Stored Electrogenerated Promoters Inducing Sustainable Enhanced Pt Catalyst Activity

THÈSE N^{O} 4690 (2010)

PRÉSENTÉE LE 30 AVRIL 2010

À LA FACULTÉ SCIENCES DE BASE

GROUPE DE GÉNIE ÉLECTROCHIMIQUE

PROGRAMME DOCTORAL EN CHIMIE ET GÉNIE CHIMIQUE

ÉCOLE POLYTECHNIQUE FÉDÉRALE DE LAUSANNE

POUR L'OBTENTION DU GRADE DE DOCTEUR ÈS SCIENCES

PAR

Cyril FALGAIRETTE

acceptée sur proposition du jury:

Dr C. Wandrey, présidente du jury
Prof. C. Comninellis, Dr G. Foti, directeurs de thèse
Prof. E. Baranova, rapporteur
Dr W. Harbich, rapporteur
Prof. D. Tsiplakides, rapporteur

ÉCOLE POLYTECHNIQUE
FÉDÉRALE DE LAUSANNE

Suisse
2010

Remerciements

Je souhaite avant tout remercier mon Directeur de thèse, le Professeur Christos Comninellis, de m'avoir encouragé à effectuer ce travail de Thèse en Génie Electrochimique au sein de son groupe de recherche à l'EPFL. Ses précieux conseils et son bienveillant encadrement au cours de ces quatre années de collaboration m'ont permis de m'épanouir tant humainement que scientifiquement.

J'aimerais également exprimer toute ma gratitude à mon Co-Directeur de thèse, le Docteur Gyorgy Foti, pour son aide inestimable, son soutien constant et sa patience légendaire qui ont été pour moi un parrainage irremplaçable.

Thank you to the other members of the jury, Professor Elena Baranova, Professor Dimitris Tsiplakides, Doctor Wolfgang Harbich and Professor Christine Wandrey for the time and effort involved in reviewing my work.

Un grand merci au Docteur Wolfgang Harbich de m'avoir invité à collaborer avec son groupe de recherche à un moment crucial de mon travail. Le généreux partage de ses installations et de ses connaissances m'a permis de porter un nouveau point de vue sur le sujet, favorisant grandement la bonne réussite de ma thèse.

Merci à Mme Ingrid Margot et à Mme Evelyne Toubes pour leur assistance dans les diverses tâches administratives ainsi qu'aux techniciens et autres membres de l'institut de chimie et de physique pour leur aide et leur disponibilité tout au long de ce doctorat.

Je remercie tous les collègues rencontrés au GGEC qui m'ont permis de travailler dans une ambiance à la fois studieuse et détendue. Merci en particulier à Méri qui, pendant plus de trois années, a su rendre mon quotidien exceptionnel, mais aussi à Xia, Stamatis, pour leur collaboration scientifique et à Stéphane, Michael H., Pietro et Aga pour tous les bons moments partagés.

Je n'oublie pas les amis de toujours qui ont été un soutien inébranlable à l'extérieur du laboratoire. Merci à Bot, Jul Mat, Séb, JM, Juyia, Maitre Nicole, Oliver Weiss, Jojo, Farlouche, Jul Jod, Keuj et Marki.

Je remercie enfin tout particulièrement ma famille qui m'a toujours apporté un soutien total au cours de mes études et qui m'a permis de les entreprendre dans d'excellentes conditions. Papa, Maman, Titi, je vous aime et je vous dédie ce travail.

Abstract

This work concerns the investigation of the electrochemical promotion of Pt/YSZ catalyst giving more emphasis to the sustainable enhanced catalytic activity after current interruption. The permanent electrochemical promotion (P-EPOC) of C_2H_4 combustion over Pt/YSZ is investigated at 375°C under atmospheric pressure. Under anodic polarization, a non-faradaic enhancement of the reaction rate is observed (ρ = 4.2 and Λ = 370). However, after current interruption, the sustainable enhanced catalytic activity (P-EPOC) increases with the holding polarization time (γ=2,2 after 10 hours) giving evidence that a storage mechanism of oxygen promoters is involved in P-EPOC. In fact, a model involving two different types of promoters is proposed. O^{δ_1-} promoters, highly mobile and reactive at the Pt/gas, are proposed to be responsible of EPOC while O^{δ_2-} promoters, slow and very stable at the Pt/gas, are proposed to account for P-EPOC.

Further electrochemical investigations of the Pt/YSZ interface realized at both atmospheric pressure and under high vacuum (HV) conditions gave strong evidence that the electrogeneration of the O^{δ_2-} promoters is related to the formation of PtO taking place during an anodic polarization. In fact, the investigations of the $O_{2(g)}$,Pt/YSZ systems at atmospheric pressure, have revealed that, under anodic polarization, two electrochemical reactions take place: PtO formation at the Pt/YSZ interface and O_2 evolution at the triple phase boundary (tpb). The current efficiencies of each process (η_{PtO} and η_{O2}) are determined allowing estimating the effective rate of PtO formation at the Pt/YSZ interface. In addition, CV-MS and DSCP-MS measurements, performed under HV conditions, have confirmed this process of oxygen storage at the Pt/YSZ interface and reveal a cooperative mechanism between O_2 evolution reaction and PtO formation which allows the slow diffusion of oxygen strongly bonded (O^{δ_2-} promoters) toward the Pt/gas interface.

Key words: NEMCA effect, EPOC effect, P-EPOC effect, Pt/YSZ interface, solid state electrochemistry, Wagner theory for metal oxidation, oxygen storage, catalysis under high vacuum

Résumé

Ce travail propose l'étude de la promotion électrochimique du catalyseur Pt/YSZ en portant une attention particulière à l'augmentation durable de l'activité calatytique observée après interruption du courant.

La promotion électrochimique permanente (P-EPOC) de la combustion de C_2H_4 sur Pt/YSZ est étudiée à 375°C sous pression atmosphérique. Pendant une polarisation anodique, une augmentation non-faradique de la vitesse de réaction est observée (ρ = 4.2 and Λ = 370). Cependant, après interruption du courant, l'augmentation durable de l'activité calatytique (P-EPOC) grandit avec le temps de polarisation (γ =2,2 après10 heures) témoignant qu'un mécanisme de stockage de promoteurs oxygène est associé à P-EPOC. Un modèle comportant deux différents types de promoteur est proposé. Les promoteurs O^{δ_1-}, très mobiles et réactifs à l'interface Pt/gaz, sont suggérés être responsables de EPOC, alors que les promoteurs O^{δ_2-}, lents et très stables à l'interface Pt/gaz, sont reliés à P-EPOC.

Les études électrochimiques de l'interface Pt/YSZ réalisées par la suite, à pression atmosphérique et sous vide poussé, ont donné une forte preuve que l'électrogénération des promoteurs O^{δ_2-} est reliée à la formation de PtO pendant la polarisation anodique. L'étude à pression atmosphérique a montré que pendant la polarisation, deux réactions électrochimiques ont lieu : la formation de PtO à l'interface Pt/YSZ et le dégagement d'oxygène à l'interface triple (tpb). Les efficacités de courant de chaque réaction (η_{PtO} et η_{O2}) sont determinées, ce qui permet d'estimer la vitesse effective de formation de PtO. En outre, les mesures CV-MS et DSCP-MS, faites sous vide poussé, ont confirmé ce procédé de stockage d'oxygène à l'interface Pt/YSZ et ont révélé un mécanisme de coopération entre le dégagement d'oxygène et la formation de PtO qui permet la diffusion lente d'oxygène fortement lié (les promoteurs O^{δ_2-}) à l'interface Pt/gaz.

Mots clés : Effet NEMCA, Effet EPOC, Effet P-EPOC, interface Pt/YSZ, électrochimie solide, théorie de Wagner pour l'oxidation des métaux, stockage d'oxygène, catalyse sous vide poussé.

Table of contents

Table of contents

CHAPTER I- INTRODUCTION

Electrochemical Promotion of Catalysis (EPOC), first observed by *Vayenas* in the 80's [1], consists of the dramatic enhancement of the catalytic activity of a conducting catalyst supported on a solid electrolyte during the application of a constant current/potential step. EPOC is a challenging interdisciplinary phenomenon regrouping the field of catalysis, surface science, electrochemistry, solid state ionic and chemical reaction engeneering. Worth to mention that EPOC has not been found to be limited to any particular electrolyte, *e.g.* cationic or anionic, any conducting catalyst, *e.g.* metal or metal oxide, or any type of catalytic reaction. As a consequence, no doubt that the investigation of EPOC phenomenon represents a subject of growing interest regrouping many fundamental and applied investigations performed by several different groups all over the world (Fig I-1).

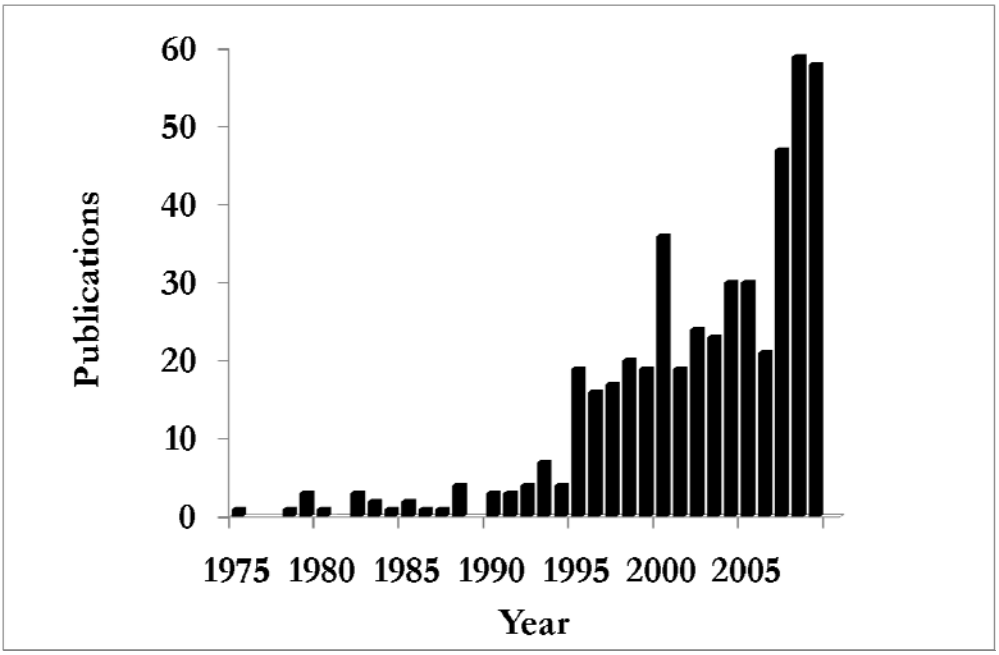

Fig I-1 : Number of EPOC publications edited over the last decades from www.scopus.com

I.1 Motivations and objectives

In most of the reported EPOC studies, after current interruption, the catalyst returns to its initial activity, *i.e.* EPOC is considered to be reversible [2]. However, after long term polarization, some systems revealed a remaining enhancement of their catalytic activity [3-5]. This intriguing behavior, first reported in our laboratory as Permanent EPOC (P-EPOC) [6] represents a challenging subject for the fundamental understanding of the phenomenon.
Previous works suggested that during polarization, promoter storage, 'hidden' from catalysis is responsible of the P-EPOC behavior [5]. However, the nature and the location of this storage represent a serious point of controversy.

This works aims to corrolate the gas exposed catalyst (Pt/gas) activity with the Pt/YSZ interface in order to understand the mechanism by which the effect of polarization at the catalyst/electrolyte interface propagates to the catalyst/gas interface. In this aim, both atmospheric and high vacuum conditions are studied. At atmospheric pressure, the investigation is performed in a large domain of temperature, by chronopotentiometry and cyclic voltammetry which are commonly used techniques to describe and get knowledge upon both anodic and cathodic behavior of electrochemical sytems. Under high vacuum (HV), a new electrochemical technique has been developed for electrochemical and electrocatalytic investigations of the Pt/YSZ interface. In this technique an electrochemical perturbation is imposed to the Pt/YSZ interface and the reaction products at the Pt/gas interface are analyzed online by mass spectrometry. The response time of this technique is less than 1s.

I.2 Outline

After description of the motivations and objectives of the work (Chapter I), the study performed herein is divided in three different parts. Part I concerns the electrochemical promotion of C_2H_4 combustion over Pt/YSZ at atmospheric pressure, Part II focuses on

the electrochemical behavior of the $O_{2(g)}$,Me/YSZ interface upon anodic/cathodic polarization at atmospheric pressure and Part III deals with the electrochemical and the electrocatalytic behavior of the Pt/YSZ interface under high vacuum conditions (HV).

I.2.1 Part I : Electrochemical promotion (EPOC and P-EPOC)

In Chapter II, the EPOC literature is reviewed. After a prolonged anodic polarization, an unexpected complex relaxation behavior, after current interruption, of the catalytic activity is reported for several systems. Depending on the experimental conditions, this catalytic enhancement is observed to be either permanent (P-EPOC : the catalytic activity reaches a sustainable higher catalytic activity after current interruption), either persistent (Pers-EPOC : the catalytic activity remains enhanced after current interruption, for a finite time, before to restore its initial state). P-EPOC is quantified by γ, the permanent enhancement factor and Pers-EPOC is quantified by Λ_{OS}, the oxygen storage efficiency.

In Chapter III, the electrochemical promotion of ethylene combustion over Pt/YSZ is studied under atmospheric pressure at 375°C by varying the reactive gas composition, the applied anodic current and the duration of the polarization step imposed. During the polarization, the electrophobic behavior of the system is confirmed (in agreement with EPOC theory). However, after current interruption, the irreversibility of the phenomenon is established to increase with increasing polarization time. This suggests that slow irreversible promoter storage takes place in parallel to the rapid mechanism of sacrificial promoter described in literature.

I.2.2 Part II : Electrochemical investigation of $O_{2(g)}$,Me/YSZ (Me:Ni,Pt) systems

In Chapter IV, the electrochemistry of generic Me/YSZ systems is reviewed. Solid state electrochemistry literature reports various possible reaction paths and reaction locations for the mechanism taking place upon an anodic/cathodic polarization of a Me/YSZ interface.

Because of these discrepancies the review is extended to the field of high temperature metal oxidation and to the literature of aqueous state electrochemistry. On this basis, the literature concerning the Ni/YSZ and the Pt/YSZ systems is subject to special focus.

In Chapter V, the $O_{2(g)}$,Ni/YSZ system is investigated under atmospheric pressure as reference system. Cyclic voltammetry measurements performed between 350°C and 450°C reveal that under anodic polarization, nickel oxide formation takes place at the Ni/YSZ interface in parallel to the oxygen evolution reaction occurring at the triple phase boundary (tpb). Current efficiencies are determined for both processes and the results are correlated to the electrochemical interpretation of the *Wagner* oxidation theory.

In Chapter VI, the $O_{2(g)}$,Pt/YSZ system is investigated by cyclic voltammetry between 250°C and 375°C at atmospheric pressure (O_2 20% in He). Under anodic polarization, PtO is formed at the Pt/YSZ interface in parallel to the oxygen evolution reaction occurring at the tpb. Depending on the applied potential, the PtO formation is found to follow a parabolic or logarithmic growth law allowing to propose a model for Pt/YSZ interface electro-oxidation in relation to the *Wagner* or the *Eley* & *Wilkinson* oxidation mechanisms.

I.2.3 Part III : Investigation under high vacuum

In Chapter VII, a new probe device is built to perform electrochemical measurements under high vacuum (HV) conditions, while monitoring simultaneously the electrochemically formed products. The short residence time of the microreactor coupled to the high sensitivity and the fast detection response (<1s) of QMS analyzer appeared as key parameters for the elaboration of such a solid electrochemical mass spectrometric investigation tool (SEMS).

In Chapter VIII, the Pt/YSZ interface is investigated under HV conditions by CV-MS measurements (coupling cyclic voltammetry to mass spectroscopy) and DSCP-MS

measurements (coupling double step chronopotentiometry to mass spectroscopy) at 400°C. The cathodic stability of YSZ and the anodic PtO formation.

In Chapter IX, the electrocatalytic behavior of the Pt/YSZ system is investigated for CO oxidation under HV conditions at 400°C. For both oxygen lean and oxygen rich conditions, the CO oxidation reaction is found to be composed of a chemical contribution and an electrochemical faradaic contribution without any synergetic effect.

Finally in Chapter X, a general discussion on the electrochemical promotion of the Pt/YSZ catalyst for gas phse reaction is proposed. On the basis of all the results obtained, a model involving two different types of promoters is proposed. First type of promoters, $O^{\delta 1-}$, are proposed to be responsible of the rapid electrochemical promotion observed during the polarization (EPOC) while second type of promoters, $O^{\delta 2-}$, more stable, are suggested to be stored during the polarization step and linked to the P-EPOC effect reported after current interruption.

I.3 References

1. Bebelis S, Vayenas CG (1989) Journal of Catalysis 118: 125

2. Vayenas CG, Bebelis S, Pliangos C, Brosda S, Tsiplakides D (2001) Electrochemical Activation of Catalysis: Promotion, Electrochemical Promotion, and Metal-Support Interactions. Kluwer Academic / Plenum Publishers, New York

3. Nicole J (1999) Etude de la promotion électrochimique de l'oxydation catalytique de l'éthylène sur des oxydes métalliques, EPFL

4. Wodiunig S (2000) Electrochemical Promotion of RuO_2 Catalysts for the Gas Phase Combustion of Ethylene, EPFL

5. Jaccoud A (2006) Electrochemical promotion of Pt catalysts for gas phase reaction, EPFL

6. Varkaraki E, Nicole J, Plattner E, Comninellis Ch, Vayenas CG /1995) Journal of Applied Electrochemistry 25:978

PART I

Electrochemical Promotion

(EPOC and P-EPOC)

CHAPTER II- STATE OF THE ART

The catalytic activity, of both metal and conductive metal oxide catalysts supported on YSZ, is found to be dramatically modified by the application of an electrochemical polarization. This phenomenon, first reported in the 80's by *Vayenas* as Non-faradaic Electrochemical Modification of Catalyst Activity (NEMCA), is in our days known as Electrochemical Promotion of Catalysis (EPOC). It has been reported that after potential (current) interruption, the catalyst is generally observed to restore rapidly its initial activity, i.e. EPOC is generally reversible and the state of the art EPOC model proposed by *Vayenas* expects such behavior.

Nevertheless, it has been found that, following a prolonged anodic polarization, at potential (current) interruption several catalysts remain in a promoted state compared to the initial open circuit activity. Moreover, an exposure to a reductive atmosphere allowed restoring the initial catalytic activity. This effect first reported in our laboratory was named Permanent EPOC (P-EPOC) and represents a challenging field of research for several years.

This chapter proposes a review of the literature of EPOC which highlights the main parameters influencing the electrochemical promotion behavior of YSZ supported catalysts with special focus on the P-EPOC phenomenon. Prolonged polarization time, t_H, oxygen rich gas mixture composition and low temperature appeared as main conditions required to the observation of P- EPOC for ethylene combustion over Pt/YSZ. This allows to define experimental conditions for the further investigation proposed in this work.

II.1 Introduction

Electrochemical promotion of catalysis (EPOC) means non-Faradaic tuning of the catalytic reaction rate by electric polarization of the interface between an electron conducting catalyst (metal or metal oxide) and an ion conducting support. Typical use is for gas phase reactions over metal or metal oxide catalysts in a solid electrolyte cell at temperatures between 300 and 600°C, where the most often used support, yttria-stabilized zirconia (YSZ), is an oxide ion (O^{2-}) conducting material. The state-of-the-art model of EPOC attributes the phenomenon to electrochemically generated species, responsible for promotion but at the same time consumed slowly in the catalytic reaction ('sacrificial' promoter). In early works already, EPOC was related to alteration of catalyst work function. Although EPOC is most often fully reversible, long-lasting polarization of both metal (Pt, Rh) and oxide (IrO_2, RuO_2) catalysts was found to cause an apparent 'permanent' effect, where the steady-state open circuit catalytic activity after current interruption exceeded significantly its initial level before polarization.

II.2 EPOC phenomenon

Controlled tuning of catalytic activity has been a long-sought goal in heterogeneous catalysis. In their pioneering work in the early 1980s *Vayenas et al.* reported the control of catalytic reactions *via* electrochemical polarization [1]. They found that the catalytic activity of thin porous metal catalyst films could be tuned in a controlled manner by polarization of the catalyst/solid electrolyte interface in an electrochemical cell of the type:

catalyst (working electrode) WE	solid electrolyte	catalytically inert metal (counter electrode) CE

where the catalyst film is the working electrode and the catalytically inert metal (typically gold) is the counter electrode. Take the example of ethylene combustion as catalytic reaction:

$$C_2H_4\,(g) + 3\,O_2\,(g) \;\rightarrow\; 2\,CO_2\,(g) + 2\,H_2O\,(g) \qquad \textbf{II-1}$$

occurring at an open-circuit reaction rate of r_o (mol O s^{-1}). Using an oxide ion (O^{2-}) conducting material (*e.g.* yttria-stabilized-zirconia, YSZ) as solid electrolyte, application of an anodic current between the counter and the working electrode (now the solid electrolyte is the source of O^{2-} ions and the working electrode is the collector of electrons) may result in the electrochemical oxidation of ethylene at the working electrode:

$$C_2H_4\,(g) + 6\,O^{2-} \;\rightarrow\; 2\,CO_2\,(g) + 2\,H_2O\,(g) + 12e^- \qquad \textbf{II-2}$$

Supposing a current efficiency of 100%, the maximum possible electrochemical reaction rate, r_{el} (mol O s^{-1}), is calculated with Faraday's law:

$$r_{el} = \frac{I}{zF} \qquad \textbf{II-3}$$

where I is the electric current, z is the charge number of the transported ions (for O^{2-}, $z = 2$), and F is the Faraday constant. If open-circuit and Faradaic reactions would be additive, Eq. 3 would give the maximum expected increase in reaction rate due to polarization.

Fig. II-1 shows the evolution of the experimentally observed reaction rate, r, in a stepwise anodic polarization cycle, *i.e.* before, during, and after galvanostatic polarization of the catalyst/YSZ interface in the combustion of ethylene (p_{C2H4} = 0.36kPa, p_{O2} = 4.6 kPa) over Pt/YSZ at 370°C, reported by *Bebelis* and *Vayenas* [1]. It is seen, that the experimental rate increase, $r - r_o$, is by orders of magnitude higher than the maximum possible rate

increase calculated from Faraday's law. Obviously, polarization of the catalyst/electrolyte interface causes a dramatic alteration in catalytic activity rather than simply contribute to the reaction rate by adding the electrochemical (Faradaic) reaction. The highly non-Faradaic character of electrochemical promotion originates its currently used synonym: non-Faradaic electrochemical modification of catalytic activity (NEMCA effect) [2].

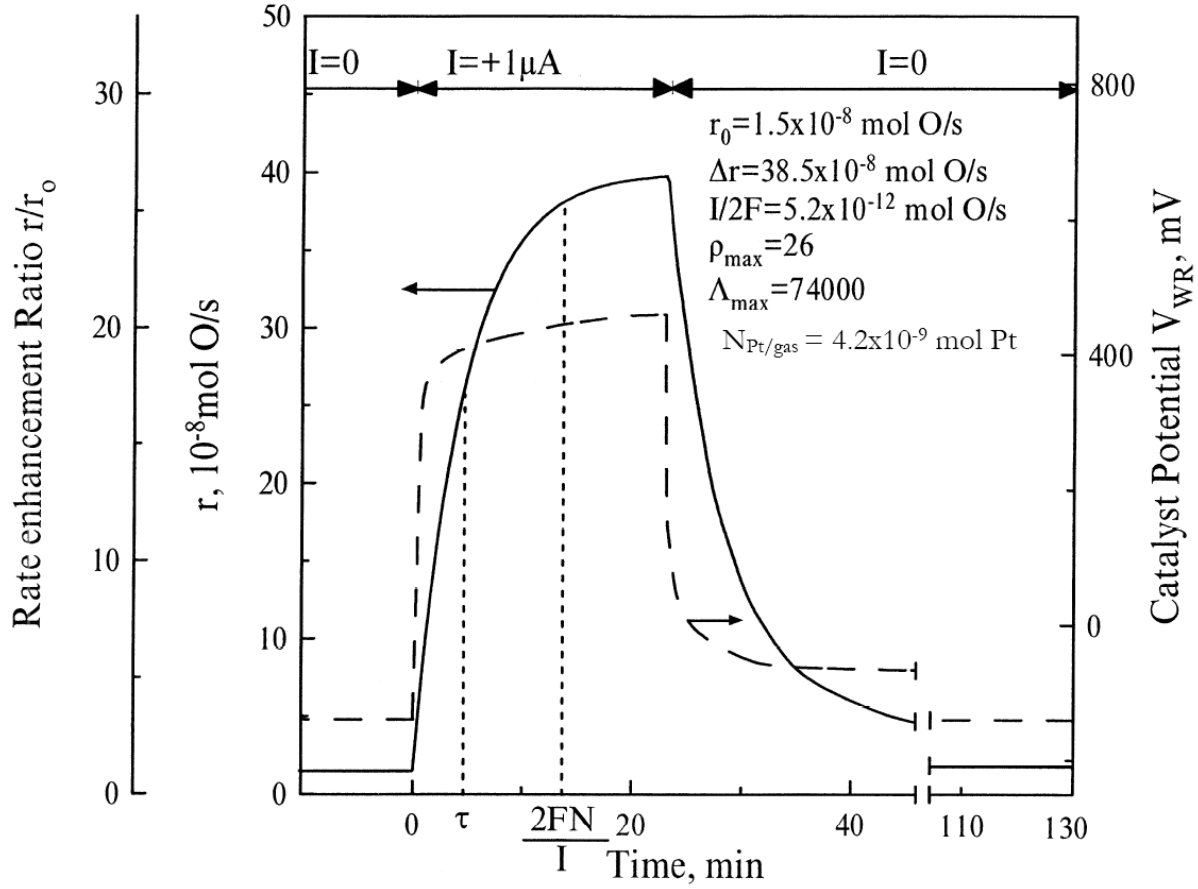

Fig. II-1 : Rate, *r*, and catalyst potential *V*, response to step changes in applied current during C_2H_4 oxidation on Pt /YSZ. *T*=370°C, P_{O2}=54.6 kPa, P_{C2H4} =0.36 kPa. The experimental (τ) and computed ($2FN_{Pt/gas}/I$) rate relaxation time constants are indicated on the figure [1]. $2FN_{Pt/gas}/$ is the number of active sites of the Pt catalyst.

EPOC is usually quantified by two parameters, ϱ and Λ. The rate enhancement factor, ϱ, is defined as the ratio of the steady-state promoted catalytic rate, r_p, to the initial open-circuit reaction rate, r_o, and is a measure of the level of promotion (equation II-4):

$$\rho = \frac{r_p}{r_0} \qquad \textbf{II-4}$$

The Faradaic efficiency, Λ, is defined as the ratio of the observed rate increase to the maximum possible electrochemical rate (equation II-5):

$$\Lambda = \frac{r_p - r_0}{\frac{I}{2F}} \qquad \textbf{II-5}$$

so $|\Lambda| > 1$ is the criterion of non-Faradaic behavior. For the example seen in Fig. II-1, the approximate steady state values are $\rho \approx 26$ and $\Lambda \approx 74000$.

Since its discovery [3], the non-Faradaic character of EPOC has been demonstrated for more than 70 catalytic reactions, and it is now well established that EPOC is not limited to any particular class of catalysts, electrolytes or reactions [2].

Electrochemical promotion induced, by application of potential difference between the working catalyst electrode and the reference results in a change in catalyst work function responsible of the enhancement of the catalytic reaction rate [4]. In fact, catalyst work function measurements performed by *Ladas et al* [5] using the Kelvin probe technique over Pt catalyst deposited on O^{2-} or Na^{+} conducting electrolytes, report a one-to-one relationship between the applied working-reference potential difference, ΔU_{WR}, and the catalyst (WE) work function change, $\Delta\Phi_W$.

$$e\,\Delta U_{WR} = \Delta\Phi_W \qquad \textbf{II-6}$$

where e is the unit electron charge.

This experimental fact was attributed by the authors to the population of the catalyst/gas interface by oxygen backspillover ions, taking place during an anodic polarization. Later, this relation (equation II–6) was theoriticaly validated by *Leiva et al* [6] for a wide range of catalyst work function (0.2eV-1eV).

The current understanding of the physicochemical origin of EPOC, based also on numerous other spectroscopic and electrochemical techniques and reviewed thoroughly [7-10], attributes the effect of electrochemical promotion to transport of ionic species through the solid electrolyte support, their discharge at the triple phase boundary (tpb) and subsequent migration of the discharged species to the catalytically active catalyst/gas interface. The discharged species act as promoters but are also consumed by the catalytic reaction and/or desorption. The resulting steady-state population of promoters at the gas exposed catalyst surface causes a potential-controlled change in the work function of this latter. According to this concept, EPOC is reversible and the catalyst restores its initial activity, typically within a few tens of minutes, after potential or current interruption.

In terms of catalytic reaction rate, the state-of-the-art model of EPOC predicts steady-state open-circuit reversibility (*i.e.* sacrificial promoters), fast response upon current imposition depending on the applied current and relatively fast relaxation (depending on Λ) upon current interruption. However, several experiments, especially when related to long lasting polarization, have revealed steady-state open-circuit irreversibility and/or current dependent complex relaxation transients. Such effect, termed 'permanent' electrochemical promotion (P-EPOC), can not be explained by the current model of EPOC.

II.3 Permanent EPOC (P-EPOC)

In our laboratory, several cases of irreversible EPOC have been reported. Such effect, termed 'permanent' electrochemical promotion (P-EPOC), was first observed with IrO_2 catalyst for ethylene combustion [11-14], and later also with RuO_2 [15-17] and Rh [18] catalysts, all interfaced with YSZ. Furthermore, it was found that reversibility of EPOC may depend strongly on the duration of polarization [19, 20]. In fact, as illustrated in Fig. II-2, in the same catalytic system short (15 min) polarization causes reversible promotion, see curve (a), while after prolonged (50 min) polarization the open-circuit catalytic reaction rate after

current interruption remains significantly higher than its initial value before current application, see curve (b).

The "permanent" rate enhancement ratio, γ, was then introduced in order to quantify the irreversibility of electrochemical promotion (equation II-7):

$$\gamma = \frac{r'}{r_0} \qquad \text{II-7}$$

where r' is the open-circuit catalytic reaction rate after the current interruption, so for γ>1 the electrochemical promotion exhibits a permanent effect.

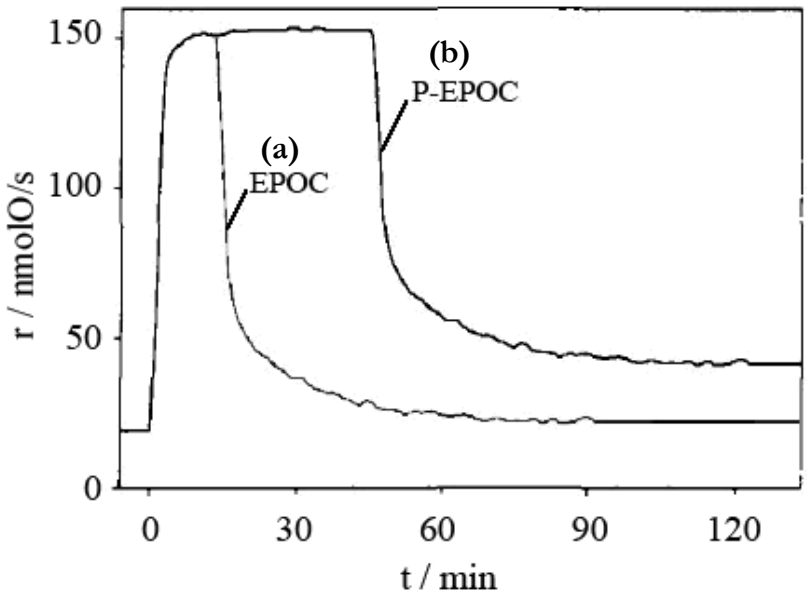

Fig. II-2 :Polarization and relaxation transients of the rate of ethylene combustion on IrO_2/YSZ catalyst due to current application (300 μA) for two different polarization times: (a) short polarization to give reversible EPOC and (b) long polarization to give P-EPOC. T = 380°C, p_{O2} = 17 kPa, p_{C2H4} = 140 Pa [19].

Nicole et al [19] reported the evolution of the permanent enhancement factor, γ, for IrO_2/YSZ catalyst in ethylene/oxygen gas mixtures at T = 380°C as a function of polarization time (Fig. II-3). For short polarization time the γ value is close to one, *i.e.*

reversible EPOC is observed. As the polarization holding time increases, the γ factor is increasing to reach a plateau after about 20 minutes of polarization. It appears that no permanent enhancement of catalytic activity process is taking place in the very first stage of polarization, but a finite polarization time is needed to permanently affect the system.

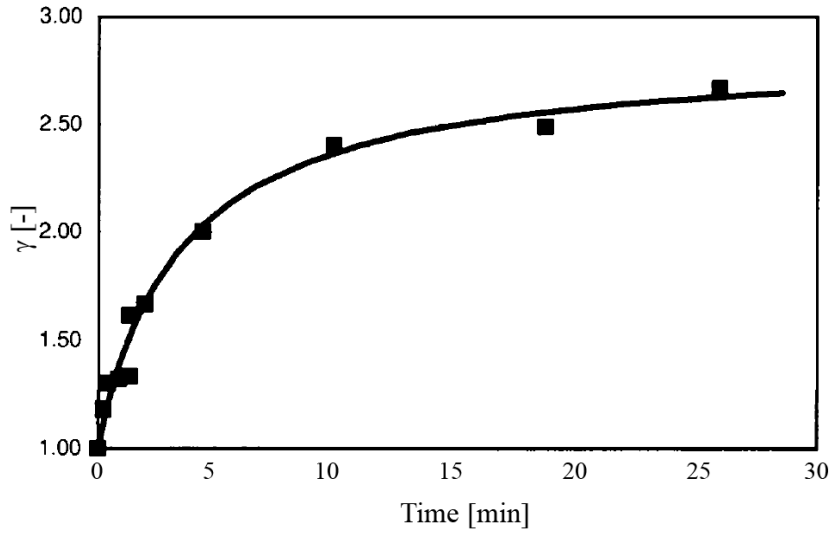

Fig. II-3 : Influence of holding time of the galvanostatic step at 300 μA on the permanent enhancement factor γ (equation II-7) for IrO_2/YSZ catalyst, T=380°C, p_{O2} = 20 kPa, p_{C2H4} = 150 Pa. [19]

A second approach to emphasis the role of duration of the polarization step is shown in Fig. II-4 which compares two ways of supplying a given charge to the IrO_2/YSZ catalytic cell. 90 mC are passed through the cell by application of either five successive pulses or one unique galvanostatic step of identical current. By pulses application, even after the final pulse, no permanent promotion enhancement is observed (γ = 1). However, if the same charge is passed through the cell by one unique galvanostatic step, the final reaction rate is enhanced by a factor of 1.4. This fact shows clearly that P-EPOC is directly linked to the polarization time since a certain delay is required to modify in a permanent way the catalytic activity of the IrO_2/YSZ system.

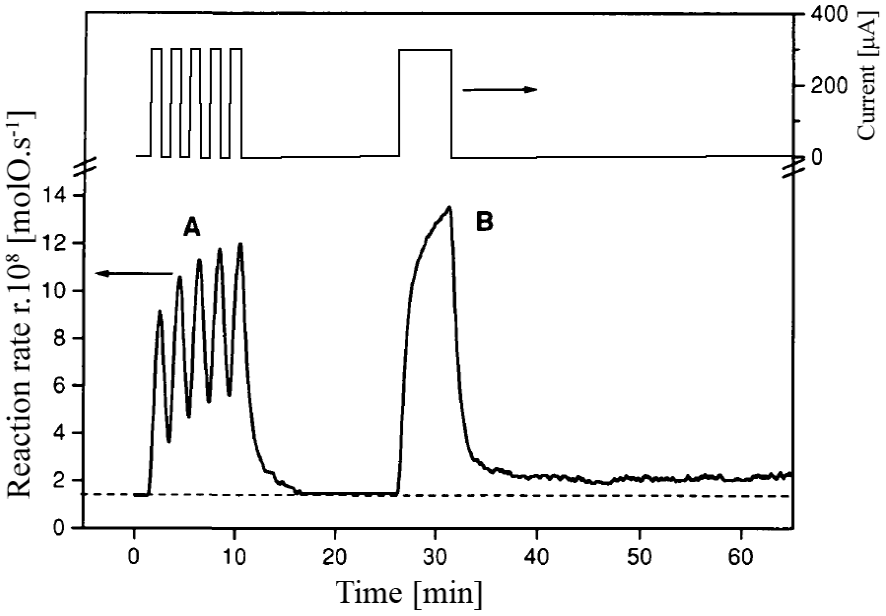

Fig. II-4 : Influence of holding time of galvanostatic step on the persistent activation of IrO_2/YSZ catalyst. A charge of 90mC is passed through the cell by application of 5 pulses (A) and 1 galvanostatic step(B), T=380°C, p_{O2} = 20 kPa, p_{C2H4} = 150 Pa. [19]

An approach to investigate electrochemical promotion by means of cyclic voltammetry consists of measuring the voltammetric charge. For this purpose, cyclic voltammetry is performed in a narrow potential range around the open-circuit potential, and the voltammetric charge is determined by integrating the area under the voltammogram. *Nicole et al.* studied the voltammetric charge of IrO_2/YSZ interfaces in ethylene/oxygen gas mixtures at T = 380°C [19]. Recorded over a range of ±25 mV around the equilibrium potential at different scan rates, fairly symmetrical cyclo-voltammograms exhibiting no peaks were obtained, as shown in Fig. II-5. The voltammetric charge was attributed to formation of an oxygen capacitor according to the reaction:

$$IrO_2 + \delta\, O^- \rightleftarrows IrO_{2+\delta} + \delta\, e^- \qquad \textbf{II-8}$$

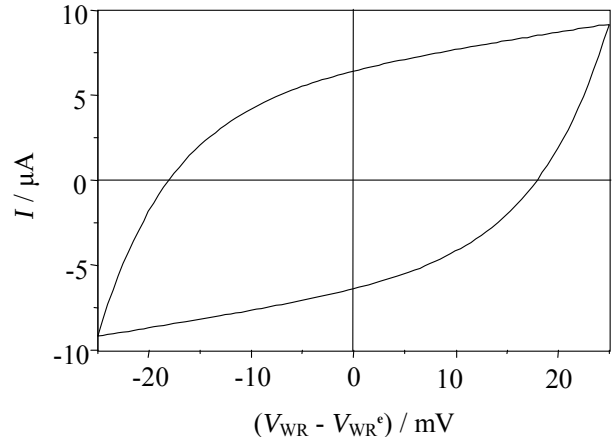

Fig. II-5 Typical cyclo-voltammogram of an IrO_2 catalyst in a narrow potential range around the equilibrium (U_{WR}^e) potential. Scan rate: 20 mV s^{-1}, p_{O_2} = 20 kPa, T = 380°C. [19]

As seen in Fig. II-6, a linear correlation was observed between the voltammetric charge and the reaction rate of ethylene combustion during open circuit relaxation of the reaction rate after current interruption. This clearly shows that the electrochemical promotion of IrO_2 catalyst is directly related to the stored charge at the catalyst (WE)/YSZ interface.

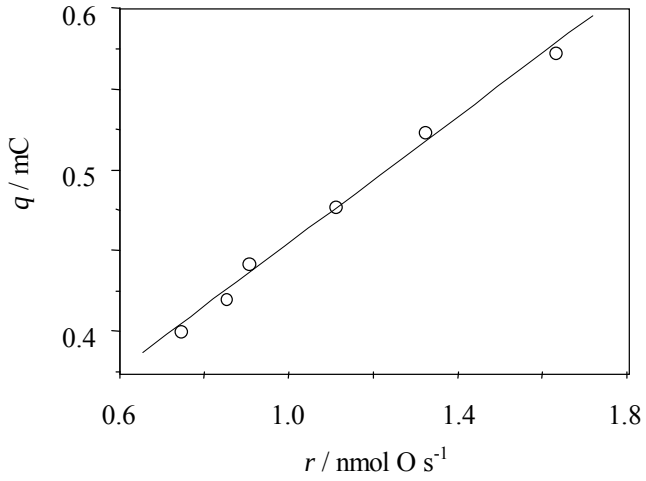

Fig. II-6 Relation between voltammetric charge and rate of ethylene combustion over an IrO_2 catalyst during open circuit relaxation. $p_{C_2H_4}$ = 120 Pa, p_{O_2} = 180 Pa, T = 380°C. [19]

Similarly, *Jaccoud et al* [20] recently observed a complex relaxation behaviour on Pt/YSZ catalytic cell after prolonged potentiostatic polarization (400mV) at 525°C and 600°C (Fig. II-7), also highly depending on the experimental temperature. At high temperature (600°C), the catalytic activity drops abruptly almost to its initial activity upon current interruption, then increases up to a promoted state before to return again to its initial state (Fig. II-7 b). At lower temperature (525°C), the first catalytic activity drop observed upon current interruption leads to an intermediate plateau value, *r'*, then it decreases slowly to its initial state (Fig. II-7 a).

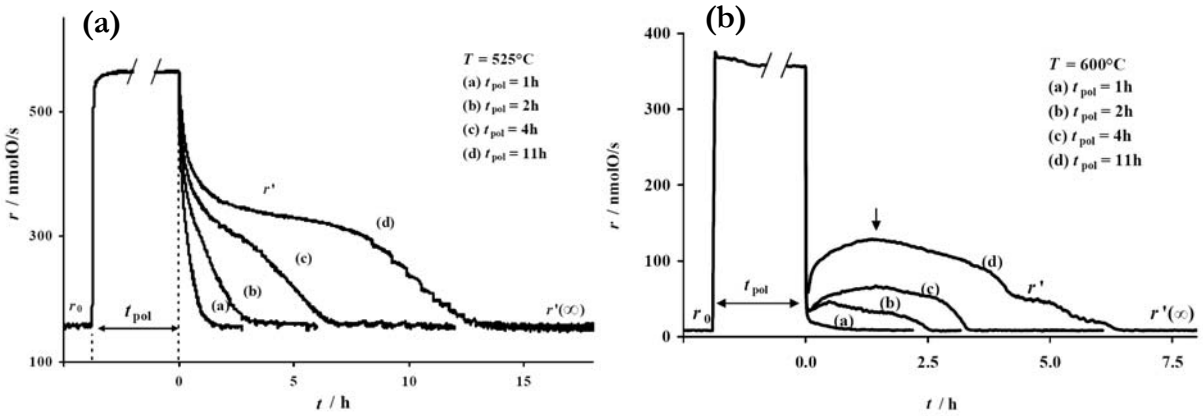

Fig. II-7 :Pers-EPOC transients observed for ethylene combustion over Pt/YSZ, (a) T = 525°C, (b) T = 525°C, E_{WR} = 400 mV, p_{C2H4} = 0.25 kPa, p_{O2} = 1 kPa; [20]

Worth to notice that under these conditions, where the catalyst activity, upon current interruption, is a complex function of time but finally returns to its initial value, the permanent enhancement factor, γ (equation II-7), is not a suitable parameter. For such case, *Jaccoud et al.* porposed to introduce an oxygen storage efficiency define as (equation II-9):

$$\Lambda_{OS} = \frac{N_r}{N_F} \qquad \textbf{II-9}$$

where $N_F = It_H/2F$ is the maximum amount of oxygen promoters supplied to the catalyst surface during the anodic polarization time t_H and N_r is the number of oxygen atoms consumed in the catalytic reaction after current interruption. As shown in Fig II-9, the so estimated values of Λ_{OS} are much higher than one (Λ_{OS} >>1) which demonstrates that the

stored oxygen acts as a promoter upon current interruption and we are not dealing with a simple consumption of oxygen stored during the preceding current imposition. Such behaviour after current interruption has been reported as persistent EPOC (Pers-EPOC).

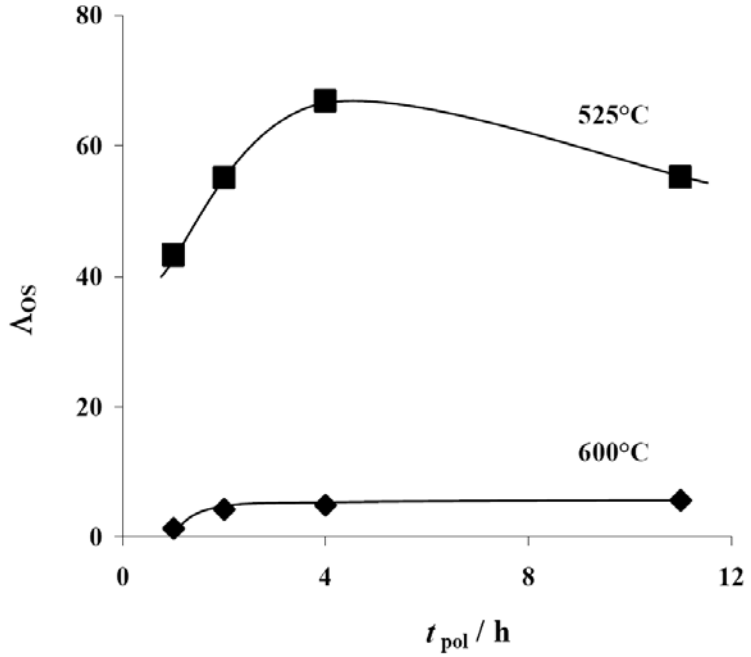

Fig. II-8 Effect of the polarization time t_{pol} on the oxygen storage efficiency Λ_{OS} at 525°C and 600°C. p_{C2H4} = 0.25 kPa, p_{O2} = 1 kPa. [20]

Investigation of P-EPOC by work function measurements confirmed the major role of the holding polarization time. Fig. II-9 displays the evolution of the catalyst work function observed by *Wodiunig et al* [17] during the imposition of a galvanostatic step to RuO_2 catalyst in ethylene/oxygen gas mixture. At current interruption, the work function decreases dramatically to an intermediate value and slowly decreases to its initial open-circuit value.

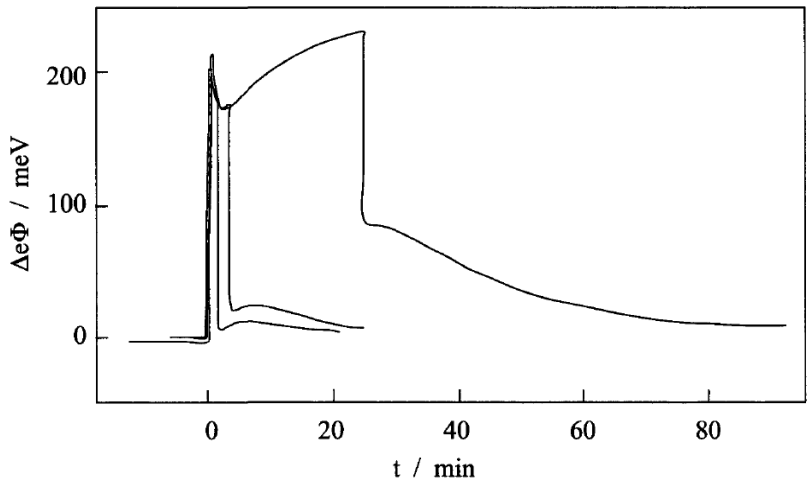

Fig. II-9 : Time dependence of the work function change during galvanostatic step of 50 μA for three polarization holding times, t = 1, 3 and 23 minutes, T=380°C, p_{O2} = 17.7 kPa, p_{C2H4} = 114 Pa. [17]

Once again, the duration of the anodic polarization step appears as a key parameter to the understanding of P-EPOC. The increase of the work function relaxation time with polarization holding time reflects the increasing amount of promoters lying at the catalyst gas exposed surface.

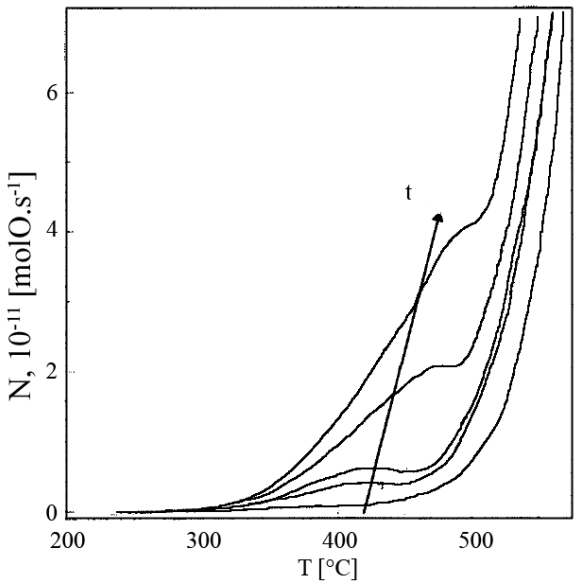

Fig. II-10 : Oxygen desorption after application of a galvanostatic step of 5μA on IrO_2/YSZ for different polarization times, t = 180, 400, 600, 1200 and 1800s, T=350°C, p_{O2} = 20 kPa, p_{C2H4} = 150 Pa [19]

Investigations by TPD experiments revealed clearly that a prolonged polarization leads to oxygen storage into the catalytic cell [21-25]. Fig. II-10 shows the influence of electrochemical pre-treatment on the thermal oxygen desorption of IrO_2/YSZ catalyst in high vacuum. When the catalyst is submitted to an anodic polarization pre-treatment, the oxygen production is greatly enhanced. In fact, after a galvanostatic step of 5 μA, a new oxygen desorption peak, which grows with increasing polarization times, appears at 400°C [19].

Nevertheless, the initial unpromoted steady state activity of the catalyst may be restored (even after prolonged polarization) by exposing the catalyst to a highly reductive atmosphere. Fig. II-11 reports the impact of a reductive atmosphere (p_{C2H4}=150 Pa) on an IrO_2/YSZ catalyst in the P-EPOC state.

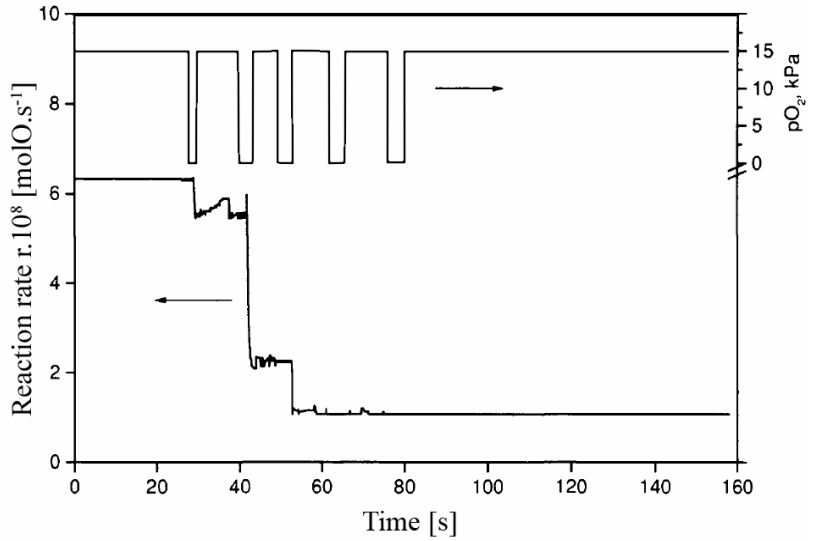

Fig. II-11 : Impact of reductive atmosphere on persistent EPOC, T=380°C, p_{C2H4} = 150 Pa, p_{O2} = 15 kPa or 0 kPa. [19]

Similar permanent enhancement of catalytic activity (P-EPOC) has also been recently reported by *Valverde* [26-28] for catalyst supported on K^+ electrolyte conductor, *e.g.* for C_3H_6 combustion over Pt/K-βAl_2O_3.

II.4 Proposed mechanism involved in P-EPOC

Several attemps have been made in order to propose a model for the experimentally observed P-EPOC phenomenon.

Nicole proposed a promoter storage mechanism taking place at the IrO_2/YSZ interface through the electrochemical formation of a high oxidation state iridium oxide species $IrO_{2+\delta}$. The $IrO_2/IrO_{2+\delta}$ system (equation II-8) is then proposed to act as a chemical capacitor able to store promoter species during the anodic polarization step and to release them upon interruption. The details of the model are given in [19].

The electrochemical investigation of Pt/YSZ cermet electrode in 20kPa O_2 in He at 450°C performed by *Jaccoud* revealed for the first time that after long polarization time, a slow platinum oxidation takes place at the Pt/YSZ [20, 29-31]. The model given by *Jaccoud* for describing the anodic polarisation of Pt/YSZ interface is the following.

- Oxygen is first rapidly stored at the catalyst/YSZ interface up to the formation of one monolayer. At 450°C, under 20kPa O_2, the process saturates within 10 minutes.
- A second type of oxygen storage in form of backspillover species is proposed to take place in parallel at the catalyst/gas interface and causes, in principle reversible, electrochemical promotion of catalysis (EPOC). The electrochemical saturation of this species appears after 80 minutes in agreement with the time needed to reach steady state during EPOC measurements of the author.
- Finally, a third type of stored oxygen, consecutive to the first process saturation, is attributed to the formation of PtO into the electrode bulk. The amount of this species is not reported to saturate even after 33h of polarization, and it is found to obey, after an induction period of a few minutes, to a $t^{1/2}$ kinetic law, typical for diffusion-controlled processes.

This model of platinum electrooxidation, obtained under unreactive atmosphere, leads the author to propose a P-EPOC model where during the anodic polarisation of the catalyst, oxygen incorporation into the bulk of the Pt electrode catalyst occurs in parallel to the

classical EPOC phenomenon. At current interruption, the so formed unstable platinum oxide, unstable at open circuit, is expected to decompose releasing promoter species to the Pt/gas interface [20, 32].

II.5 Conclusion

Electrochemical Promotion of Catalysis consists of application of small current/potential to a conductive catalyst supported on a solid electrolyte. It induces a non faradaic modification of the catalyst activity described by the state of the art EPOC theory proposed by *Vayenas* in the late 80's. In theory, and also in practice the, EPOC phenomenon is reversible, *i.e.* after current interruption the promoted reation rate returns rapidly to its initial unpromoted state. However, after long term polarization, several supported catalysts (metal and metal oxide), revealed that the classical EPOC theory may not explain the transient behaviour observed. The main statements proposed upon years and reviewed in this chapter may be summarized as follows :

- The open circuit catalytic activity of the catalyst can be increased by prolonged (>30 min) polarization (P-EPOC phenomenon)
- The temperature has a major influence on the P-EPOC phenomenon.
  - At low temperature (<400°C), the relaxation transient reaches a new enhanced open circuit steady state characterizing a Permanent EPOC (P-EPOC) quantified by γ.
  - At high temperature, although no P-EPOC is observed, the relaxation transient is very slow and complex characterizing a Persistent EPOC (Pers-EPOC) quantified by Λ_{OS}.
- Permanent-EPOC (P-EPOC) is characterized by the "permanent" enhancement factor γ which is defined by the ratio of open-circuit steady state reaction rates after, r', and before, r, polarization (equation II-7).

$$\gamma = \frac{r'}{r} \qquad \text{II-7}$$

γ values up to five can be achieved.

● Persistent-EPOC (Pers-EPOC), due to prolonged anodic polarization of a catalyst interfaced with O^{2-} conducting solid electrolyte, is characterized by the "oxygen storage efficiency" Λ_{OS} which is defined as the ratio of the maximum amount of oxygen promoters supplied to the catalyst surface during anodic polarization, N_F, to the number of oxygen atoms consumed in the catalytic reaction after current interruption, N_r.

$$\Lambda_{OS} = \frac{N_r}{N_F} \qquad \textbf{II-9}$$

● Both P-EPOC and Pers-EPOC are observed only for long polarization times (one to several hours).

● Changing the feed composition allows returning from P-EPOC to the initial un-promoted catalytic rate.

● The catalyst work function follows the catalytic rate after current interruption.

● Both P-EPOC and Pers-EPOC seem to be related with the charge stored at the catalyst/electrolyte interface during the polarization step.

II.6 References

1. Bebelis S, Vayenas CG (1989) Journal of Catalysis 118: 125
2. Vayenas CG, Jaksic MM, Bebelis SI, Neophytides SG (1996) In: Bockris JOM (ed) Modern Aspects of Electrochemistry, vol 29. Plenum Press, New York p 57
3. Vayenas CG, Lee B, Michaels J (1980) Journal of Catalysis 66: 36
4. Vayenas CG, Bebelis S, Neophytides S (1988) Journal of Physical Chemistry 92: 5083
5. Ladas S, Bebelis S, Vayenas CG (1991) Surface Science 251/252: 1062
6. Leiva EPM, Sánchez CG (2003) Journal of Solid State Electrochemistry 7: 588
7. Luerßen B, Gunther S, Marbach H, Kiskinova M, Janek J, Imbihl R (2000) Chemical Physics Letters 316: 331
8. Janek J, Luerßen B, Imbihl R, Rohnke M (2000) Phys. Chem. Chem. Phys. 2: 1935
9. Tsaofang Chao, Walsh KJ, Fedkiw PS (1991) Solid State Ionics 47: 277
10. Vayenas CG, Ioannides A, Bebelis S (1991) Journal of Catalysis 129: 67

11. Nicole J, Comninellis C (1996) In: Janssen LJJ (ed) Contemporary Trends in Electrochemical Engineering. Institute of Chemical Technology, Prague p 1
12. Nicole J, Tsiplakides DT, Wodiunig S, Comninellis C (1997) Journal of the Electrochemical Society 144: L312
13. Nicole J, Comninellis C (1998) Journal of Applied Electrochemistry 28: 223
14. Nicole J, Mousty C, Comninellis C (1998) L'Actualité chimique: 57
15. Wodiunig S, Comninellis C, Mousty C (1997) In: Electrochemistry TESaTISo (ed) The 1997 Joint International Meeting, vol 97-2, Paris
16. Wodiunig S, Comninellis C (1999) Journal of the European Ceramic Society *19*: 931
17. Wodiunig S (2000) Electrochemical Promotion of RuO_2 Catalysts for the Gas Phase Combustion of Ethylene, Ecole Polytechnique Fédérale
18. Foti G, Lavanchy O, Comninellis C (2000) Journal of Applied Electrochemistry 30: 1223
19. Nicole J (1999) Etude de la promotion électrochimique de l'oxydation catalytique de l'éthylène sur des oxydes métalliques, EPFL
20. Jaccoud A (2006) Electrochemical promotion of Pt catalysts for gas phase reaction, EPFL
21. Vayenas CG, Lambert RM, Ladas S, Bebelis S, Neophytides S, Tikhov MS, Filkin NC, Makri M, Tsiplakides D, Cavalca C, Besocke K (1997) In: Xin CLaQ (ed) Spillover and Migration of Surface Species on Catalysts. Elsevier Science B. V.
22. Neophytides S, Tsiplakides D, Vayenas CG (1998) Journal of Catalysis 178: 414
23. Tsiplakides D, Neophytides S, Vayenas CG (2000) Solid State Ionics 136-137: 839
24. Li X, Gaillard F, Vernoux P (2005) Ionics 11: 103
25. Li X, Gaillard F, Vernoux P (2007) Topics in Catalysis 44: 391
26. de Lucas-Consuegra A, Dorado F, Valverde JL, Karoum R, Vernoux P (2007) Journal of Catalysis 251: 474
27. de Lucas-Consuegra A, Dorado F, Jimenez-Borja C, Valverde JL (2008) Applied Catalysis B: Environmental 78: 222

28. de Lucas-Consuegra A, Dorado F, Valverde JL, Karoum R, Vernoux P (2008) Catalysis Communications 9: 17
29. Jaccoud A, Foti G, Comninellis C (2006) Electrochimica Acta 51: 1264
30. Jaccoud A, Falgairette C, Foti G, Comninellis C (2007) Electrochimica Acta 52: 7927
31. Jaccoud A, Foti G, Wuthrich R, Jotterand H, Comninellis C (2007) Topics in Catalysis 44: 409
32. Falgairette C, Jaccoud A, Foti G, Comninellis C (2008) Journal of Applied Electrochemistry 38: 1075

CHAPTER III- EPOC AND P-EPOC FOR C_2H_4 COMBUSTION OVER Pt/YSZ

The catalytic oxidation of C_2H_4 over a Pt/YSZ/Au electrochemical cell was studied under excess of O_2 at 375°C. Both catalytic and electrocatalytic properties of the catalyst were investigated with regard to the EPOC model proposed by *Vayenas*. It turns out that for short term polarization transients, the electrocatalytic cell behaves as expected (*e.g.* reversible as predicted by EPOC theory). On the other hand, long term polarization revealed unexpected relaxation transient behavior highly depending on the polarization time. In these experimental conditions, using both chronopotentiometry and cyclic voltammetry combined with mass spectrometry, it has been found that after current interruption, the catalytic rate remains in a highly active P-EPOC steady state, where it is almost twice as high as the initial open-circuit rate. During this highly active steady state, the application of a similar negative current for a similar time period has been found to result in the return of the catalytic rate to the initial open-circuit state. Similar reversibility of the rate has been observed in cyclic voltammetry experiments where after a complete potential cycle the open-circuit rate is almost the same to that before polarization.

On this basis, a mechanism is proposed for the origin of P-EPOC, based on the storage of promoting species via migration through the three phase boundaries to the metal/gas interface during current application.

III.1 Introduction

As reviewed in previous Chapter, the nature of modification of the catalyst activity (EPOC, P-EPOC or Pers-EPOC phenomenon) observed upon electrochemical polarization is highly depending on the experimental conditions, *e.g.* polarization time, t_H, temperature, T, and oxygen partial pressure, p_{O2}. It turns out that short term polarization leads to the observation of the well known reversible EPOC behaviour, while application of longer t_H conducts to Pers-EPOC at high temperature or to P-EPOC at low temperature. Oxygen rich atmosphere is known to favour not only the efficiency of electrochemical promotion (ρ and Λ) in electrophobic catalytic systems but also its remaining influence after current interruption (γ and Λ_{OS}).

Based on the conclusions of Chapter II, it was decided in this chapter to revisit and generalize the mechanism of electrochemical promotion. For this purpose, one focuses on the permanent electrochemical promotion, P-EPOC, (t_H up to 10 hours) of the ethylene combustion reaction over Pt/YSZ catalyst under oxygen rich atmosphere (p_{O2}/p_{C2H4}=40) and at low temperature (375°C) to avoid any complex Pers-EPOC behavior.

III.2 Experimental setup

The general experimental setup used in this part for both catalytic and electrochemical investigations is depicted in Fig. III-1. The reactant gases used were Carbagas certified standards of 20% O_2/He, 1% C_2H_4/He (99.95% purity) and He (99.996% purity). Mass flow controllers (E-5514-FA, Bronkhorst) were used to control the gas feed composition and to keep the gas flow continuously at 200ml/min to feed the electrochemical reator.

The reactor, already characterized in previous work [1], was an atmospheric single-chamber type quartz tube of 90ml (Fig. III-2). The single-pellet three-electrode cells were suspended in the reactor with the three gold wires serving as electrical contacts to the electrodes. A K-type (NiCr-Ni) thermocouple placed in proximity of the surface of the working electrode was used to measure the temperature of the system. The reactor was put into a furnace (XVA271, Horst) equipped with a heat control system (HT30, Horst).

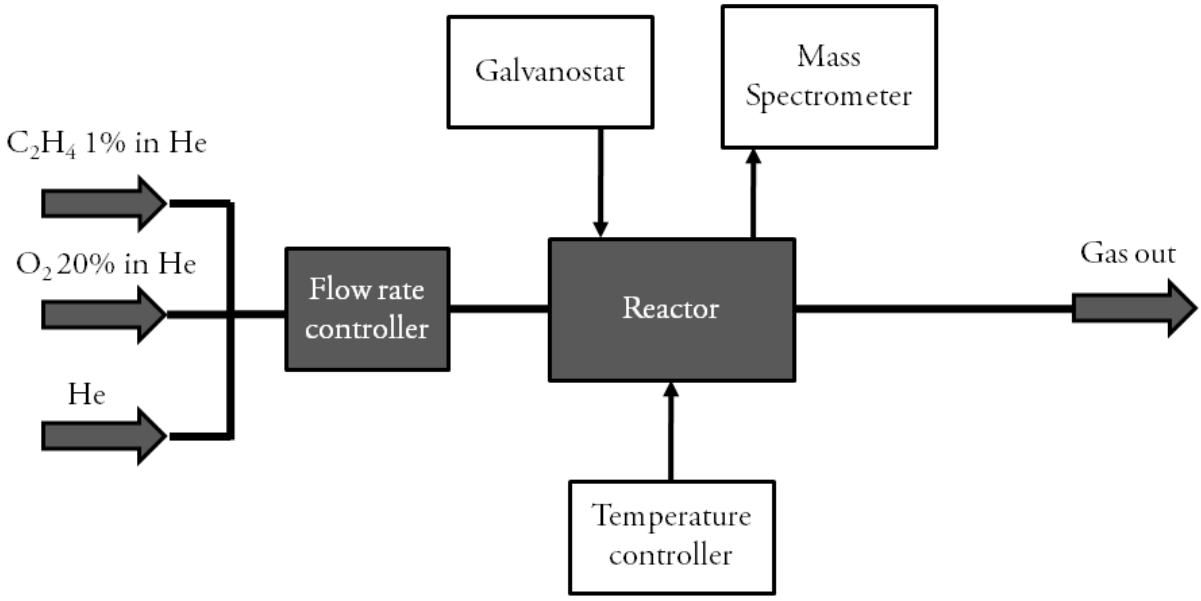

Fig. III-1 : Schematic representation of the general set-up.

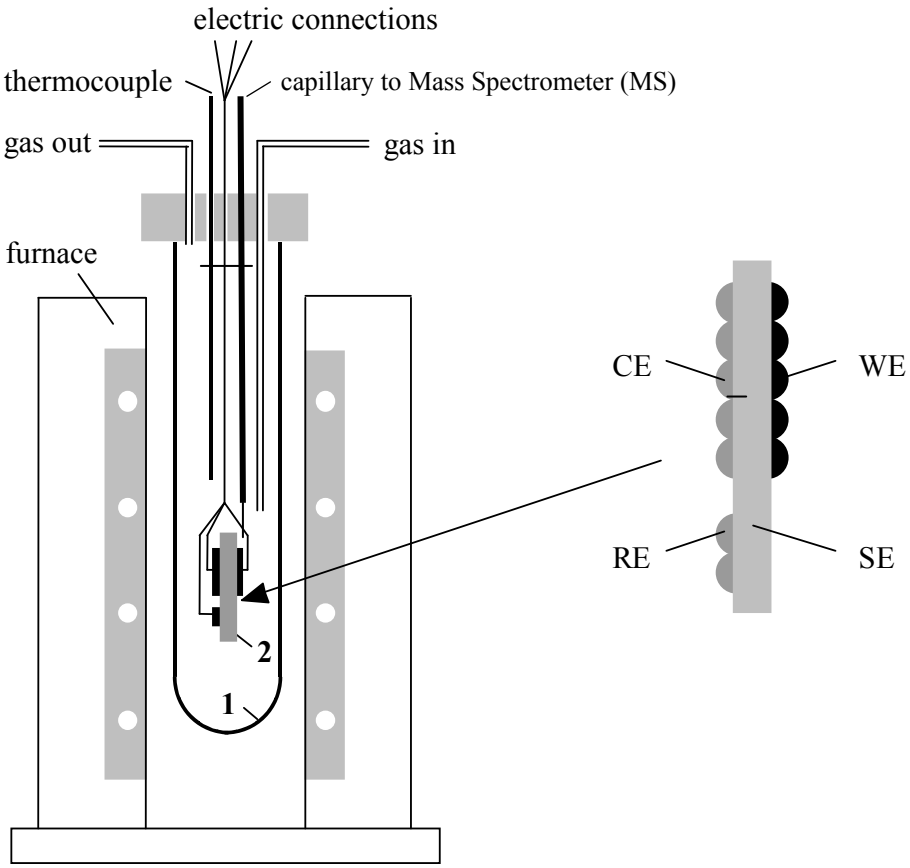

Fig. III-2 : Scheme of the atmospherique reactor. 1: quartz tube; 2: electrochemical cell

A heated capillary tube (120°C), placed in the vicinity of the working electrode, was connected to a mass spectrometer (MS, Prolab-Thermo Onix) allowing on-line monitoring of the gas composition in the reactor.

Electrochemical mass spectrometry (EMS) measurements was used to control the gas composition in the reactor, *i.e.* the reaction products (CO_2 and H_2O) were detected on-line by MS (Prolab-Thermo Onix) during potential sweep using a galvanostat–potentiostat (Autolab, Model PGSTAT30, EcoChemie).

III.2.1 Pt and Au deposition on YSZ

The solid electrochemical cell consisted of a thin (1mm) rectangular YSZ pellet (8mol% Y_2O_3-stabilized ZrO_2 Technox 802, Dynamic Ceramic Ltd) supporting the three electrodes: working, counter and reference. The Pt working electrode (thickness of 1μm) was deposited by magnetron sputtering technique in inert atmosphere (Ar) at room temperature. Direct current (dc) mode was used with a discharge of 330 V at an argon pressure of 10^{-2} mbar, resulting in a metal deposition rate of 0.09 nm s^{-1}. For structure stabilization a calcination pretreatment step at 700°C for 4h in air was performed. Gold counter and reference electrodes were deposited on the other side of the pellet by application of metalorganic paste (Gwent Electronic Materials Ltd. - C70219R4) followed by calcination at 550°C. The influence of the thermal pretreatment on the sputtered Pt film microstructure was already described by *Jaccoud* [2]. The author mentions that the calcinations step leads to sintering of the Pt film forming a percolated network with a macroporous structure at the YSZ surface. In this work the surface characterization of the sputtered Pt film was performed by scanning electron microscopy (SEM) and X-ray diffraction (XRD) and lead to similar observation as *Jaccoud* got. Results are given in the second part of this work (Chapter VII).

The electrodes size is 7 x 5 mm giving a geometric surface of 0.35 cm^2 for each of them. The working and counter electrodes were located in a symmetrical face-to-face arrangement on the opposite sides of the YSZ pellet (Fig. III-3). This ensures a symmetrical current distribution in the cell during the electrochemical investigation [3].

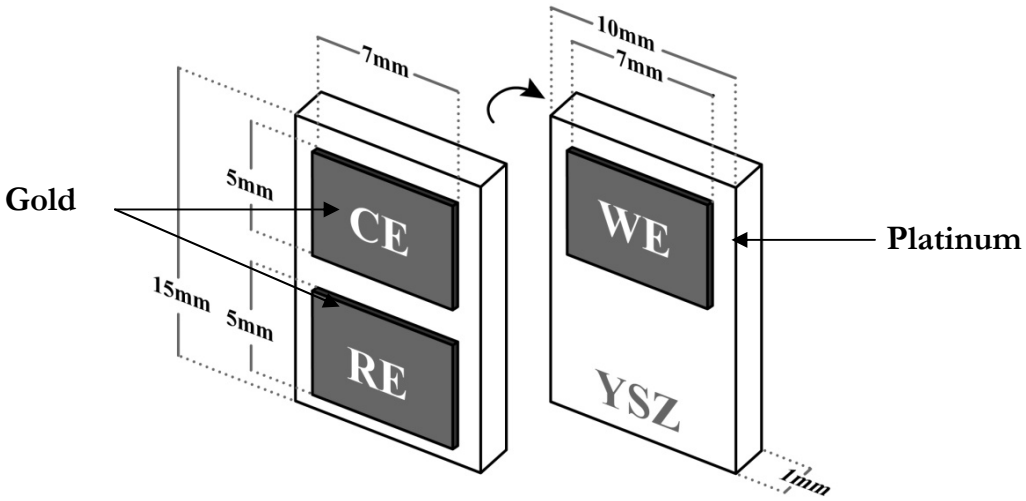

Fig. III-3 : Placement and dimensions of the Pt electrodes prepared by sputtering. WE: Pt working electrode; CE: Au counter electrode; RE: Au reference electrode.

Electrochemical promotion involving the use of a Pt metal supported film as both normal catalyst and working electrode, it is important to distinguish the catalytic and the electrocatalytic properties of the Pt catalyst electrode. This can be performed by estimating the ethylene combustion catalytic active surface area of the Pt/YSZ catalyst, *i.e.* the Pt gas exposed interface $A_{Pt/gas}$ and I_0, the exchange current of the Pt/YSZ interface.

III.2.2 Surface titration of the Pt/YSZ catalyst

The determination of the catalytic active surface area, i.e. Pt/gas interface area $A_{pt/gas}$, is carried out by isothermal titration technique as described by *Vayenas* [4]. This experiment was performed at 375°C under a constant gas flow of 200ml/min in the previously described reactor as follows:

- The reactor is first purged with pure He during 20 minutes.
- The catalyst surface is then exposed for 5 minutes to 20% O_2 in He in order to reach an oxygen coverage near to saturation at the Pt/YSZ catalyst surface.
- The reactor is then purged with pure He for different desorption time t_d.
- The catalyst is then immediately exposed to a 1% C_2H_4 in He flow in order to chemically titrate the remaining oxygen adsorbed at the catalyst surface.

$$3O_{2(g)} + C_2H_4 \rightarrow 2CO_2 + 2H_2O \qquad \text{III-1}$$

- The catalytic rate of CO_2 formation is monitored with a mass spectrometer (Fig. III-4) and integration of the obtained peak allows the determination of the amount of adsorbed oxygen N_O after desorption time t_D.

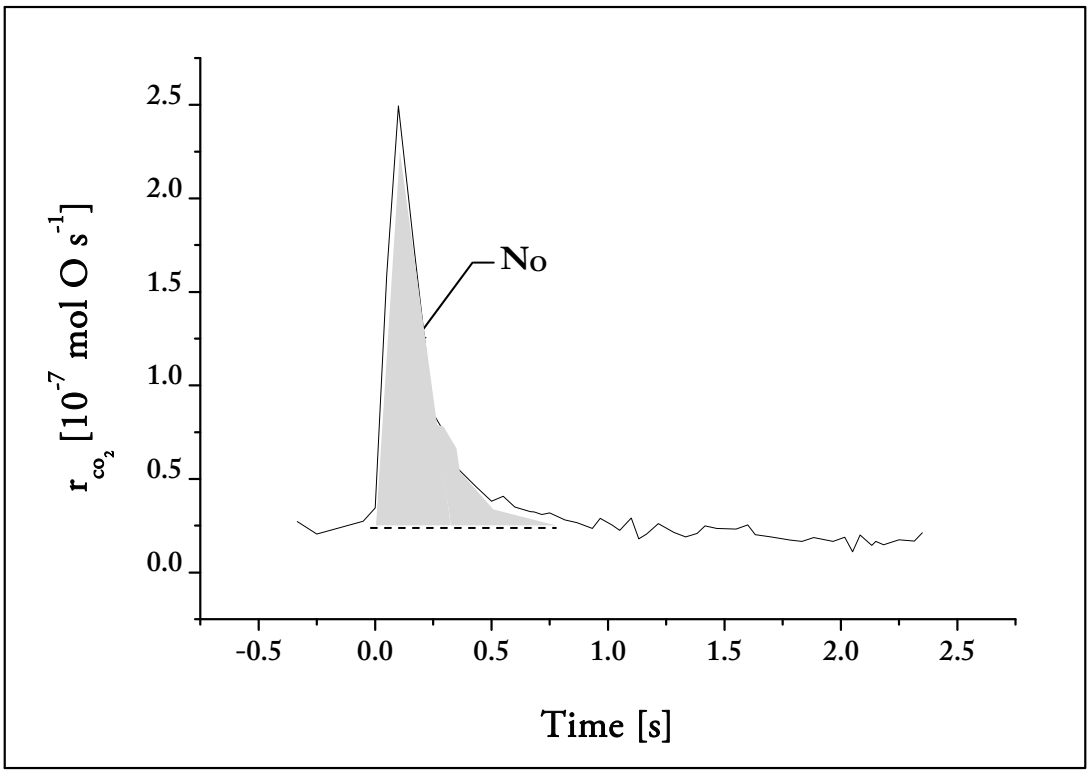

Fig. III-4 : Determination of N_O by integration of the CO_2 formation transient monitored by MS during the C_2H_4 titration step at 375°C.

The y-intercept obtained by plotting the amount of oxygen adsorbed at the catalyst surface, N_O, versus the desorption time, t_D, represents the number of active sites at the catalyst surface $N_{Pt/gas}$. The number of active sites at the Pt film investigated herein is then estimated to be 109 nmol (Fig. III-5).

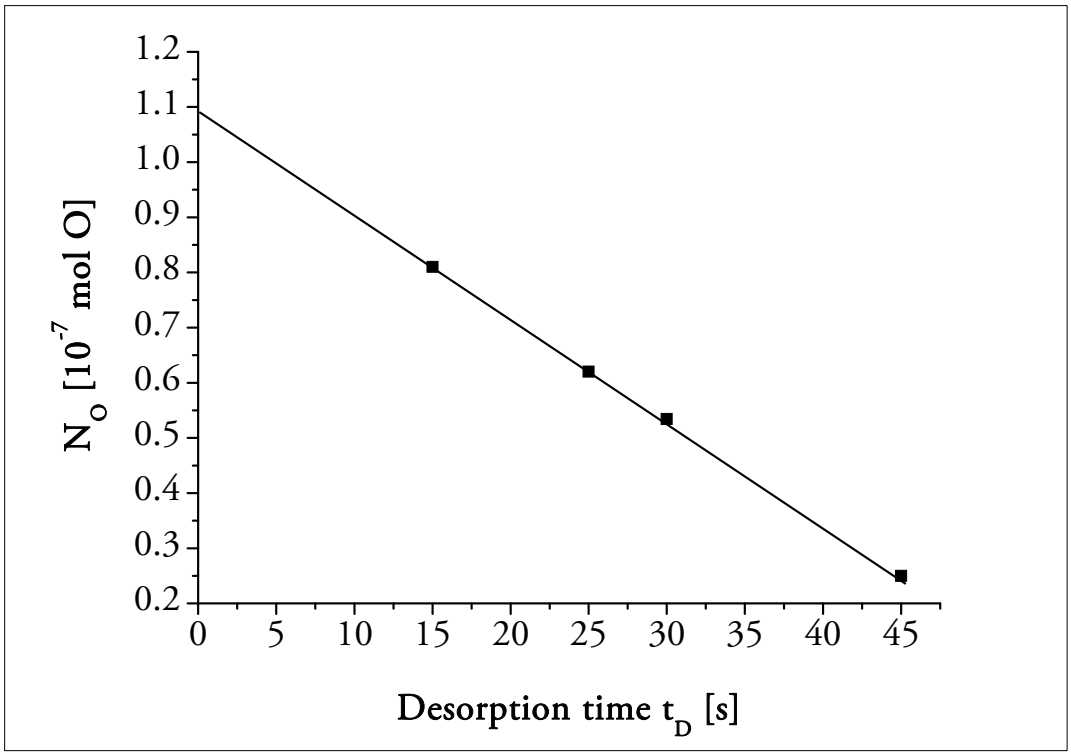

Fig. III-5 : Determination of $N_{Pt/gas}$ by plotting N_O as a function of desorption time t_D at 375°C.

III.2.3 Exchange current of the Pt/YSZ catalyst

The overall electrocatalytic activity of the O_2/O^{2-} redox system in the reaction medium may be estimated by the measure of the exchange current I_0. In case of a multistep process, the overall kinetic will be dictated by the rate limiting step (rds) and the Buttler Volmer equation, describing the current-potential characteristic (equation III-2):

$$I = I_0 \left[e^{\frac{\alpha_a F}{RT}\eta_{act}} - e^{-\frac{\alpha_c F}{RT}\eta_{act}} \right] \qquad \text{III-2}$$

where α_a and α_c are the anodic and cathodic transfer coefficient, η_{act} is the activation potential of the working catalyst electrode, R is the ideal gas constant (8.32 J.mol^{-1}.K^{-1}), F the Faraday constant (96500 C.mol^{-1}) and T the temperature.

Considering the high field approximation (η_{act}>100mV), the Buttler-Volmer equation is reduced to equation III-3 :

$$\ln I = \ln I_0 + \alpha_a \frac{F}{RT}\eta_{act} \qquad \text{III-3}$$

The exchange current, I_0, for the Pt/YSZ/Au electrocatalytical cell is then determined in different ethylene/oxygen gas mixtures from a Tafel plot (Fig. III-6).

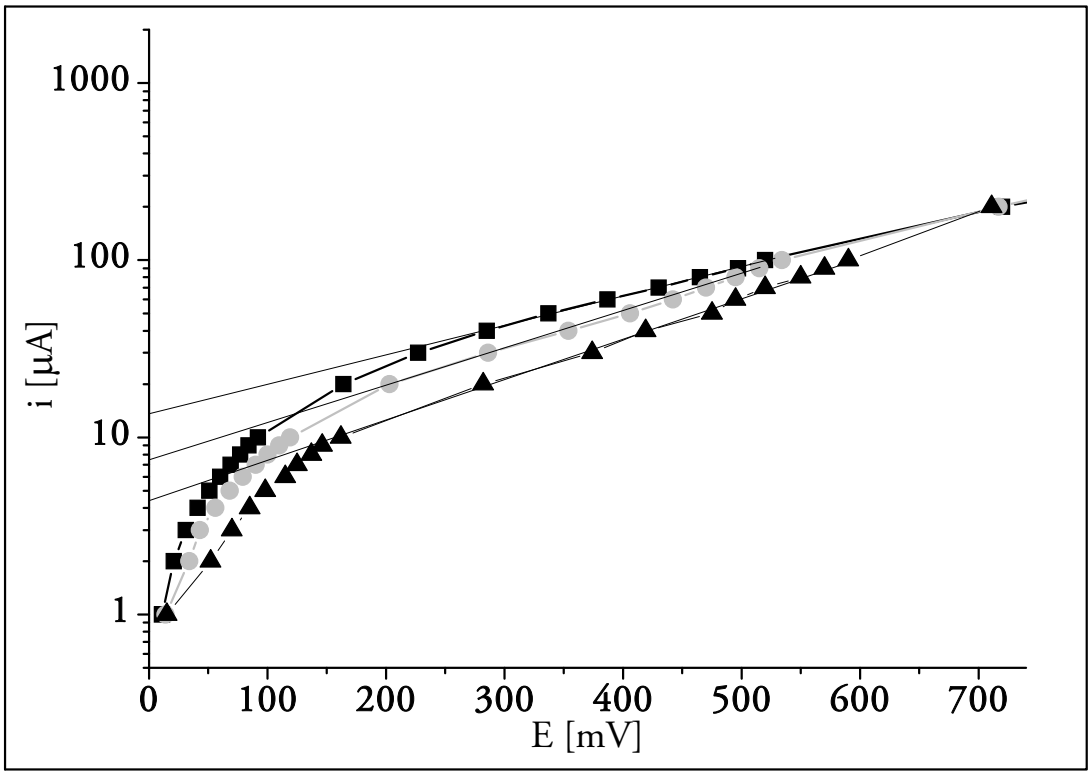

Fig. III-6 : Determination of I_0 by plotting Tafel plot measured for 2 different oxygen partial pressure P_{O2}=8.2kPa (▲), P_{O2}=2kPa (●), P_{O2}=1kPa (■). P_{C2H4}=0.2 kPa T=375°C

Oxygen partial pressure [kPa]	Exchange current [μA]
1 kPa	13.4 μA
2 kPa	7.2 μA
8.2 kPa	4.1 μA

Table III-1 : The exchange current i_0 in the Pt/YSZ/Au cell as a function of oxygen partial pressure P_{O2}, P_{C2H4}=0.2 kPa T=375°C

As expected the exchange current is observed to be dependant of the surrounding gas composition. This gas composition dependence has been subject to many studies and was related to the oxygen coverage at the catalyst surface by *Vayenas* [5] who proposed, by

considering a Langmuir-type adsorption of oxygen, the following relationship between the exchange current and the oxygen coverage θ_O :

$$I_0 \sim \left[\theta_O \left(1-\theta_O\right)\right]^{1/2} \qquad \textbf{III-4}$$

or in terms of oxygen partial pressure p_{O2} :

$$I_0 \sim \frac{K_0 p_{O_2}^{1/4}}{\left(1+K_0 p_{O_2}\right)^{1/2}} \qquad \textbf{III-5}$$

As C_2H_4 is added to the gas mixture, I_0 is modified in two ways :

- θ_O is directly affected by the C_2H_4 coadsorption, θ_{C2H4}, at the catalyst surface
- C_2H_4 molecule of the gas phase may react with the electrochemically produced O^{2-} promoter at the catalyst surface.

Worth to notice that this implies that I_0 represents an important parameter in the EPOC theory. Actually, *Vayenas* observed experimentally that the faradaic enhancement factor, Λ, is commonly related to I_0 according to equation III-6 [4]:

$$\left|\Lambda\right| \approx \frac{2Fr_0}{I_0} \qquad \textbf{III-6}$$

Hence, to obtain high Λ values, the electrode catalyst should present a low I_0 value, *i.e.* the interface must be highly polarizable. The magnitude of I_0 being proportional to the tpb length, the morphology of the Pt film should have a dramatic influence on its electrochemical behavior.

III.3 Results and discussion

III.3.1 Open circuit ethylene combustion over Pt/YSZ catalyst

The combustion of ethylene over Pt/YSZ catalyst is reported to take place above 280°C according to the following global reaction :

$$3O_{2(g)} + C_2H_{4(g)} \rightarrow 2CO_{2(g)} + 2H_2O_{(g)} \qquad \text{III-7}$$

Fig. III-7 displays the influence of the gas composition on the catalatic rate of reaction III-7, the experiment is performed at 375°C under constant flow rate of 200mL/min. Two approaches are proposed, the variation of ethylene partial pressure at fixed oxygen partial pressure and the variation of oxygen partial pressure at fixed ethylene partial pressure.

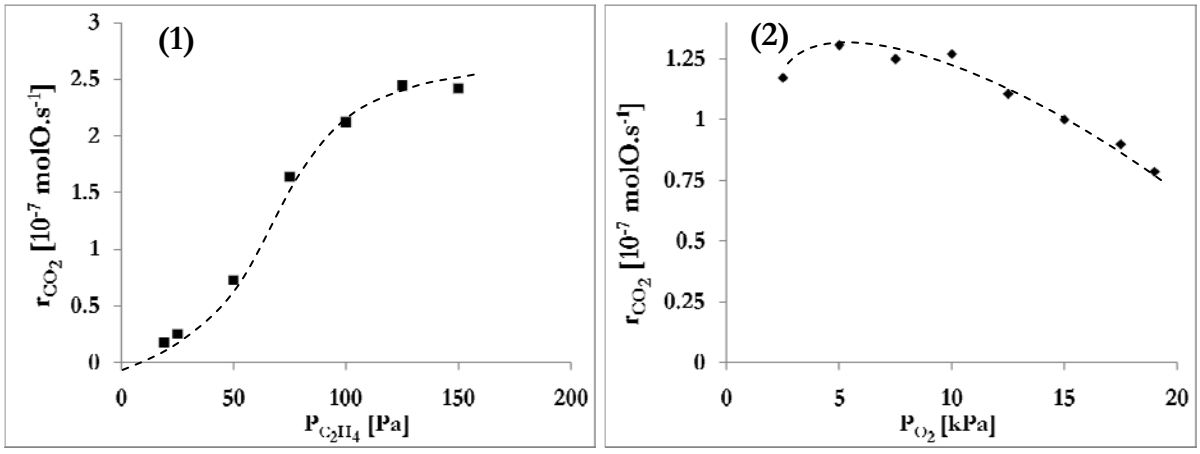

Fig. III-7 : Catalytic reation rate of CO_2 production as a function of gas composition. (1) dependence on ethylene partial pressure at P_{O2}=10kPa, (2) dependence on oxygen partial pressure at P_{C2H4}=50Pa, T=375°C

Worth is to notice that $p_{O2} >> p_{C2H4}$ in both cases. Under these conditions, the reaction rate is of positive order with respect to ethylene and negative order with respect to oxygen. Pt/YSZ/Au presents the expected electrophobic behavior for C_2H_4 combustion reaction, *i.e.* oxygen is strongly adsorbed at the catalyst surface while ethylene is weakly chemisorbed.

The rate of CO_2 formation in terms of equivalent O mol.s^{-1} may also be given as a function of the ratio p_{O2}/p_{C2H4} (Fig. III-8). Two different regimes are observed depending on the oxidative/reductive properties of the gas mixture.

- For p_{C2H4}/p_{O2}, <5.10^{-3} the surrounding gas mixture is oxygen rich such as PtO is favored at the platinum surface. In this case, ethylene combustion may be approximated to a pseudo first order reaction in ethylene.

- On the other hand, for p_{C2H4}/p_{O2}>0.02, the oxygen amount in the gas mixture is low, stabilizing the metallic form of platinum. In this case, ethylene combustion may be approximated to a pseudo first order reaction in oxygen.

- A transition domain, corresponding to a transition state of Pt/PtO, is observed for 5.10^{-3}<p_{C2H4}/p_{O2} <0.02. In this region both form, *i.e.* Pt and PtO, are expected to be present at the same time at the catalyst surface, however, this region is dramatically affected by the initial (reductive/oxidative) composition of the gas mixture.

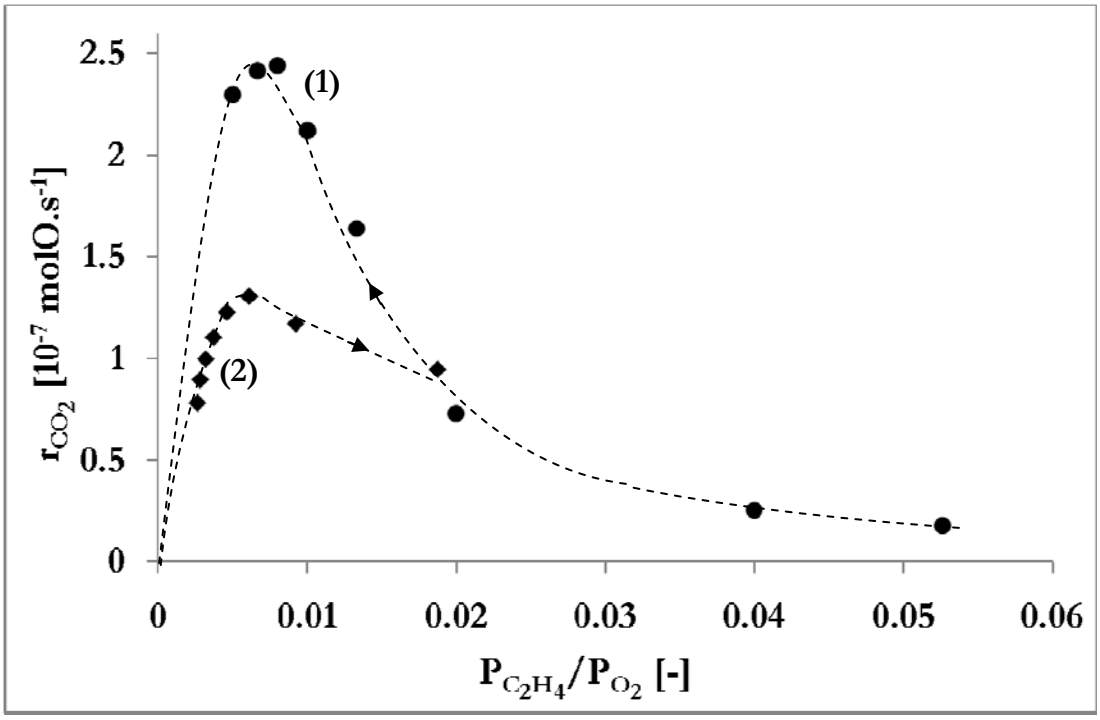

Fig. III-8 : Catalytic reation rate of CO_2 production as a function of p_{C2H4}/p_{O2}. From (1) and (2) data of Fig. III-7. T=375°C

These experimental observations may be interpreted quantitatively by the following kinetic scheme [4] :

$$\frac{1}{2}\left\{\begin{matrix} O_{2(g)} \rightarrow O_{2(a)} \\ O_{2(a)} \rightarrow 2O_{(a)} \end{matrix}\right\} \qquad \textbf{III-8}$$

$$C_2H_{4(g)} + O_{(a)} \rightarrow P + \frac{5}{2}O_{2(g)} \rightarrow 2CO_2 + 2H_2O \qquad \textbf{III-9}$$

Where $O_{(a)}$ is a molecular adsorbed oxygen adsorbed and P is a highly reactive intermediate.

The rates of both step may be written respectively as :

$$r = k_{ad} P_{O_2} \left(1 - \theta_O\right) \qquad \textbf{III-10}$$

$$r = k\ P_{C_2H_4} \theta_O \qquad \textbf{III-11}$$

Where k_{ad} is the oxygen adsorption rate constant, k is the rate constant of formation of the reactive intermediate P and θ_O is the molecular oxygen coverage at the catalyst surface.

Assuming a Langmuir isotherm for atomic oxygen chemisorption one may express the oxygen coverage as

$$\theta_O = \frac{1}{1 + \frac{k p_{C_2H_4}}{k_{ad}\, p_{O_2}}} \qquad \textbf{III-12}$$

And the whole mechanism may then be described by the following equation :

$$r = \frac{k\ k_{ad} P_{O_2} P_{C_2H_4}}{k\ P_{C_2H_4} + k_{ad} P_{O_2}} \qquad \textbf{III-13}$$

Then on the oxygen rich side ($k_{ad}p_{O2} >> kp_{C2H4}$), the oxygen coverage at platinum surface is near unity and step III-9 is the rate determining step of the mechanism. The equation of the reaction rate may be reduced to a pseudo first order :

$$r_0 = k\ P_{C_2H_4} \qquad \textbf{III-14}$$

On the other extreme condition, *i.e.* oxygen lean side ($k_{ad}p_{O2} << k_p p_{C2H4}$), oxygen adsorption step is the rate determining step, oxygen coverage is close to zero and the reaction rate of the ethylene combustion may be reduced to :

$$r_0 = k_{ads} P_{O_2} \qquad \text{III-15}$$

III.3.2 EPOC and P-EPOC on the Pt/YSZ/Au system

III.3.2.1 Influence of the gas composition

A typical catalytic reaction rate transient obtained at 375°C for ethylene combustion over Pt/YSZ/Au cell during a short galvanostatic polarization step (5min) is reported in Fig. III-9. Initially, *i.e.* at open circuit conditions, the catalytic ethylene combustion over Pt takes place at the unpromoted catalytic reaction rate, r_0 = 300 nmolO s^{-1}.

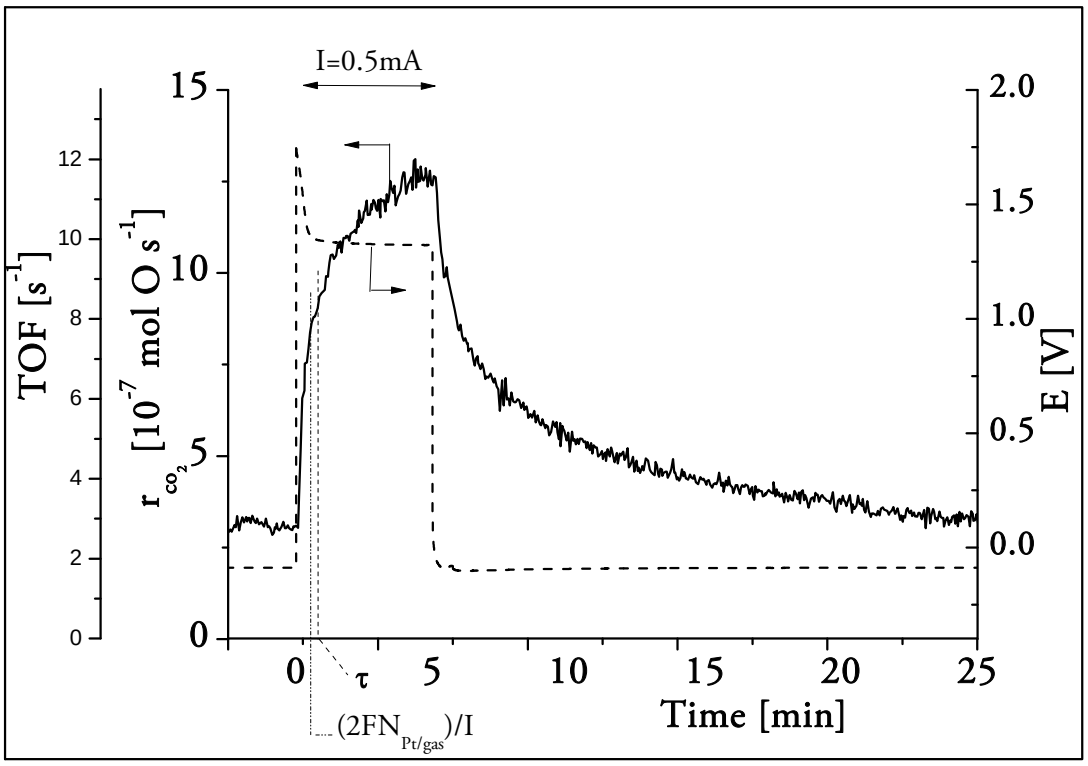

Fig. III-9 : Transient effect of a constant applied anodic current on the CO_2 formation catalytic rate (left) and on the working (Pt) - reference (Au) potential difference (right). P_{O2}=8.2kPa. P_{C2H4}=0.2 kPa T=375°C

Considering the number of reactive sites at Pt/gas interface, $N_{Pt/gas}$, previously determined (section III.2.2), the corresponding open circuit turnover frequency can be calculated using equation III-16*:*

$$TOF_0 = \frac{r_0}{N_{Pt/gas}} = 2.7s^{-1} \qquad \textbf{III-16}$$

Considering the previously mentioned relationship between Λ and I_0 (equation III-6), the faradaic efficiency factor of this reaction is expected to be of the order of magnitude of $2Fr_0/I_0$, *i.e.* 14000.

At t = 0, a constant anodic galvanostatic polarization of 0.5mA is applied between the Pt working electrode and the gold counter electrode, this corresponds to a faradaic supply of O^{2-} ions to the Pt catalyst from the YSZ electrolyte at $r_F=I/2F$. As a consequence, the catalytic rate, r, increases rapidly within the first seconds, and then more slowly to a new steady state promoted value, r_p=1260 nmolO.s^{-1}, which is 4.2 times higher than r_0. This catalytic rate increase, $\Delta r=r_p - r_0$, is 370 times larger than the faradaic rate of O^{2-} supply, *i.e.* r_F, highlighting the non faradaic character of the electrochemical promotion. One may notice the deviation of 2 orders of magnitude for the actual value of Λ to the value predicted from the experimental relation between r_0 and I_0. However, a new promoted value of TOF_p, *i.e.* under anodic polarization, is estimated according to equation III-17:

$$TOF_p = \frac{r_p}{N_{Pt/gas}} \qquad \textbf{III-17}$$

Fig. III-10 displays the influence of the gas mixture composition on the electrochemical promotion observed at 375°C. Three different ratio of p_{O2}/p_{C2H4} are given, the general EPOC phenomenon previously described (consisting of the dramatic catalytic rate increase with concomitant potential increase) was observed in each case directly after the application of a constant anodic current (0.5mA).

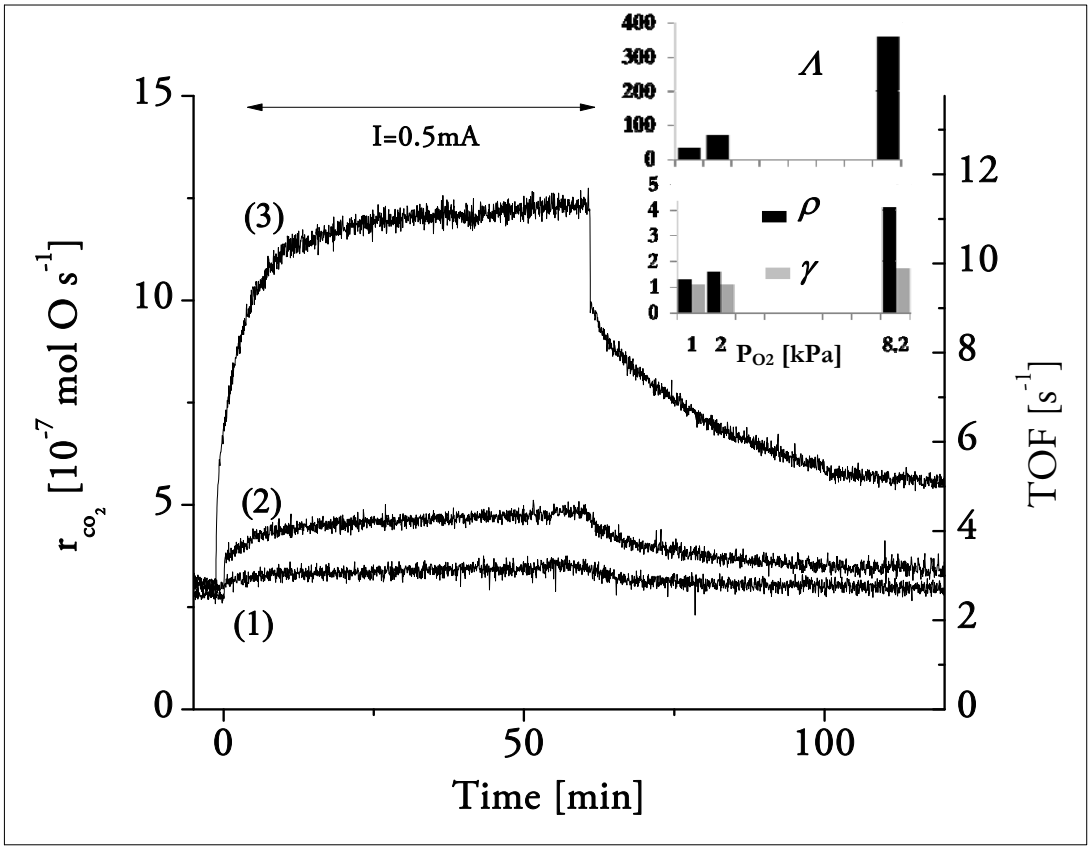

Fig. III-10 : Reaction rate transients during application of a constant anodic current on the CO_2 formation catalytic rate (left) and on the turnover frequency (right) for 3 different oxygen partial pressures P_{O2} . (1)P_{O2}=1kP , (2)P_{O2}=2kPa and (3)P_{O2}=8.2kPa. P_{C2H4}=0.2 kPa T=375°C

The estimation of the EPOC parameters (Table III-2) showed that decreasing the oxygen partial pressure in the gas mixture strongly decreses both ρ and Λ values. Similarly, *Bebelis* reported a strong influence of the gas composition on both ρ and Λ values for ethylene oxidation over Pt/YSZ catalyst [6, 7].

P_{O2}	1 kPa	2 kPa	8.2 kPa
TOF_0	$2.5s^{-1}$	$2.6s^{-1}$	$2.7s^{-1}$
TOF_p	$2.8s^{-1}$	$4.3s^{-1}$	$11.5s^{-1}$
ρ	1.3	1.6	4.2
Λ	31	70	370

Table III-2 : Experimental EPOC parameters as a function of P_{O2}. Conditions as in Fig. III-10.

According to *Vayenas* [4], upon current interruption, the flow of the electrogenerated promoter O^{2-} supplied from the tpb to the gas exposed Pt catalyst stops and the catalytic reaction rate returns slowly to its initial unpromoted value because of the gradual consumption by C_2H_4 (or desorption) of the promoters from the Pt/gas interface. Considering the value of TOF_p for the electrochemically promoted reaction ($11.5s^{-1}$) and the obtained Λ value (370) one can estimate the average life time (τ_D) of the promoter upon current interruption from the relation

$$\tau = \frac{\Lambda}{TOF_p} = 32s \qquad \text{III-18}$$

One should then expect that after about 32s, the catalytic activity of the system would have return to its initial state. Experimentally (Fig. III-9), even if a dramatic drop of catalytic reaction rate is initially observed upon current interruption, the relaxation time needed for the catalyst to return to its initial catalytic activity is more than one order of magnitude longer (>1200 s).

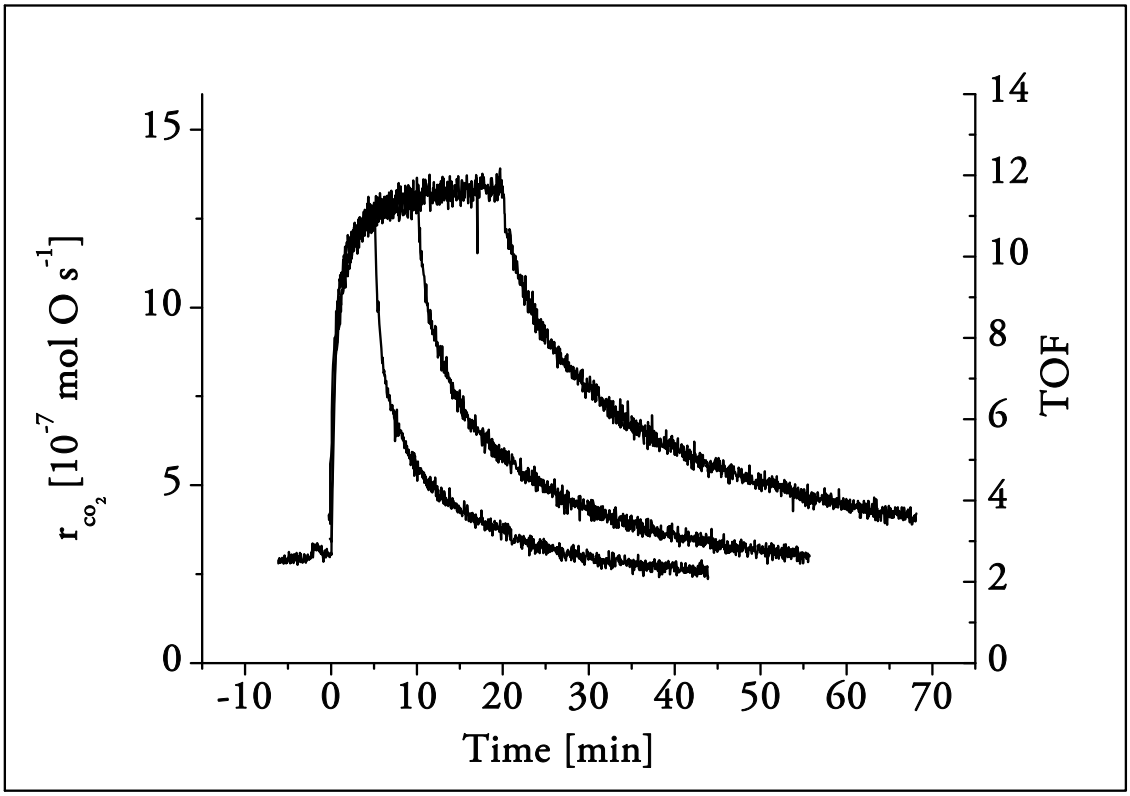

Fig. III-11 : Open circuit relaxation transients obtained by increasing the duration of a constant applied anodic current on the CO_2 formation catalytic rate (left) and on the corresponding turnover frequency (right). P_{O2}=8.2kPa. P_{C2H4}=0.2 kPa T=375°C

In addition, the increase of the polarization time, t_H, leads to even slower relaxation transients (Fig. III-11). In fact, increasing the polarization time, slows down the relaxation rate upon current interruption reaching a new steady state, *r'*, where the catalytic rate is higher than the initial unpromoted catalytic rate, r_0. The ratio *r'* to *r* is defined as the permanent enhancement factor γ (equation II-7)

Furthermore, the increase of p_{O2} has a dramatic impact not only on EPOC (Table III-2) but also on P-EPOC (Fig. III-10). In fact under less oxidizing atmosphere, the phenonomenon of electrochemical promotion seems to be reversible, *i.e.* returns rapidly to its initial catalytic activity upon current interruption, contrary to more strongly oxidizing atmosphere where a remaining promoted activity slowly decreases without reaching its initial catalytic state even after two anodic polarization time periods, *i.e.* herein after 120 minutes (P-EPOC).

III.3.2.2 Influence of polarization time on γ values

Fig. III-12 shows the transient effect of a constant applied anodic current of +0.5 mA for 170 min, on the catalytic rate of CO_2 formation, r_{CO2} (equation III-9), expressed as consumed mol O and on the working (Pt) - reference (Au) potential difference (U_{WR}) at 375°C.

Initially, under open-circuit conditions r_0 = 300 nmolO.s^{-1}, while positive current application causes a 4.2-fold increase of the catalytic rate, *i.e.* ρ = 4.2, reaching 1260 nmolO.s^{-1}. The Faradaic efficiency, Λ, equals 370 indicating a non-Faradaic process. Worth to note is the fact that even after 170 min of anodic polarization the system is not at steady-state, but the catalytic rate increases slowly.

After current interruption, the catalytic rate decreases until it is stabilized at a new steady-state, called P-EPOC steady-state, where the catalytic activity is higher than that in the initial open-circuit state. After an anodic current application for 170 min γ equals 1.7, since in the P-EPOC state CO_2 formation rate is 70% higher than r_o.

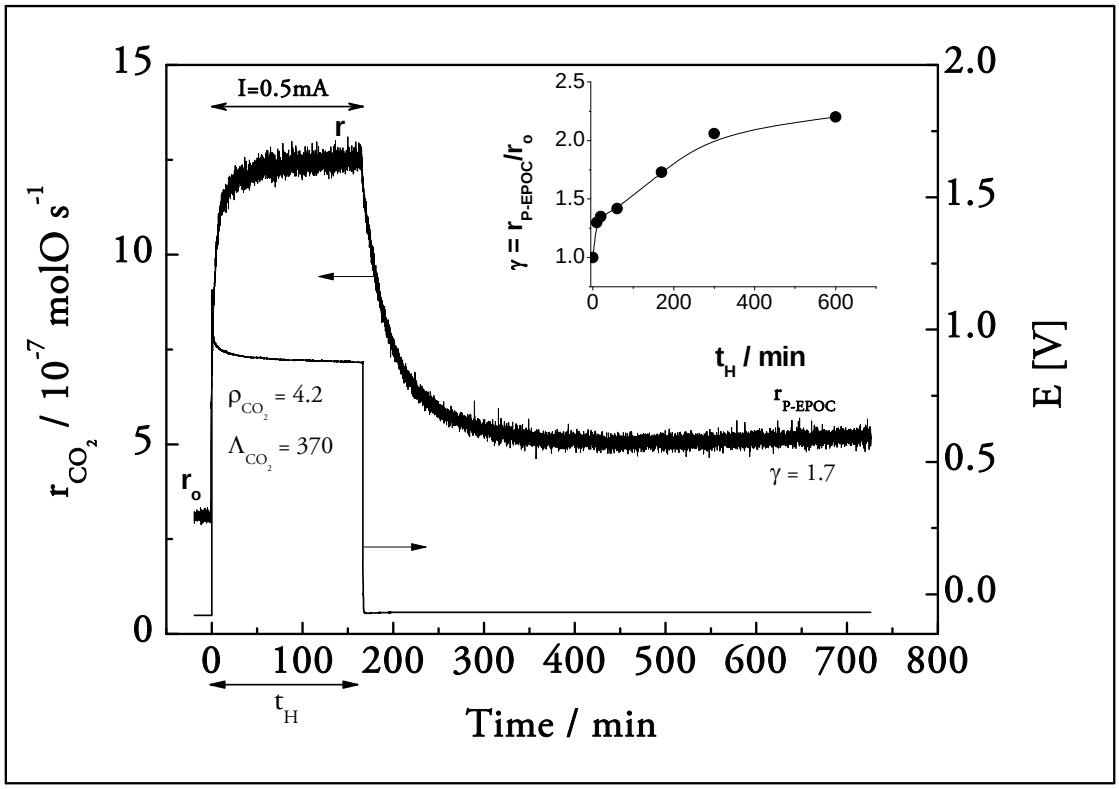

Fig. III-12 : Transient effect of a constant applied anodic current on the CO_2 formation catalytic rate (left) and on the working (Pt) - reference (Au) potential difference (right). P_{O2}=8.2kPa. P_{C2H4}=0.2 kPa T=375°C

The effect of anodic current application time, t_H, on the "permanent" rate enhancement ratio, γ, is shown in the insert in Fig. III-12. As shown, γ increases by t_H toward a plateau in agreement with previous studies using IrO_2 [8-11].

III.3.2.3 Influence of cathodic polarization on the P-EPOC state

Fig. III-13 a) shows the effect of four constant negative current application steps of 0.1mA for 4 min each, on the CO_2 formation rate after current interruption. As shown, negative polarization causes a decrease in the CO_2 formation rate; while by interruption of the negative current the catalytic rate increases again up to a state of lower activity than that of the free relaxation case which leads to P-EPOC (shown in Fig. III-12). The application of successive negative current steps leads to the gradual shift from the P-EPOC steady-state towards the initial open-circuit state in a period of shorter time.

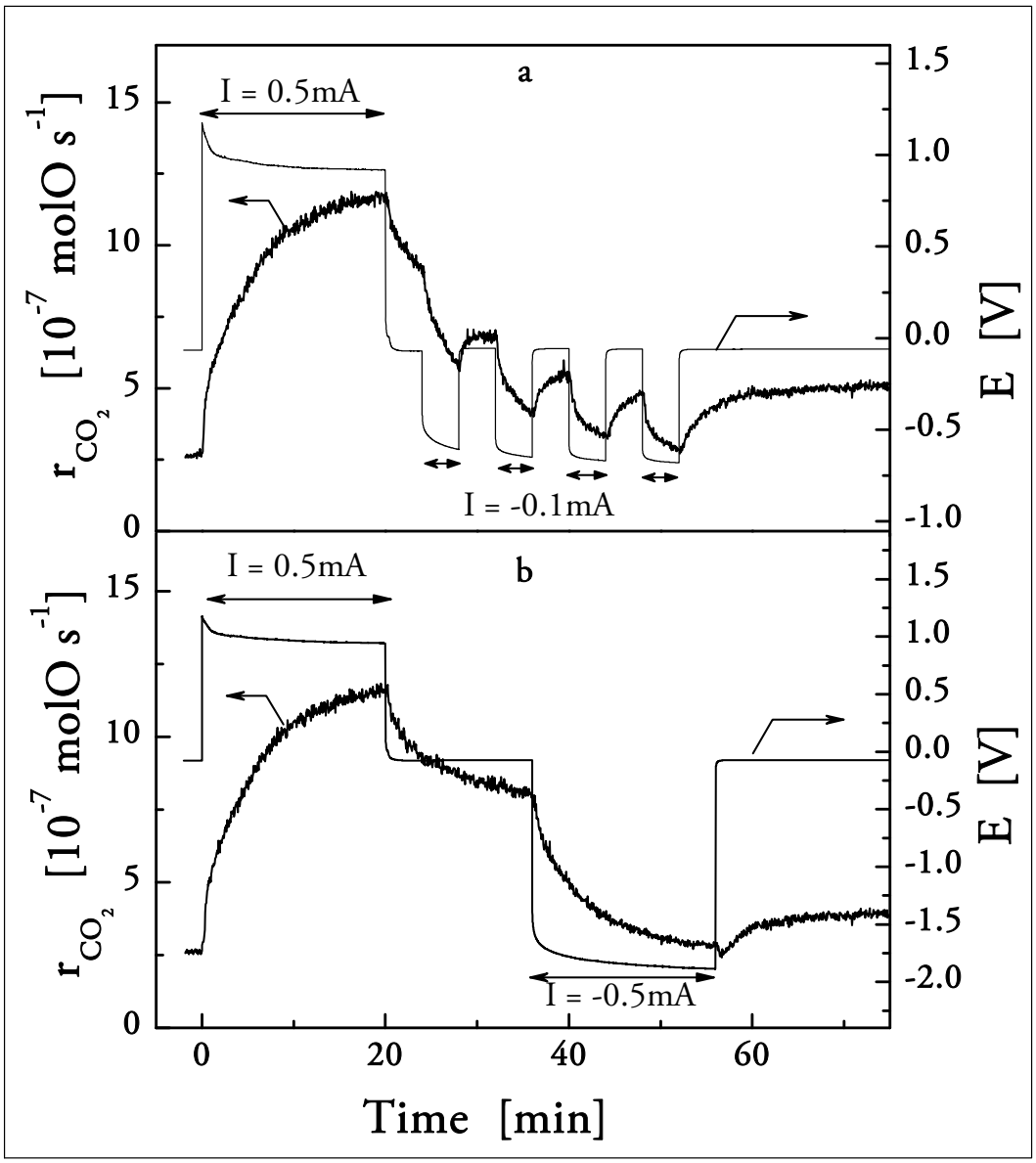

Fig. III-13 : Transient effect of cathodic current application during depolarization on the CO_2 formation catalytic rate (left) and on the working-reference potential difference (right). P_{O2}=8.2kPa. P_{C2H4}=0.2 kPa T=375°C.

Also, worth to note is that the charge supplied during each step of negative current application is 4% of that supplied during the positive current application, thus a complete return of the rate to the initial state could be obtained after about 25 steps considering the same current efficiency for both charge storage (upon anodic current application) and charge release (upon cathodic current application).

The effect of negative current application, of similar charge to that applied during the preceding positive polarization, on the catalytic rate after current interruption is shown in

Fig. III-13 b). Negative current application has a significant decreasing effect on the catalytic rate. Moreover, after negative current interruption the reaction rate increases and is stabilized in a steady-state much lower than that obtained in Fig. III-13 a) and close to the initial. This indicates the direct correlation between the charge stored during positive polarization and the P-EPOC steady-state. Negative polarization serves as a fast and efficient way for the release of the stored charge.

III.3.2.4 Transient behavior upon linear potential sweep.

Fig. III-14 shows the transient effect of linear potential sweep on the faradaic rate of O^{2-} transport, $I/2F$, on the CO_2 and H_2O formation rates and on the rate enhancement ratio for the CO_2 production, ρ_{CO2}, obtained by EMS using a sweep rate of 1 mV s^{-1}. As shown, linear increase of the potential from 0 V to anodic maximum potential (+1 V) results in increase of the catalytic rates.

During the reverse potential sweep from +1 to 0 V, a hysteresis on the CO_2 and H_2O formation rate was observed. At 0V r_{CO2} is 760 nmolO s^{-1}, 260% higher than the initial open-circuit rate. Similar experiments under faster sweep rates revealed that when slow sweep rates (< 5 mV s^{-1}) are used, any possible delay between the potential application and the MS measurement can be neglected. Also, from previous catalytic studies [1] it has been found that the used hourly space velocity (HSV=133 h^{-1}) is high enough to avoid any accumulation – mass transport limitations phenomena in the reactor. Accounting for the above, it can be concluded that the hysteresis presented here is not due to EMS delay, but due to both the inexistence of a stable electropromoted steady-state (as mentioned in Fig. III-12, rate increases slowly) and to the remain of the system in a more activated P-EPOC steady state after current interruption. Similar behavior has been detected for the H_2O formation rate. On the other hand, negative polarization causes a decrease in the catalytic rate, in agreement with previous EPOC studies [4]. Additionally, almost no permanent state was observed at the end of the cathodic sweep. This is attributed to the fact that during the negative potential scan any promoting species stored during positive polarization are pumped back to the electrolyte.

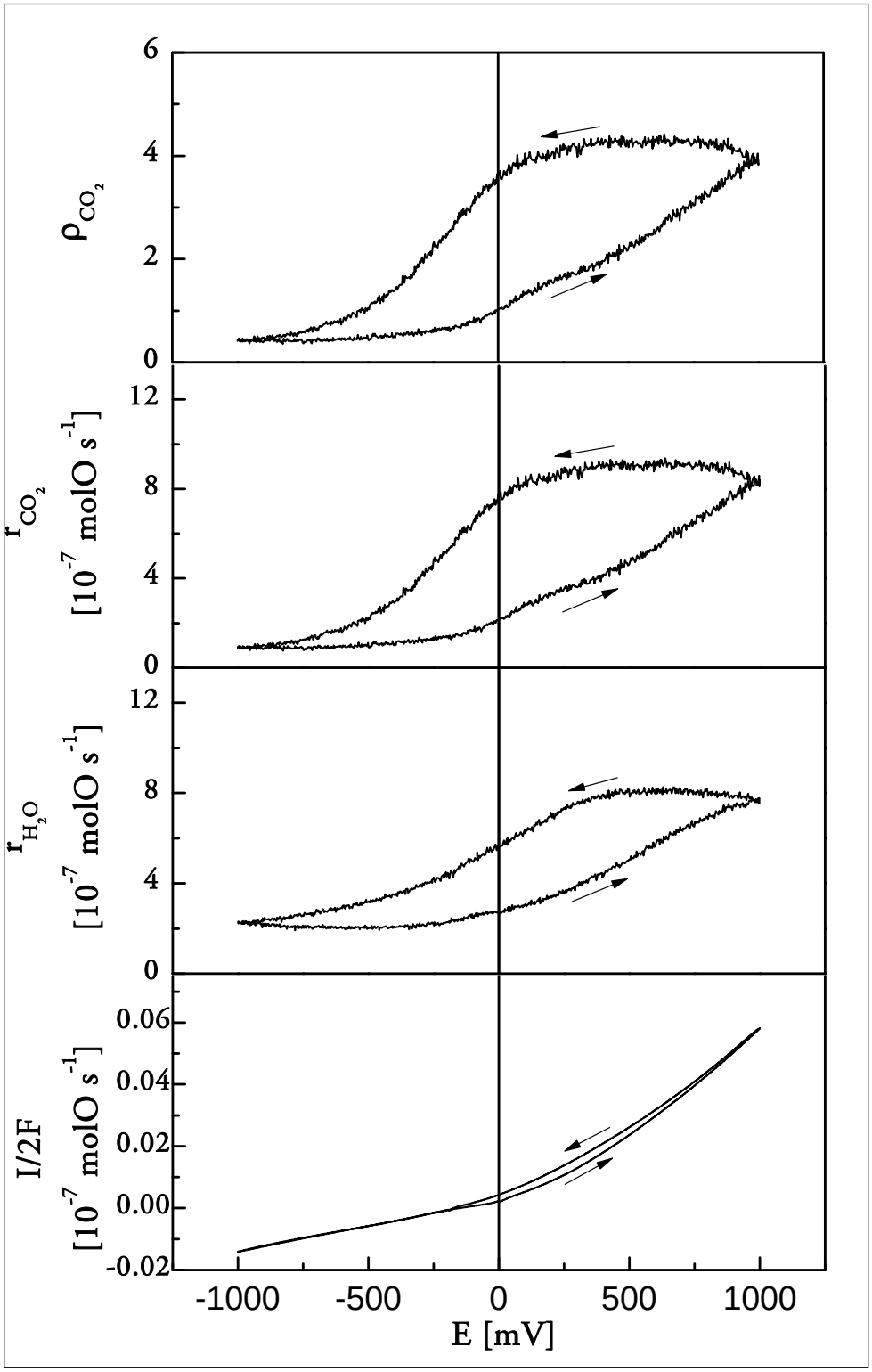

Fig. III-14 : Effect of linear potential sweep on the simultaneously recorded faradaic rate of O^{2-} transport, CO_2 and H_2O formation rates and rate enhancement ratio of CO_2 production, ρ_{CO2}. υ=1mV.s^{-1}, P_{O2}=8.2kPa. P_{C2H4}=0.2 kPa T=375°C

III.3.3 General discussion

The ethylene combustion reaction over Pt/YSZ/Au catalyst has been studied under both open circuit (classical catalysis) and closed circuit conditions for both short (EPOC) and long (P-EPOC) anodic polarization times at 375°C.

The first characterization of the sample by isothermal titration method allowed the determination of the gas exposed active surface area of the catalyst $N_{Pt/gas}$. Investigation of the classical catalytic reaction of ethylene combustion was then performed by varying the gas mixture composition (Fig. III-8). The results revealed an electrophobic catalytic behaviour of the system in agreement with the kinetic mechanism reported in literature (equation III-13):

The electrochemical promotion of ethylene combustion has been studied by applying anodic polarization step to the working Pt catalyst electrode in different gas mixture compositions (Fig. III-10). It turns out that a high oxygen partial pressure in the gas mixture is favourable to both EPOC and P-EPOC phenomenon. Under these oxidizing conditions, the kinetics of the ethylene combustion is reduced to a pseudo first order reaction with respect to ethylene and the Pt/YSZ catalyst exhibited strong electrophobic EPOC behaviour (Fig. III-9), in good agreement with the sacrificial promoter mechanism of electrochemical promotion [4]. According to this mechanism, anodic polarization produces oxygen promoters via (presumably partial) discharge of O^{2-} arriving from the solid electrolyte (equation III-19).

$$Pt + O^{2-}_{YSZ} \rightarrow Pt - O^{\delta-}_{ads} + (2-\delta)e^{-} \qquad \textbf{III-19}$$

The resulting $O^{\delta-}$ promoters migrate with their mirror charge through the triple phase boundary and progressively cover the catalyst/gas interface. They increase the work function of the metal and consequently weaken the Pt–O bond of chemisorbed oxygen atoms, which leads to an increase of the catalytic activity. As postulated in the state-of-the-art sacrificial promoter model of EPOC, the electrochemically produced backspillover species are consumed both by reaction with the reactant (ethylene) and by desorption.

When balance between electrochemical production and consumption is reached, the electropromoted rate of the catalytic reaction (ethylene oxidation in the present case) reaches a steady-state and it remains constant during the whole polarization period, meaning that no more alteration of the catalyst/gas interface occurs.

However, upon current interruption, the relaxation transient expected to be rapid appears to be rather slow. In addition, increasing the anodic polarization time seems to slow down further the relaxation transient. This is an indication that the polarization time has a positive effect on the stability of promoters. In fact, as displayed in Fig. III-15, the estimated lifetime of the promoter τ_D (the determination of τ_D is shown schematically in Fig. III-15) is found to increase linearly with the square root of the anodic polarization time (insert of Fig. III-15).

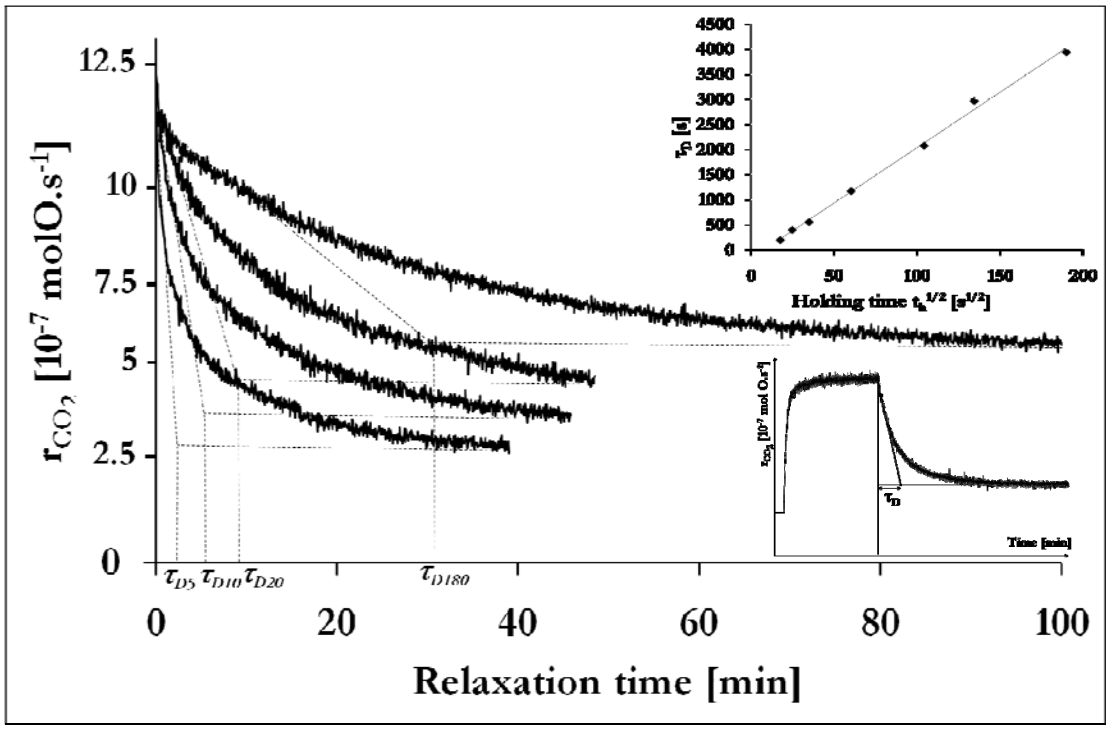

Fig. III-15 : Effect of increasing anodic holding time t_H on the relaxation rate transient after current interruption. (1) 5min (2) 10min (3) 20 min and (4) 180 min P_{O2}=8.2kPa. P_{C2H4}=0.2 kPa T=375°C. Insert : Linear realationship between τ_D and $t_H^{1/2}$

In addition to the long relaxation period a new enhanced steady state reaction rate, *r'*, is reached. This behaviour, characteristic of P-EPOC phenomenon, is described by the γ parameter (equation II-7). Experimentally, γ is found to increase linearly with the square root of the holding polarization time (insert in Fig. III-12). However the involved time

constant indicates that the permanent alteration (P-EPOC) is linked to very slow processes certainly related to diffusion process.

In the filed of EPOC, the alteration of the catalytic reaction rate observed during polarization is commonly described by an experimental relation linking the change in reaction rate to the change of catalyst work function.

$$\ln\left(\frac{r}{r_0}\right) = \frac{\alpha(\Phi - \Phi^*)}{k_b T} \qquad \textbf{III-20}$$

where Φ is the catalyst work function, Φ^* is a constant, and α the EPOC coefficient which is positive for electrophobic reactions and negative for electropholic ones.
So, the influence of polarization time observed on the relaxation transients implies a modification of the catalyst work function after current interruption. As previously mention in Chapter II, for the same EPOC reaction over RuO_2/YSZ catalytic system, *Wodiunig et al.* observed such catalyst work function transient, *i.e.* depending on polarization time after current interruption (Fig II-9). Worth to notice that the work function Φ is directly related to the coverage θ_j of the promoting species, *j*, according to the Helmoltz equation :

$$\Delta\Phi = \frac{eN_M}{\varepsilon_0}\sum_j P_j \Delta\theta_j \qquad \textbf{III-21}$$

where *e* is the electron charge, N_M is the surface atom density of the catalyst surface, ε_0 is the vacuum permittivity and P_j the dipole moment of the *j* species, which is coverage dependent with typical values of 1 to 5 Debye. The herein reported P-EPOC phenomenon, implying a permanent change of catalyst work function should then be related to the coverage of the catalyst surface with stable promoters with relatively high dipole moment P_j, *i.e.* the dipole moment of the oxygenpromoter formed during prolonged polarization and remained on the catalyst surface upon current interruption (P-EPOC) seems to be higher than that of the promoters formed by short term polarization (EPOC).

The extreme reducing conditions (multistep electrochemical reduction or use of ethylene) needed in order to restore the initial catalytic activity of a P-EPOC state can be explained by the low chemical reactivity of the involved promoters.

Furthermore these promoters seem to desorb at high temperatures (600°C). As previously reviewed in Chapter II, increasing temperature is unfavorable to both EPOC and P-EPOC. In fact, it is well known that the classical EPOC phenomenon disappears at temperature exceeding 600°C [5, 12, 13]. Furthermore, at moderate temperature (525°C and 600°C) the P-EPOC investigation on ethylene combustion over Pt/YSZ catalyst performed by *Jaccoud et al.* revealed complex relaxation transients and the oxygen storage efficiency (equation II-9) decreases strongly with increasing temperature [14].

III.4 Conclusions

In this chapter, the electrochemical promotion of catalytic ethylene oxidation over a Pt/YSZ/Au electrochemical cell was studied under excess of oxygen at 375°C. The gas exposed active area of the cell was determined by isothermal titration technique and under open circuit conditions (classical catalysis) the catalysis followed the expected kinetic mechanism already reported in literature. Upon anodic current application (EPOC and P-EPOC), a strong non Faradaic enhancement of the catalyst activity was observed (Λ = 370), corresponding to a 4.2-fold increase of the reaction rate, in agreement with the sacrificial promoter EPOC theory. However after longer polarization time, at current interruption, the relaxation transients slowed down (τ_D increases) and the catalytic rate remained in a highly active P-EPOC steady state r_p (depending on duration of the previous anodic polarization t_H and characterized by γ>1). Worth is to notice that once the catalyst is in the P-EPOC highly active steady state, the application of a similar negative current for a similar time period results in the return of the catalytic rate to the initial open-circuit state. Similar results for the reversibility of the rate have been observed in cyclic voltammetry experiments. After completion of the potential cycling the open-circuit rate is almost the same as that measured before polarization.

All those results suggested that during the polarization a slow (current independant) irreversible promoter storage process takes place at the gas exposed catalyst surface in parallel to the rapid sacrificial promoter storage/release process imposed by the current. The second part of this work focuses on the formation mechanism of this stable promoter. An electrochemical investigation of the $O_{2(g)}$,Pt/YSZ system is proposed, with

regard to the platinum aqueous state electrochemistry and high temperature oxidation theory, in order to gain knowledge on the high temperature platinum film solid electrochemistry.

III.5 References

1. Nicole J (1999) Etude de la promotion électrochimique de l'oxydation catalytique de l'éthylène sur des oxydes métalliques, EPFL
2. Jaccoud A, Foti G, Wuthrich R, Jotterand H, Comninellis C (2007) Topics in Catalysis 44: 409
3. Eaves J (2003)
4. Vayenas CG, Jaksic MM, Bebelis SI, Neophytides SG (1996) In: Bockris JOM (ed) Modern Aspects of Electrochemistry, vol 29. Plenum Press, New York p 57
5. Vayenas CG, Bebelis S, Pliangos C, Brosda S, Tsiplakides D (2001) Electrochemical Activation of Catalysis: Promotion, Electrochemical Promotion, and Metal-Support Interactions. Kluwer Academic / Plenum Publishers, New York
6. Vayenas CG, Bebelis S, Neophytides S (1988) Journal of Physical Chemistry 92: 5083
7. Bebelis S, Vayenas CG (1989) Journal of Catalysis 118: 125
8. Nicole J, Mousty C, Comninellis C (1998) L'Actualité chimique: 57
9. Tsiplakides D, Nicole J, Vayenas CG, Comninellis C (1998) Journal of the Electrochemical Society 145: 905
10. Nicole J, Comninellis C (2000) Solid State Ionics 136-137: 687
11. Nicole J, Tsiplakides D, Pliangos C, Verykios XE, Comninellis C, Vayenas CG (2001) Journal of Catalysis 204: 23
12. Neophytides S, Tsiplakides D, Vayenas CG (1998) Journal of Catalysis 178: 414
13. Tsiplakides D, Neophytides S, Vayenas CG (2000) Solid State Ionics 136-137: 839
14. Jaccoud A (2006) Electrochemical promotion of Pt catalysts for gas phase reaction, EPFL

PART II

Electrochemical investigation of $O_{2(g)}$,Me/YSZ systems

CHAPTER IV- STATE OF THE ART

This chapter proposes a review of the relevant litterature of the $O_{2(g)}$,Me/YSZ system, presenting the various reaction paths and reaction locations such as the different models and rate determining steps proposed for the mechanism taking place upon an anodic/cathodic polarization. To get a clearer picture of the interaction between oxygen species and YSZ supported metal, the review is extended to the field of high temperature metal oxidation, recalling the main *Wagner* metal oxidation theory and its electrochemical interpretations given by *Mott* & *Cabrera* and *Eley* & *Wilkinson*.

On this basis, the literature concerning the Ni/YSZ and the Pt/YSZ systems is subject of special focus. The field of solid state electrochemistry appearing to be subject to controversial interpretations, the literature of aquaeous state electrochemistry and high temperature oxidation of both systems are given as it may be useful to the understanding of the phenomena investigated.

IV.1 $O_{2(g)}$,Me/YSZ electrochemistry

IV.1.1 The O_2(g),Me/YSZ system

The field of high temperature solid electrochemistry is related to several technologies such as electrochemically promoted catalysts (EPOC) [1], gas sensors [2-6] , gas pumps [7, 8], solid oxide fuel cells (SOFCs) [9] and electrolysis cells [10, 11].

As depicted in Fig. IV-1, the O_2(g),Me/YSZ system is composed of three different phases. A solid electrode is deposited on a solid electrolyte and this electrochemical system is hanging into a gaseous atmosphere. This geometry implies three double interfaces respectively Me/gas, Me/YSZ and YSZ/gas and a triple phase boundary where the three phases are present. Each of those interfaces has different properties and involves different physical and chemical mechanisms contributing to the overall electrochemical reaction taking place in the cell. For this reason the determination of the oxygen evolution reaction sites and reaction mechanism is still misunderstood and no clear agreement can be found in the extensive literature.

Fig. IV-1 : Schematic representation of an $O_{2(g)}$, Me/YSZ solid electrolyte cell indicating the triple phase boundary (tpb).

IV.1.2 Yttria Stabilized Zirconia as solid electrolyte

A solid electrolyte is an ionically conducting solid medium. Due to the presence of intrinsic or extrinsic point defects in their structures, mobile sublattices allow the ionic conduction in

a rigid framework [12-14]. Specific ions are able to migrate, into the solid, along those defects.

Zirconium dioxide, ZrO_2, presents three different states at ambient pressure: a non conducting monoclinic structure at low temperature, a tetragonal one between 1100 and 2400°C, and at higher temperatures ZrO_2 changes to a conducting cubic structure [15-17]. The face-centered cubic structure is fluorite type as shown in Fig V-2.

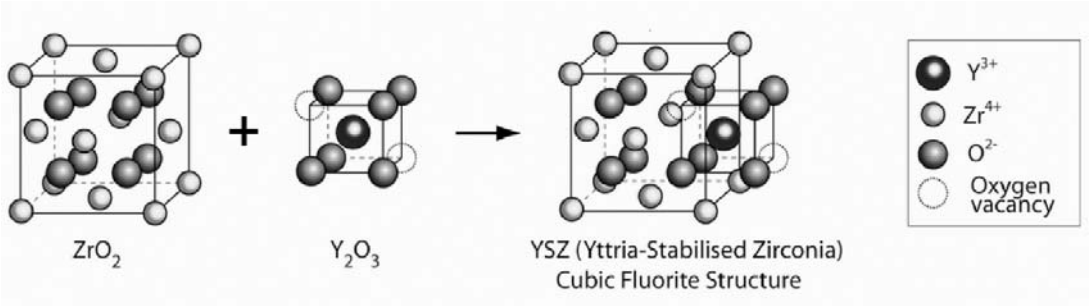

Fig. IV-2 : Schematic representation of stabilization of zirconium oxide fluorite structure by yttria dopping

Each metal cation is surrounded by eight oxygen atoms and each oxygen anion is coordinated with four metal cations. Common defects of this structure are vacancies and interstitials. Vacancies are sites that would be occupied in the ideal structure but are empty in the real solid, they are reported as Schottky defects. On the other hand interstitials would be empty in the ideal structure but in the real solid electrolyte ions may move from their original location in the lattice to an interstitial site, they are reported as Frenkel defects. Both Schottky and Frenkel defects allow different migration mechanism. Vacancy migration consists of the hopping of an O^{2-} ion from a vacancy to another one located nearby (Schottky defects). Interstitial migration implies the migration of ions moving through the interstice of the regular lattice (Frenkel defects). The cubic conducting structure of zirconia can be stabilized down to room temperatures by doping the lattice with aliovalent ions. In addition to this structural stabilization, the doping leads to the creation of vacancies to maintain electroneutrality of the crystal lattice. Then by doping zirconia with yttria, oxygen vacancies are created by charge compensation with respect to the following equation [18-20]:

$$Y_2O_3 \xrightarrow{ZrO_2} 2Y'_{Zr} + V_{\ddot{O}} + 3O_{O^x} \qquad \text{IV-1}$$

The maximal conductivity of the resulting yttria stabilized zirconia electrolyte is observed for a 9% mol Y_2O_3 concentration at 1000°C [21, 22] and decreases with increasing dopant concentration because of defect association and electrostatic interactions. At lower temperatures, the conductivity is maximal close to the stability limit of the cubic phase corresponding to 8% at 600°C 0[23, 24]. A key factor for a solid to be seen as an electrolyte, their electronic transport number should be as low as possible. Over a wide range of temperature and pressure, YSZ can be seen as a purely ionic conductor independent of oxygen partial pressure. At 700°C, *Weppner* reported [25] the YSZ electronic conductivity to be 10^{-7} $Ohm^{-1}cm^{-1}$ at 20kPa oxygen while the ionic conductivity was 10^{-3} $Ohm^{-1}cm^{-1}$. Electronic conductivity is found to be significant only at extremely high (p-type) or low (n-type) oxygen partial pressures. Under normal conditions of operation, YSZ 8%, can then be considered as a purely O^{2-} ionic conductor, with a transference number of unity ($t_h+t_e < 0.01 \bullet t_{ion}$) and a temperature depend conductivity, σ, expressed by Kilner [26] as :

$$\sigma T = Ae^{\left(\frac{-E_m}{k_b T}\right)} \qquad \text{IV-2}$$

where A is a constant, k_b is the Boltzman constant and E_m the energy for hopping.

IV.1.3 Possible reaction path at $O_{2(g)}$,Me/YSZ system

By investigating the $O_{2(g)}$,Me/YSZ system, authors conclude a complex dependence upon several experimental parameters as oxygen partial pressure, temperature, polarization potential, polarization time but also on electrode preparation method and their consequences on electrode microstructure [27-47]. Several reaction paths were proposed as depicted in Fig. IV-3.

(1)"Triple phase boundary process" :

Dissociative adsorption of oxygen on metal surface followed by diffusion of adsorbed oxygen species on the gas exposed electrode surface toward the tpb, where the electrochemical reaction takes place. The reduced oxygen O^{2-} enters the solid electrolyte by association with an oxygen vacancy V_O.

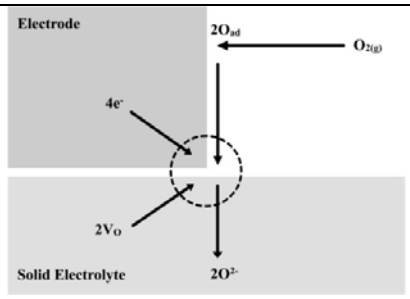

(2) "Electrolyte process":

Dissociative adsorption of oxygen on YSZ surface immediately followed by the electrochemical reaction at YSZ/gas interface. The reduced oxygen O^{2-} enters the solid electrolyte by association with an oxygen vacancy V_O and electrons originating from metal.

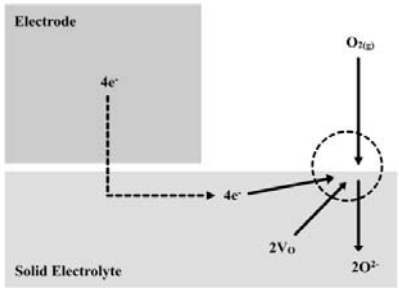

(3) "Surface process"

Dissociative adsorption of oxygen on metal surface followed by the electrochemical reaction at Me/gas interface. The reduced oxygen species diffuses from the gas exposed electrode surface toward the tpb to be incorporated into the electrolyte.

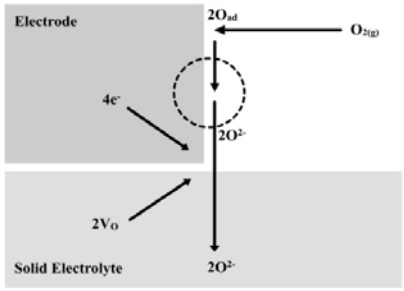

(4) "Interface process" :

Dissociative adsorption of oxygen on metal surface followed by diffusion of adsorbed oxygen species on the gas exposed electrode surface toward the electrolyte/electrode interface where the electrochemical reaction takes place.

Electrochemical reaction takes place over the entire Me/YSZ interface instead of being confined to the tpb.

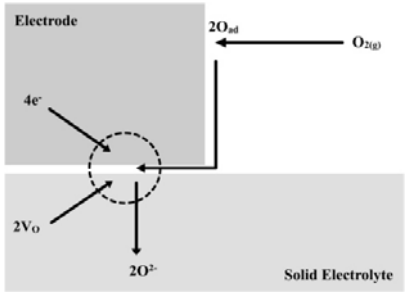

(5) "Electrode process" :

Dissociative adsorption of oxygen on metal surface followed by diffusion of adsorbed oxygen species trough the electrode to the reaction sites at the electrode/electrolyte interface.

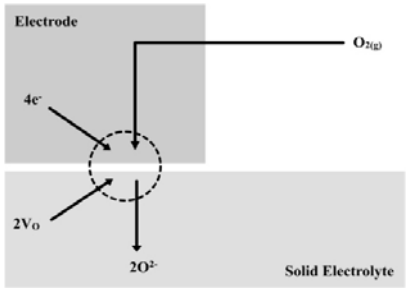

Fig. IV-3: Possible pathways for the oxygen exchange reaction (cathodic case)

● Process 1 [41, 44, 48-51] is the most straightforward one as the triple phase boundary is supposed to be the only electrochemical active part of the system. YSZ electrolyte acts as sink/source of O^{2-} anions, metal electrode acts as current acceptor/donor of electrons and gas atmosphere is the source/sink of oxygen. Electrolyte/metal interface is inactive to electrochemical reaction acting as a blocking interface. However, since the triple phase boundary is geometrically represented by a line (zero width), the site of the electrochemical reaction (ERS) is often reported to extend toward an adjacent interface.

● Process 2 [49, 52-54] considers the extension of tpb to electrolyte surface (process 2) implies that YSZ acts, at least partially, as an electronic conductor. As previously reported (§ IV.1.2), YSZ,8% is most likely a pure ionic conductor under atmospheric atmosphere, this process is then limited by lack of YSZ electronic conduction. However, local partial reduction of YSZ, by application of a strong cathodic current or a low O_2 partial pressure, can produce significant electronic conductivity and lead to a mixed ionic-electronic conductor (MIEC) [6, 55]. The mixed conductivity can also be achieved by implantation of an electronic conductor in the near surface YSZ layers [56-63].

Process 3 [49, 52-54] allows for the extension of the tpb to the metal/gas interface, assumes the stability of charged oxygen species at metal gas exposed surface. Stability and diffusion of this particular oxygen at metal surface has been extensively discussed in many works and especially in the field of Electrochemical Promotion of Catalysis, with regard to the promoter backspillover theory.

● Process 4 [1, 46, 47], proposes the extension of electrochemical reaction sites to the whole Me/YSZ interface by analogy to liquid state electrochemistry where the reaction sites are located at the electrode/electrolyte interface. Diffusion of oxygen along this interface was found possible with a limited rate [55], and accumulation of oxygen at the Me/YSZ interface occurs by formation of metal oxide [27, 41, 64, 65]. This process is largely accepted for oxygen permeable metal electrode, *e.g.* Ni [53], and controversed for metal electrode presenting low oxygen solubility, *e.g.* Pt [54, 65, 66].

- Process 5 [49], involves oxygen diffusion across the metal bulk electrode to the electroactive reactive sites at the Pt/YSZ interface. This process concerns only the metal electrodes presenting sufficiently high oxygen solubility, *e.g.* Ag.

IV.1.4 Metal oxidation at high temperture

In this work the reactivity of oxygen with metal at high temperature is of particular interest. The rich literature of high temperature metal oxidation reports that depending on experimental conditions (*P, p_{O2}, T*), and on the initial state of the metal surface, three different oxidation kinetics are commonly considered for metal oxidation.

IV.1.4.1 Linear reation rate

In case of a pure metallic surface, *i.e.* there is no oxide layer barrier at the metal surface, the oxidation rate is expected to be constant with time as the reaction is controlled by one of the charge transfer steps of the mechanism rather than by a transport process. The linear oxidation rate can then be expressed as :

$$x = k_L t \qquad \text{IV-3}$$

where x is the mass or the thickness of the oxide formed and k_L is the linear rate constant.
The oxidation never slows down until complete formation of metal oxide. This process is observed at the very first oxidation stage and later on if a porous unprotective oxide is formed at the metal surface.

IV.1.4.2 Parabolic reation rate

In case of diffusion controlled mechanism where diffusion of ions through a compact oxide layer at the interface is the rate determining step, a parabolic growth of oxide is observed [67-72]:

$$x = k_P t^{1/2} \qquad \text{IV-4}$$

where x is the mass (thickness) of the oxide formed and k_p is the parabolic rate constant.

The electrochemical potential acting as driving force, the oxide grows and diffusion length increases slowing down the reaction rate with increasing polarization times.

Wagner first observed experimentally this kinetic growth law at high temperature and proposed a commonly accepted high temperature metal oxidation theory model involving the displacement of charged species as rate determining step [73, 74]. A scheme of *Wagner* model is presented in Fig. IV-4, assumptions made are the following.

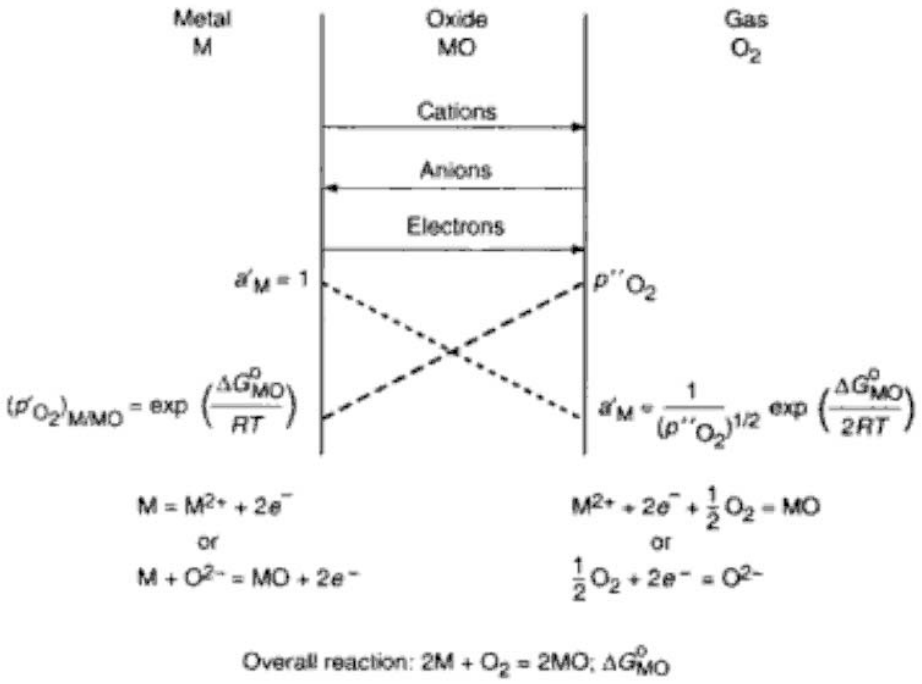

Fig. IV-4:Diagram scale formation according to Wagner's theory [74].

The oxide layer is dense and adherent to the metal, migration of charged species (ions, electrons or holes) is the rate determining step of oxidation process, both metal/oxide and oxide/gas interface are in thermodynamical equilibrium, the oxide formed is stochiometric and solubility of oxygen into the oxide layer is neglected. The resulting electrochemical potential gradient in the oxide layer is the driving force of the process. The resulting ions flux, F_i, can then be written as :

$$F_i = -C_i u_i \frac{d\mu_i^*}{dx} = -C_i u_i \left(\frac{d\mu_i}{dx} + z_i F \frac{d\Phi}{dx} \right) \qquad \text{IV-5}$$

where C_i is the ion concentration in the oxide, u_i its mobility and μ_i^* the electrochemical potential and Φ the Galvani potential . Considering the Nernst-Einstein equation which relates the mobility of the ion to its diffusion coefficient, D_i, the equation becomes :

$$F_i = -D_i \frac{dC_i}{dx} + C_i u_i z_i F \frac{d\Phi}{dx} \qquad \textbf{IV-6}$$

Considering displacement of cations, electroneutrality of the film implies a coupled displacement of electrons into the film with a similar flux.

The derivation of this model, for the formation of metal oxide of stochiometry MeO, leads *Wagner* to the determination of a parabolic law for the growing oxide layer as follows:

$$\frac{dx}{dt} = -3D_i \frac{\Delta C_i}{x} V_{ox} \qquad \textbf{IV-7}$$

where V_{ox} indicates the number of moles of metal required to form one mole of oxide, *e.g.* for MeO, V_{ox}=1.

However, because of the basic restrictive assumptions made the experimental results were usually found deviating from model predictions. Upon oxide growth, the layer formed is unlikely compact, similarly oxide stochiometry is rarely observed. Moreover, ionic transport may also occur through grain boundary diffusion especially in case of few structure defects in the layer.

IV.1.4.3 Logarithmic and inverse logarithmic reation rate

At low temperatures, after formation of a thin barrier oxide layer at the metal surface, the oxidation rate is commonly measured as logarithmic or inverse logarithmic growth. Oxidation rate is then expressed respectively as [67-71, 75-79]:

$$x = k_{Log} \log(at+1) \text{ or } \frac{1}{x} = b - k_{Log} \log(t) \qquad \textbf{IV-8}$$

where x is the mass or the thickness of the oxide formed, k_{Log} is the logarithmic rate constant, a and b are constants. Experimental distinction between the two laws is unrealistic because in the mathematical analysis of the results, both equations have constants (a and b) which can be adjusted to fit almost perfectly the data [67].

However for logarithmic and inverse logarithmic oxide growth, oxidation is limited by mass transport across the oxide film, the driving force being the electric field across the film. In these conditions, three main theories were developed upon years of research, *i.e.* limitation by electron mass transport, by cation mass transport and by cation incorporation into the oxide film.

● Electron tunneling : Mixed Ionic-Electronic Conductivity

Thin metal oxide films commonly behave as mixed ionic-electronic conductors (MIEC)[58, 59, 80-82], electrons can then enter into the film by overpassing an energy barrier, ΔU_e, corresponding to the energy difference of the Fermi level in the metal and the conduction band of the oxide. This mechanism can take place through a classical thermal emission but also by electron tunneling effect if the energy barrier is much larger than the electron thermal energy as depicted in Fig. IV-5.

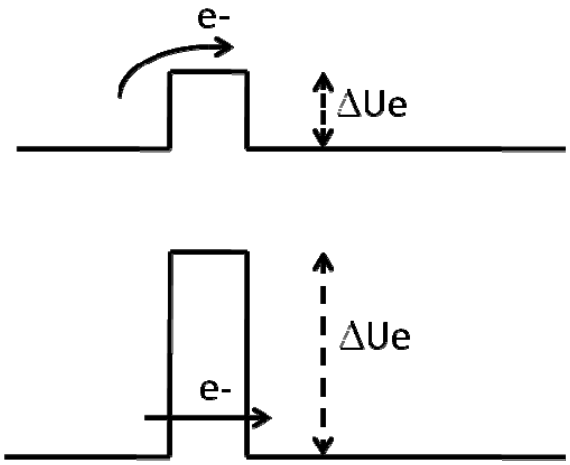

Fig. IV-5 : Electron emission from metal in presence of oxide film, thermal emission and emission by tunneling

In the latter case, the probability, *W*, that an electron enters into the oxide can be written [79]:

$$W = e^{\left(-\frac{L}{L_t}\right)} \text{ with } \frac{1}{L_t} = \frac{4\pi}{h}(2m_e\Delta U_e) \qquad \text{IV-9}$$

where L_t represents the critical tunneling distance of the order of several angstroms at which the film begins to attenuate the electron tunnel current, h is the Planck constant, m_e the electron mass and , ΔU_e, the energy difference of the Fermi level in the metal and the conduction band of the oxide .

● Cation diffusion through the oxide: High Field Theory

Mott and Cabrera developed a theory which is probably the most established and accepted one for metal thin film oxidation (x is less than 10nm) [68-71]. They assume that growth is limited by cation migration across the oxide film.

At the metal/metal oxide interface, a metal ion must pass into the oxide (potential barrier W) and moves into the metal by hopping mechanism (potential barrier U). Similarly as proposed by *Wagner*, oxygen is dissociatively adsorbed at the metal oxide/gas interface, producing sink for electron, however solid state diffusion is assumed too slow to play a significant role and motion of cations is due to the apparition of a strong electric field with a constant drop through the oxide layer thickness, decreasing the migration energy of cations by

$$\frac{qaE}{2x} \qquad \textbf{IV-10}$$

where x is the oxide layer thickness, q is the charge of the metal ion, a the cation hopping distance and E the potential drop.

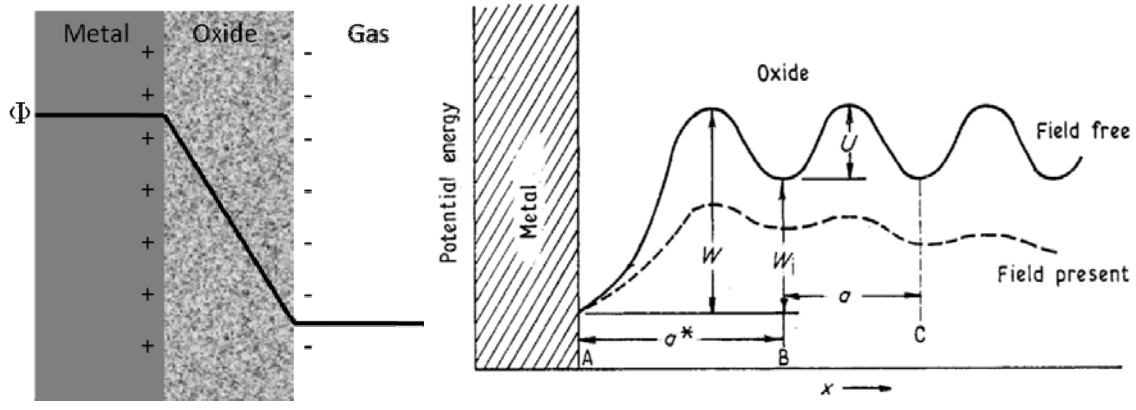

Fig. IV-6 : Electric field in the oxide and schematic representation of its effect on the charge transfer at the interface.

Final assumption is that every leaving metal cation is pulled across the oxide layer and reacts with oxygen adsorbed. The oxide growth is then determined in case of high field by :

$$\frac{dx}{dt} = N\Omega\upsilon e^{\left(-\frac{W}{kT}\right)} e^{\left(-\frac{qaE}{2xkT}\right)} \qquad \textbf{IV-11}$$

where N is the number of metal atoms at the metal/metal oxide interface, Ω is the volume of oxide per metal ion, υ is the vibrational frequency of metal lattice and q the charge of the metal ion.

This equation cannot be analytically integrated but *Mott* & *Cabrera* approximate the solution to a inverse logarithmic law.

● Cation incorporation into the oxide: Place exchange mechanism

Eley & *Wilkinson* [73, 83, 84] proposed a mechanism of place exchange between adsorbed oxygen and underlying platinum. In this case, the incorporation of metal or oxygen ion into the oxide lattice is the rate determining step.

The description previously made holds but the electric field created acts on the rate of place exchange rather than on the cation migration. The activation barrier is supposed to increase linearly with the thickness so by assuming that each leaving metal ion reacts with oxygen, oxide growth is determined by :

$$\frac{dx}{dt} = Ap^n e^{\left(-\frac{W}{kT}\right)} e^{(-\mu x)} \qquad \textbf{IV-12}$$

where x is the oxide layer thickness, p^n is the pressure dependency, μ and A are constants depending on the oxide structure.

The mathematical derivation is the same as the one previously proposed, *i.e.* no difference can be made between the lowering of the penetration energy into the film and the lowering of the cation migration across the film. The place exchange limitation mechanism leads then also to a logarithmic law for the oxide growth rate.

However, the dominance of this process is suggested for low oxygen pressure, while at higher oxygen partial pressure the cation and electron migration mechanism, pressure independent, become the rate determining step.

IV.2 $O_{2(g)}$,Ni electrochemistry

IV.2.1 $O_{2(g)}$,Ni/YSZ electrochemistry

The Ni-YSZ system is widely used in the field of solid oxide fuel cell, SOFC, as anode material because of its low charge transfer resistance and its very good electrocatalytic ability for hydrogen oxidation. Under polarization, oxygen evolution reaction takes place at the triple phase boundary (reaction V-13) and NiO is formed in the bulk of the metal electrode through the Ni/YSZ interface (reaction V-14).

$$O^{2-} \rightarrow \frac{1}{2}O_2 + 2e^- \qquad \text{IV-13}$$

$$O^{2-} + Ni \rightarrow NiO + 2e^- \qquad \text{IV-14}$$

In fact, the nickel oxidation reaction induces a large volume change in the Ni electrode which leads to cracks and breaks if the formation of NiO overpasses 60% [116]. In their SOFC study [117], *Birss et al.* report by thermogravimetric analysis (TGA) a parabolic formation of NiO at 700°C while the reduction reaction is pseudo first order (Fig. IV-7). By analogy to *Hoar* & *Price's* electrochemical interpretation of the *Wagner* oxidation theory [118], the authors propose a mechanism where Ni^{2+} diffusion toward the NiO scale is the limiting step.

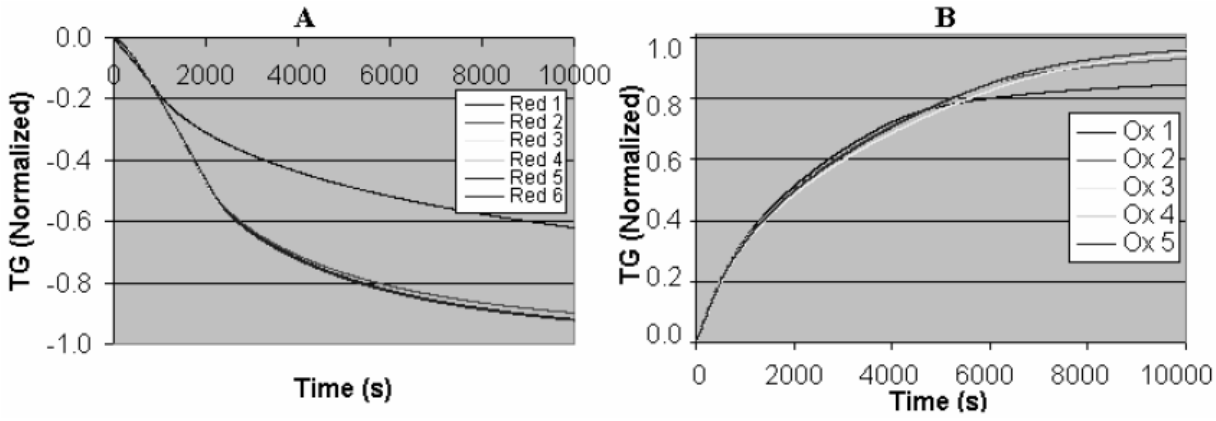

Fig. IV-7 : TGA analysis during successive Ni-YSZ oxidation and reduction steps during redox cycling at: (A) reduction at 700°C, (B) oxidation at 700°C. [86]

IV.2.2 Nickel aquaeous electrochemistry

In neutral and alkaline electrolyte media the Ni electrochemical behavior is commonly described by the reaction scheme proposed by Bode [88,89]. The author proposed to interpret the typical cyclic voltammograms obtained in such conditions by separating three different domains (namely A, B and C in Fig. IV-8).

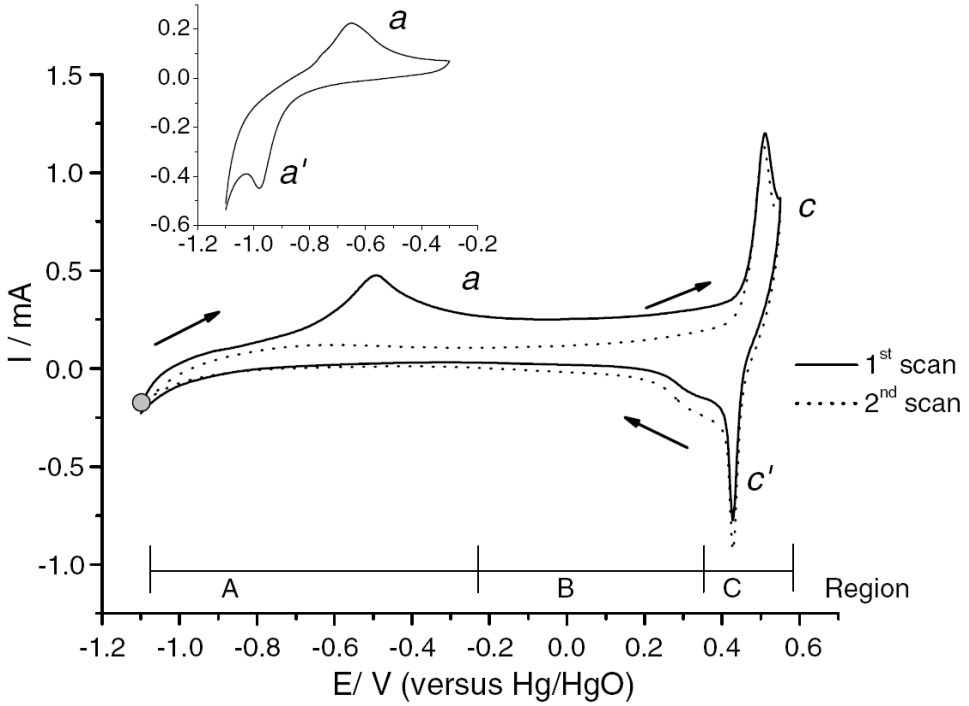

Fig. IV-8 : Cyclic voltammograms of Ni(111) in 1M KOH. The Ni(111)crystal was prepared by thermal annealing in a hydrogen atmosphere. The first scan and subsequent sweep are highlighted. Sweep rates:main plot 50 mV s^{-1}, inset 10 mV s^{-1} [89].

● Region A, corresponding to the more negative potential in the voltammogram (insert in Fig. IV-8), is reported as the Ni(II) region where, according to Pourbaix, Ni behaves like an electropositive metal. The lower negative limit of the voltammogram corresponds to hydrogen evolution reaction and hydrogen absorption into the nickel bulk electrode. Upon anodic potential sweep, the observed anodic peak *a*, is assigned to the formation of a slightly soluble nickel oxide : α-$Ni(OH)_2$ with concomitant expulsion of absorbed hydrogen from the bulk [88,89].

$$Ni + 2OH^- \rightleftarrows \alpha - Ni(OH)_2 + 2e^- \qquad \text{IV-15}$$

If the potential is cycled in this Ni(II) region (insert in Fig. IV-8)„ upon cathodic potential sweep, the reduction peak *a'* is observed corresponding to the reduction of : α-$Ni(OH)_2$ back to metallic Ni [88,89].

● In region B (intermediate potential domain in Fig. IV-8), according to the *Bode* oxidation model, α-$Ni(OH)_2$ is irreversibly transformed by dehydration in a more dense phase, β-$Ni(OH)_2$ [88,89].

$$\alpha - Ni(OH)_2 \rightarrow \beta - Ni(OH)_2 \qquad \text{IV-16}$$

As a consequence, the peaks *a* and *a'* previously observed in region A diminish and may even disappear, due to the irreversible formation of β-$Ni(OH)_2$ which can not be reduced back to Ni by the successive cathodic sweeps. Worth is to mention that the irreversible formation of β-$Ni(OH)_2$ phase may also take place by aging of the α-$Ni(OH)_2$ oxide layer[89].

● Region C, known as Ni(III) region, correspond to the oxidation of the hydroxide Ni(II) layer to Ni(III) by ejection of a proton taking place before the oxygen evolution reaction. In highly alkaline media, the further oxidation of β-$Ni(OH)_2$ phase leads to the formation of an hydrous Ni(III) oxide, β-NiOOH (equation IV-17) which may lead to nickel over-oxidation state in a neutral electrolyte , *i.e.* NiO_2.

$$\beta - Ni(OH)_2 \rightleftarrows NiOOH + H^+ + e^- \qquad \text{IV-17}$$

IV.2.3 High temperature nickel oxidation

The overall reaction of nickel oxidation at high temperature may be written as :

$$Ni + \frac{1}{2}O_{2(g)} \rightleftarrows NiO \qquad \text{IV-18}$$

This process has been widely studied and is well described at high temperature (T > 700°C) by the *Wagner* oxidation theory, *i.e.* a parabolic oxide growth law (Fig. IV-9). The parabolic rate constant is proportional to the surrounding oxygen partial pressure and commonly

reported to vary according to $k_p \propto p_{O_2}^{1/6}$ [90]. The mechanism is governed by a bulk diffusion process of single or doubly charged nickel vacancies [91].

However, at lower temperature, the reaction rate decreases and a sub-parabolic growth law is reported. At those temperatures, oxidation behaviour of Ni is reported to be highly dependant on the pretreatment of the metal prior the oxidation [92]. Nevertheless, worth to notice that even if short circuit transport mechanisms play a role, the mechanism of inward transport of oxygen toward the Ni bulk for the NiO layer formation remains.

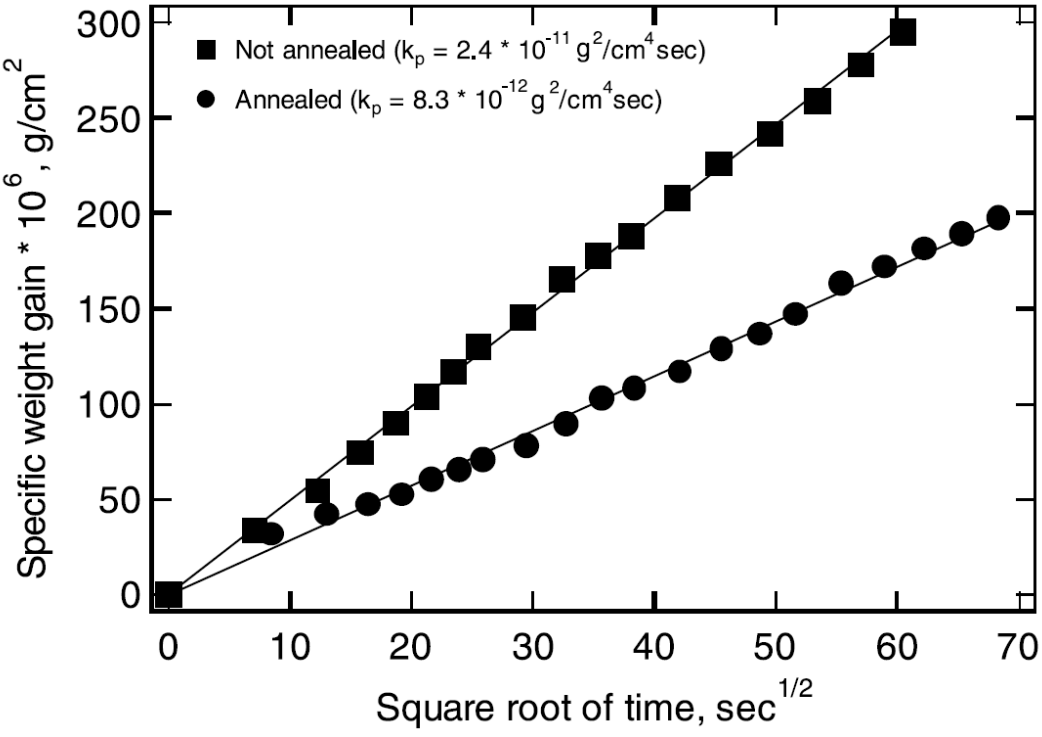

Fig. IV-9 : NiO parabolic growth kinetics : Ni weight gain as a function of the square root of time during the first hours of oxidation at 900°C in 0.02 atm O_2 [90]

IV.3 $O_{2(g)}$,Pt electrochemistry

IV.3.1 $O_{2(g)}$,Pt/YSZ electrochemistry

As the solubility of oxygen in platinum metal is much lower than that of nickel, two major ways of thought can be distinguished according to the reaction sites involved in the Pt/YSZ polarization and the resulting mechanism proposed.

- A first class of authors focuses on the major role of the triple phase boundary supposed to be the only electrochemical active part of the system as the oxygen evolution reaction IV-21 involves species present in each phase (processes 1 to 3).
- A second group of authors, with regard to the aquaous state theory of platinum electrochemistry, emphases the role of the binary Pt/YSZ interface and platinum multilayer oxidation (processes 4 and 5). Oxygen evolution taking place at the triple phase boundary is commonly seen as a side reaction occurring in parallel to platinum oxidation.

A rapid survey of both approaches and the resulting proposed mechanisms follows.

IV.3.1.1 Triple phase boundary acting as only reaction site

The mechanism of O_2(g),Pt/YSZ system under polarization can then be reduced to oxygen evolution reaction over platinum catalyst as follows :

$$O_{2(g)} \rightleftarrows 2O_{Pt}^{ads} \qquad \textbf{IV-19}$$

$$O_{Pt}^{ads} \rightleftarrows O_{tpb}^{ads} \qquad \textbf{IV-20}$$

$$O_{tpb}^{ads} + 2e_{Pt}^{-} \rightleftarrows O_{YSZ}^{2-} \qquad \textbf{IV-21}$$

Since the charge transfer takes place at the triple phase boundary, its length**,** l_{tpb}, is one of the most important factors influencing the electrode performance. *Radhakrishnan et al.* [41, 48] found, by electrochemical impedance spectroscopy measurements, a direct influence of l_{tpb} on the polarization resistance R_p and concluded to a charge transfer limited reaction. *Mizusaki et al* [8, 48, 51, 93, 94] proposed two different limiting steps for this mechanism depending on the experimental temperature.

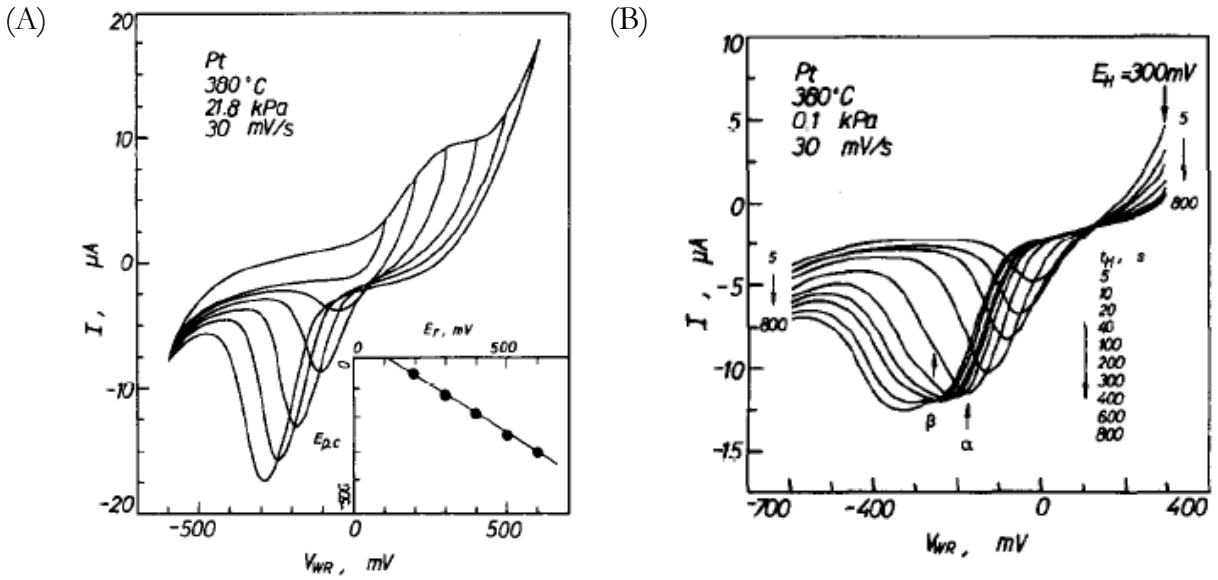

Fig. IV-10: Effect of reversal potential (A) and of anodisation holding time (B) on the cathodic potential peak. [95]

Above 600°C, oxygen atom surface diffusion to/from the triple phase boundary was found to be rate determining while at temperatures below 500°C, oxygen dissociation on platinum surface was proposed as RDS.

By studying Electrochemical Promotion of Catalysis (EPOC), *Vayenas et al* [96] conducted kinetic analysis at lower temperatures (380°C) involving cyclic voltammetry and Tafel measurements and concluded to electrochemical adsorption limitations at the tpb. Observation of one cathodic peak in the voltamogramms has been reported in literature in a wide range of temperature and oxygen partial pressure with electrodes prepared by several methods [41, 44]. Anodic reverse potential and anodisation time was found to have a dramatic influence on voltammograms as shown in Fig. IV-10. After long polarization times two peaks were usually observed, and explained by two different types of chemisorbed oxygen at platinum surface supporting the spillover theory of EPOC [1].

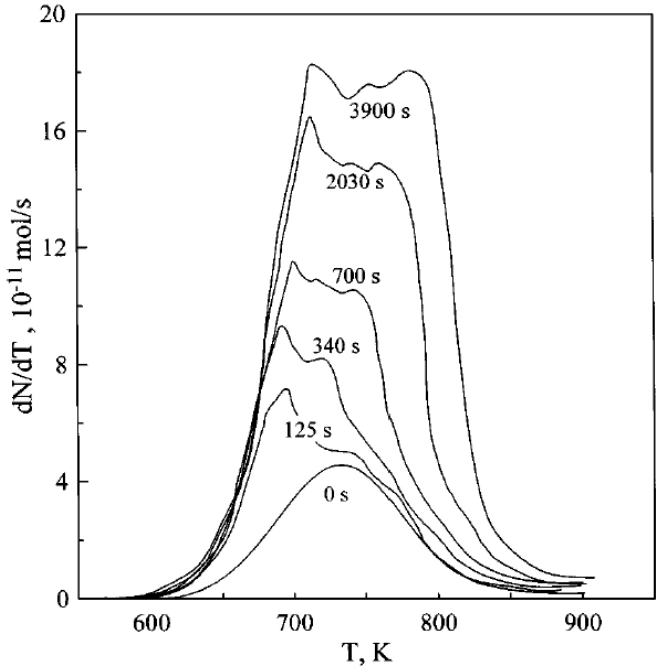

Fig. IV-11: Thermal desorption spectra of oxygen on Pt/YSZ film after gaseous oxygen adsorption at 673 K and an O_2 pressure of $4 \cdot 10^{-6}$ Torr for 1800 s followed by electrochemical O^{2-} supply (I = 15 μA) for various time periods.[96]

Temperature Programmed Desorption measurements performed by *Vayenas* [97, 98] and *Vernoux* [34, 99] show that anodic polarization of the Pt/YSZ cell leads to formation of $O^{\delta-}$ species, which had a different behavior than the chemisorbed oxygen originating from the gas. TPD measurements presented in Fig. IV-11 show the progressive apparition of back-spillover anions, reported as promoters in EPOC theory, with increasing anodic polarization times. Promoters desorb at higher temperature than the oxygen formed via gaseous adsorption without polarization indicating a strongly bonded oxygen on platinum surface, however because of the observation of a parallel increase in catalytic activity and platinum oxide being known of low catalytic activity, platinum oxidation reaction was then excluded from the mechanism [1].

IV.3.1.2 Pt/YSZ binary interface and tpb acting as reaction sites

If binary Pt/YSZ interface is electrochemically active, platinum oxidation reaction should be considered in the mechanism taking place at $O_{2(g)}$,Pt/YSZ system under polarization. Several authors support then that the observed cathodic peak reduction is more likely related to the platinum oxidation reaction at Pt/YSZ interface rather than to the oxygen evolution taking place at the triple phase boundary. However they do all agree that oxygen evolution reaction take place at the triple phase boundary as a side reaction process, equation IV-22.

$$O^{2-} \rightleftarrows \frac{1}{2} O_{2(g)} + 2e^{-} \qquad \text{IV-22}$$

Chao et al. [27] proposed, for the interpretation of the voltammograms presented in Fig. IV-12, that a slow oxidation process is taking place at Pt/YSZ interface limited by oxygen adsorption in the electrolyte subsurface. This was supported by confrontation of the large amount of charges involved in the cathodic reduction process to the rather limited triple phase boundary length.

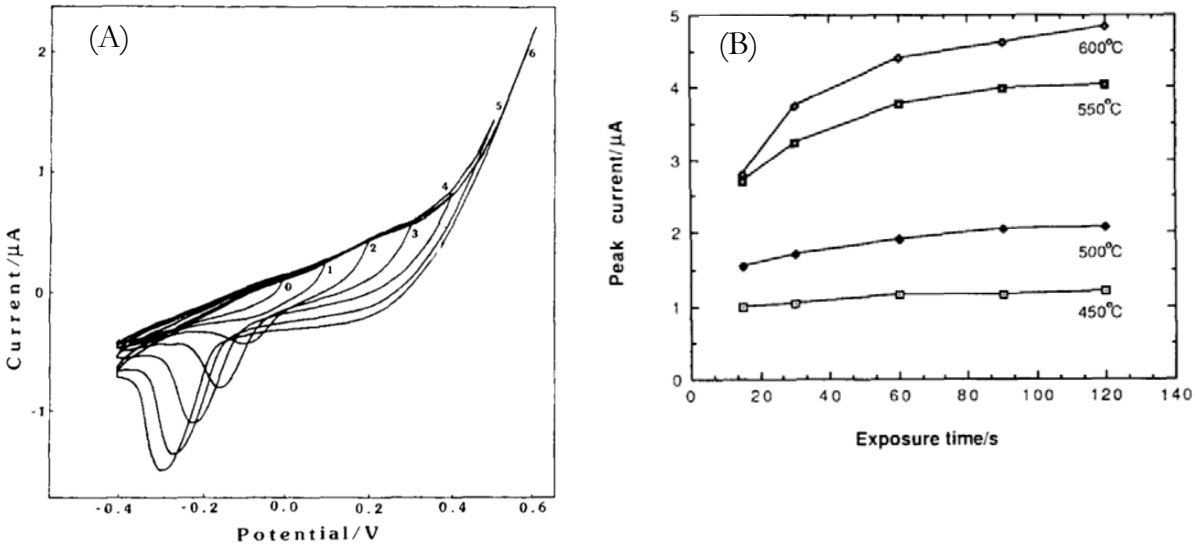

Fig. IV-12 : Effect of reversal potential (A) and of anodisation holding time (B) on the cathodic current peak. [27]

Through the electrochemical investigation of a screen printed Pt/YSZ electrode , *Jaccoud et al.* [65,66,100,101] observed for the first time a third cathodic process after long lasting

anodic polarization of the cell as shown in Fig. IV-13 : In order to explain this behavior, the authors proposed a mechanism involving three oxygen storage locations into the $O_{2(g)}$,Pt/YSZ system which can be summerized as follows:

$$Pt + O^{2-} \rightleftarrows PtO + 2e^{-} \qquad \textbf{IV-23}$$

$$PtO_{tpb} \rightleftarrows PtO_{Pt/gas} \qquad \textbf{IV-24}$$

$$PtO_{Pt/YSZ} + O^{2-} \rightleftarrows PtO_{bulk} + 2e^{-} \qquad \textbf{IV-25}$$

A first monolayer adsorbed rapidly at the Pt/YSZ binary interface during the initial times of anodic polarization, equation IV-23. This first oxygen storage is assumed to be rather limited and will then rapidly reach saturation. In parallel, similar reaction takes place at the triple phase boundary but the formed strongly bonded oxygen diffuses toward the gas exposed platinum surface being a second larger oxygen storage location, equation IV-24. Finally, after the completion of the first process, an incorporation and subsequent diffusion of oxygen into the platinum bulk is proposed as a third oxygen storage location, equation IV-25. This last oxygen sink was proposed to explain the third cathodic peak observed for the first time by *Jaccoud* [65].

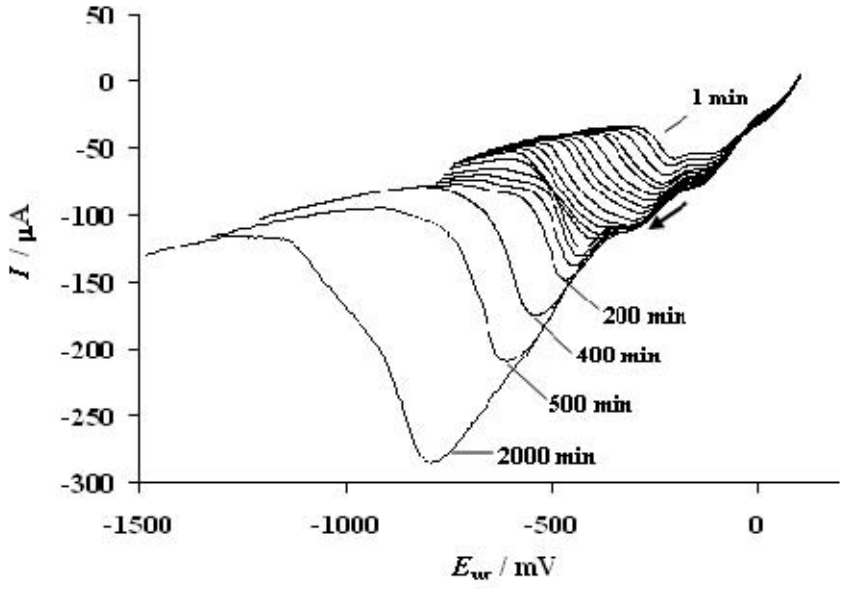

Fig. IV-13 : Effect on the anodic polarization time on the shape of the first linear cathodic sweep. [65]

IV.3.2 $O_{2(g)}$,Pt aqueous electrochemistry

Jerkiewicz et al. combined CV and electrochemical quartz-crystal nanobalance (EQCN) measurements where nanogram interfacial mass changes can be measured and directly correlated with the cyclic voltammogram as shown in Fig. IV-14 [104]. This corresponds to an in-situ determination of the molecular weight increase of the Pt surface oxide.

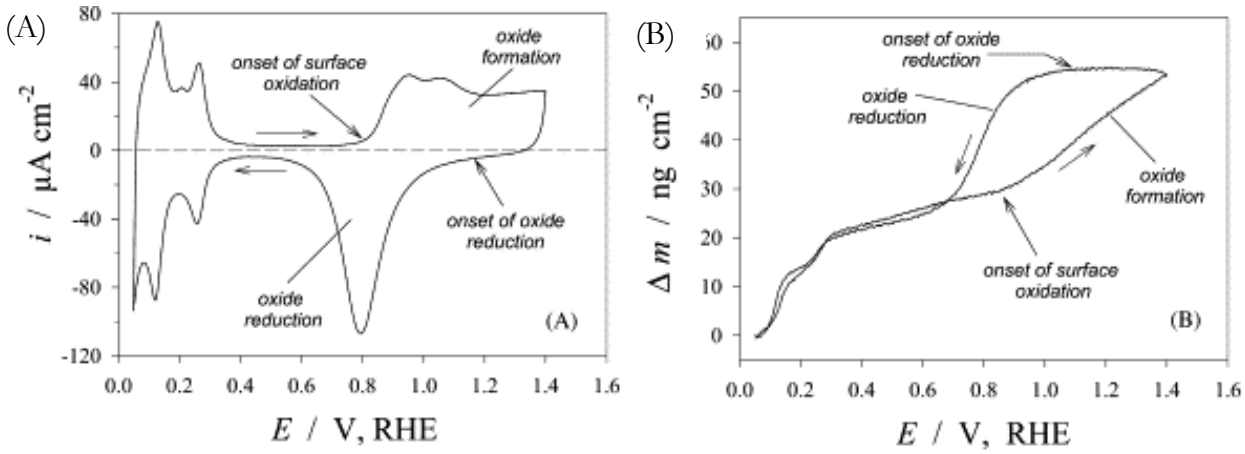

Fig. IV-14 : Cyclic-voltammetry profile (A) and mass-response profile (B) for a Pt electrode in 0.5 M aqueous H_2SO_4 solution recorded at ν=50 mV s^{-1} and T=25°C.

The voltammogram obtained is similar to that presented in previous literature [102-107], however evolution of masses during the potential sweeps shows a continuous almost linear increase with increasing potential in the oxide formation region. *Jerkiewicz et al.* proposed that one O atom is added to the surface, and PtO is the oxide species formed. It was also ascertained that the surface oxide was anhydrous, and that the process did not involve OH_{ads} as an intermediate. The mechanism proposes that surface oxidation proceeds via a progressive coordination of chemisorbed O adatoms (O_{chem}) to the Pt substrate as depicted schematically in Fig. IV-15 [106, 107].

The first step is an interaction of H_2O molecules with the Pt electrode at potential values between 0.27 and 0.85 V. At these potentials the Pt surface atoms carry a partial positive charge that attracts the negatively charged oxygen atoms in the dipolar water molecules (Eq.

V-26) and is characterized by a strong physisorption. In the second step, the discharge of half a monolayer (ML) of H_2O molecules takes place and results in the formation of 0.5 ML of $O_{chem.}$ (Eq. V-27). This process is accompanied by charge transfer. The third step is discharge of the second half-monolayer of H_2O molecules exhibiting strong interfacial interactions with the Pt surface. As the second half-monolayer of O_{chem} starts to build up, strong lateral repulsive dipole-dipole interactions set in which involve the dipole moment of the $(Pt\text{-}Pt)^{\delta+}\text{-}O_{chem}^{\delta-}$ surface compound. These interactions lead to an interfacial place exchange process of the initial half-monolayer of O_{chem} adatoms with the Pt surface atoms producing a surface PtO lattice in which the repulsive interactions are minimized. This place exchange is accompanied by completion of the charge transfer from Pt to O_{chem}, which leads to a quasi-3D surface lattice built up from Pt^{2+} and O^{2-} (Eq. V-28).

$$Pt + H_2O \rightarrow Pt^{\delta+}\text{-}O^{\delta-}H_2 \qquad \textbf{(IV-26)}$$

$$(Pt\text{-}Pt)\text{-}H_2O \rightarrow (Pt\text{-}Pt)^{\delta+}\text{-}O_{chem}^{\delta-} + 2H^+ + 2e^- \qquad \textbf{(IV-27)}$$

$$Pt\text{-}O_{chem} + H_2O \rightarrow (Pt^{2+}\text{-}O^{2-})_{quasi\text{-}3D} + 2H^+ + 2e^- \qquad \textbf{(IV-28)}$$

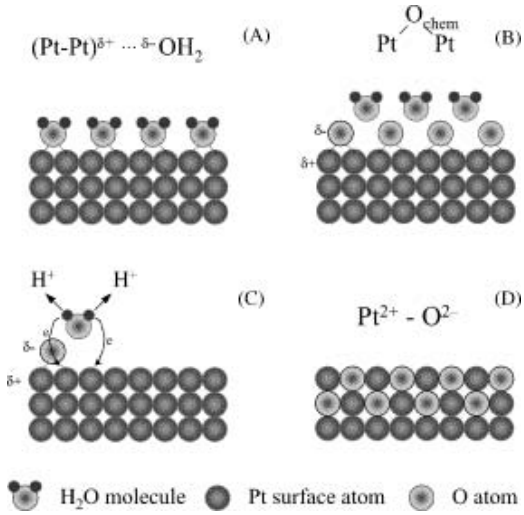

Fig. IV-15 : Mechanism and schematic representation of platinum electrooxidation in acidic media, model proposed by *Jerkiewicz*. [104]

IV.3.3 High temperature platinum oxidation

The overall oxidation reaction of platinum at the gas exposed suface may be written as :

$$Pt + \frac{1}{2}O_{2(g)} \rightleftarrows PtO \qquad \textbf{IV-29}$$

The driving force of this process is the variation of free energy, *i.e.* the formation of platinum oxide requires that oxygen partial pressure is larger than the dissociation pressure of the oxide .

Berry, proceeding to resistance measurements on platinum wires at high temperature, reports the evolution of oxide layer thickness for varying conditions of oxygen partial pressure and temperature [108].

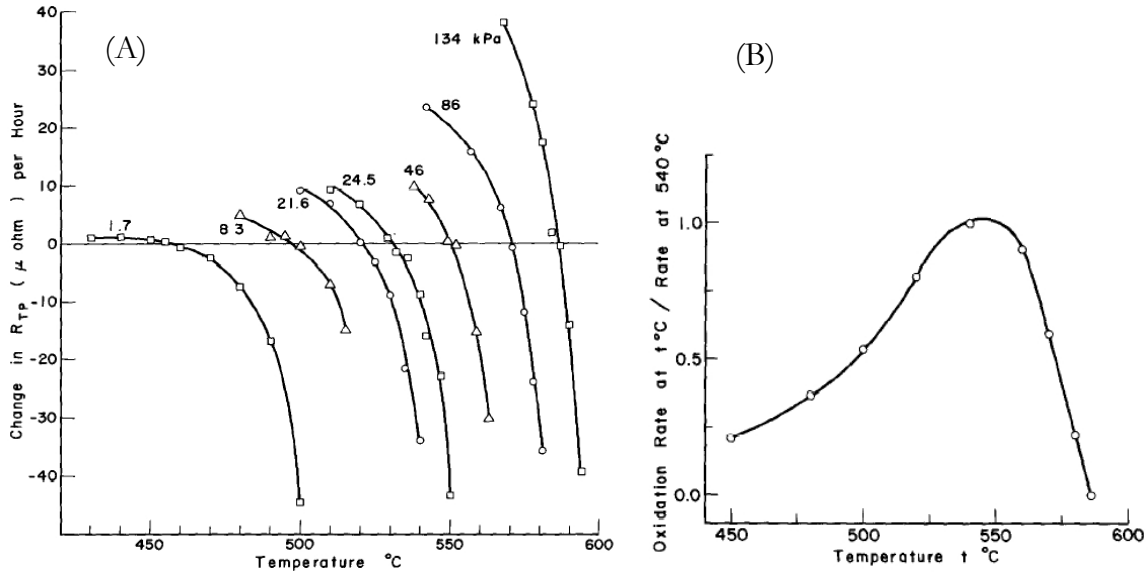

Fig. IV-16 : Isobaric change in resistance (A) and of normalized oxidation rate as function of temperature (B). [108]

Upon temperature increase the oxidation rate first increases and then decreases at temperatures higher than 550°C because the platinum oxide becomes thermodynamically less favourable than metal platinum.

Berry estimated ΔH and ΔS for the formation of platinum oxide at platinum wire surface [108]. *Vayenas et al* proposed similar thermodynamic values [109]. Using the ΔH and ΔS values, one may calculate the dissociation oxygen partial pressure p_{O2}* at any given temperature T:

$$\ln \frac{p_{O_2}^{*}}{p^{\circ}} = \frac{\Delta G_{PtO}}{RT} = \frac{\Delta H - T \cdot \Delta S}{RT} \qquad \textbf{IV-30}$$

where p^0 = 100kPa is set as the reference oxygen partial pressure.

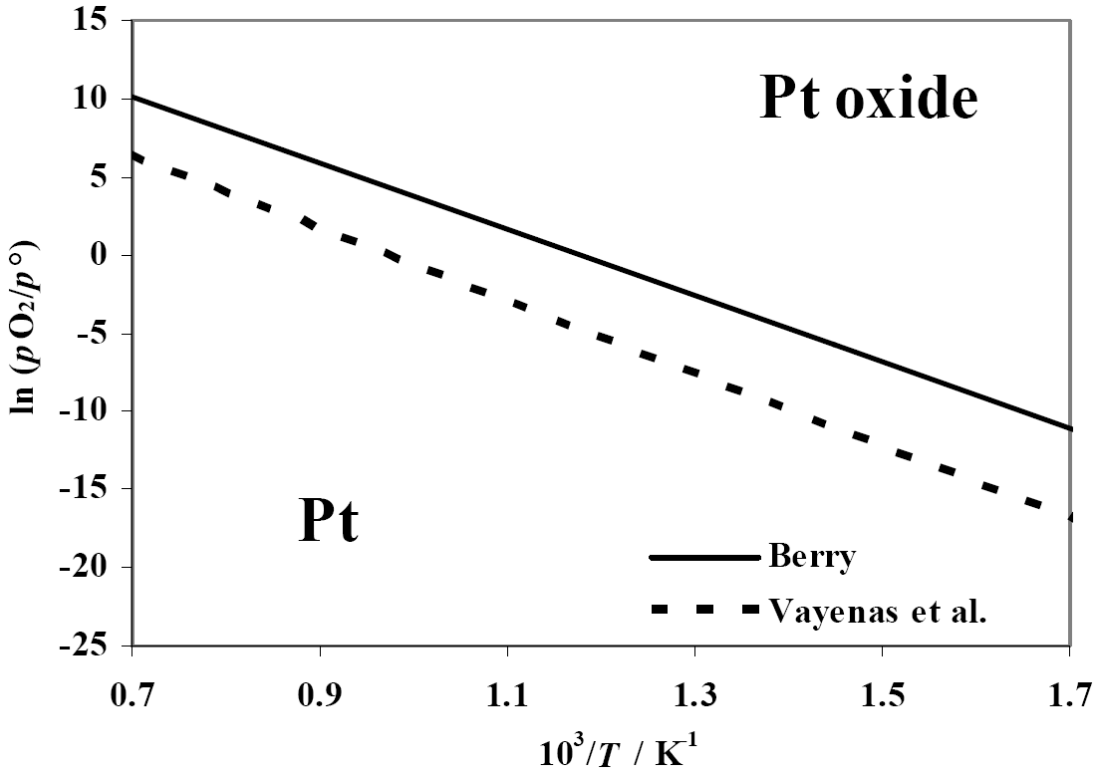

Fig. IV-17 : Stability domain of surface platinum oxide (Berry [108] and Vayenas et al. [109]), p° = 100 kPa.

IV.4 References

1. Vayenas CG, Bebelis S, Pliangos C, Brosda S, Tsiplakides D (2001) Electrochemical Activation of Catalysis: Promotion, Electrochemical Promotion, and Metal-Support Interactions. Kluwer Academic / Plenum Publishers, New York
2. Kawai T, Hayakawa N, Yamada T (1995), United State
3. Takao Murase, Yoshimura T (1992). NGK Insulators, Ltd., US
4. Yasushi HKO (1987). Honda Giken Kogyo Kabushiki Kaisha, United State
5. Visser JH, Logothetis EM, Rimai L, Soltis RE (1994). Ford Motor Company, US
6. Wiemhofer HD (1995) Solid State Ionics 75: 167
7. Deportes C (1994) Electrochimie des solides. Presses Universitaires de Grenoble
8. Mizusaki J, Amano K, Yamauchi S, Fueki K (1987) Solid State Ionics 22: 313

9. Kordesch KV, De Olivera JCT (1989) Ullmann's Encyclopedia of Industrial Chemistry, vol A12. Wiley, New York
10. Subbarao EC (1980) Solid Electrolytes and their Applications. Plenum Press, New York
11. Tao G, Sridhar KR, Chan CL (2004) Solid State Ionics 175: 615
12. Kumar B, Chen C, Varanasi C, Fellner JP (2005) Journal of Power Sources 140: 12
13. Li PW, Chyu MK (2005) Journal of Heat Transfer 127: 1344
14. Padma Kumar P, Yashonath S (2006) Journal of Chemical Sciences 118: 135
15. Nakamura A, Wagner JJB (1986) Journal of The Electrochemical Society 133: 1542
16. Ratkje SK, Forland KS (1991) Journal of the Electrochemical Society 138: 2374
17. Ratkje SK, Tomii Y (1993) Journal of the Electrochemical Society 140: 59
18. Manning PS, Sirman JD, Kilner JA (1996) Solid State Ionics 93: 125
19. Manning PS, Sirman JD, De Souza RA, Kilner JA (1997) Solid State Ionics 100: 1
20. Park J-H, Blumenthal RN (1989) Journal of the Electrochemical Society 136: 2867
21. Badwal SPS (1992) Solid State Ionics 52: 23
22. Badwal SPS (1995) Solid State Ionics 76: 67
23. Badwal SPS, Ciacchi FT, Haylock JW (1988) Journal of Applied Electrochemistry 18: 232
24. Backhaus-Ricoult M, Badding M, Thibault Y (2006) Ceramic Transactions, vol 179 p 173
25. Schwandt C, Weppner W, Schwandt C (1998) Solid State Ionics 112: 229
26. Tannhauser DS, Kilner JA, Steele BCH (1983) Nuclear Instruments & Methods in Physics Research 218: 504
27. Tsaofang Chao, Walsh KJ, Fedkiw PS (1991) Solid State Ionics 47: 277
28. Yoon SP, Nam SW, Kim S-G, Hong S-A, Hyun S-H (2003) Journal of Power Sources 115: 27
29. Tsiakaras PE, Douvartzides SL, Demin AK, Sobyanin VA (2002) Solid State Ionics 152-153: 721

30. Vernoux P, Gaillard F, Bultel L, Siebert E, Primet M (2002) Journal of Catalysis 208: 412
31. Kaloyannis A, Pliangos CA, Yentekakis IV, Vayenas CG (1995) Ionics 1: 159
32. Katsaounis A, Nikopoulou Z, Verykios XE, Vayenas CG (2004) Journal of Catalysis 222: 192
33. Katsaounis A, Nikopoulou Z, Verykios XE, Vayenas CG (2004) Journal of Catalysis 226: 197
34. Li X, Gaillard F, Vernoux P (2005) Ionics 11: 103
35. Bultel L, Vernoux P, Gaillard F, Roux C, Siebert E (2005) Solid State Ionics 176: 793
36. Jacobsen T, Bay L (2002) Electrochimica Acta 47: 2177
37. Poppe J, Schaak A, Janek J, Imbihl R (1998) Berichte der Bunsen-Gesellschaft 102: 1019
38. Imbihl R, Janek J (2000) Solid State Ionics 136-137: 699
39. Luerßen B, Gunther S, Marbach H, Kiskinova M, Janek J, Imbihl R (2000) Chemical Physics Letters 316: 331
40. Luerßen B, Janek J, Imbihl R (2001) Solid State Ionics 141-142: 701
41. Kenjo T, Yamakoshi Y, Wada K (1993) Journal of Electrochemical Society 140: 2151
42. Kenjo T, Takiyama H (1994) Electrochimica Acta 39: 2685
43. Kenjo T, Nakagawa T (1996) Journal of the Electrochemical Society 143: L92
44. Kenjo T, Shiroichi N (1997) Electrochimica Acta 42: 3461
45. Mitterdorfer A, Gauckler LJ (1999) Solid State Ionics 120: 211
46. Mitterdorfer A, Gauckler LJ (1999) Solid State Ionics 117: 187
47. Mitterdorfer A, Gauckler LJ (1999) Solid State Ionics 117: 203
48. Radhakrishnan R, Virkar AV, Singhal SC (2005) Journal of the Electrochemical Society 152
49. Siebert E (1994) Electrochimica Acta 39: 1621
50. Mogensen M, Skaarup S (1996) Solid State Ionics 86-88: 1151
51. Fukunaga H, Ihara M, Sakaki K, Yamada K (1996) Solid State Ionics 86-88: 1179
52. Wang DY, Nowick AS (1981) j. Electrochem . Soc. 128: 55

53. Fleig J (2002) Journal of Power Sources 105: 228
54. Velho LR, Bartlett RW (1972) Metallurgical Transactions 3: 65
55. Gopel W, Wiemhofer HD (1990) Berichte der Bunsen-Gesellschaft für physikalischemie 94: 981
56. Riess I (1992) Journal of the Electrochemical Society 139: 2250
57. Riess I (1992) Solid State Ionics 52: 127
58. Riess I (1995) Solid State Ionics 80: 129
59. Riess I (2005) Zeitschrift fur Physikalische Chemie 219: 1
60. Rutman J, Raz S, Riess I (2006) Solid State Ionics 177: 1771
61. Shkerin SN (2004) Russian Journal of Electrochemistry 40: 510
62. Shkerin SN (2003) Russian Journal of Electrochemistry 39: 863
63. Schouler EJL, Kleitz M (1987) Journal of the Electrochemical Society 134: 1045
64. Breiter MW, Leeb K, Fafilek G (1997) Journal of Electroanalytical Chemistry 434: 129
65. Jaccoud A, Foti G, Comninellis C (2006) Electrochimica Acta 51: 1264
66. Jaccoud A, Falgairette C, Foti G, Comninellis C (2007) Electrochimica Acta 52: 7927
67. Lawless KR (1974) p 231
68. Mott NF (1939) Transactions of the Faraday Society 35: 1175
69. Mott NF (1940) Transactions of the Faraday Society 35: 472
70. Mott NF (1947) Transactions of the Faraday Society 43: 429
71. Cabrera N, Mott NF (1949) Reports on Progress in Physics 12: 163
72. Wagner C (1933) Z. Phys. Chem. B21: 25
73. Landolt D (2007) Materials Today 10: 57
74. Wagner C (1933) Z. Phys. Chem. B21: 25
75. Zhang L, Macdonald DD, Sikora E, Sikora J (1998) Journal of the Electrochemical Society 145: 898
76. Macdonald DD (2004) Meeting Abstracts p 812
77. Macdonald DD (2005) Meeting Abstracts p 297

78. Sun A, Franc J, MacDonald DD (2006) Journal of the Electrochemical Society 153: B260
79. Bao J, Macdonald DD (2007) Journal of Electroanalytical Chemistry 600: 205
80. Riess I (1991) Solid State Ionics 44: 207
81. Riess I (1992) Materials science & engineering. B, Solid-state materials for advanced technology B12: 351
82. Rosenstock Z, Feldman I, Gil Y, Riess I (2005) Journal of Electroceramics 14: 205
83. Eley DD, Wilkinson PR (1960) Proceedings of the Royal Society of London. Series A. Mathematical and Physical Sciences 254: 327
84. Robertson NL, Michaels JN (1991) Journal of the Electrochemical Society 138: 1494
85. Pihlatie M, Kaiser A, Mogensen M (2009) Solid State Ionics 180: 1100
86. Young JL, Vedahara V, Kung S, Xia S, Birss VI (2007) ECS Transactions, vol 7 p 1511
87. Hoar TP, Price LE (1938) Transactions of the Faraday Society 34: 867
88. White Ed RE, Bockris Ed JO, Conway Ed BE (1990)
89. Medway SL, Lucas CA, Kowal A, Nichols RJ, Johnson D (2006) Journal of Electroanalytical Chemistry 587: 172
90. Haugsrud R (2003) Corrosion Science 45: 211
91. Bailey JM, Ritchie IM (1988) Oxidation of Metals 30: 405
92. Haugsrud R (2003) Corrosion Science 45: 1289
93. Mizusaki J, Amano K, Yamauchi S, Fueki K (1987) Solid State Ionics 22: 323
94. Kawada T, Sase M, Kudo M, Yashiro K, Sato K, Mizusaki J, Sakai N, Horita T, Yamaji K, Yokokawa H (2006) Solid State Ionics 177: 3081
95. Yi J, Kaloyannis A, Vayenas CG (1993) Electrochimica Acta 38: 2533
96. Neophytides S, Tsiplakides D, Vayenas CG (1998) Journal of Catalysis 178: 414
97. Neophytides SG, Vayenas CG (1995) Journal of Physical Chemistry 99: 17063
98. Vayenas CG, Lambert RM, Ladas S, Bebelis S, Neophytides S, Tikhov MS, Filkin NC, Makri M, Tsiplakides D, Cavalca C, Besocke K (1997) In: Xin CLaQ (ed) Spillover and Migration of Surface Species on Catalysts. Elsevier Science B. V.

99. Li X, Gaillard F, Vernoux P (2007) Topics in Catalysis 44: 391
100. Foti G, Jaccoud A, Falgairette C, Comninellis C (2007) Journal of Electroceramics: 1
101. Jaccoud A (2006) Electrochemical promotion of Pt catalysts for gas phase reaction, EPFL
102. Zolfaghari A, Jerkiewicz G (1999) Journal of Electroanalytical Chemistry 467: 177
103. Radovic-Hrapovic Z, Jerkiewicz G (2001) Journal of Electroanalytical Chemistry 499: 61
104. Jerkiewicz G, Vatankhah G, Lessard J, Soriaga MP, Park Y-S (2004) Electrochimica Acta 49: 1451
105. Jerkiewicz G, Tremiliosi-Filhoa G, Dall'Antoniaa LH (2005) Journal of Electroanalytical Chemistry 578: 1
106. Alsabet M, Grden M, Jerkiewicz G (2006) Journal of Electroanalytical Chemistry 589: 120
107. Jerkiewicz G, Alsabet M, Grden M, Varela H, Tremiliosi-Filho G (2009) Journal of Electroanalytical Chemistry 625: 172
108. Berry RJ (1978) Surface Science 76: 415
109. Vayenas CG, Michaels JN (1982) Surface Science 120: L405

CHAPTER V- ELECTROCHEMICAL INVESTIGATION OF THE Ni/YSZ SYSTEM

In this chapter, cyclic voltammetry has been used for the investigation of the oxidation-reduction reactions of a model metal electrode deposited over an YSZ pellet, during anodic and cathodic polarization, respectively. The choice of Nickel as working electrode was motivated by its oxidation mechanism following the *Wagner* theory at high temperature. Electrodes were deposited by sputtering on YSZ and investigated at temperatures between 350°C and 450°C, in 20 kPa O_2 and under atmospheric pressure. It has been found that a NiO scale is formed during anodic polarization at the Ni/YSZ interface and then is reduced during the subsequent cathodic potential sweep resulting in a significant cathodic peak. A correlation between cyclic voltammetric findings and metal oxidation theories has been obtained for the NiO formation rate. Finally, an original model is proposed for the electrochemically induced formation and growth of NiO at the Ni/YSZ interface.

V.1 Introduction

Nickel is a material commonly used in solid oxide fuel cells (SOFC) for environmentally acceptable energy production and, in addition, it is considered as a reference material for fundamental studies on the mechanism of high temperature oxidation of metals. Numerous studies have been devoted to both fields. However, only few fundamental studies using electrochemical techniques have been published on the $O_{2(g)}$,Ni/YSZ system [1-4]. An investigation by cyclic voltammetry of the electrochemically induced oxidation of this reference system is then proposed.

V.2 Eperimental

V.2.1 General setup

The reactor was an atmospheric single-chamber type quartz tube of 90ml (Fig. V-1). The single-pellet three-electrode cells were suspended in the reactor with the three gold wires serving as electrical contacts to the electrodes. A K-type (NiCr-Ni) thermocouple placed in proximity of the surface of the working electrode was used to measure the temperature of the system. The reactor was put into a furnace (XVA271, Horst) equipped with a heat control system (HT30, Horst).

The reactant gases used were Carbagas certified standards of 20% O_2/He, 1% C_2H_4/He (99.95% purity) and He (99.996% purity). Mass flow controllers (E-5514-FA, Bronkhorst) were used to control the gas feed composition and to keep the gas flow continuously at 200ml/min to feed the electrochemical reator.

Electrochemical stimulation and data acquisition are performed by using a galvanostat–potentiostat (Autolab, Model PGSTAT30, EcoChemie). Unless otherwise specified, the potential of the working electrode is given with respect to the reference Pt electrode exposed to oxygen partial pressure of 20 kPa.

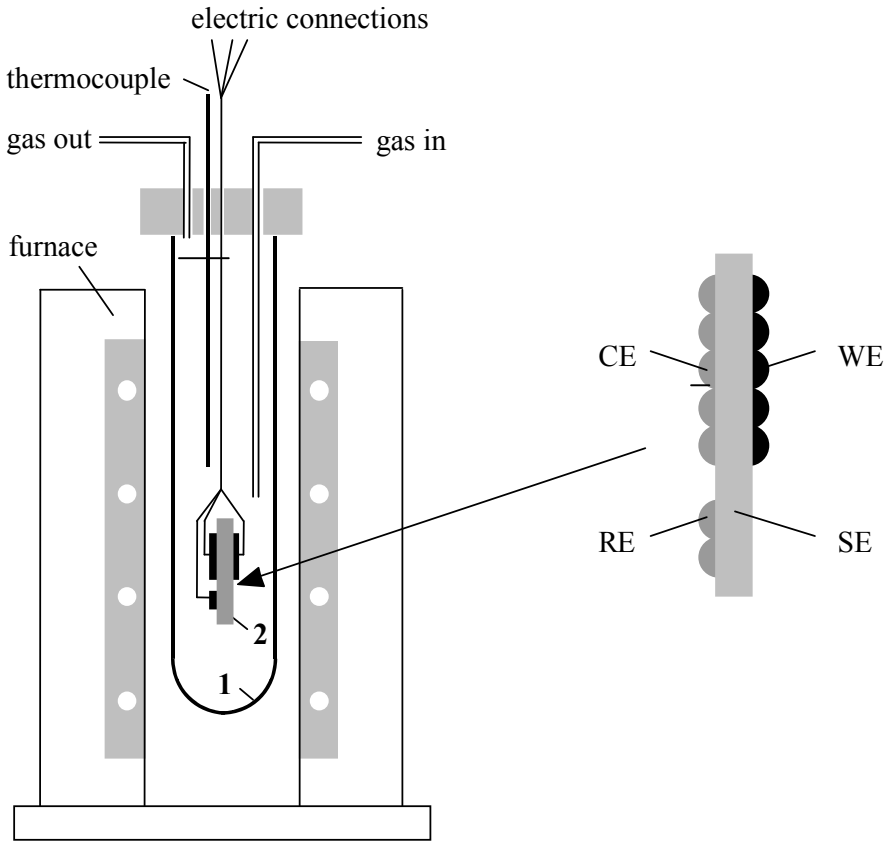

Fig. V-1 : Scheme of the atmospherique reactor. 1: quartz tube; 2: electrochemical cell

V.2.2 Deposition of Ni and Pt on YSZ

The solid electrolyte cell consists of a rectangular YSZ (8%mol Y_2O_3-stabilized ZrO_2 Technox 802, Dynamic Ceramic Ltd) pellet (10 mm x 15 mm) of 1mm thickness supporting the three electrodes: working, counter and reference. The Ni working electrode (thickness of 880 nm) was deposited by magnetron sputtering on one side of the electrolyte pellet in inert atmosphere (Ar) at room temperature. Direct current (dc) mode was used with a discharge of 455 V at an argon pressure of 4.3×10^{-3} mbar, resulting in a nickel deposition rate of 0.05 nm/s. The mask used during the deposition allowed to deposit one rectangular (7 x 5mm) film on the YSZ surface (working electrode). Platinum counter and reference electrodes were deposited on the other side of the electrolyte pellet by magnetron sputtering technique in inert atmosphere (Ar) at room temperature. Direct current (dc) mode was used with a discharge of 330 V at an argon pressure of 10^{-2} mbar. Under these conditions, a 1 μm thick

Pt electrode was deposited with a deposition rate of 0.09 nm s^{-1} on the YSZ pellet, as determined by profilometric measurement (Alphastep, Model 500) of the film deposited on smooth silicon samples processed simultaneously. The mask used during the deposition allowed to deposit two rectangular (7 x 5mm) films on the YSZ surface (counter and reference electrodes).

The working and counter electrodes were located in a symmetrical face-to-face arrangement on the opposite sides of the YSZ pellet (Fig. V-2), ensuring a symmetrical current and potential distribution in the cell during electrochemical investigations [10].

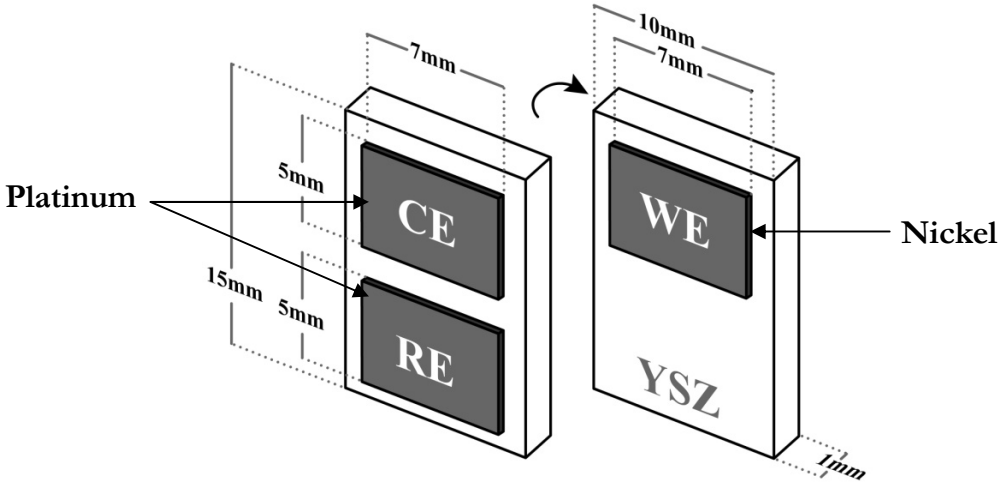

Fig. V-2 : Placement and dimensions of the Pt electrodes prepared by sputtering. WE: working electrode; CE: counter electrode; RE: reference electrode.

Before use, a pretreatment process including a calcination step at 700°C for 4h in air was performed in order to obtain a stable surface structure during the electrochemical measurements in the whole examined temperature range [10].

V.3 Electrochemical investigation

The electrochemical oxidation of YSZ supported Ni working electrode was studied at atmospheric pressure with 20kPa O_2 in He. The influence of anodic reverse potential, anodic holding time and temperature on the nickel working electrode oxidation mechanism was investigated by cyclic voltammetry.

V.3.1 Influence of the anodic reverse potential

Fig. V-3 shows the effect of the anodic reverse potential, E_r, on the cyclic voltammograms of Ni/YSZ system at 350°C. The increase of the anodic reverse potential leads to the formation of a single cathodic peak. The latter becomes more significant and shifts to lower potential values, with increasing reverse potential.

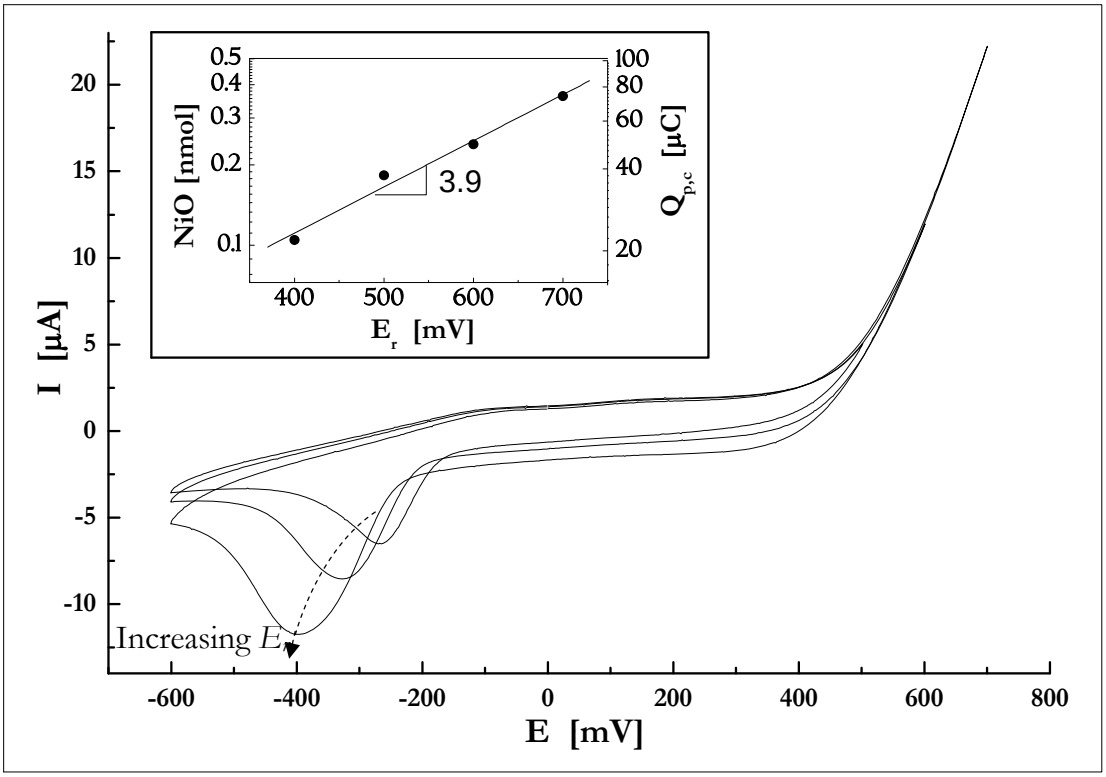

Fig. V-3: Effect of the anodic reverse potential, E_r on the voltammogram of Ni/YSZ system. Insert: effect of E_r, on the amount of formed NiO (nmol) (left axis) and corresponding reduction charge (µC) (right axis). p_{O2}=20kPa, ν=20mV s^{-1} and T=350°C.

Worthy to note is the fact that when the anodic reverse potential is set to values lower than ~150 mV the reduction peak does not appear on the voltammogram. This threshold potential indicates that the reduction peak is more likely related to the reduction of an electrochemically formed NiO equation V-1, rather than to the reduction of an oxide formed chemically by the surrounding oxygen equation V-2.

$$O_{YSZ}^{2-} + Ni \rightarrow NiO + 2e^{-} \qquad \text{V-1}$$

$$1/2O_2(g) + Ni \rightarrow NiO \qquad \text{V-2}$$

An estimation of the formed oxide (nmol) is performed by integrating the cathodic peak considering equation V-1, then plotted as a function of the anodic reverse potential (insert in Fig. V-3). This figure shows that increasing the anodic reverse potential results in an increase of the formed nickel oxide.

V.3.2 Influence of the anodic holding time

Fig. V-4 displays the voltammograms obtained after anodic polarization of the Ni electrode for increasing holding time. By holding the anodic potential up to 5 minutes at 400mV, the cathodic peak related to NiO reduction grows and shifts to more negative potentials.

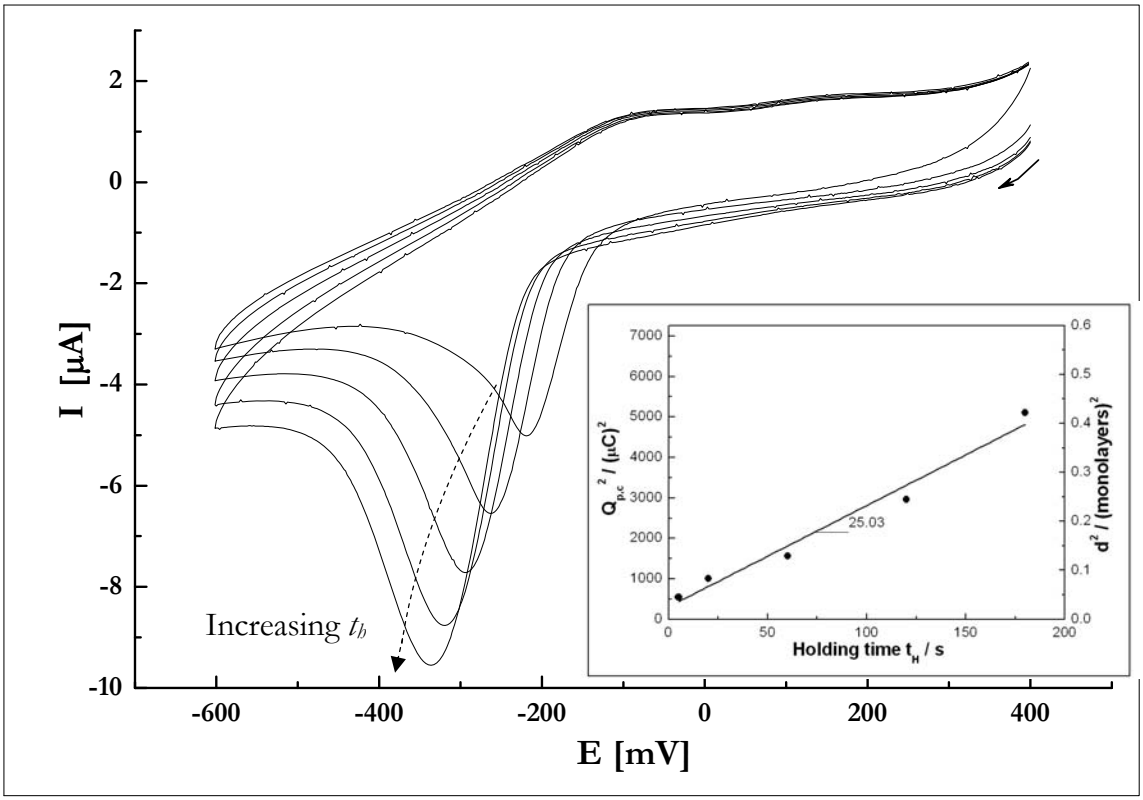

Fig. V-4 : Linear potential sweep voltammograms of Ni after holding the potential at +400mV for various holding times t_H (1) 5s, (2) 20s, (3) 60s, (4) 120s and (5) 180s. Insert gives the estimated charges of the cathodic peak and the equivalent nickel oxide thickness formed. P_{O2}=20 kPa, υ=20mV/s and T=350°C.

As shown in the insert, the anodic polarization of the Ni electrode leads to a parabolic growth of NiO. However, during anodic polarization oxygen evolution (equation V-3) takes place in parallel to the nickel oxide formation. The current efficiency for NiO formation (η_{NiO}) and for oxygen evolution (η_{O2}) during anodic polarization is defined by equation V-4 and equation V-5, respectively:

$$O^{2-} \rightarrow 1/2\,O_2 + 2e^- \qquad \text{V-3}$$

$$\eta_{NiO} = Q_{NiO}/Q_{Total} \qquad \text{V-4}$$

$$\eta_{O_2} = 1 - \eta_{NiO} \qquad \text{V-5}$$

where, Q_{NIO} is the charge involved in the reduction of NiO peak and Q_{Total} is the charge passes during the holding time t_H of the anodic potential step.

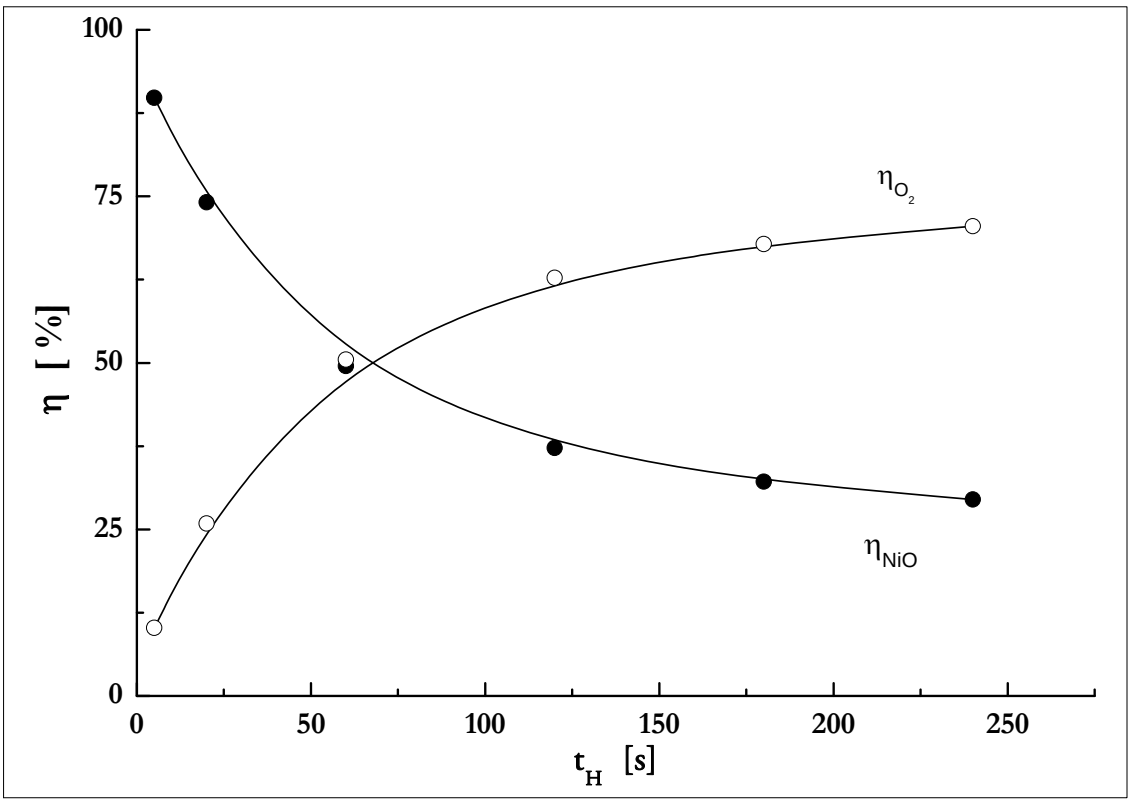

Fig. V-5 : Effect of holding time, t_H, on the current efficiencies of NiO formation, η_{NiO}, and O_2 evolution, η_{O2}, under E_r=400mV. P_{O2}=20 kPa and T=350°C.

Fig. V-5 shows the effect of holding time at a fixed anodic potential (E_r = 400mV) on the current efficiency of both NiO formation (η_{NiO}) and O_2 evolution (η_{O2}). This figure shows that the initial current efficiency of NiO formation (η_{NiO}) is close to 100% and then decreases rapidly with a concomitant increase of the current efficiency of O_2 evolution (η_{O2}). This is certainly related to the different mechanism of the involved reactions (equation V-1 and equation V-3). In fact, it seems that oxide scale formation acts as a barrier for further oxide growth without any influence on the O_2 evolution reaction.

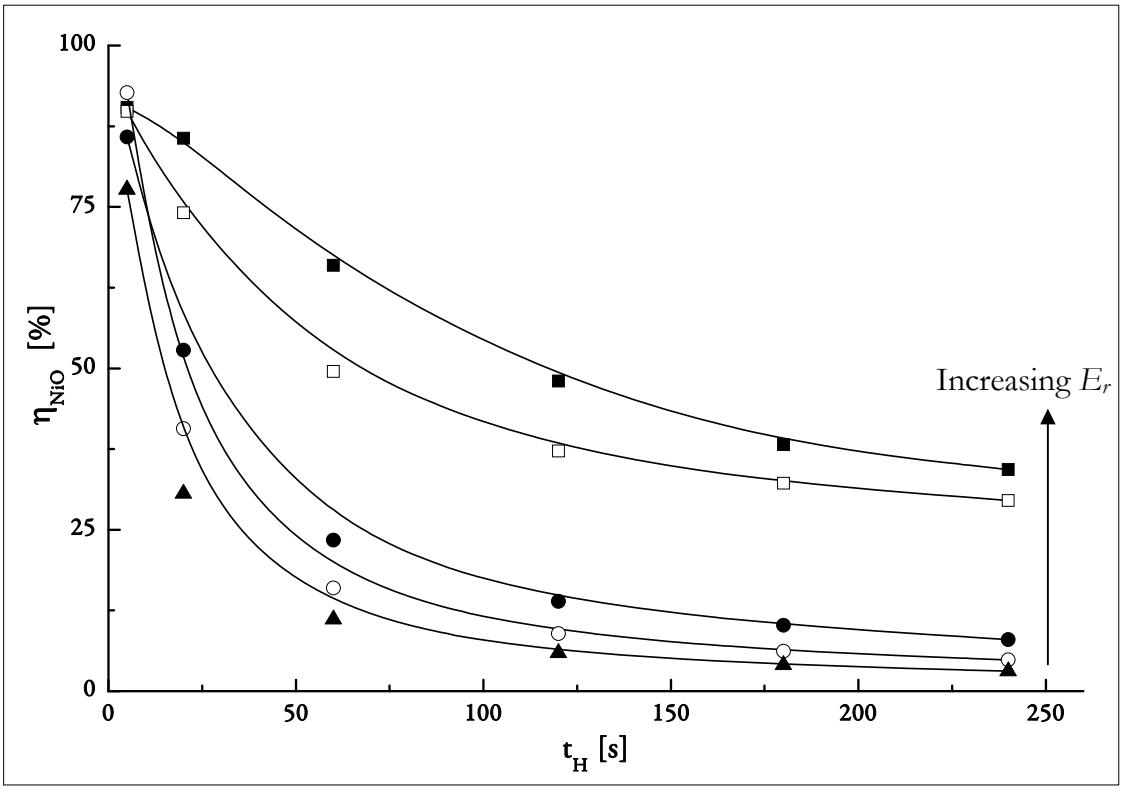

Fig. V-6 : Effect of holding time, t_H, on the current efficiency of NiO formation, η_{NiO}, for increasing holding potentials, E_H. P_{O2}=20 kPa and T=350°C.

Furthermore, the current efficiency for NiO formation (η_{NiO}) depends strongly on the applied holding potential as shown in Fig. V-6.

In order to estimate the effective rate (R_{eff}) of NiO formation, the following equation has been used (equation V-6):

$$R_{eff} = I_{eff}/2F = I\eta_{NiO}/2F \qquad \text{V-6}$$

where, I is the applied current during the anodic polarization and I_{eff} is the effective current used for NiO formation.

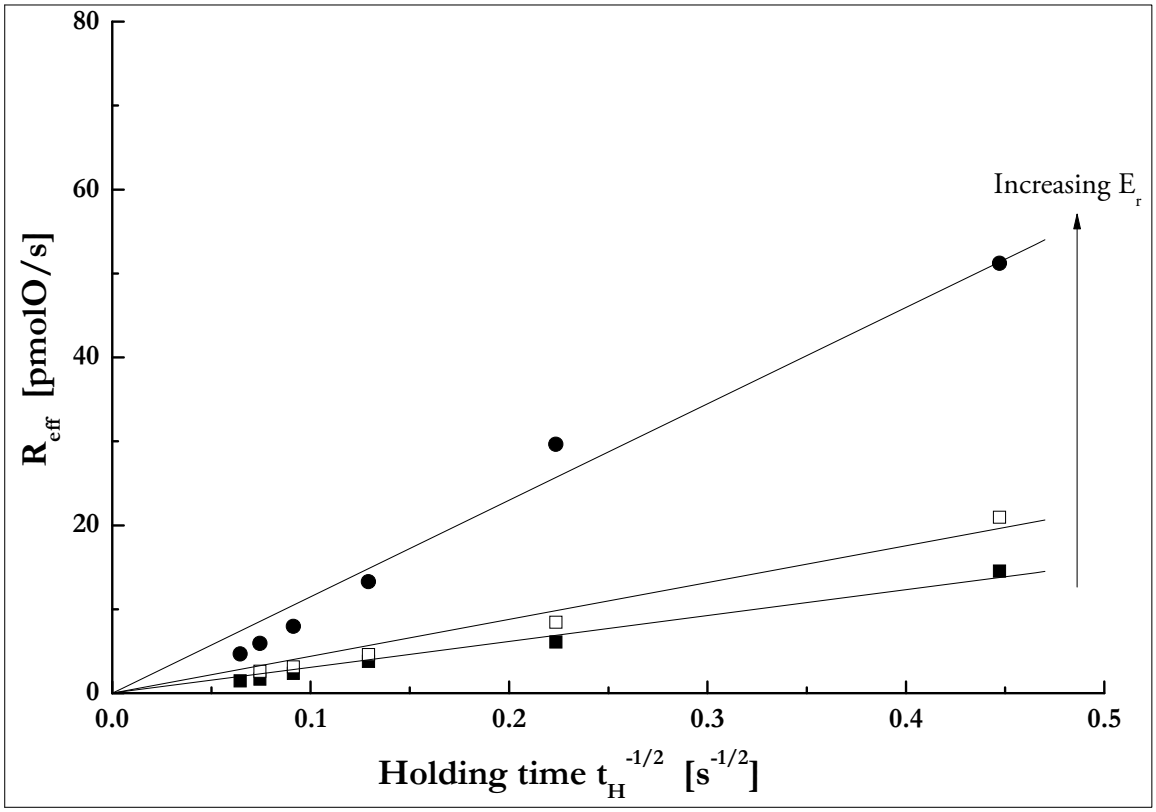

Fig. V-7 : Effective rate of NiO formation (eq. 5) as a function of $t_H^{1/2}$ for different holding potentials. P_{O2}=20 kPa and T=350°C.

Fig. V-7 shows the variation of R_{eff} (equation V-6) with the reciprocal square root of the holding time, $t_H^{-1/2}$, for three different potentials at 350°C. As shown, a linear correlation between the effective rate (pmolO/s) of the NiO formation and the $t_H^{-1/2}$ is observed.

V.3.3 Influence of temperature

In order to evaluate the effect of temperature on the effective rate of NiO formation, similar experiments were performed at higher temperatures.

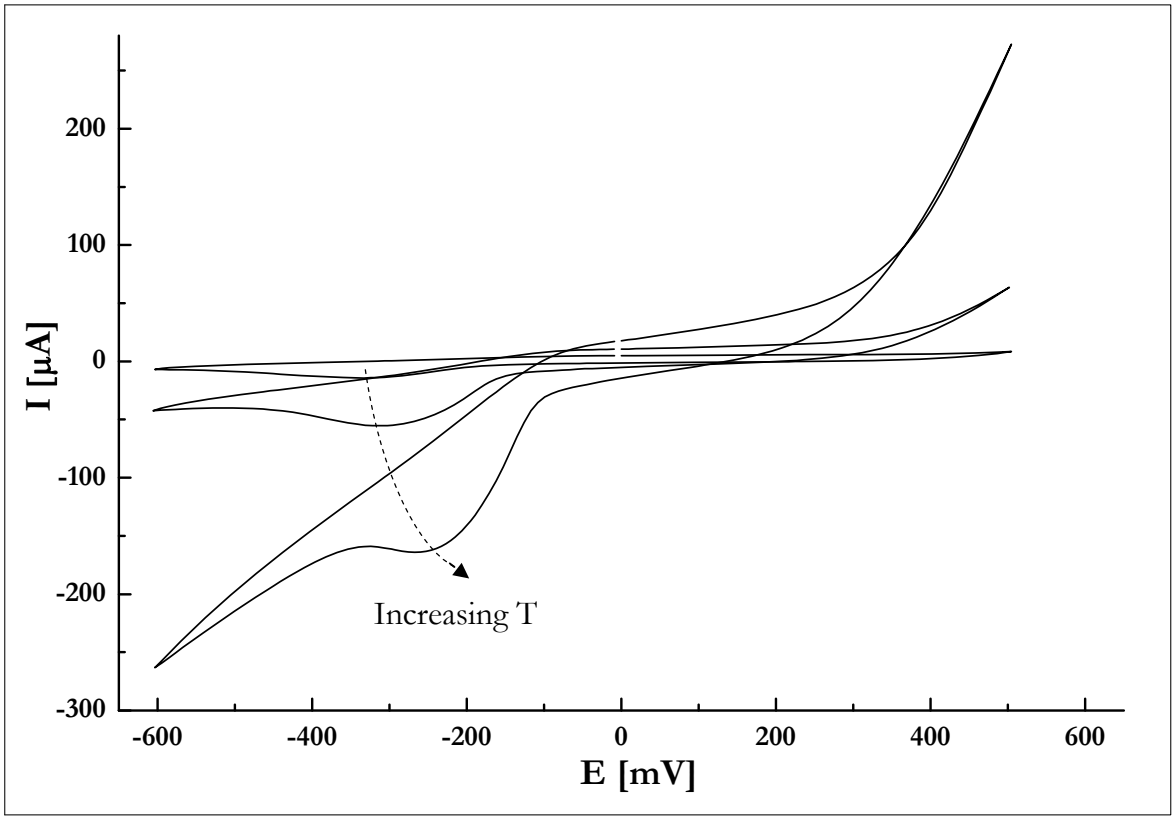

Fig. V-8 : Effect of temperature on the voltammogram of Ni/YSZ system. P_{O2}=20 kPa, υ=20mV/s and T=350°C.

Fig. V-8 shows voltammograms of the Ni /YSZ system carried out at 350, 400 and 450°C. This figure shows that increasing the temperature, the general shape of the voltammogram remains almost the same; however, the current peak increases strongly. The calculated current efficiency for NiO formation (η_{NiO}) at holding potential E_H = 400mVand for three different temperatures 350, 400, and 450°C is presented in Fig. V-9. This figure shows that increasing temperature results in a rapid decrease of η_{NiO}.

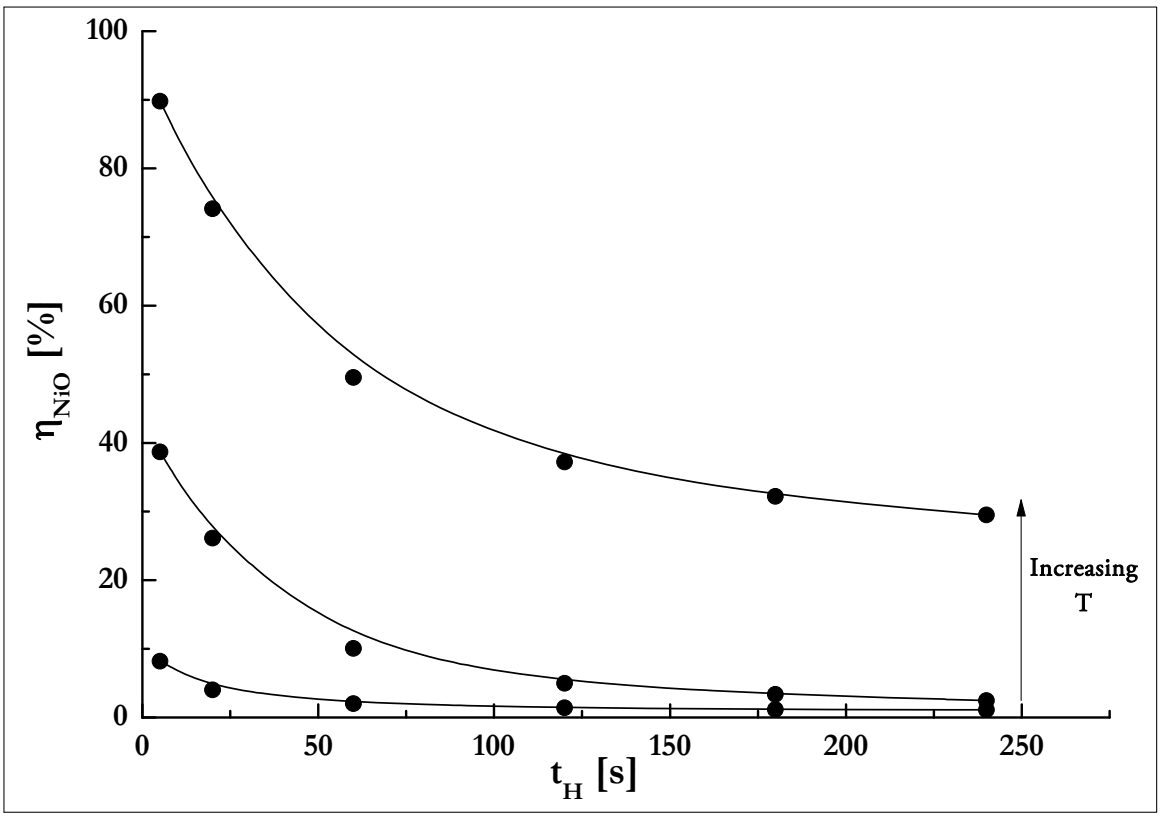

Fig. V-9 : Effect of holding time, t_H, on the oxidation efficiency of NiO formation, η_{NiO}, for three different temperatures; 350°C, 400°C and 450°C. P_{O2}=20 kPa, Ea=400mV

V.4 General discussion

Upon anodic polarization of the Ni/YSZ interface two parallel reactions take place:

- Formation of NiO (equation V-1)
- Oxygen evolution (equation V-3)

For low polarization times the NiO formation is the main reaction. However, after few seconds of polarization the reaction of oxygen evolution dominates. This behavior is certainly related with the formation of NiO scale which seems to induce an auto-inhibition of NiO growth without effecting the oxygen evolution reaction.

The $t^{1/2}$ dependence of the effective rate of NiO formation (Fig. V-7) allows to suggest the following parabolic law (equation V-6) for the effective rate of NiO formation upon anodic polarization:

$$R_{eff} = k_p(\eta, T)t_H^{-1/2} \qquad \text{V-7}$$

where, $k_p(\eta,T)$ is the parabolic law constant, depending on the applied overpotential (η) and temperature (T).

This approach is similar to the model proposed by *Wagner* [5] and *Hoar* & *Price* [6] for high temperature oxidation of metals exposed to oxygen.

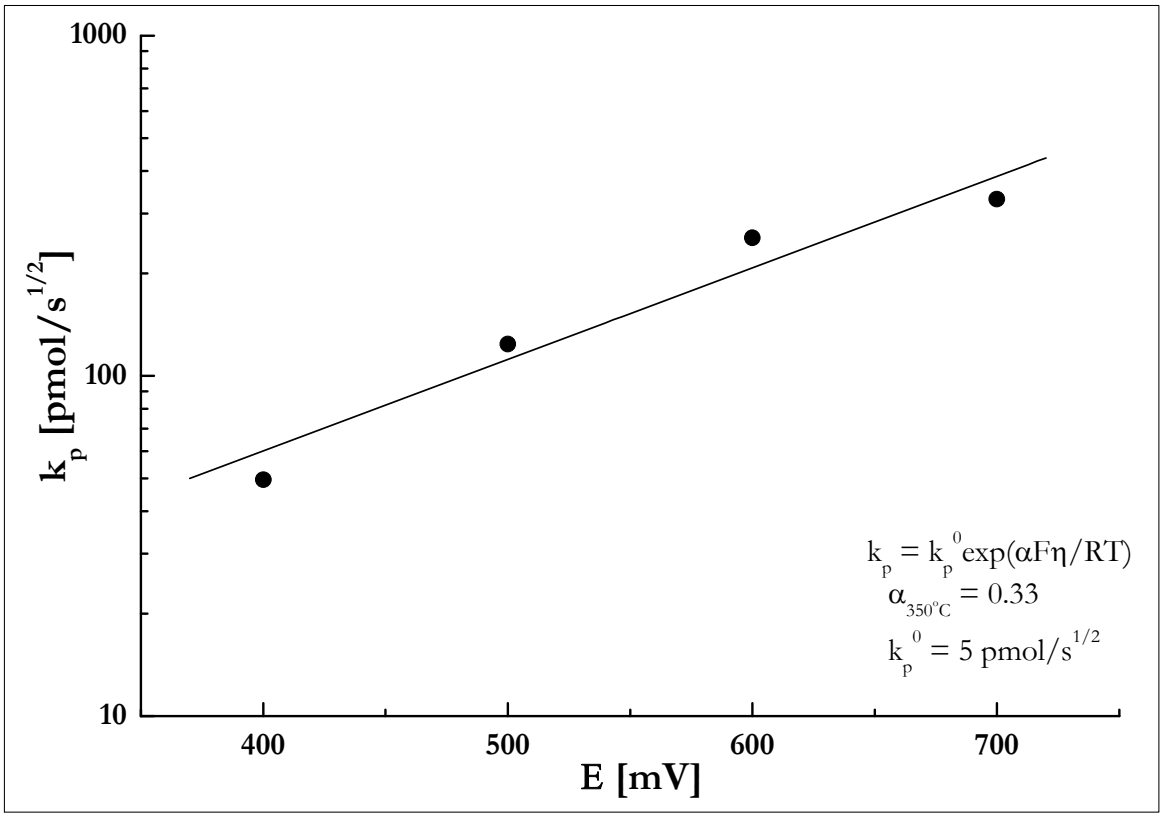

Fig. V-10 : Effect of holding anodic potential, E_H, on the parabolic law constant, k, (equation V-7). P_{O2}=20kPa T=350°C.

The dependence of the parabolic law constant on the applied potential can be given by the relation:

$$k_p = k_p^0 \exp(\alpha F\eta / RT) \qquad \text{V-8}$$

where, k_p^0 is the parabolic law constant at open circuit (η = 0), *a* the charge transfer coefficient, *F* the Faraday number and $\eta = E\text{-}E_{oc}$ (E_{oc}: open circuit potential).

The two parameters of this relation (k_p^0 and α) can be calculated from Fig. V-10 where *log(k_p)* is plotted as a function of overpotential, η, at 350°C.

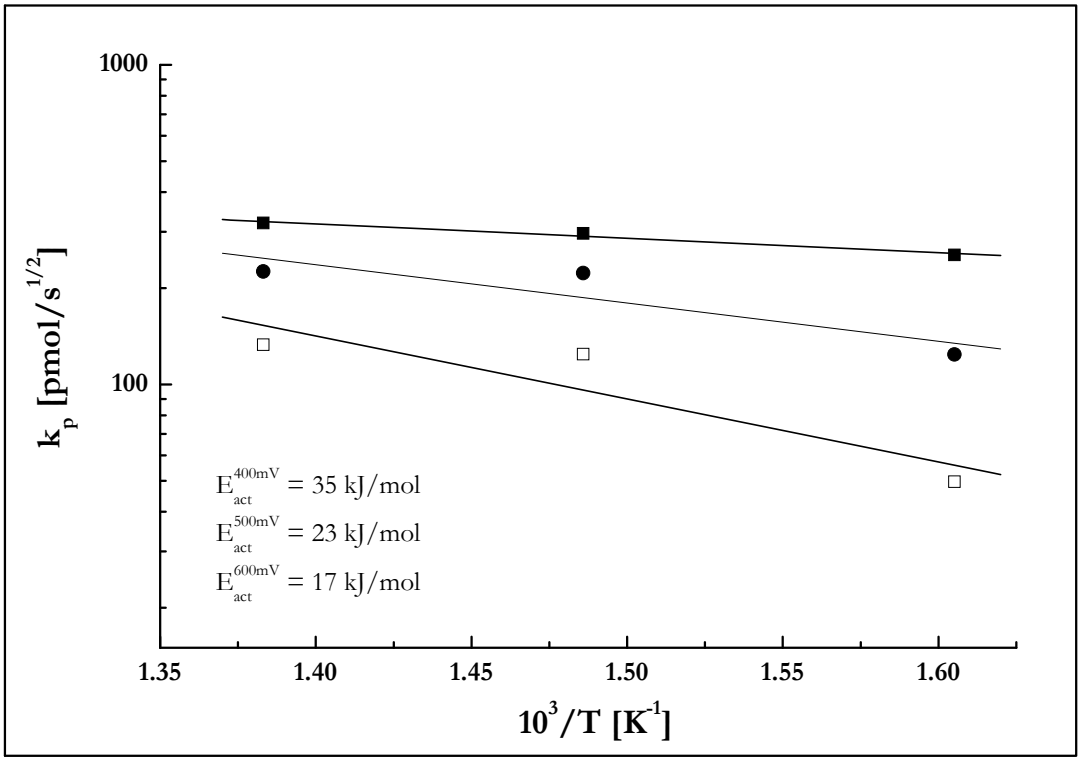

Fig. V-11 : Typical Arrhenius plot of the NiO formation kinetics for 3 anodic holding potential values; 400, 500 and 600 mV. P_{O2}=20kPa T=350°C.

The dependence of parabolic law constant, k_p, on applied overpotential at 350°C can be given by the relation:

$$k_p = 5\exp(0.33F\eta / RT) \text{ / pmol/s}^{1/2} \qquad \text{V-9}$$

The influence of temperature on the rate constant of NiO growth can be evaluated from activation energy determination using Arrhenius plots at different applied potentials (Fig. V-11). The obtained apparent activation energy (E_{act}) decreases from 35 kJ/mol to 17 kJ/mol by increasing the anodic overpotential form 400 to 600 mV.

V.5 Proposed model

Initially, before any anodic polarization, one can consider a pure Ni electrode, and thus a Ni/YSZ interface. By anodic potential application, NiO formation occurs at the interface with high η_{NiO}. This is a two step process; oxidation of Ni to Ni^{2+} (equation V-10) and the combination of Ni^{2+} with O^{2-} (equation VI-12) coming from the reduction of O_2 at the cathode, according to (equation VI-11):

Anode : $Ni \rightarrow Ni^{2+} + 2e^{-}$ **V-10**

Cathode : $1/2O_2(g) + 2e^{-} \rightarrow O^{2-}$ **V-11**

Interface : $Ni^{2+} + O^{2-} \rightarrow NiO$ **V-12**

The global cell reaction is:

$$Ni + 1/2O_2(g) \rightarrow NiO \quad \textbf{V-13}$$

After anodic polarization resulting in a complete coverage of the Ni surface by a NiO layer, two new interfaces are created; Ni/NiO and NiO/YSZ together with the three phase boundary (t.p.b.) NiO/YSZ/O_2.

The rate of NiO formation at the NiO/YSZ interface is controled by reaction V-12 involving outward diffusion of Ni^{2+} (when fresh NiO is formed at the NiO/YSZ interface) or inward diffusion of O^{2-} through the oxide film (NiO is formed at the Ni/NiO interface).

It is worthwhile to mention that this ionic diffusion process, in the domain of working temperature (<450°C), is not a bulk diffusion but takes place along grain boundaries. Moreover, as the reported diffusivity of Ni^{2+} in NiO is ~10 orders of magnitude greater than O^{2-} diffusivity [16] we can consider that Ni^{2+} diffusion through the NiO scale, resulting in the formation of fresh NiO at the NiO/YSZ interface, is the rate determining step in NiO growth under anodic polarization.

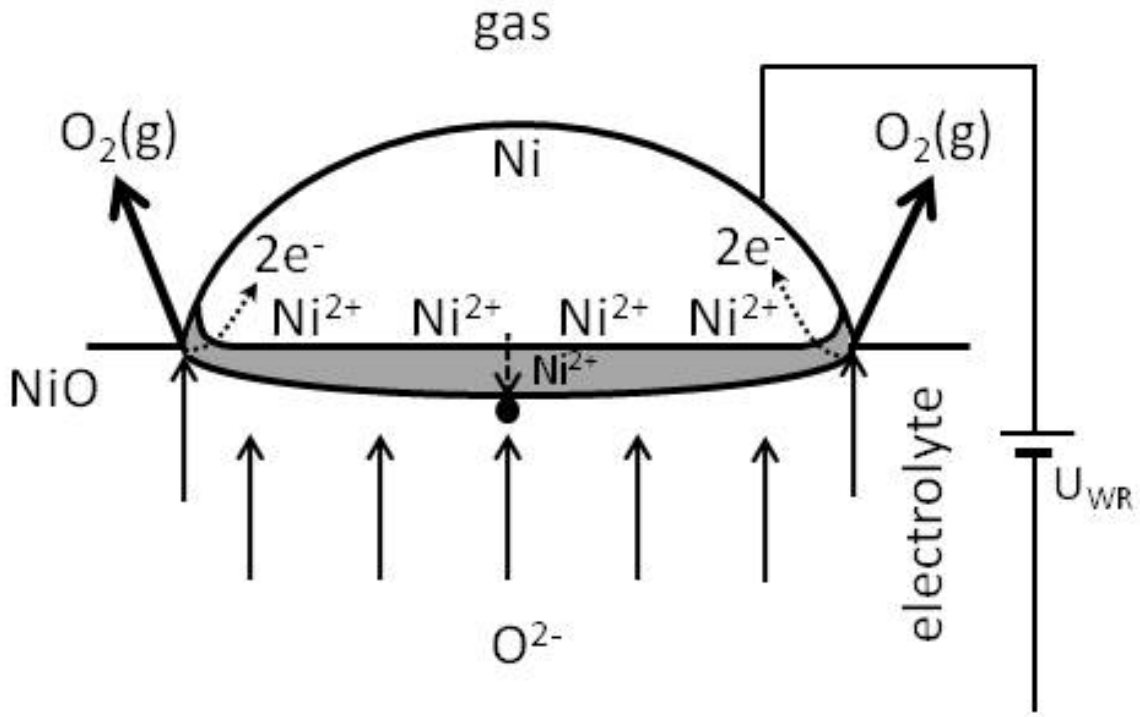

Fig. V-12 : Schematic representation of the oxidation process during anodic polarization.

The above consideration of Ni^{2+} diffusion as rate determining step is similar to *Wagner's* theory at high temperatures [5]. A difference between *Wagner's* (chemical oxidation with $O_{2(g)}$) and the current model constitutes the mean of oxygen supply for Ni oxidation, *i.e.* O_2 from the gas phase or O^{2-} from the electrolyte support, respectively. The parabolic growth law proposed by *Wagner* in the chemical oxidation of Ni by O_2 is also applied in our study (equation V-13), as in both systems the r.d.s. is the diffusion of Ni^{2+} through NiO. Concerning O_2 evolution reaction, which takes place at the t.p.b., the rate of this reaction is not firmly affected by the presence of the oxide scale, since electron transfer can occur by electron tunneling through NiO to the Ni electrode resulting in O_2 evolution at the NiO-YSZ-$O_{2(g)}$ t.p.b. (Fig. V-12).

V.6 Conclusions

In this study, the cyclic voltammetry technique has been used for the electrochemical investigation of a Ni electrode supported over an YSZ solid electrolyte pellet in the temperature range between 350° and 450°C. It has been found that NiO is electrochemically formed by the O^{2-} species supplied from the electrolyte upon anodic polarization. Moreover, the NiO scale grows according to the parabolic growth law, in agreement with *Wagner's* oxidation theory of metals at high temperatures. A model for the NiO initial formation has been proposed, where NiO is formed at the Ni/YSZ interface and grows by the outward diffusion of Ni^{2+} species through the NiO layer, which is determined as the rate limiting step. This implies for the auto-inhibition of NiO formation by its continuous growth. This is similar to *Wagner's* theory; however, a difference between *Wagner's* and the current model is the mean of supplying oxygen for the oxidation of Ni, which is the O_2 of the gas phase or O^{2-} from the electrolyte support, respectively. Also, it has been found that O_2 evolution reaction is not firmly affected by the oxide formation, since it occurs and is controlled by electron tunneling though NiO to the Ni electrode. An apparent activation energy of the limiting outward Ni^{2+} diffusion process has been calculated (35 kJ/mol under E_H = 400 mV) and has been found to decrease by increasing potential.

V.7 References

1. C.Y. Yang and H.S. Isaacs, J. Electroanal. Chem., 123, 411 (1981).
2. C.Y. Yang and W.E. O'Grady, J. Vac. Sci. Technol., 20, 925 (1982).
3. D. Gozzi, M. Tomellini, L. Petrucci and P.L. Cignini, J. Electroch. Soc., 134, 278 (1987).
4. P.A. van Manen, R. Weevver and J.H.W. de Wit, J. Electrochem. Soc., 139(4), 1130 (1992).
5. C. Wagner, Z. Physik. Chem., B21, 25 (1933).
6. T.P. Hoar and L.E. Price, Transactions of the Faraday Society, 34, 867 (1938).
7. D. Landolt, Materials Today, 10, 57 (2007)

8. A. Jaccoud, C. Falgairette, G. Fóti and C. Comninellis, Electrochim. Acta, 52, 7927 (2007).
9. G. Fóti, A. Jaccoud, C. Falgairette and C. Comninellis, J. Electroceram., 23, 175 (2009).
10. A. Jaccoud, G. Fóti, R. Wuthrich, H. Jotterand, C. Comninellis, Top. Catal., 44, 409 (2007).
11. C. Falgairette, A. Jaccoud, G. Fóti and C. Comninellis, J. Appl. Electrochem., 38, 1075 (2008).
12. A.J. Bard and L.R. Faulkner, Electrochemical Methods: Fundamentals and Applications, J. Wiley, New York (1980)
13. N. Birks, G.H. Meier and F.S. Pettit, High temperature oxidation of metals, Cambridge (2006).
14. A. Atkinson and R.I. Taylor, J. Mater. Sci., 13, 427 (1978).
15. W.W. Smeltzer and D.J. Young, Progress in Sol. St. Chem., 10(1), 17 (1975).
16. A. Atkinson, D.P. Moon, D.W. Smart and R.I. Taylor, J. Mater. Sci., 21, 1747 (1986).

CHAPTER VI- ELECTROCHEMICAL INVESTIGATION OF THE Pt/YSZ SYSTEM

The electrochemical investigation of a sputtered platinum electrode is performed at atmospheric pressure (20 kPa O_2 in He) in the temperature range of 250°C-375°C. Under anodic polarization two reactions take place, oxygen evolution reaction at the triple phase boundary and PtO formation at the Pt/YSZ interface. Cyclic voltammetric investigation was used to quantify the influence of both processes by determining their respective current efficiencies. PtO formation is found to be an auto-inhibited reaction with different kinetic regimes depending on the applied potential. Finally, with regard to the *Wagner* oxidation theory and the *Eley* & *Wilkinson* place exchange mechanism, an original electro-oxidation model is proposed for the $O_{2(g)}$,Pt/YSZ system.

VI.1 Introduction

The great majority of studies involving Pt/YSZ interface, are performed at high temperature (T > 300°C) and under atmospheric pressure [1]. However, in the field of solid state electrochemistry, the preparation procedure of the sample is of primary importance. In fact, although the chemical composition of a conductive electrode is identical, depending on the deposition technique (paste thermal decomposition, screen printing, sputtering or pulsed laser deposition) the experimental results obtained and their interpretation may greatly differ [2-6]. In addition, the cell microstructure which has a major impact on the electrochemical behavior may also be affected by temperature increase (sintering effects) and upon extensive use (aging effects). Worth to notice that these morphological impacts are comonly the source of reproducibility problems and that they are frequently discussed or mentioned in the literature [7, 8].

In this work, in order to minimize these problems, it was chosen to prepare the working electrode by magnetron sputtering technique and to stabilize its structure by thermal pre-treatment. The morphological investigation performed on the so prepared Pt/YSZ samples revealed a stable Pt film, statistically (111) oriented and presenting a macroporous structure, *i.e.* a large amount of triple phase boundaries (tpb). Investigation by cyclic voltammetry is performed at high temperature (250°C < *T* < 375°C) under atmospheric pressure in the previously described setup.

VI.2 Experimental

VI.2.1 Deposition of Pt on YSZ by sputtering

Platinum film electrodes were deposited by magnetron sputtering technique in inert atmosphere (Ar) at room temperature on a rectangular YSZ (8mol% Y_2O_3-stabilized ZrO_2 Technox 802, Dynamic Ceramic Ltd) pellet (10 mm x 15 mm) of 1 mm thickness. Direct current (dc) mode was used with a discharge of 330 V at an argon pressure of 10^{-2} mbar.

Under these conditions, 1 μm thick Pt electrodes were deposited with a deposition rate of 0.09 nm s^{-1} on the YSZ pellet, as determined by profilometric measurement (Alphastep, Model 500) of the film deposited on smooth silicon samples processed simultaneously.

The solid electrochemical cell used in this work consists of three electrodes deposited on YSZ solid electrolyte. The working and counter electrodes were located in a symmetrical face-to-face arrangement on the opposite sides of the YSZ pellet ensuring a symmetrical current and potential distribution in the cell during electrochemical investigations [9]. The electrodes size is 7 x 5 mm giving a geometric surface of 0.35 cm^2 for each of them (Fig. VI-1).

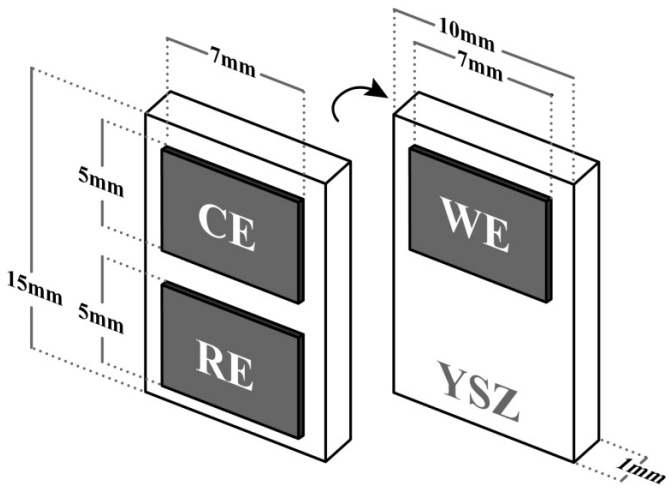

Fig. VI-1 : Placement and dimensions of the Pt electrodes prepared by sputtering. WE: working electrode; CE: counter electrode; RE: reference electrode.

Before use, a pretreatment process including a calcination step at 700°C for 4h in air was performed in order to obtain a stable surface structure during the electrochemical measurements in the whole examined temperature range [8].

VI.3 Pt/YSZ film morphological characterization

Each sample morphology was characterized before any electrochemical investigation by high-resolution scanning electron microscopy (HRSEM, Leo Gemini 982). The

crystallographic structure and orientation were analyzed by X-ray diffraction (XRD, 2 θ = 10°–90°, Bragg–Brentano diffraction geometry, Cu–Kα radiation, V = 40 kV, I = 30 mA).

VI.3.1 Scanning Electron Microscopy

The as-sputtered platinum electrode (left image inFig. VI-2) presents a very compact layer with nearly no porosity, as expected for the sputtering deposition technique. The layer follows the topography of the YSZ substrate. However, after heat treatment at 700 °C in 20 kPa of O_2 for 4 h, the Pt film is strongly modified resulting in the formation of agglomerates and the appearance of YSZ substrate, (right image in Fig. VI-2). This film discontinuity, observed after the thermal treatment, has been already reported by *Jaccoud* [8, 10]. From SEM images we can estimate that in this new structure only 60% of the YSZ is covered by Pt. The estimated three phase boundary (tpb) length can be estimated from SEM images to 370m/cm^2.

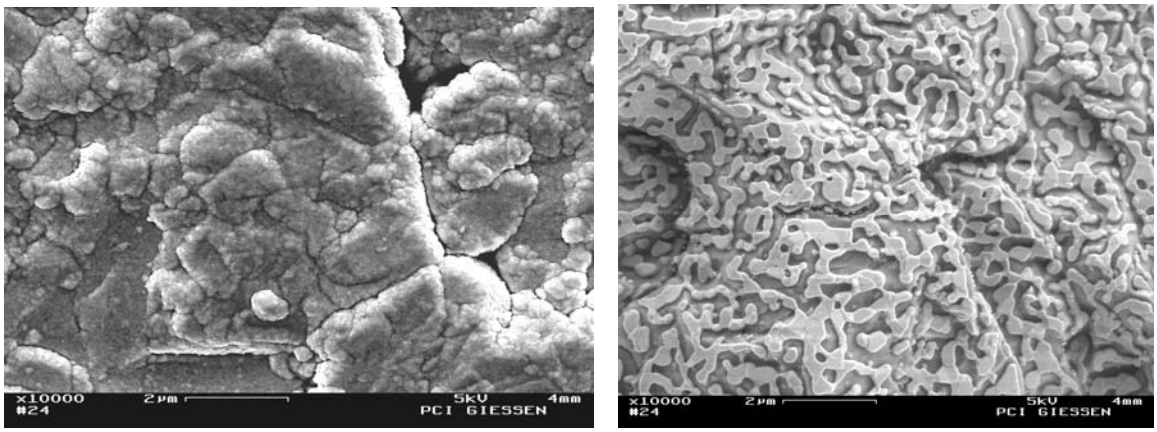

Fig. VI-2 : SEM pictures of the as-sputtered electrode (left) and after heat treatment at 700 °C in 20 kPa of O_2 for 4 h (right).

VI.3.2 X-Ray Diffraction

XRD analysis was performed on both polycrystalline YSZ(8%) substrate (Fig. VI-3) and YSZ Pt sputtered electrode (Fig. VI-4). Even if several crystallite orientations are observed, majority of the crystallites has a (111) orientation, and the substrate can then be considered as statistically (111) oriented.

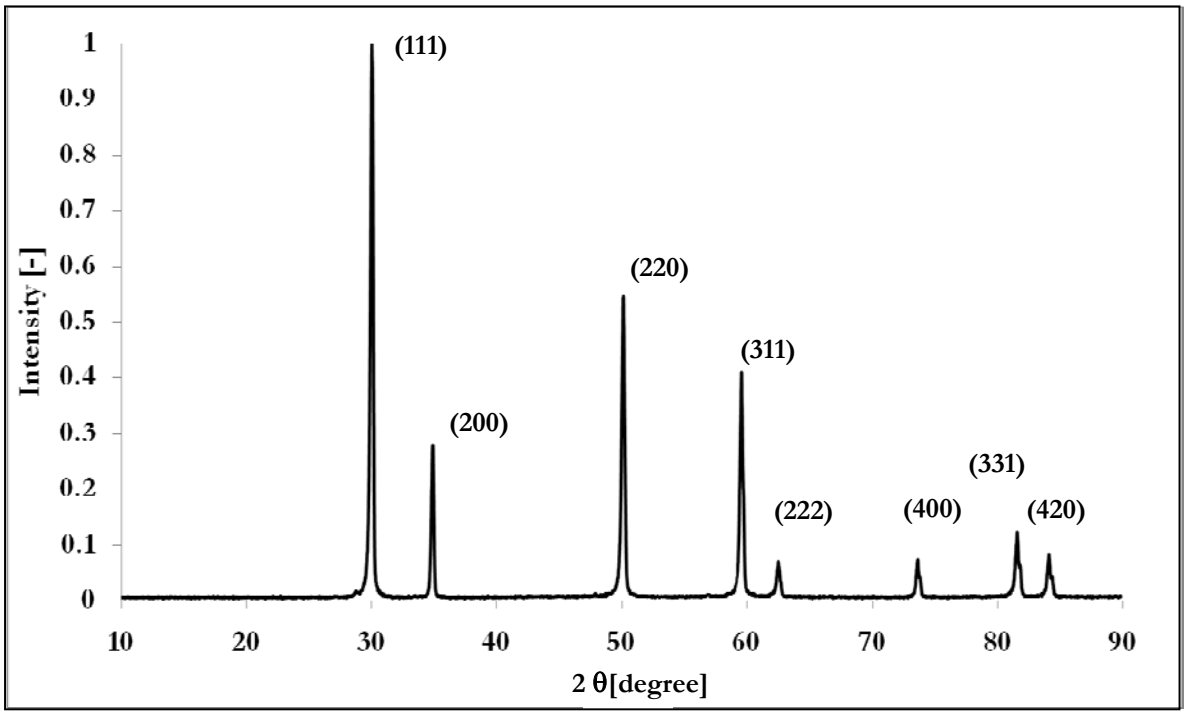

Fig. VI-3 : XRD pattern of polycrystalline YSZ(8%)

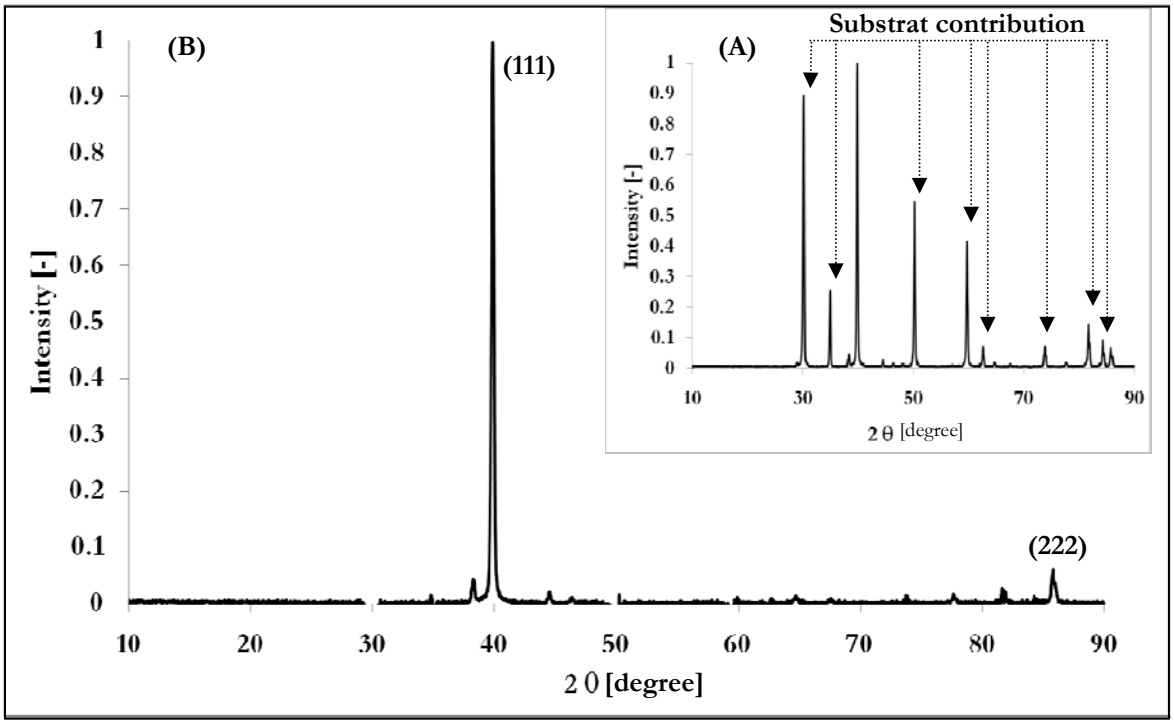

Fig. VI-4 : XRD pattern of sputtered platinum electrode. YSZ substrate before (A) and after (B)substraction of the XRD pattern of YSZ.

The XRD pattern of the Pt sputtered electrode after treatment at 700°C (20kPa O_2, 4h) is presented in Fig. VI-4 before (A) and after (B) subtraction of the XRD pattern of YSZ substrate. This figure shows that the platinum crystallites are mainly (111) oriented. Furthermore, by using the Scherrer equation the crystallite average size is estimated to be 32 nm.

VI.3.3 Discussion

Deposition of Pt by sputtering on YSZ substrate leads to an uniform film following the substrate topography. However, the as-deposited film did not show a good stability upon long term electrochemical measurements. *Jaccoud* [8] proposed to stabilize the structure by thermal pretreatment at 700°C for 4 hours in 20 kPa O_2. This pretreatment leads to a dramatic change of the film leading to a network of (111) oriented crystallites covering only 60% of the YSZ substrate and resulting in the formation of macro pores of few hundreds of nanometers. This results in an increase of the triple phase boundary length (estimated at 370m/cm^2) and concomitant binary Pt/YSZ interface decrease (0.2cm^2).

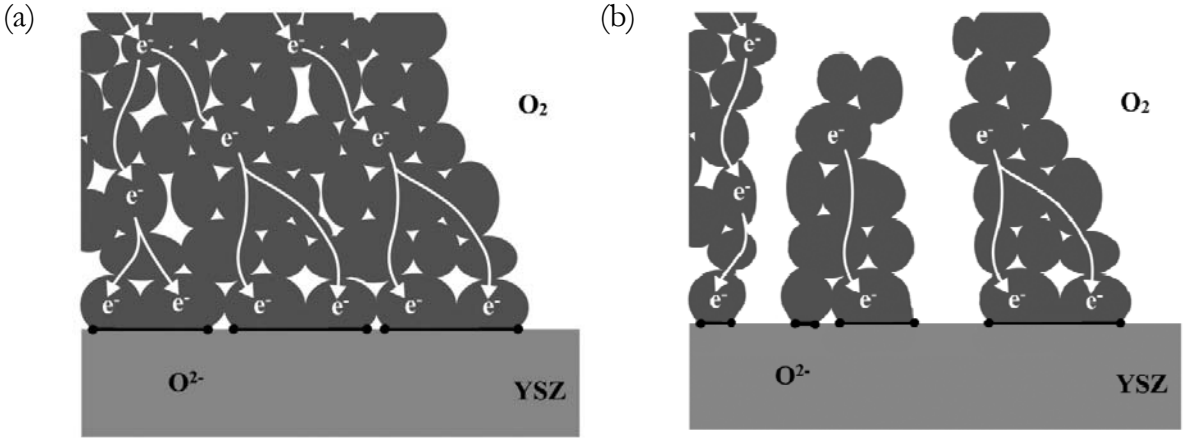

Fig. VI-5 : Schematic morphology of sputtered Pt/YSZ electrode before (a) and after (b) thermal treatment at 700°C during 4 hours.

VI.4 Electrochemical investigation

This electrochemical investigation of platinum film sputtered on YSZ(8%) polycrystalline substrate (Pt/YSZ) is performed by cyclic voltammetry in 20kPa O_2 in He. The influence of anodic reverse potential, temperature, anodic holding time and oxygen partial pressure has been first investigated.

VI.4.1 Influence of anodic reverse potential

In this first series of experiment, the potential of the Pt working electrode is cycled (20 mV s^{-1}) in a defined domain of potential at 325°C in 20% O_2 in He. The lower limit is fixed at E_c=-500mV while the upper limit, *i.e.* the anodic reverse potential, E_a, is increased from 50mV to 500mV by steps of 50mV (Fig. VI-6).

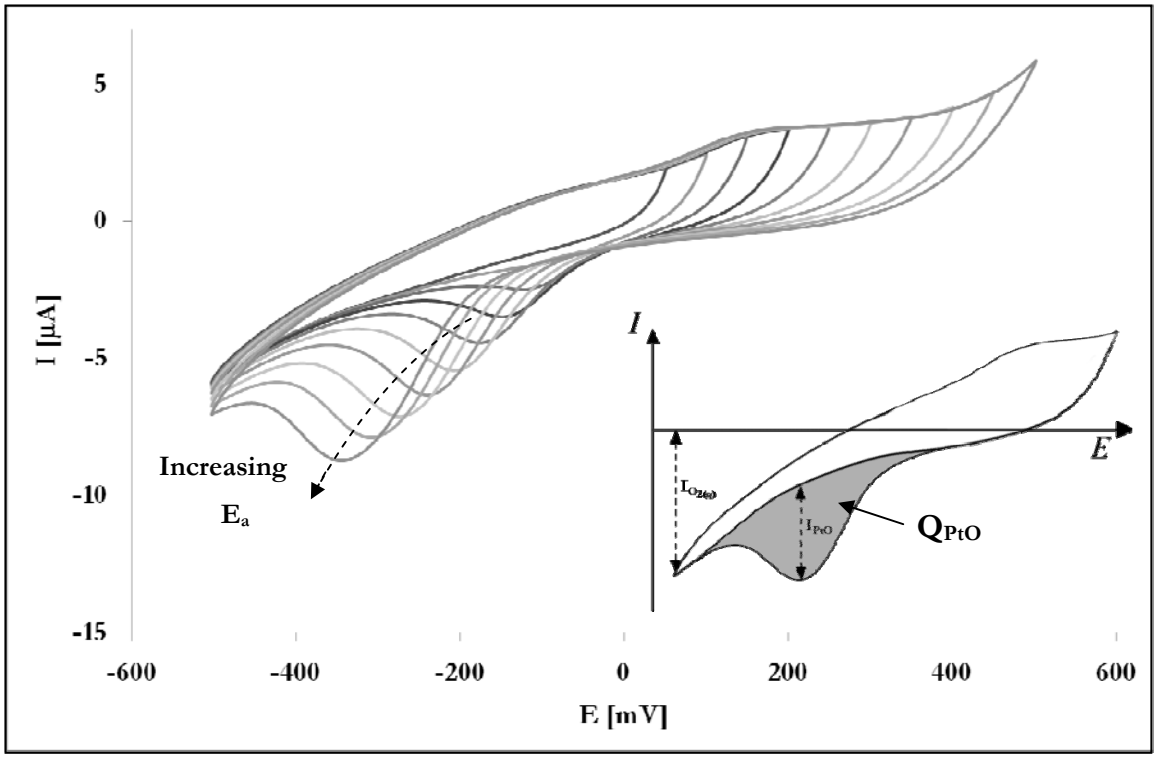

Fig. VI-6 : Effect of anodic reverse potential E_{ra} increase from 50mV to 500mV by steps of 50mV on the cyclic voltagemogram of Pt/YSZ. Insert : determination of the charge involved in the cathodic peak related to PtO reduction. T=325°C, p_{O2}=20 kPa, v=20mV s^{-1}.

For anodic reverse potentials lower than 100mV, no cathodic peak is observed, however as the anodic reverse potentials is set at 150mV, a small cathodic peak is observed at -100mV. By increasing E_{ra}, the cathodic peak grows and shifts to more negative values. In the anodic part of the voltammograms the current forms a plateau at 3μA between 150mV and 450mV and at higher anodic overpotential it increases sharply.

Upon an electrochemical stimulation of the $O_{2(g)}$,Pt/YSZ system, two electrochemical reactions may take place, *i.e.* the oxygen evolution/reduction reaction (equation VI-1) taking place at the triple phase boundary and the oxidation/reduction of platinum electrode (equation VI-2) occurring mainly at the binary Pt/YSZ interface.

$$O^{2-} \rightleftarrows \frac{1}{2} O_{2(g)} + 2e^{-} \qquad \textbf{VI-1}$$

$$Pt + O^{2-} \rightleftarrows PtO + 2e^{-} \qquad \textbf{VI-2}$$

The measured voltammograms is then composed of both contributions.

The amount of the formed PtO is performed by integration of the cathodic peak (insert of Fig. VI-6) considering equation VI-2 then plotted as a function of the anodic reverse potential. This represents the amount of platinum oxide formed and stored in the electrochemical cell during the anodic polarization (Fig. VI-7). This figure shows that between 50mV and 500mV, a linear relationship is obtained between the amount of formed PtO and the anodic reverse potential. Considering that 60% of the YSZ is covered by Pt and a Pt monolayer consists of 10^{15} atoms, the estimated amount of formed PtO corresponds to about 0.5 equivalents PtO monolayer at 500mV.

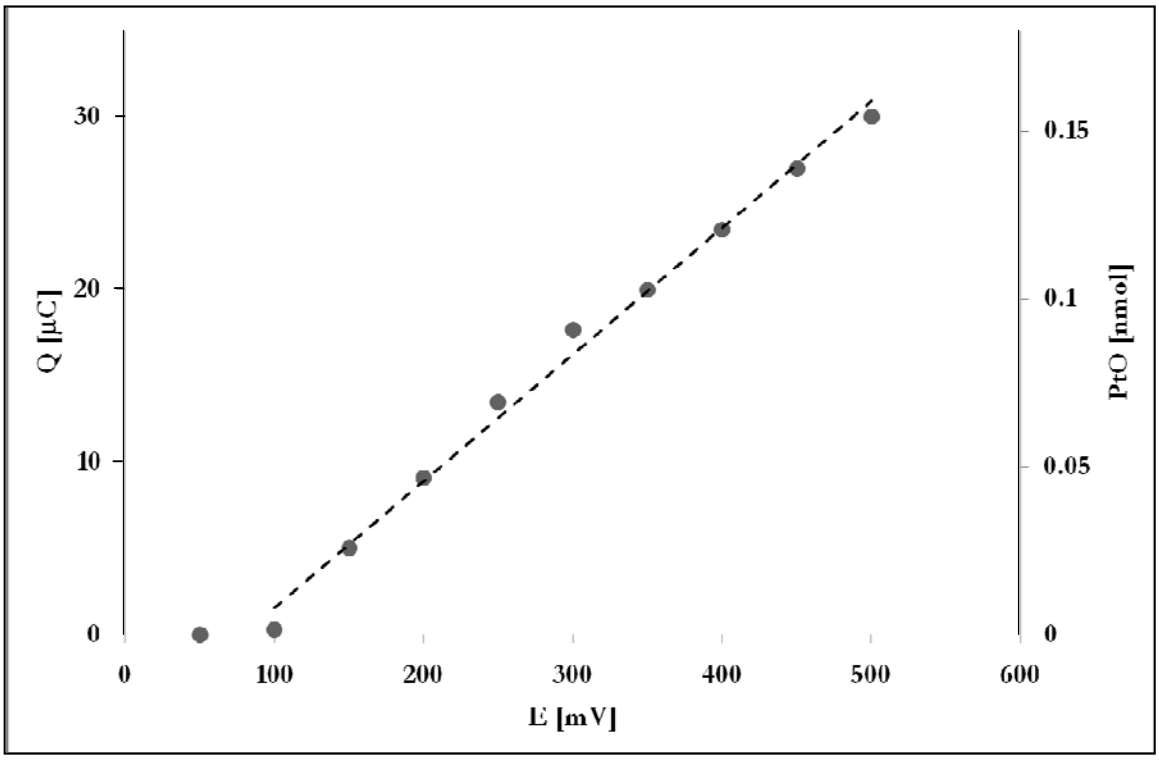

Fig. VI-7 : Evolution of the cathodic charge estimated by peak integration and equivalent amount of formed PtO upon the increase of the anodic reverse potenital. T=325°C, p_{O2}=20 kPa, v=20mV s^{-1}.

VI.4.2 Influence of the scan rate

The influence of scan rate on the voltammogram is presented inFig. VI-8. The experiments are performed at 325°C under 20kPa O_2 in He in a fixed potential domain (+400mV/-600mV).

Both in the anodic and cathodic part of the voltammogram, the current increases with scan rate. Furthermore, the peak potential for PtO reduction shifts to more negative values as the scan rate is increased. As presented in the insert of Fig. VI-8, a linear relationship is obtained between the peak potential of PtO reduction and the logarithm of the scan rate. Furthermore, both the anodic current (at 400mV) and cathodic peak current depend linearly on the inverse square root of the scan rate. Finally, the cathodic charge of PtO reduction decreases with the scan rate.

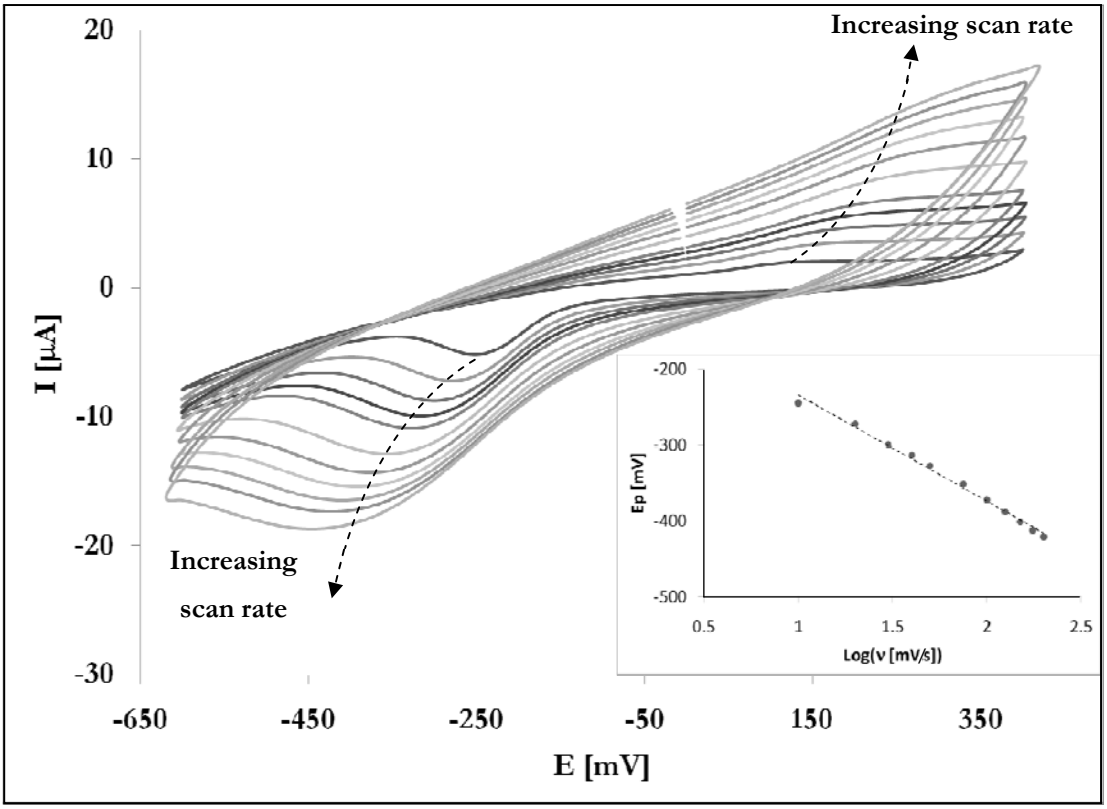

Fig. VI-8 :Influence of scan rate on the measured voltammograms. (1) 10mV s^{-1}, (2) 20mV s^{-1}, (3) 30mV s^{-1}, (4) 40mV s^{-1}, (5) 50mV s^{-1}, (6) 75mV s^{-1}, (7) 100 mV s^{-1}, (8) 125mV s^{-1} (9), 150mV s^{-1}, (10) 175mV s^{-1} and (11) 200mV s^{-1}. Insert gives the dependence of the cathodic peak potential on the logarithm of the scan rate. T=325°C, p_{O2}= 20kPa.

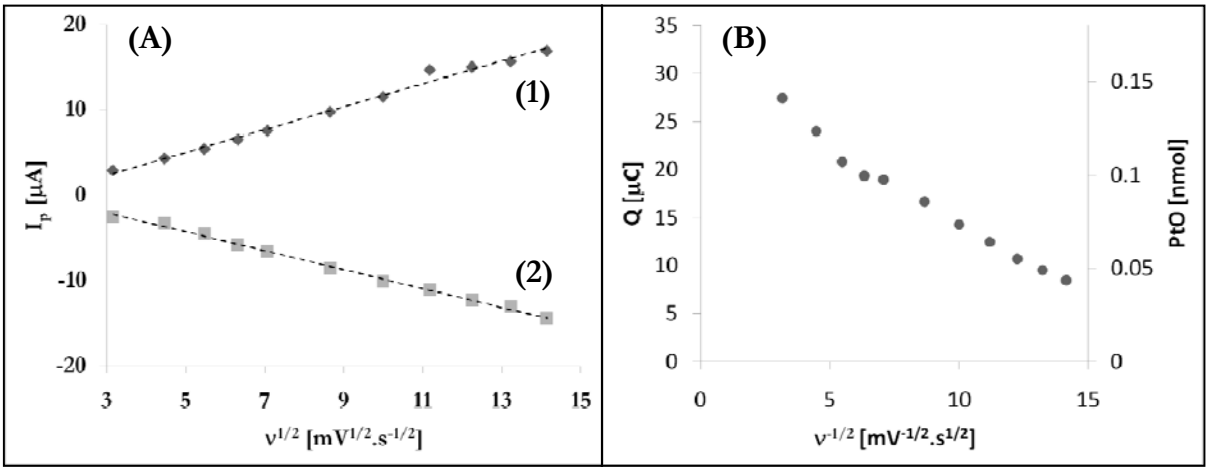

Fig. VI-9 : (A) Evolution of the anodic current at 400mV (1) and cathodic peak current (2) with the inverse square root of the scan rate, and (B) Scan rate dependence of the cathodic charge estimated by peak integration and the equivalent amount of PtO formed. T=325°C, p_{O2}= 20kPa.

The large separation between the anodic and cathodic peaks (Fig. VI-8), the variation of the cathodic peak potential with scan rate (insert of Fig. VI-8) and the decrease of the cathodic charge (related to PtO reduction) with scan rate (Fig. VI-9 B) shows clearly that the electrode presents a fraction of the Pt/YSZ active sites less accessible (inner surface) to reactants. Furthermore, the observed $I\text{-}\nu^{1/2}$ dependence (Fig. VI-9A) gives evidence that limitations due to mass transport are involved in this system.

VI.4.3 Influence of anodic holding time

The anodic holding time of the polarization at 400mV has been varied from 1 to 10 minutes by step of 1 minute in a 20% O_2 in He atmosphere at 325°C. The subsequent cathodic linear potential scans are presented in Fig. VI-10.

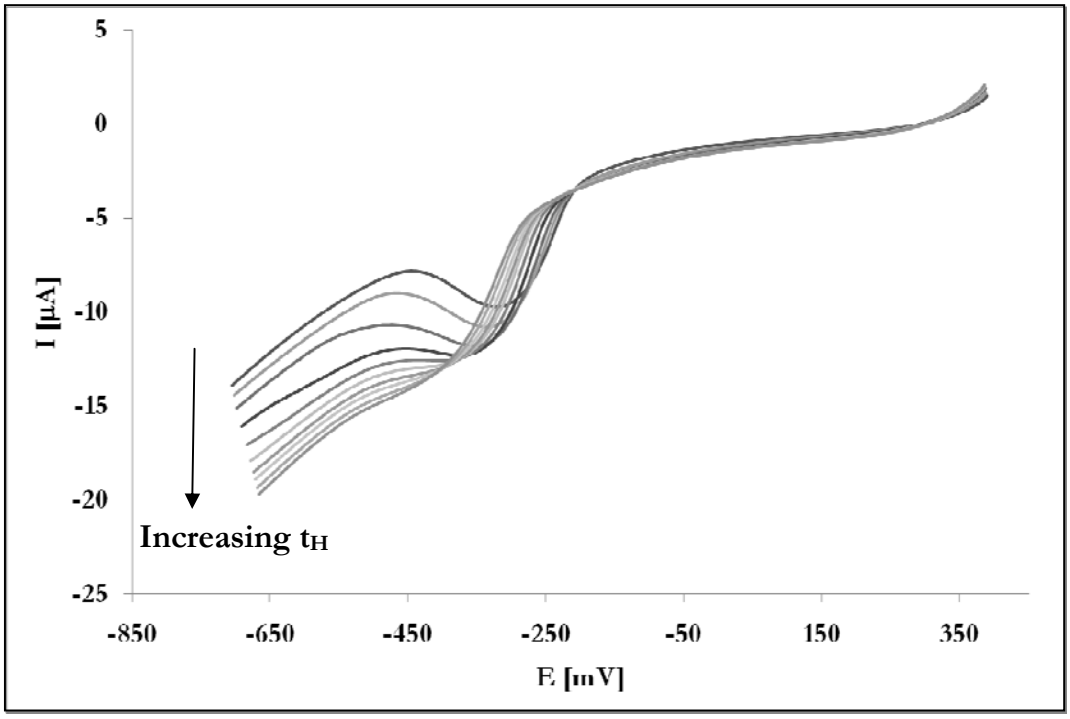

Fig. VI-10 : Linear sweep voltammograms of the sputtered Pt/YSZ electrode. Effect of the holding time t_H = 0s, 60s, 120s, 180s, 240s, 300s, 360s, 420s, 480s, 540s and 600s, at E_{ra}=400mV on the first cathodic scan. T=325°C, p_{O2}=20kPa, ν=20mV s^{-1}

The cathodic reduction peak appears at -250 mV, and then increases and shifts to more negative potentials with increasing holding times. After 10 minutes of anodic polarization the cathodic peak seems to reach saturation. Worthy to notice the increase of current at high cathodic potential (*i.e.* in the domain where oxygen reduction dominates) with increasing holding time.

In order to quantify this behavior of the Pt/YSZ interface under anodic polarization, it is proposed to define the current efficiency for PtO formation (η_{PtO}) by equation VI-3 and for oxygen evolution (η_{O2}) by equation VI-4 during anodic polarization:

$$\eta_{PtO} = \frac{Q_{PtO}}{Q_{Total}} \qquad \textbf{VI-3}$$

$$\eta_{O_{2(g)}} = 1 - \eta_{PtO} \qquad \textbf{VI-4}$$

where Q_{PtO} is determined as shown in Fig. VI-6 (insert) and Q_{Total} is the anodic charge passing through the cell during the anodic polarization step.

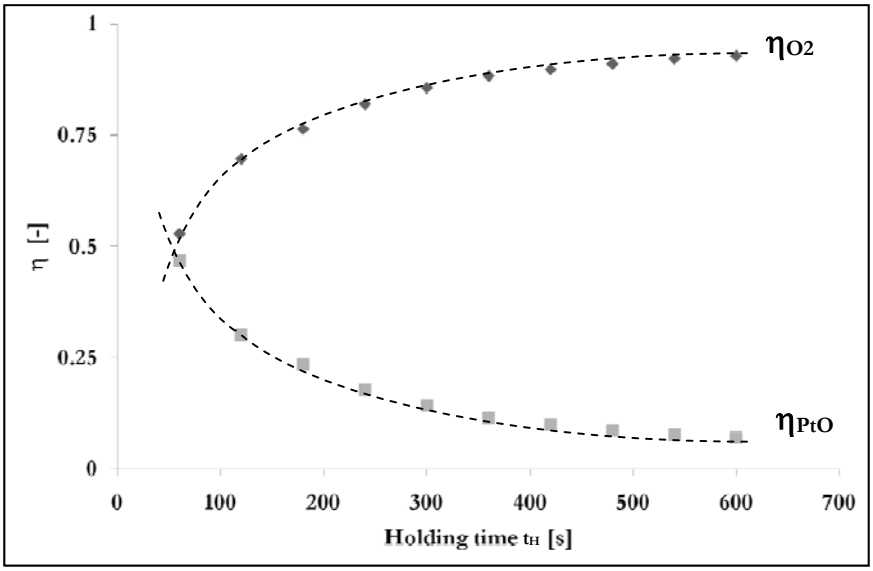

Fig. VI-11 : Effect of the holding time on the current efficiency of PtO formation and O_2 evolution. E_a=400mV, p_{O2}=20kPa, T=325°C.

Fig. VI-11 shows the effect of holding time at a fixed anodic potential (400mV) on both the current efficiency of PtO formation and O_2 evolution. The initial rapid decrease of η_{PtO} and

the concomitant increase of η_{O2} suggest that the forming PtO layer acts as barrier to further oxide growth without effecting the oxygen evolution reaction. Decreasing the value of the holding potential leads to a similar behavior but with a slower kinetic (Fig. VI-12).

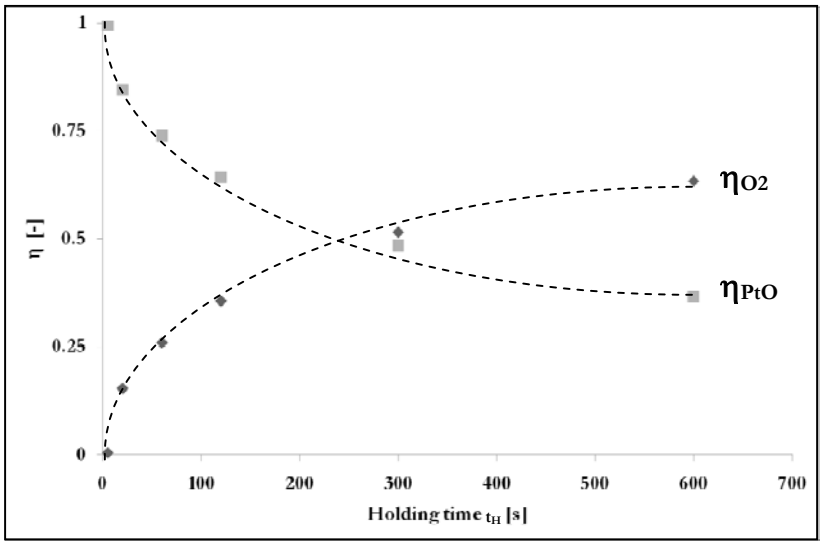

Fig. VI-12 : Effect of the holding time on the current efficiency of PtO formation and O_2 evolution. E_a=100mV, p_{O2}=20kPa, T=325°C.

VI.4.4 Influence of temperature

Fig. VI-13 presents the IR-drop corrected linear sweep voltammograms (20mV s^{-1}) obtained between 400mV and -700mV at various temperatures after anodic polarization of the Pt/YSZ interface at 400mV for 1 hour in 20kPa O_2 in He.

For all investigated temperatures, a reduction plateau is firstly obtained at negative potentials certainly related to platinum oxide reduction (equation VI-2) mainly at the Pt/YSZ interface followed by a rapid increase in current at more negative potentials corresponding to the oxygen reduction reaction (equation VI-1) taking place at the triple phase boundary. However, increasing temperature has a dramatic effect on both reduction potential and current of PtO and O_2 reduction (equation VI-2, VI-1).

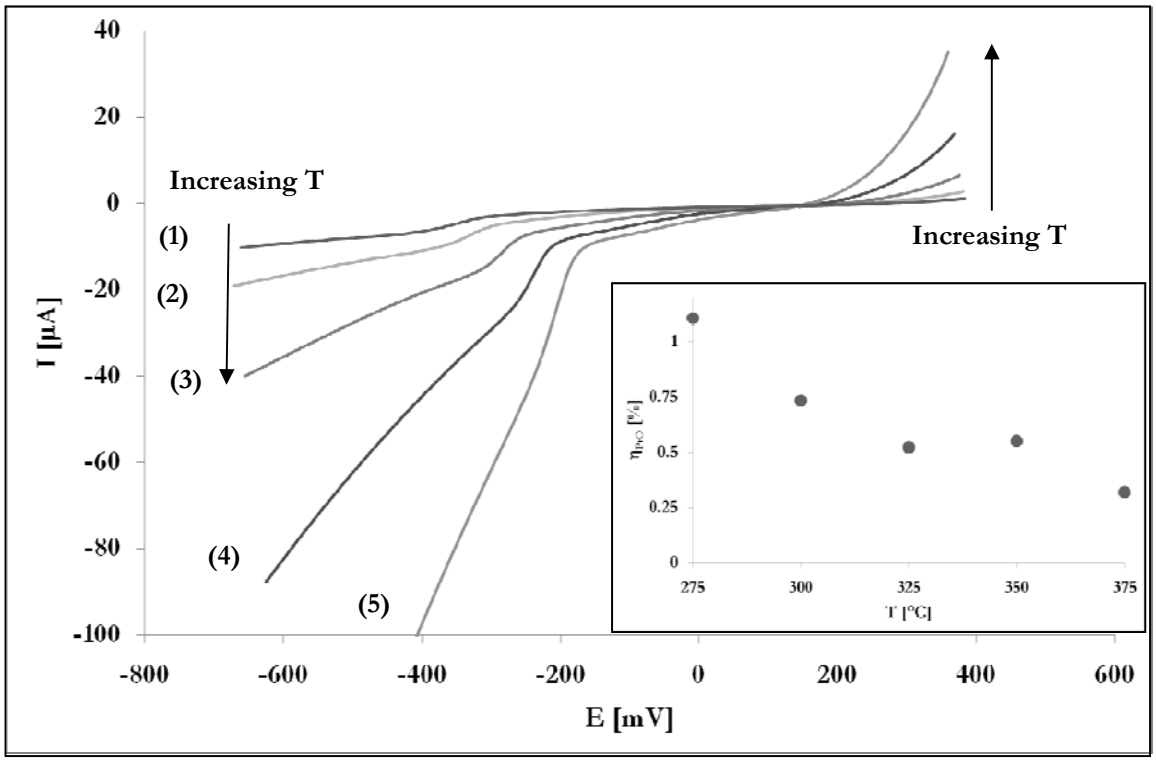

Fig. VI-13 : Linear sweep voltammetry in O_2(g),Pt_{sputt}/YSZ system. Effect of temperature on the first cathodic scan after 1 hour of anodic polarization at 400mV. 275°C (1), 300°C (2), 325°C (3), 350°C (4) and 375°C (5). pO_2=20kPa, ν =20mV/s

In fact the reduction plateau potential of PtO is shifted (from -420mV at 275°C to -280mV at 375°C) while the plateau current increases (from 10µA at 275°C to 45µA at 375°C). Moreover, at higher overpotential the current of O_2 reduction increases strongly, this shows the dramatic impact of temperature on the oxygen reduction reaction at the tpb.

The linear dependence of both PtO and O_2 reduction with respect to the square root of the scan rate found previously allows estimating their activation energy. In case of mass transfer limitation, supposing a semi-infinite linear diffusion of oxidative species, the faradaic current measured in CV is proportional to the square root of the scan rate and the current peak is according to equation VI-5:

$$I_p = 0.99FA\left(\frac{\alpha 2F}{RT}\right)^{1/2} D_{Ox}^{1/2} C_{Ox}^{*} \nu^{1/2} \qquad \textbf{VI-5}$$

where A is the electrode surface area, α is the charge transfer coefficient, D_{Ox} the diffusion coefficient of the O species, C_{Ox}^{*} the concentration of O in the bulk, ν is the scan rate, F, R and T have their usual meanings.

By assuming that the pre-exponential factor of the diffusion coefficient, D_{ox}, does not depend on temperature, the dependence of D_{ox} on temperature can be given by an Arrhenius type relation (equation VI-6)

$$D_{Ox} = D_{Ox}^{0} e^{\left(\frac{-E_a}{RT}\right)} \qquad \textbf{VI-6}$$

Equation VI-7 can be rearranged as follows :

$$I_p^2 T = cst \bullet e^{\left(\frac{-E_a}{RT}\right)} \qquad \textbf{VI-7}$$

Fig. VI-14 presents the linear dependence of $ln(I_p^2 T)$ on the inverse of the temperature for both platinum oxide and oxygen reduction reaction. From the slopes, activation energies of PtO reduction and O_2 reduction reaction are estimated to be 113kJ mol^{-1} and 190kJ mol^{-1} respectively. These values show clearly that the O_2 reduction reaction is more sensible to the increase in temperature than the PtO reduction. In fact at high temperatures (>375°C) the current due to PtO reduction is completely hidden by the oxygen reduction reaction.

To estimate the influence of temperature on the kinetics of PtO formation, the anodic holding time of the Pt/YSZ interface at 400mV has been varied from 1 to 10 minutes by steps of 1 minute in 20% O_2 in He atmosphere in the temperature range between 250°C and 375°C. For all temperatures and holding times only one reduction peak is observed. Furthermore, the peak current and peak potential are strongly influenced by both temperature and holding time. Worthy to notice the increase of current at high cathodic

potential, (*i.e.* in the domain where oxygen reduction dominates), with increasing holding time.

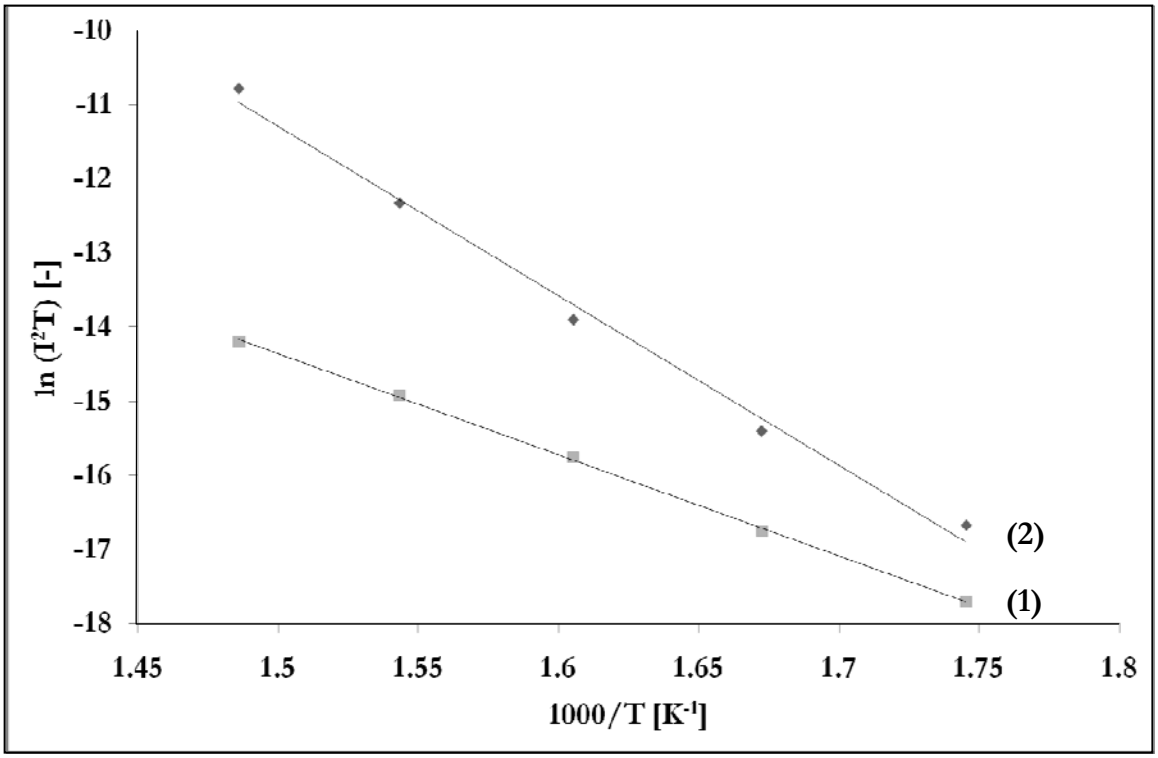

Fig. VI-14 : Determination of activation energy using equation VI-6. (1) PtO reduction, (2) O_2 reduction.

The charges involved in the reduction of PtO formed during the anodic polarization step are estimated by integration of the cathodic peak and plotted versus the anodic holding time (Fig. VI-15) and ln(t_H) (insert). The linear *Q-ln(t)* dependence obtained at high holding potential (E_a = 400mV) gives strong evidence that the PtO growth may be related to a *Mott* & *Carbrera* or place exchange mechanism. However, worth to mention that at lower holding potential (E_a = 100mV), a $Q\text{-}t^{1/2}$ dependence is observed, which gives evidence that diffusion and *Wagner* oxidation theory should be considered.

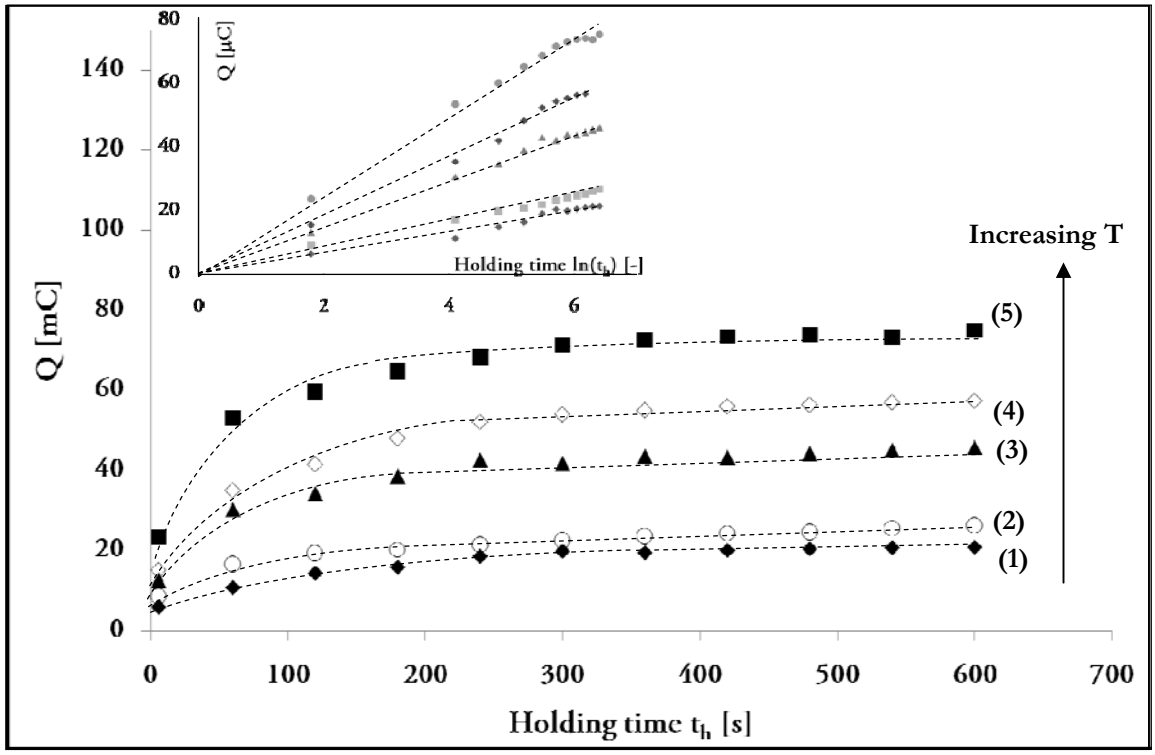

Fig. VI-15 : Evolution of Q_{PtO} as a function of anodic holding time. 250°C (1) , 275°C (2), 300°C (3), 325°C (4), 350°C (5), E_a = 400mV p_{O2}=20kPa Insert : Plot of Q_{PtO} as a function of ln(t)

Fig. VI-16 displays the decrease of platinum oxide formation efficiency, η_{PtO} (equation VI-5), with increasing temperature. This decrease of η_{PtO} is accompanied with a concomitant increase of η_{O2} according to equation VI-6.

As shown in Fig. VI-17, decreasing the potential to 100mV leads to a slower kinetics as previously expected. Nevertheless, holding the potential at 100mV leads to a similar decrease of the current effiency η_{PtO} with both increasing holding time and temperature.

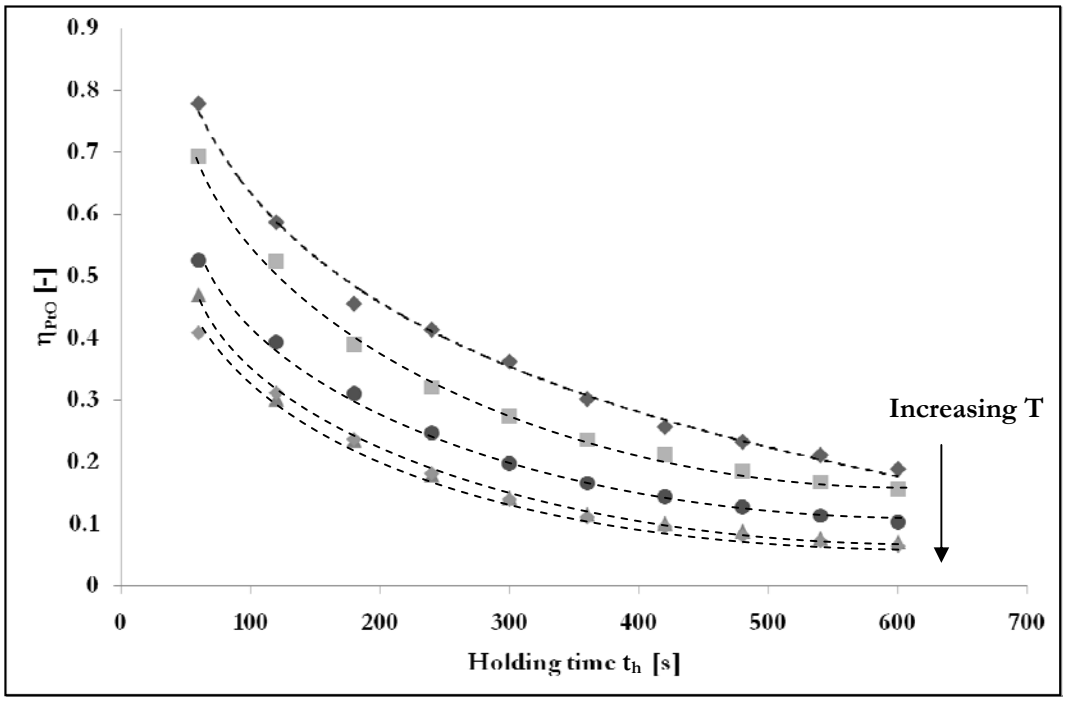

Fig. VI-16 : Evolution of η_{PtO} as function of anodic holding times. 250°C (1) , 275°C (2), 300°C (3), 325°C (4), 350°C (5), E_a=400mV, p_{O2}=20kPa

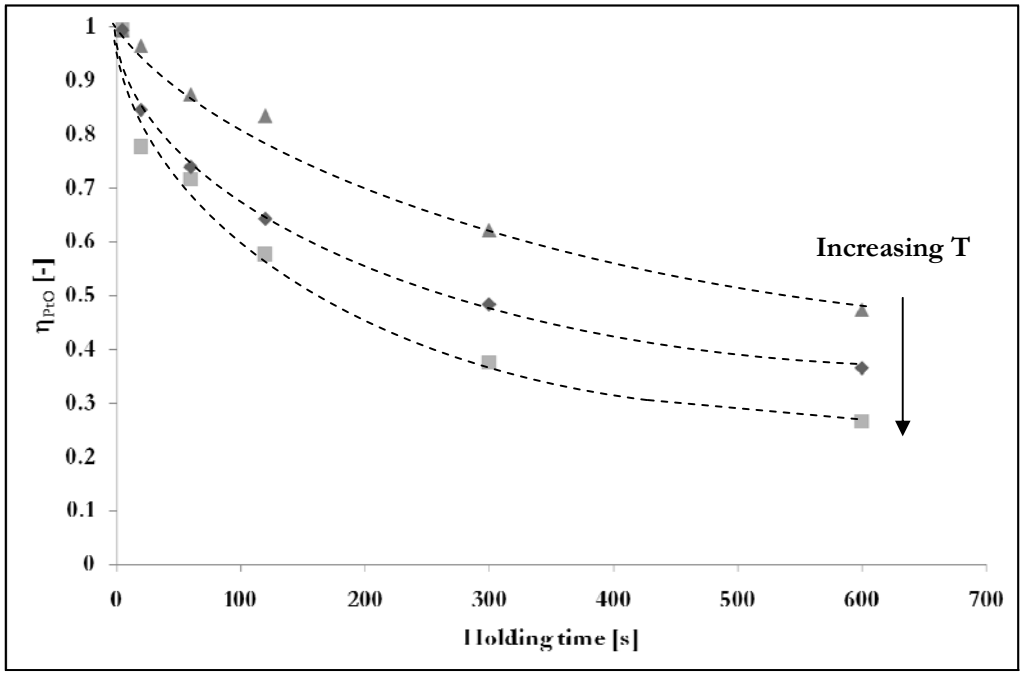

Fig. VI-17 : Evolution of η_{PtO} as function of anodic holding times. 250°C (1) , 275°C (2), 300°C (3), 325°C (4), 350°C (5), E_a=100mV, p_{O2}=20kPa

VI.4.5 Influence of oxygen partial pressure, p_{O2}

The influence of oxygen partial pressure p_{O2} on the voltammograms of the Pt/YSZ electrode was studied at 450°C. In this measurements the oxygen partial pressure, p_{O2}, has been determined by analysis the gas phase using a mass spectrometer. Furthermore the potential of the reference electrode has been corrected using the Nernst equation VI-8.

$$E_{\mathrm{WR}}(20\,\mathrm{kPa}) = E_{\mathrm{WR}}(p_{\mathrm{O_2}}) + \frac{RT}{4F}\ln\left(\frac{p_{\mathrm{O_2}}}{20\,\mathrm{kPa}}\right) \qquad \textbf{VI-8}$$

where $E_{WR(pO2)}$ is the experimental potential difference between the working and the reference electrodes exposed to the varying p_{O2}. $E_{WR(20\ kPa)}$ is the corrected working electrode potential.

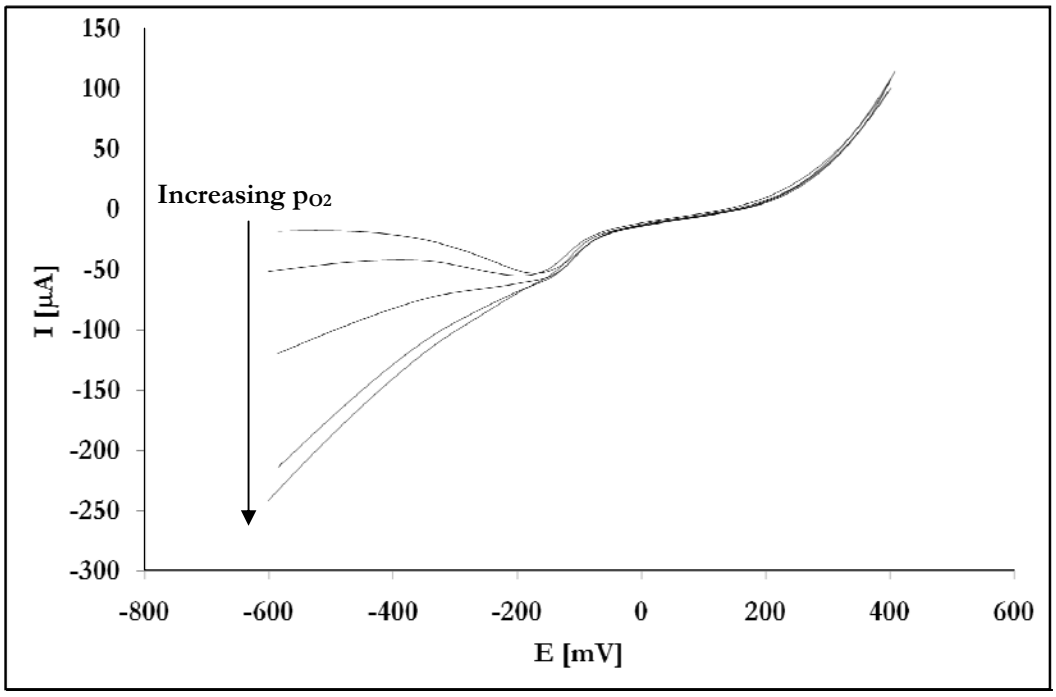

Fig. VI-18 : Effect of oxygen partial pressure on the voltammogram measured between 400mV and -600mV. (1) 10 Pa, (2) 20 Pa, (3) 350 Pa, (4) 2.5 kPa, (5) 20 kPa. T=450°C, ν =20mV/s

As shown in Fig. VI-18, increasing p_{O2} in the gas phase leads to an important change of the voltammograms. In fact, increasing the oxygen partial pressure results in a dramatic increase of the O_2 reduction reaction without a sensible effect of the PtO reduction current.

VI.5 General discussion

The morphological characterization of the thermally pretreated sputtered Pt electrode revealed a porous (111) oriented platinum film presenting a percolated macroporous structure with holes of few hundred μm diameter at the YSZ electrolyte surface. An estimation of the platinum coverage lead to an active surface of 60% of the geometric electrode surface area. Similarly the tpb length was estimated to be of 370m/cm^2.

The electrochemical investigation showed that upon anodic polarization two parallel reactions take place, i.e oxygen evolution and platinum oxide formation.

- Formation of PtO (equation VI-2)
- Oxygen evolution (equation VI-1)

A current efficiency for PtO formation, η_{PtO}, is introduced to reflecting the current contribution to platinum oxidation. The latter is found to be relatively close to unity at initial time of polarization (Fig. VI-16), but a rapid auto inhibition of platinum oxide growth is observed while the side oxygen evolution reaction is not affected.

The effective rate of platinum oxide formation may be estimated according to the following equation :

$$R_{eff} = \frac{I_{eff}}{2F} = \frac{I \bullet \eta_{PtO}}{2F} \qquad \text{VI-9}$$

where I is the applied current during the anodic polarization and I_{eff} is the effective current for PtO formation.

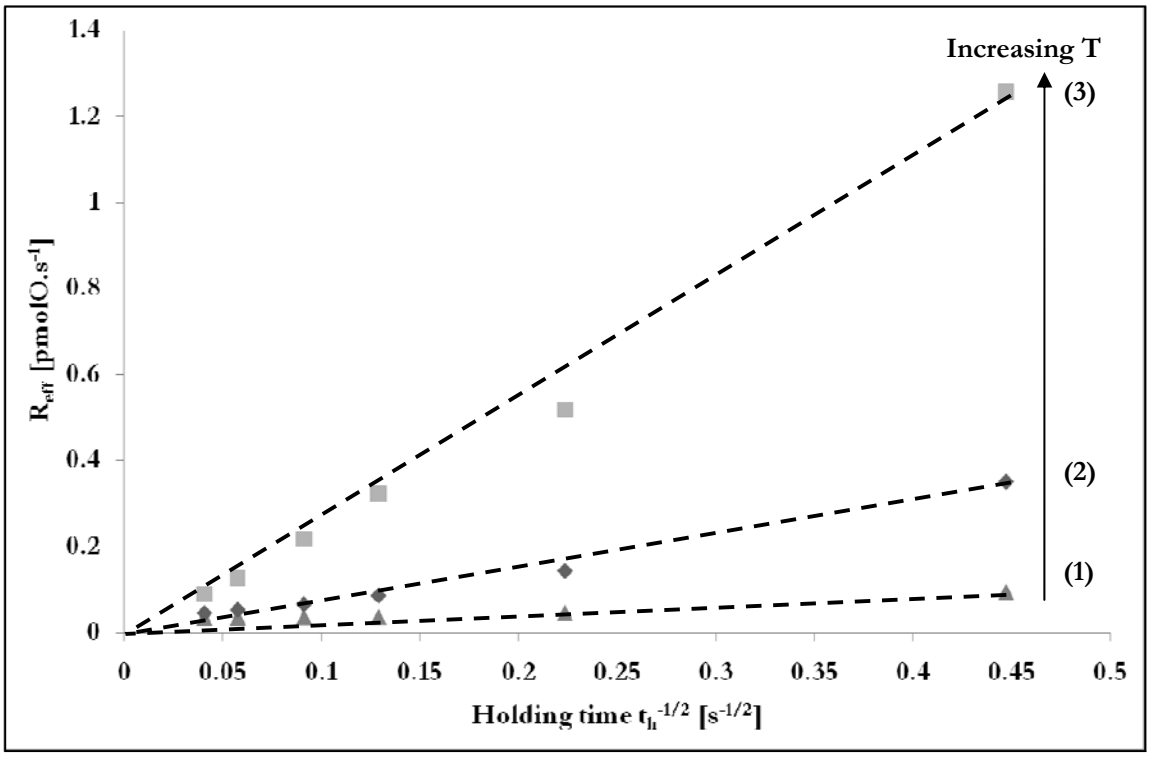

Fig. VI-19 : Effective rate of PtO formation as function of the inverse of the square root of the anodic holding time for different temperatures. 300°C (1), 325°C (2), 350°C (3) E_a = 100mV, p_{O2}=20kPa

The $t^{-1/2}$ dependence of the effective rate of PtO formation R_{eff} observed at 100mV (Fig. VI-23) suggested a *Wagner* type parabolic growth for the electrochemical formation of PtO. A similar approach to that proposed in the previous chapter allows to write :

$$\frac{dQ_{PtO}}{dt} = k_{(\eta,T)} t^{-1/2} \qquad \textbf{VI-10}$$

with

$$k_{(\eta,T)} = K_0 e^{\left(-\frac{E_a}{RT}\right)} \qquad \textbf{VI-11}$$

An Arrhenius plot alows to estimate the apparent activation energy of the PtO formation at 100mV to give E_{act} = 146 kJ/mol.

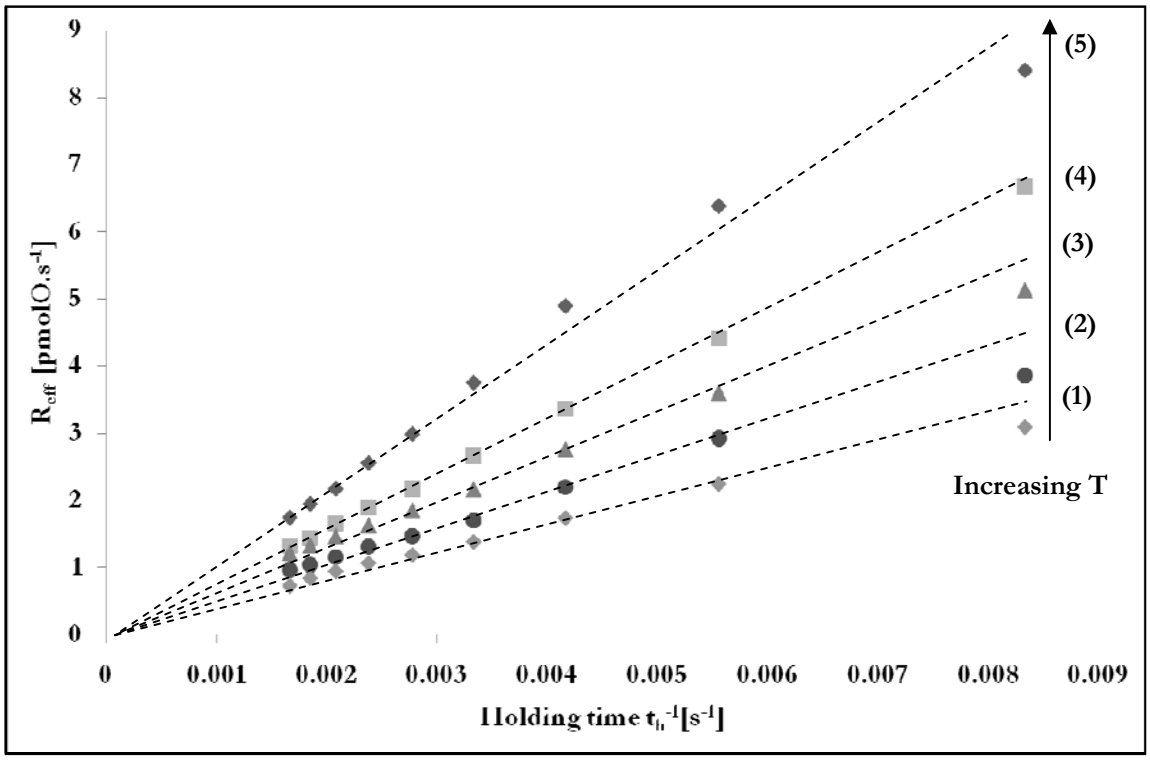

Fig. VI-20 : Effective rate of PtO formation as function of the inverse of the anodic holding time for different temperatures. 250°C (1) , 275°C (2), 300°C (3), 325°C (4), 350°C (5) E_a = 400mV, p_{O2}=20kPa

Fig. VI-20 shows the variation of the estimated effective rate of PtO formation with the inverse of the anodic holding polarization time at 400mV. For each temperature a linear relationship passing through the origin is observed. The PtO growth appears then to follow a logarithmic type growth as proposed by *Conway* in aqueaous electrolyte and by *Mott* & *Cabrera* in their electrooxidation model. The following kinetic regime is then observed :

$$\frac{dQ_{PtO}}{dt} = k_{(\eta,T)} t^{-1} \qquad \textbf{VI-12}$$

with

$$k_{(\eta,T)} = K_0 e^{\left(-\frac{E_a}{RT}\right)} \qquad \textbf{VI-13}$$

An Arrhenius plot alows to estimate the apparent activation energy of the PtO formation at 400mV to give E_{act} = 29 kJ/mol.

VI.6 Proposed model

The model of platinum electrochemical oxidation proposed herein, considers an approach similar to the electrochemical interpretation of *Wagner's* theory given by *Hoar* & *Price* [11] at low overpotential and considers the *Mott* & *Cabrera* mechanism [12-15] at high overpotential. In addition, the model takes into account the state of the art EPOC backspillover theory implying the migration of O^{2-} promoter at the Pt/gas surface. Fig. VI-21 illustrates the mechanism proposed to take place upon an anodic polarization of such a cell.

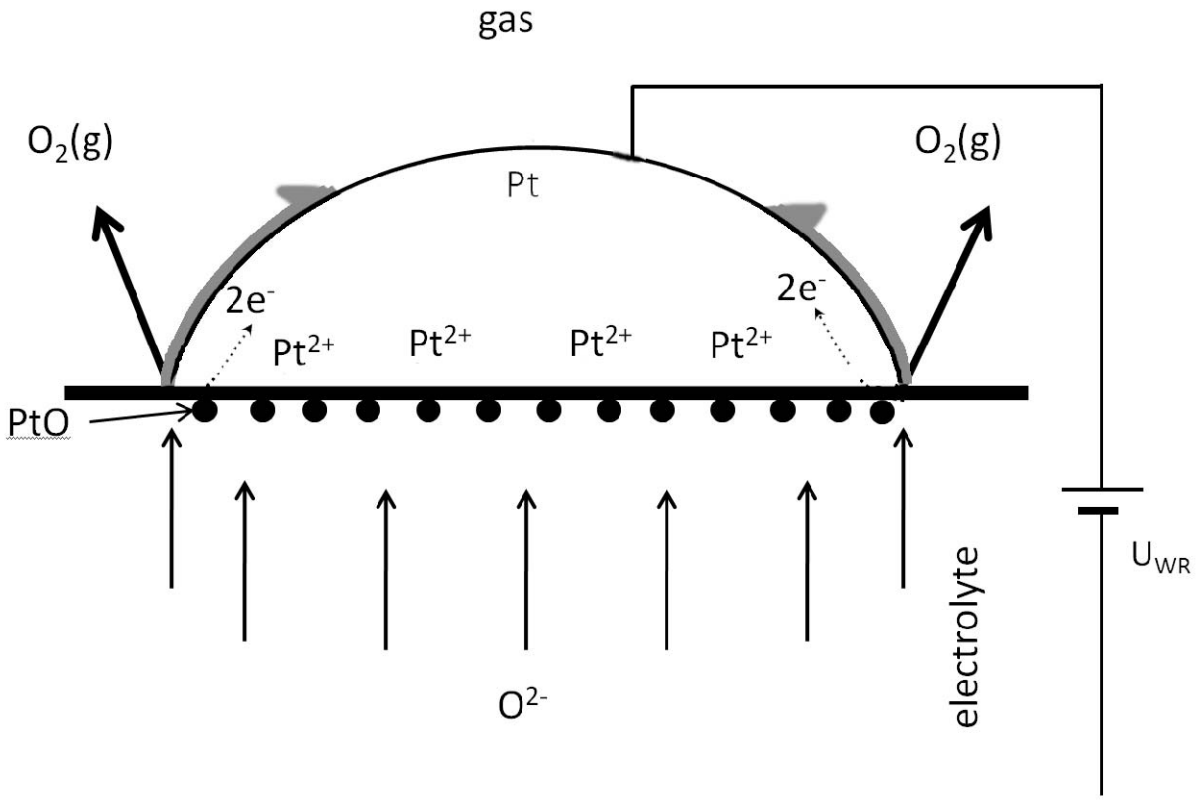

Fig. VI-21 : Schematic representation of the oxidation process during anodic polarization of theplatinum sputtered electrode

Initially the electrode is assumed as a purely metallic platinum film lying on the YSZ electrolyte. By applying an anodic polarization platinum oxidation takes place at the Pt/YSZ interface in two steps, *i.e.* the oxidation of Pt to Pt^{2+} (equation VI-14) and the subsequent instantaneous combination of Pt^{2+} and O^{2-} originating from the electrolyte (equation VI-15).

$$Pt \rightarrow Pt^{2+} + 2e^{-} \qquad \text{VI-14}$$

$$Pt^{2+} + O^{2-} \rightarrow PtO_{Pt/YSZ} \qquad \text{VI-15}$$

This occurs with a high η_{PtO} within the first times of polarization but slows down rapidly to reach a saturation amount of PtO formed at the Pt/YSZ interface. This oxide layer acts then as a barrier to further oxide formation. However, a very slow process of PtO formation toward the platinum bulk is suggested to take place upon prolonged polarization time (reaction VI-16).

$$PtO_{Pt/YSZ} \rightarrow PtO_{bulk} \qquad \text{VI-16}$$

According to litterature, oxygen penetration into the oxide scale is the most probable rate determining step of oxidation mechanism. The Pt^{2+} migration model proposed by *Wagner* appears to be valid only at low overpotential. A process of oxygen diffusion across PtO proposed by *Mott* & *Cabrera* [15] or a place exchange mechanism between platinum and strongly adsorbed oxygen proposed by *Wilkinson* [16] are more likely to be observed in the higher potential domain. However, experimentally this process of long term PtO formation toward the Pt bulk electrode appears to be very slow and only significant after long lasting anodic polarization of the Pt working electrode. In this case platinum bulk may be considered as a long term oxygen storage location into the Pt/YSZ system. Moreover, according to the theory Electrochemical Promotion Of Catalysis [17-19], oxygen promoters originating from the triple phase boundary populates the Pt/gas interface during the anodic polarization (reaction VI-17).

$$PtO_{tpb} \rightarrow Pt{\bullet}O_{Pt/gas} \qquad \text{VI-17}$$

The nature of those oxygen promoter species is subject to controversy but all authors refer to strongly bonded oxygen at the Pt/gas interface. As this species is formed at the triple phase boundary before populating the Pt/gas interface, it seems reasonable to suppose that oxygen bonding at the Pt/gas interface and at the Pt/YSZ interface are of the same nature. However, worth to mention that this migrating oxygen species should be in equilibrium with the oxygen present in the surrounding gas phase (reaction VI-18) in agreement with the long residence time of the promoters reported by the authors of the EPOC field.

$$Pt{\bullet}O_{Pt/gas} \rightleftarrows Pt + O_{2(g)} \qquad \text{VI-18}$$

Finally the side reaction of oxygen evolution (equation VI-19) taking place at the tpb is proposed to be not firmly affected by the formation of a thin platinum oxide at the binary Pt/YSZ interface as electrons may cross rapidly the oxide layer formed there, by tunneling effect to the Pt electrode, while gaseous oxygen will evolve to the gas phase.

$$O^{2-} \rightarrow \frac{1}{2}O_{2(g)} + 2e^{-} \qquad \text{VI-19}$$

VI.7 Conclusion

In this chapter, morphological characterization of the sputtered platinum electrode allowed to estimate the electroactive surface area of the platinum film as well as its structural properties. Subsequent electrochemical investigation, performed by cyclic voltammetry, allowed to identify two electrochemical process taking place at the electrode/electrolyte interface. The efficiency of the platinum oxidation reaction was estimated and correlated to *Wagner's* theory of metal oxidation at low holding potential and to place exchange mechanism at higher potential to propose a model of the electrochemically induced oxidation of platinum.

VI.8 References

1. Vayenas CG, Bebelis S, Pliangos C, Brosda S, Tsiplakides D (2001) Electrochemical Activation of Catalysis: Promotion, Electrochemical Promotion, and Metal-Support Interactions. Kluwer Academic / Plenum Publishers, New York

2. Badwal SPS, Ciacchi FT (1986) Solid State Ionics 18-19: 1054

3. Emery DA, Luke RJC, Middleton PH, Metcalfe IS (1999) Journal of the Electrochemical Society 146: 2188

4. Emery DA, Middleton PH, Metcalfe IS (1999) Journal of the Electrochemical Society 146: 2194

5. Janek J, Korte C (1999) Solid State Ionics 116: 181

6. Mutoro E, Gunther S, Luerssen B, Valov I, Janek J (2008) Solid State Ionics 179: 1835

7. Mutoro E, Luerssen B, Gunther S, Janek J (2009) YSZ: Influence of impurities and electrode morphology on cyclic voltammograms 180: 1019

8. Jaccoud A, Foti G, Wuthrich R, Jotterand H, Comninellis C (2007) Topics in Catalysis 44: 409

9. Eaves J (2003) Promotion electrochimique des catalyseurs à base de rhodium et d'iridium, EPFL

10. Jaccoud A (2006) Electrochemical promotion of Pt catalysts for gas phase reaction, EPFL

11. Hoar TP, Price LE (1938) Transactions of the Faraday Society 34: 867

12. Mott NF (1939) Transactions of the Faraday Society 35: 1175

13. Mott NF (1940) Transactions of the Faraday Society 35: 472

14. Mott NF (1947) Transactions of the Faraday Society 43: 429

15. Cabrera N, Mott NF (1949) Reports on Progress in Physics 12: 163

16. Eley DD, Wilkinson PR (1960) Proceedings of the Royal Society of London. Series A. Mathematical and Physical Sciences 254: 327

17. Luerßen B, Gunther S, Marbach H, Kiskinova M, Janek J, Imbihl R (2000) Chemical Physics Letters 316: 331

18. Luerßen B, Mutoro E, Fischer H, Günther S, Imbihl R, Janek J (2006) Angewandte Chemie International Edition 45: 1473

19. Vayenas CG, Jaksic MM, Bebelis SI, Neophytides SG (1996) In: Bockris JOM (ed) Modern Aspects of Electrochemistry, vol 29. Plenum Press, New York p 57

PART III

Investigation under High Vacuum (HV)

CHAPTER VII- SOLID ELECTROCHEMICAL MASS SPECTROMETRY (SEMS)

In the field of electrochemical promotion of catalysis (EPOC) several investigation devices are based on the coupling of analytical techniques to electrochemistry. However, most of them are performed under atmospheric pressure conditions where the promotion mechanism is still subject to controversy. In order to obtain a clearer mechanistic picture of the phenomenon, *Imbihl et al.* proposed to investigate EPOC under high vacuum (HV) conditions. Surface analysis tools like PEEM and SPEM were combined with success to electrochemical methods allowing the authors to directly observe the migration of O^{2-} promoters at the catalyst surface during anodic polarization. Few years later, *Vayenas et al.* proposed an EPOC investigation of CO oxidation using labeled oxygen confirming the EPOC sacrificial promoter model suggested for atmospheric conditions.

In order to shed more light on the intriguing P-EPOC behavior of Pt/YSZ interface reported in this work, a new probe device, coupling electrochemistry and mass spectroscopy techniques, is developed for the investigation of a solid electrochemical cell under high vacuum conditions (HV). Two configurations are realized, single and dual chamber type reactors, for the investigation of both the electrochemical and electrocatalytical behavior of the Pt/YSZ system. Compared to a conventional setup we can readily select the pressure (down to 10^{-8}mbar) and access to much shorter response time (less than 1s).

VII.1 Introduction

Coupling electrochemistry to another analytical technique represents a constant effort in the field of research as it allows to gain valuable information for the elucidation of complex electrochemical mechanisms. Surface analysis techniques, *e.g.* Auger electron spectroscopy, X-ray photoelectron spectroscopy (XPS) [1,2], scanning photoelectron spectroscopy (SPEM) [3-5], photoelectron emission microscopy (PEEM)[4-7], scanning tunneling microscopy (STM), are usually coupled to electrochemistry to investigate electrochemical deposition and adsorption at the electrode while spectroscopic techniques, *e.g.* infrared-spectroscopy, gas chromatography (GC) [8-9], mass spectrometry (MS)[8-11], may be coupled to monitor (qualitatively and quantitatively) the products of an electrochemical reaction. Relatively recently, the field of aqueous electrochemistry yielded important insight from the development of differential electrochemical mass spectrometry (DEMS) technique allowing online detection of electrochemically formed products and intermediates [12,13].

Here, a new probe device is built to perform electrochemical measurements (under HV conditions, while monitoring the electrochemically formed products. Actually, a microreactor configuration equipped with a gas analyser quadrupole mass spectrometer (QMS) is proposed for the investigation of solid state electrochemical systems. The high sensitivity and the fast detection response of QMS analyzer appeared as key parameters for the elaboration of such a solid electrochemical mass spectrometry investigation tool (SEMS).

VII.2 Experimental setup

Two different HV setup configurations are proposed, a single chamber type configuration (Fig. VII-1 a), designed for the electrochemical investigation of a metal electrode supported on a solid electrolyte, Pt/YSZ electrochemistry, and a dual chamber type configuration (Fig. VII-1 b), adapted to the investigation of CO oxidation over Pt/YSZ catalyst.

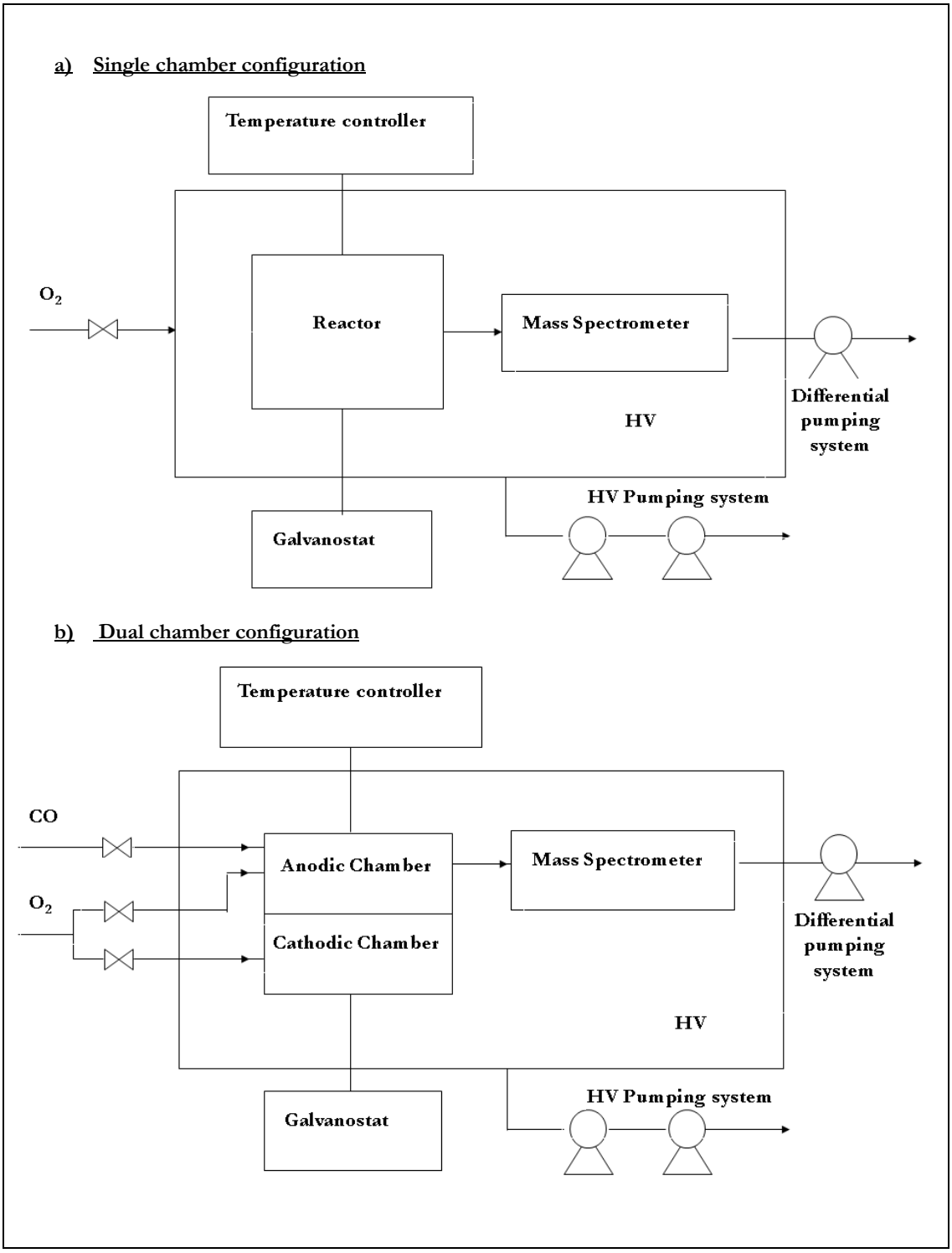

Fig. VII-1 : Scheme of the high vacuum experimental setup. (a) single chamber configuration, (b) dual chamber configuration

These two configurations mainly differ by the electrochemical reator and the gas supply to the system. The HV chamber, heating system, current application/measurement and MS gas sampling are the same (Fig. VII-2). The general setup consists of two key parts namely the electrochemical reactor and the mass spectrometric equipment placed in the HV chamber.

VII.2.1 HV chamber and vacuum setup

The whole HV chamber (V_{HV} = 10 L) is maintained typically at 10^{-8} mbar by a pumping system composed of a turbomolecular pump (Pfeiffer TMU 521, 520 L/s) and a second molecular pump (Peiffer TMU 071P, 60 L/s), which are connected to a rotary pump (Trivac D16B, 16 m^3/h). The total volume and the effective pumping speed of the system yields to a time constant of 20ms.

A manipulator allowing 3 translational and 2 rotational degrees of freedom supports the heating system and the electrochemical reactor containing the sample. This manipulator is fixed on the top of the device positioning the sample in the middle of the HV chamber. The mass spectrometer equipment is placed on the side and can be moved next to the electrochemical reactor during the experiments. The gases used as reactants (O_2 (46 purity) and CO (60 purity) carbagas certified) are introduced in the system via HV leak valves and capillary gas lines. A pressure gauge (Balzer CPG 300), added on the other side of the device, allows measuring the total pressure in the HV chamber.

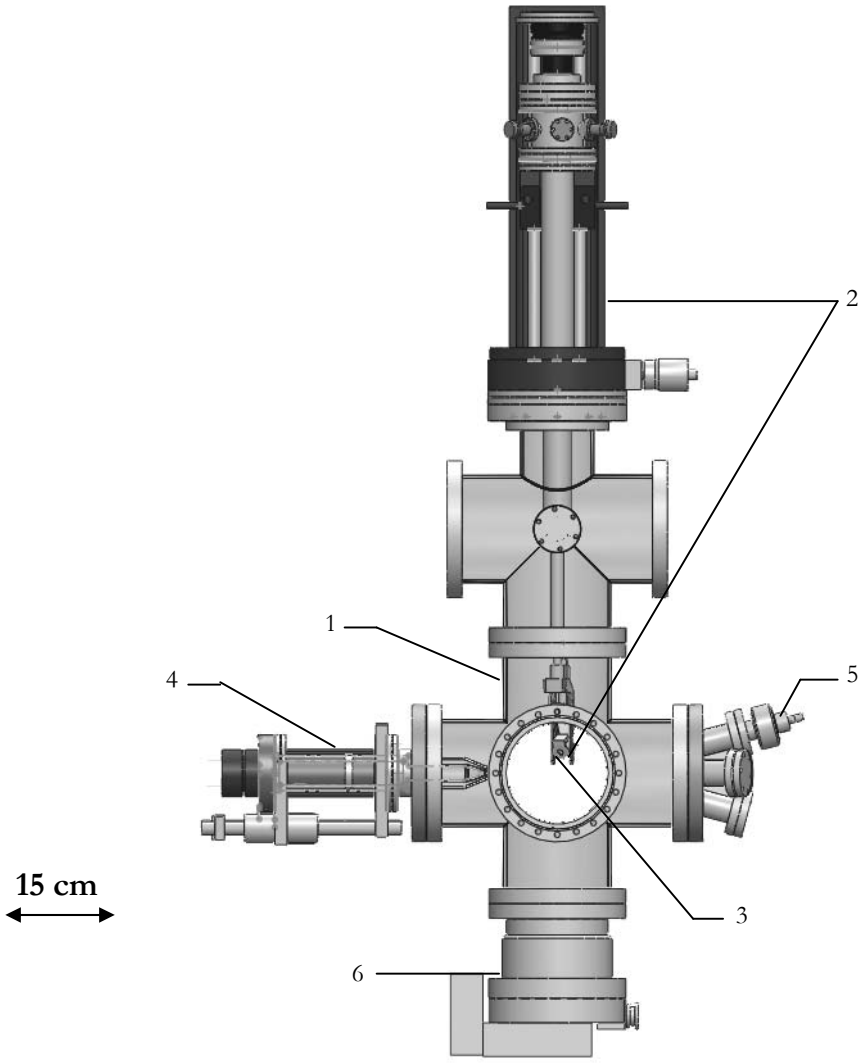

Fig. VII-2 : Scheme of the high vacuum experimental setup. 1: main chamber; 2: manipulator and support, 3 : electrochemical reactor 4: mass spectrometer and sniffer, 5 : pressure gauge and 6: molecular pump.

VII.2.2 Heating system

The scheme of the heating system is shown in Fig. VII-3. The sample is mounted in a copper reactor block. The block is fixed to a base copper piece which is heated by radiation and electron bombardement from a tungsten filament (12V, 50W). During the heating, the electrons emitted by the filament are confined in the base copper piece ensuring that they all contribute to its heating and do not perturbate the electrochemical measurements.

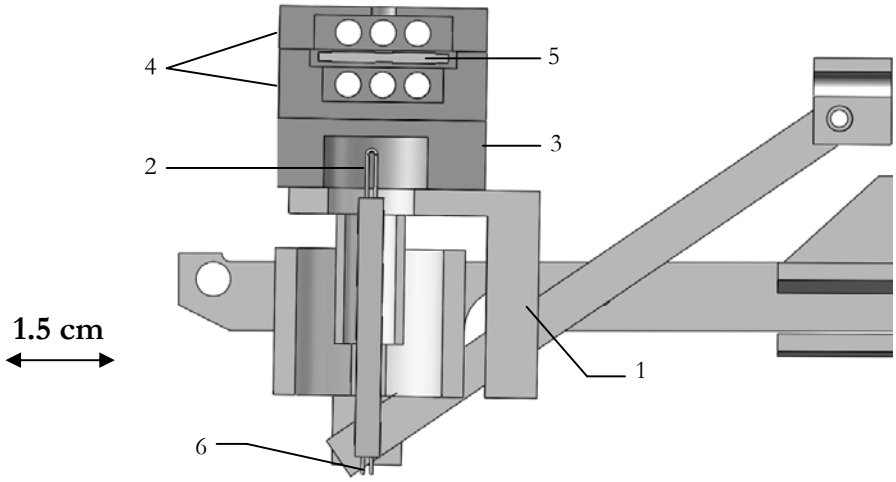

Fig. VII-3 : Scheme of the heating system, cross view. 1: manipulator holder; 2: filament, 3: base cupper piece connected to thermocouple K-type, 4 : electrochemical reactor, 5: sample and 6: electrical connections.

In addition, two high voltage power sources (Delta Electronika ESO 300-0.45) are connected to the base copper piece and to the filament. This tuning system, operating at about 500V, is used to create a strong electric field which accelerates the electrons emitted by the filament, heating efficiently the reactor because of the excellent heat conductivity of copper. As a consequence, the whole contains of the reactor (sample and reactive gas mixture) is homogeneously heated by radiation up to 500°C with small deviation from the imposed reactor temperature.

VII.2.3 Mass spectrometric equipment

The mass spectrometric equipment, designed herein, is similar to the one used and characterized by *Valloton* during his PhD work [14]. A residual gas analyser (Pfeiffer, Prisma200) quadrupole MS is enclosed in the so called "sniffer" composed of multi-cylindric stainless steel tubes (Fig. VII-4). The "sniffer" aims to collect maximum of gases desorbing from the sample surface. Its unique front opening (3.5mm diameter) is placed in the vicinity of the gas feed to be analysed and its cone shape ensures the diffusion of non collected molecules away from the electrochemical reactor, *i.e.* avoides gas back mixing.

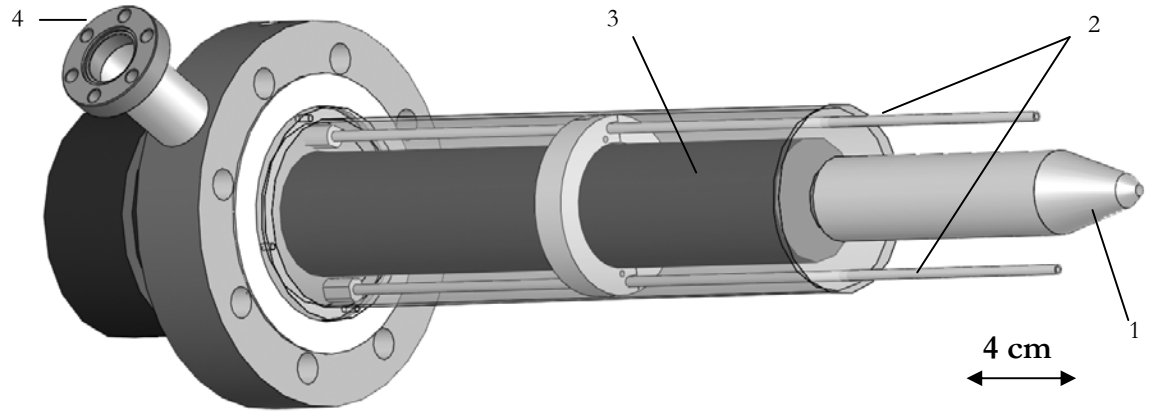

Fig. VII-4 : Scheme of the sniffer. 1: cone shape collector; 2: inlet gases capillary tubes, 3 : quadrupole MS, 4: differential pumpimg.

In addition, reactant gases are introduced by two gas capillary tubes built on both sides of the "sniffer". For the single chamber type reactor configuration, the oxygen gas source is released in the main HV chamber in order to set a similar p_{O2} value in both anodic and cathodic chamber of the reactor (electrochemical investigation). On the contrary, for the dual chamber type reactor configuration, reactant gases are directly transfered to the anodic and to the cathodic chambers by connecting the capillary tubes to the gas inlet of electrochemical cell with Teflon tubes avoiding gas loss into the HV main chamber (catalytic measurements).

The volume of the ionic detection chamber is connected to a molecular pump (PS = 60 L/s) to ensure a continuous forced convection of analysed gases.

The time constant detection τ of a given species is directly given by the ratio of the ionization chamber volume to the differrential pumping speed.

$$\tau = \frac{V_0}{PS} \qquad \textbf{VII-1}$$

where τ is the detection time constant, V_0 is the volume of the ionisation chamber and PS is the actual pumping speed of the ionic chamber. Worth to notice that due to the complex

multi-section structure of the whole "sniffer", its actual efficient pump speed is modified according to equation VII-2:

$$PS = 1/\sum(1/C_i) \qquad \textbf{VII-2}$$

where C_i representing the conductance of each section of the sniffer, is estimated according to the Molecular flow theory [15] (equation VII-3).

$$C_i = KS_i\left(\frac{RT}{2\pi M_X}\right)^{1/2} \qquad \textbf{VII-3}$$

where K is the Clausing's factor , S the section of the sniffer entrance, T the temperature, M_X the molecular mass of the analysed gas. Considering the so estimated pumping speed (0.63 L/s) and the volume of the gaz collector (V_0 = 0.38 L), the detection time constant is determined to be 0.6s.

VII.2.4 Electrochemical reactors

As previously mentioned, two types of reactor were designed in this work, a single chamber type reactor well suited for electrochemical investigation of the Pt/YSZ system and a dual chamber type reactor adapted to catalytic investigation (EPOC and P-EPOC).

VII.2.4.1 Single chamber type reactor

The electrochemical reactor is composed of two copper pieces (Fig. VII-5). The sample is loosely fixed in the middle of the electrochemical reactor with an inert ceramic paste (Feuerfestkitt, Firag AG), differentiating a working compartment (containing WE and thermocouple, $V_{working}$=0.7 cm^3) and a reference compartment (containing CE and RE, $V_{reference}$=0.5 cm^3) but permitting free gas circulation in the whole reactor. The sides of each compartment present six openings (3mm diameter holes), two holes were isolated by alumina ceramic tubes and were used for the output of electrical connections (gold wires) connected to the electrodes and of the thermocouple fixed at the Pt/YSZ sample surface. The four other holes ensure the free circulation of gases in both compartments, *i.e.* the reactor is similar to a single chamber reactor as the gas inlet is located in the main HV

chamber. The gas analysis of the working compartment is performed via an additional 3mm diameter hole placed on the top face of the reactor.

The pumping speed of the reactor, determined by the gas flow at the openings, is estimated to be 0.64 L/s. Considering the volume of the reactor, this results in a time constant of 1ms, much faster than the vaccum system and we can consider the reactor in constant homogeneous pressure conditions (CSTR).

The temperature is measured by two (NiCr-Ni) thermocouples, connected to the sample next to the working electrode and connected to the reference compartment of the reactor respectivelly.

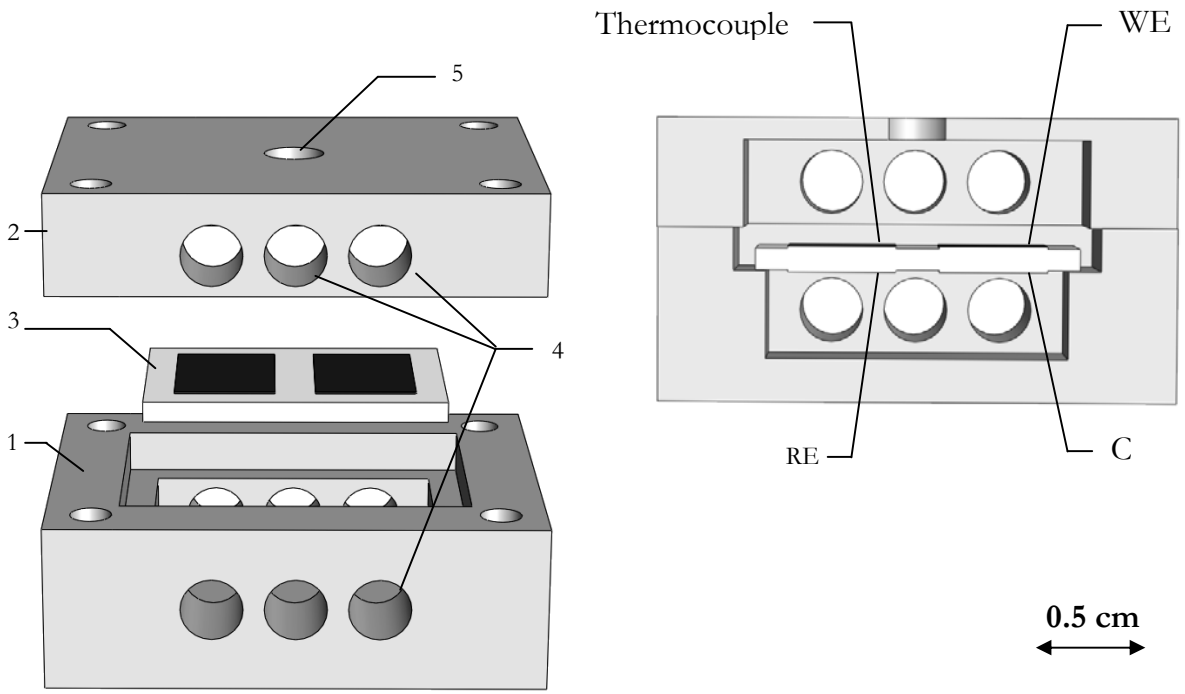

Fig. VII-5 : Scheme of the electrochemical reactor. 1: bottom part; 2: top part, 3 : sample 4: holes ensuring both connection and free gas circulation 5 : hole to MS detection. WE: working electrode, CE: counter electrode, RE: reference electrode.

VII.2.4.2 Dual chamber type reactor

The sample is sealed gas tight in the reactor with an inert ceramic paste (Feuerfestkitt, Firag AG), separating two independent compartments: the working compartment (containing WE

and thermocouple, $V_{working}$=0.7 cm^3) and the reference compartment (containing CE and RE, $V_{reference}$=0.5 cm^3) (Fig. VII-6). The working compartment is efficiently pumped by seven openings (3mm diameter holes) while the reference compartment is effectively sealed since the openings are used as feedthroughs for the gas inlet and electrical connections. In fact, the direct feed of reactant is ensured by stainless steel inlet gas lines (2.8 mm diameter) connected to two openings of the working compartment (O_2 and CO) and to one opening of the reference compartment (O_2). Temperature monitoring and gas analysis of the dual chamber type reactor is similar to the one previously described for the single chamber type reactor.

The pumping speed of the reactor is determined to be 0.9 L/s which correspond to a reactor time constant of 0.8ms (CSTR).

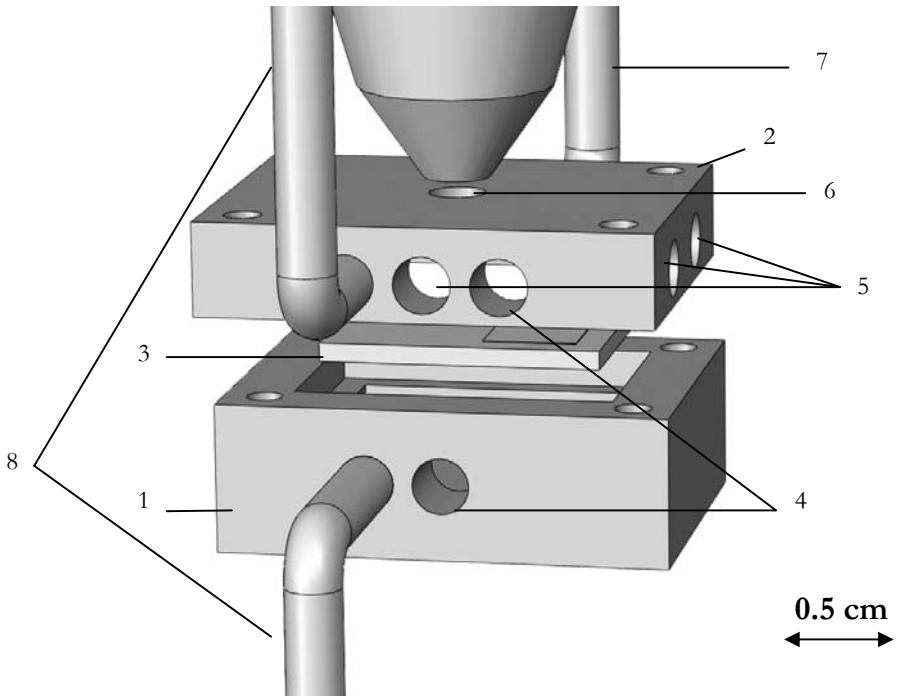

Fig. VII-6 :: Scheme of the dual chamber electrochemical reactor. 1: reference compartiment; 2: working compartiment, 3 : sample 4: holes ensuring electrical and thermocouple connections, 5 : holes ensuring free gas circulation 6 : top hole facing the entrance of the sniffer (MS detection), 7 CO inlet gasline, 8 : O_2 inlet gasline.

During experiments involving electrochemical measurements, worth is to notice that in this reactor, the actual measured potential difference ΔU_{WR} does not correspond to the cell overpotential η because the oxygen partial pressure present in the two compartments are differents**.** To get the value of η**,** the potential of the reference electrode has to be corrected using the Nernst equation VII-4.

$$\eta = \Delta U_{\mathrm{WR}}(p_{\mathrm{O_2}}^{working}) + \frac{RT}{4F}\ln\left(\frac{p_{\mathrm{O_2}}^{working}}{p_{\mathrm{O_2}}^{reference}}\right) \qquad \textbf{VII-4}$$

where $\Delta U_{WR(pO2)}$ is the experimental potential difference between the working and the reference electrodes exposed to different p_{O2} and η is the working electrode overpotential.

VII.2.5 Preparation of the Pt/YSZ samples

Commercial YSZ 8%mol pellet (Technox 802, Dynamic Ceramic Ltd) were used as substrate on which platinum electrode was deposited by magnetron sputtering in inert atmosphere (Ar) at room temperature. Direct current (dc) mode was used with a discharge of 330 V at an argon pressure of 10^{-2} mbar. Under these conditions, a 1 μm thick Pt electrode was deposited with a deposition rate of 0.09 nm s^{-1} on the YSZ pellet, as determined by profilometric measurement (Alphastep, Model 500) of the film deposited on smooth silicon samples processed simultaneously.

For electrochemical investigation (single chamber configuration) a Pt/YSZ/Pt cell is constructed so platinum counter and reference electrodes have been deposited on the reverse side of the pellet using the same sputtering procedure (Fig. VII-7).

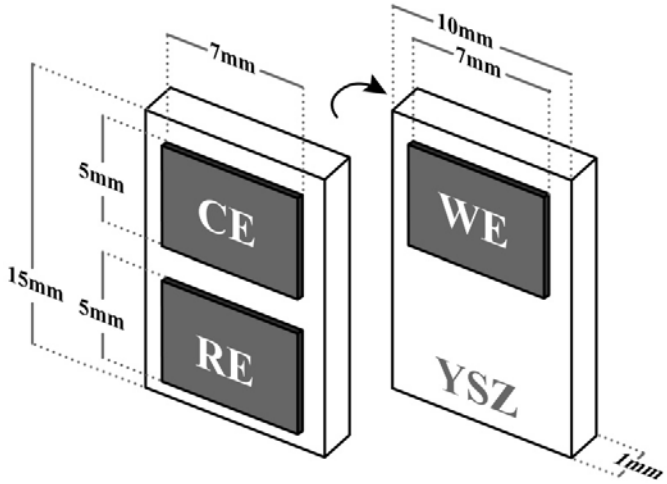

Fig. VII-7 : Placement and dimensions of the Pt electrodes prepared by sputtering. WE: working electrode; CE: counter electrode; RE: reference electrode.

On the contrary, catalytic measurements (dual chamber configuration) are performed over a Pt/YSZ/Au system. This ensures the catalytic inertness of gold counter and reference electrodes which are deposited on the other side of the pellet by application of metalorganic paste (Gwent Electronic Materials Ltd. - C70219R4) followed by calcination at 550°C. Before any investigation, the cells have been treated at 700°C in 20 kPa O_2 during 4 hours in order to stabilize the platinum films.

The electrode size is 7 x 5 mm giving a geometric surface of 0.35 cm^2. The working and counter electrodes were located in a symmetrical face-to-face arrangement on the opposite sides of the YSZ pellet. This geometry ensured a symmetrical current and potential distribution in the cell.

VII.3 Results

VII.3.1 Heating system

Upon increasing temperature, the heating system revealed a good homogeneous heating of the sample (Fig VII-8) with little deviation from the imposed temperature, *i.e.* $T_{reactor}$. One

should mention that in consequence, during the heating , the open circuit potential of the Pt/YSZ/Pt cell remained at 0V.

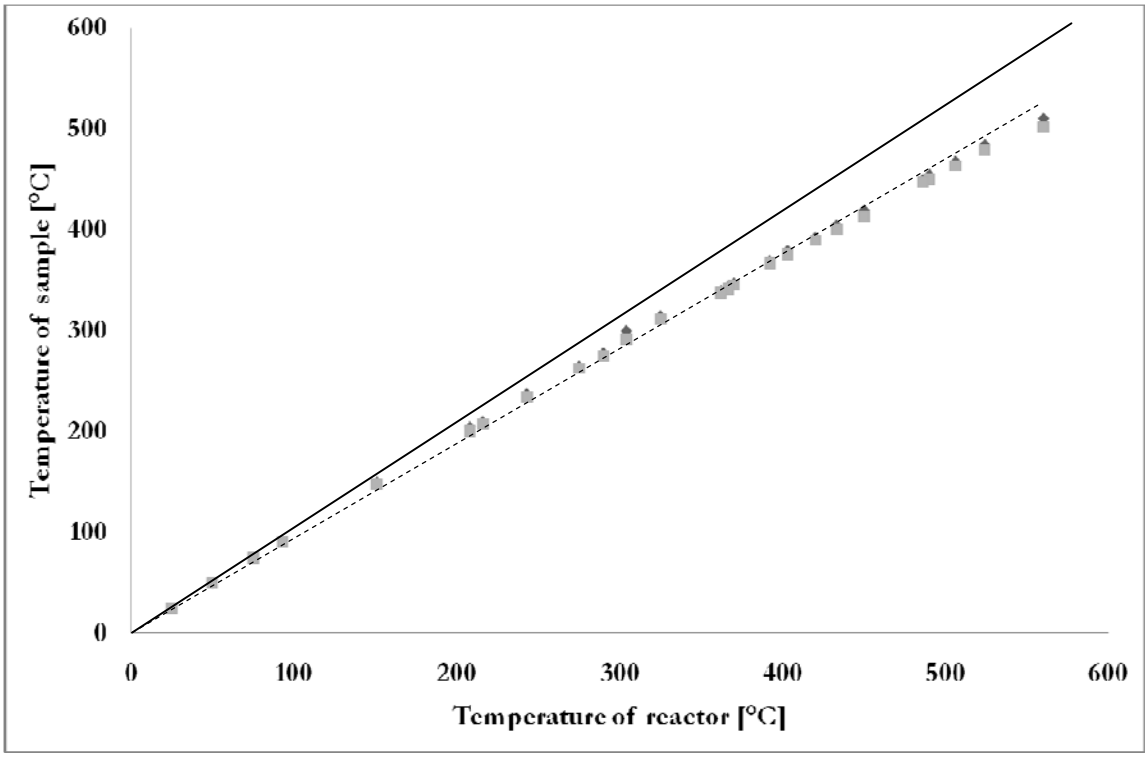

Fig. VII-8: Linear dependence of temperature of the sample on the temperature of the copper reactor. Dashed line is experimental linear regression while solid line displays the ideal case where $T_{reactor} = T_{sample}$.

VII.3.2 QMS gas analyzer calibration

The online analysis of the gas composition consist of measuring the ionic current of each gas with the quadrupole mass spectrometer. The ion current intensity, I_i, being directly proportional to the gas pressure, $p_X^{sniffer}$, in the sniffer, one may write:

$$I_X = K_X p_X^{Sniffer} \qquad \text{VII-5}$$

where K_X is a constant containing all mass spectrometer settings and ionization probability.

Calibration of the mass spectrometer, *i.e.* determination of *K*, can be performed by removing the electrochemical reactor from the sniffer gas inlet and stop the differential pumping to

insure a homogeneous pressure in the whole HV chamber and in the "sniffer". In this conditions, the relationship between ion current, I_X, and analysed gas pressure, p_X^{HV}, in the HV chamber is given as:

$$I_X = K_X^0 p_X^{HV} \qquad \text{VII-6}$$

where the constant K_X^0 coefficient, similar to K, contains all MS parameters under stationary conditions and can be estimated experimentally (Fig. VII-9, Table VII-1).

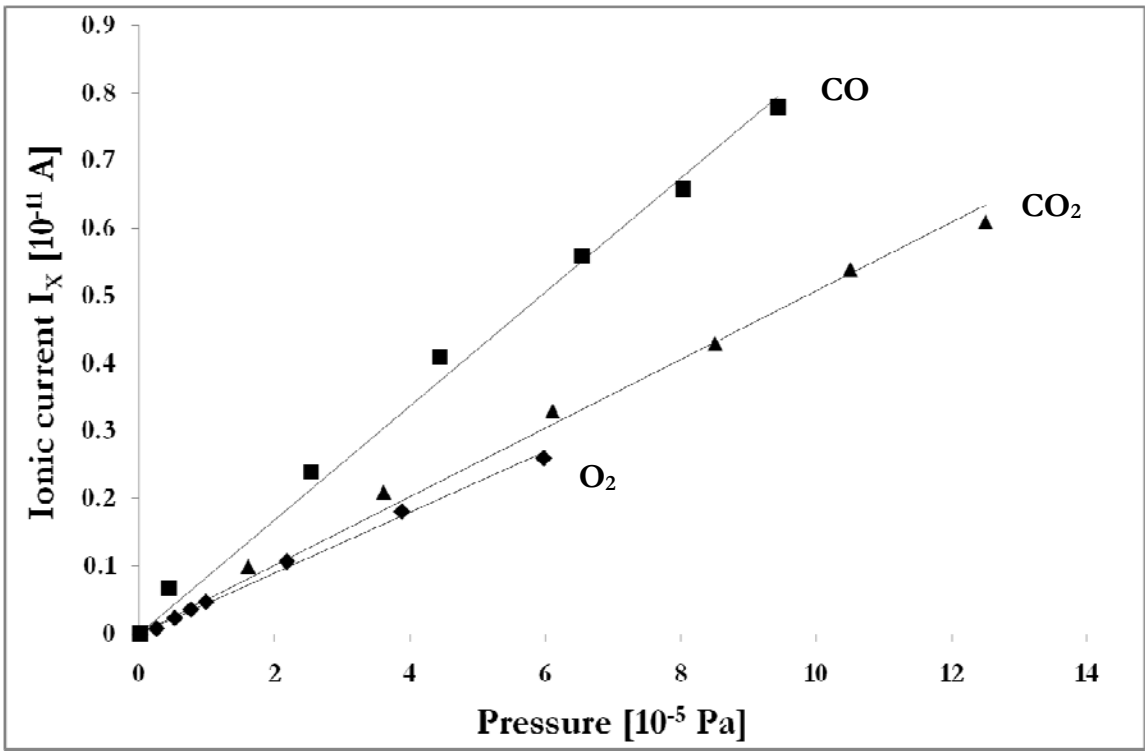

Fig. VII-9: Linear relation between the HV chamber pressure and the measured ionic current intensity of the calibrated gas. (1) $O_{2(g)}$, (2) $CO_{(g)}$ and (3) $CO_{2(g)}$

$K^0_{O_2}$	$4.5.10^{-8}$ A Pa^{-1}
K^0_{CO}	8.10^{-8} A Pa^{-1}
$K^0_{CO_2}$	5.10^{-8} A Pa^{-1}

Table VII-1 : Calibration coefficient K_X^0 for $O_{2(g)}$, $CO_{(g)}$ and $CO_{2(g)}$

VII.3.3 SEMS calibration

The gas analysis of the working compartiment is performed through an additive 3mm diameter hole placed on the top face of the reactor. Under anodic polarization O^{2-} ions migrate to the Pt/YSZ interface where they electrochemically react according to reaction VII-7 at the Pt/YSZ interface and according to reaction VII-8 at the triple phase boundary:

$$O^{2-}_{(s)} + Pt(s) \rightarrow PtO_{(s)} + 2e^- \qquad \textbf{VII-7}$$

$$2O^{2-}_{(s)} \rightarrow O_{2(g)} + 4e^- \qquad \textbf{VII-8}$$

However, only $O_{2(g)}$ is released into the gas phase during this process, *i.e.* $O_{2(g)}$ is the only product wich may be sampled by the MS. In addition reaction VII-8 dominates largely at high overpotential [13]. In this domain, assuming 100% current effieciency for the oxygen evolution reaction taking place at the tpb, the electrochemical oxygen flow produced by an anodic polarization of the working electrode is related to the faradaic current flowing through the Pt/YSZ/Pt cell as follows:

$$J_{O_2}^{sample} = \frac{I_f}{4F} \qquad \textbf{VII-9}$$

where I_f is the faradaic current imposed to the cell, $J_{O_2}^{sample}$ is the flow of electrochemically formed oxygen flow and F the Faraday constant.

Nevertheless, only a fraction of the gas coming out of the working compartiment goes in the "sniffer". One defines the total efficiency N by the ratio of the amount of species detected by the MS to the total amount of species produced electrochemically.

$$J_{O_2}^{sniffer} = NJ_{O_2}^{sample} \qquad \textbf{VII-10}$$

where $J_{O2}^{sniffer}$ is the oxygen flow entering the sniffer, N the transfer effieciency and J_{O2}^{sample} the electrochemically produced oxygen flow.

Considering the relation between the oxygen pressure in the sniffer and the sniffer incoming oxygen flow :

$$p_{O_2}^{sniffer} = \frac{RT}{PS} J_{O_2}^{sniffer} \qquad \text{VII-11}$$

and so

$$I_{O_2} = K_{O_2}^0 \frac{RT}{PS} J_{O_2}^{sniffer} \qquad \text{VII-12}$$

Combining equations VII-10 and VII-12 one can finally write equation VII-13.

$$I_{O_2} = NK_{O_2}^0 \frac{RT}{PS} \frac{I_f}{4F} \qquad \text{VII-13}$$

where, I_{O2} is the oxygen ion current intensity measured by MS, I_f is the faradaic current imposed to the cell by the galvanostat, K^0 the MS calibration constant, F the Faraday constant and N is the total efficiency.

A plot of I_{O2} vs I_f allows the determination of N, which is estimated to be 0.098 for this setup (Fig. VII-10).

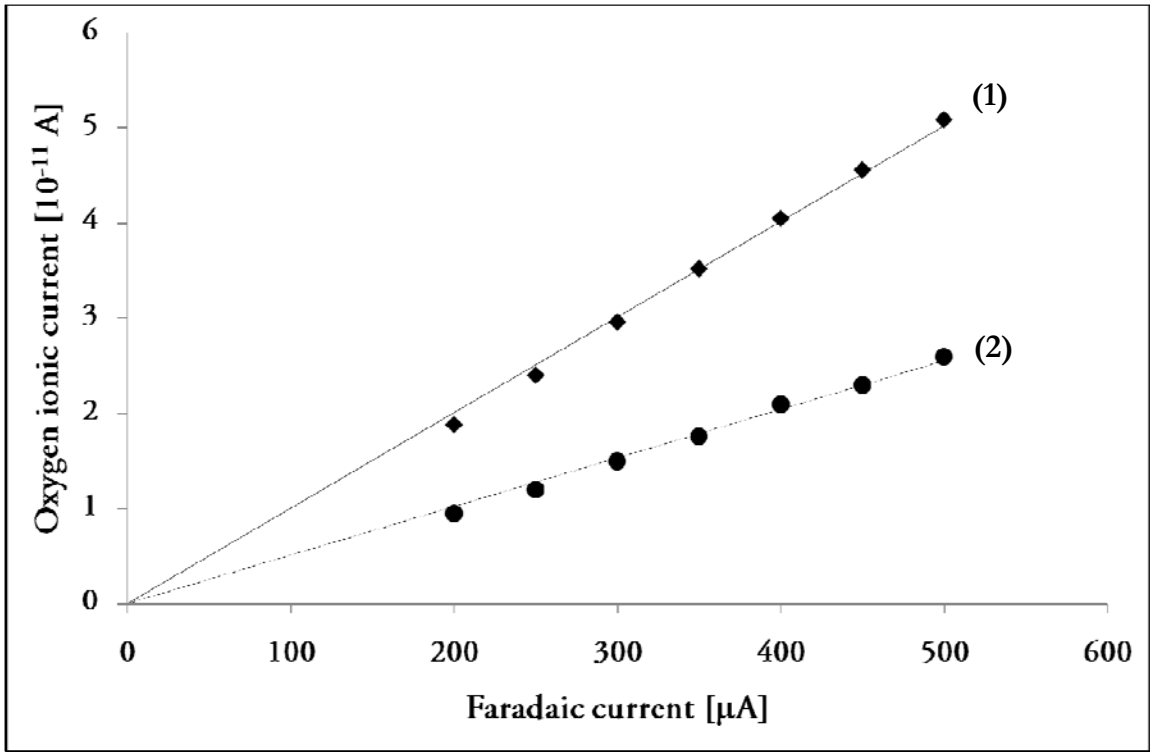

Fig. VII-10: Dependence of oxygen ionic current intensity on the applied faradaic current. Application of the current is performed during 60s under background oxygen partial pressure of 10^{-7} mbar at T=400°C. Single chamber reactor (1) dual chamber reactor (2).

One should notice that the total effieciency *N* is composed of a collection efficiency, *C,* and a detection effieciency, *D*.

The collection efficiency reflects the ratio of product flow guided to the "sniffer" entrance, $J_{O_2}^{Top\,Reactor}$, to the total electrochemically formed oxygen flow $J_{O_2}^{sample}$.

$$C = \frac{J_{O_2}^{Top\,Reactor}}{J_{O_2}^{sample}} = 0.2 \qquad \textbf{VII-14}$$

This factor depends on the reactor time constant, *i.e.* on its design.

The detection efficiency reflects the ratio of the mass spectroscopically detected oxygen flow in the "sniffer" $J_{O_2}^{sniffer}$ to the product flow guided to the "sniffer" entrance, $J_{O_2}^{Top\,Reactor}$:

$$D = \frac{J_{O_2}^{Sniffer}}{J_{O_2}^{Top\,Reactor}} = 0.49 \qquad \textbf{VII-15}$$

This factor depends on the detection time constant of the "sniffer" and of its distance to the top hole of the reactor.

A similar calibration is performed for the dual chamber type reactor, *e.g.* under background pressure of oxygen in both compartments (p_{O2} = 10^{-7} mbar). Doing so, the oxygen ionic current recorded with the MS I_{O2} is related to the faradaic current imposed with the galvanostat I_f, allowing to determine the total detection efficiency N=0.069 for the dual chamber type reactor composed of the collection efficiency C= 0.14 and the detection efficiency D= 0.48.

VII.4 Discussion

The elaboration of a new probe accessory for the investigation of solid state electrochemical systems under HV condition leads to the development of two differential solid electrochemical mass spectrometry apparatus. The main characteristic of these devices are

summarized in Table VII-2 which gives the relevant parameters of the different constituting parts of each configuration, *i.e.* vaccum system, heating system, mass spectrometry analysis, reactant gas supply and electrochemical reactor.

The heating system was carefully designed in order to avoid any temperature gradient in the YSZ electrolyte, *i.e.* to insure that in the single chamber reactor OCV = 0V. In fact because of the HV conditions, the only heat transport mechanism which can be used to heat the sample is radiation (convection being inexistent under HV and thermal conductivity of YSZ being too low, *i.e.* 2.5 $W.m^{-1}.K^{-1}$ [22]). The use of a single filament placed in the vicinity of the working electrode, as commonly seen in most UHV/TPD experimental setups [3-11], would create a large temperature gradient between the two sides of the sample. Herein, the sample was heated indirectly by the reactor which acts as a radiative heat source allowing to supply a homogeneous heating for the sample up to 500°C. Worth to mention that, as a consequence, adding openings at the reactor sides, *e.g.* to decrease the reactor time constant, decreases dramatically the performance of the heating system. Another important limitation of the heating system concerns the oxygen partial pressure in the HV chamber, which should be kept below 10^{-5} mbar to avoid the combustion of the tungsten filament, *i.e.* the break of the heat source.

The two electrochemical reactors realized, single and dual chamber type, features low-volume of reactants and very small time constant (about 1ms) allowing a fast sampling of the electrochemical products. Because of their microreactor properties, these two reactors presented a low collection efficiency (0.2 for the single chamber type and 0.14 for the dual chamber type). However, this collection efficiency parameter, which might be easily improved by sealing some openings on the sides of the reactors, should be intentionally kept low because of the MS analysis limitations.

Similarly, because of the limitation of the QMS detector which should not be exposed to high pressure ($<10^{-5}$mbar), only a small fraction of the electrochemical product must be submitted to the MS gas flow analysis to prevent the break of MS filament, *i.e.* the collection effieciency of the reactor must be small.

		Single chamber configuration	Dual chamber configuration
Vacuum system			
	Volume	10 L	10 L
	Pumping speed	520 L.s^{-1}	520 L.s^{-1}
	Time constant	20 ms	20 ms
	Minimum attainable pressure	10^{-7} mbar	10^{-7} mbar
Heating system			
	$T_{sample}=k_0 T_{reactor}$	$k_0=0.93$	$k_0=0.9$
	Main power supply	7V/3A	7V/3A
	Tunning electrical potential	500V	550V
	T_{sample}^{max}	500°C	500°C
	Maximum oxygen pressure	10^{-5} mbar	10^{-5} mbar
MS analyser			
	Ionisation volume	0.38 L	0.38 L
	Pumping speed	0.63 L s^{-1}	0.63 L s^{-1}
	Time constant	500 ms	500 ms
	Potential applied to the filament	800 V	800 V
	Limit detection pressure	10^{-5} mbar	10^{-5} mbar
	$K_{O_2}^0$	4.5×10^{-8} A Pa^{-1}	4.5×10^{-8} A Pa^{-1}
	K_{CO}^0	-	8.10^{-8} A Pa^{-1}
	$K_{CO_2}^0$	-	5.10^{-8} A Pa^{-1}
Reactant gas supply			
	O_2 (46) garbagas certified	HV chamber	Reactor (both sides)
	CO (60) garbagas certified	-	Working compartiment
Electrochemical reactor		**Single chamber**	**Dual chamber**
	Working compartiment volume	7×10^{-4} L	7×10^{-4} L
	Reference compartiment volume	5×10^{-4} L	5×10^{-4} L
	Pumping speed	0.64 L s^{-1}	0.9 L s^{-1}
	Time constant	1 ms	0.8 ms
	Collection efficiency	0.2	0.14
	Total efficiency	0.098	0.069
	Applied/measured potential	$\Delta U_{WR} = \eta$	$\Delta U_{WR} \neq \eta$

Table VII-2 : Main parameters and characteristics for each configuration.

VII.5 Conclusion

A new probe device, coupling electrochemistry and mass spectroscopy techniques, is developed for the investigation of a solid electrochemical cell under high vacuum conditions (HV). Two configurations are proposed, single and dual chamber type reactors, for the investigation of both the electrochemical and electrocatalytical behavior of the Pt/YSZ system. At this molecular level, the fast detection response of the herein built solid electrochemical mass spectrometry (SEMS) device allowed to observe on line the electrochemically formed oxygen during an anodic polarization with a total efficiency of 0.11. Worth to mention that this low efficiency is related to a poor collection efficiency induced by the low time constant of the electrochemical microreactors designed.

VII.6 References

1. Williams FJ, Palermo A, Tikhov MS, Lambert RM (2000) Journal of Physical Chemistry B 104: 615

2. Williams FJ, Palermo A, Tikhov MS, Lambert RM (2001) Surface Science 482-485: 177

3. Luerßen B, Janek J, Imbihl R (2001) Solid State Ionics 141-142: 701

4. Luerßen B, Gunther S, Marbach H, Kiskinova M, Janek J, Imbihl R (2000) Chemical Physics Letters 316: 331

5. Imbihl R, Janek J (2000) Solid State Ionics 136-137: 699

6. Poppe J, Völkening S, Schaak A, Janek J, Imbihl R (2000) Phys. Chem. Chem. Phys. 1: 5241

7. Janek J, Luerßen B, Imbihl R, Rohnke M (2000) Phys. Chem. Chem. Phys. 2: 1935

8. Vayenas CG, Bebelis S, Pliangos C, Brosda S, Tsiplakides D (2001) Electrochemical Activation of Catalysis: Promotion, Electrochemical Promotion, and Metal-Support Interactions. Kluwer Academic / Plenum Publishers, New York

9 Neophytides SG, Vayenas CG (1995) Journal of Physical Chemistry 99: 17063

10. Katsaounis A, Nikopoulou Z, Verykios XE, Vayenas CG (2004) Journal of Catalysis 222: 192

11. Katsaounis A, Nikopoulou Z, Verykios XE, Vayenas CG (2004) Journal of Catalysis 226: 197

12. Anastasijevic NA, Baltruschat H, Heitbaum J (1989) Journal of Electroanalytical Chemistry 272: 89

13. Baltruschat H (2004) Journal of the American Society for Mass Spectrometry 15: 1693

14. Jaccoud A, Foti G, Comninellis C (2006) Electrochimica Acta 51: 1264

15. Foti G, Jaccoud A, Falgairette C, Comninellis C (2009) Journal of Electroceramics 23:175

16. Jaccoud A, Falgairette C, Foti G, Comninellis C (2007) Electrochimica Acta 52: 7927

17. Falgairette C, Jaccoud A, Foti G, Comninellis C (2008) Journal of Applied Electrochemistry 38: 1075

18.] K. Judai, S. Abbet, A. Woerz, M. Roettgen, and U. Heiz, Int J Mass Spectrom 229, 99

(2003).

19. Valloton R. (2009) EPFL Thesis n°4365

20. Handbook of Vacuum Science and Technology, Hoffman, Singh and Thomas, Academic Press, 1998

21 Foti G, Stankovic V, Bolzonella I, Comninellis C (2002) Journal of Electroanalytical Chemistry 532: 191

22. Tan Y, Longtin JP, Sampath S (2006) Journal of Thermal Spray Technology 15: 545

CHAPTER VIII- Pt/YSZ ELECTROCHEMICAL INVESTIGATION UNDER HV

In this chapter, the Pt/YSZ interface is investigated under high vacuum (HV) conditions in absence of oxygen (p_{O2}=10^{-7}mbar) at 400°C. Transient and steady state electrochemical techniques are coupled to mass spectrometric gas analysis using the single chamber type configuration of the previously described SEMS monitoring device.

Under anodic polarization, both platinum oxidation and oxygen evolution reaction are identified. It turns out that PtO was present at both Pt/YSZ and Pt/gas interface according to two different mechanisms. The PtO formation taking place at the Pt/YSZ interface is electrochemical process and follows a parabolic growth law while the other one involves diffusion of PtO formed at the triple phase boundary toward the Pt/gas interface. In fact, it is proposed that the side oxygen evolution reaction stabilizes thermodynamically the PtO diffusion toward the gas exposed interface during the anodic polarization.

Under cathodic polarization, the lack of oxygen in the gas phase induced the reduction of the YSZ solid electrolyte which acts as oxygen source for the formation of O^{2-} ions migrating to the anode. In fact, the reaction front of zirconia reduction moves in direction of the anode and creates an electron conductive zone in the YSZ subsurface at the cathode.

VIII.1 Introduction

In this work a new electrochemical technique has been developed for the electrochemical investigation of the Pt/YSZ interface under HV condition. In this technique an electrochemical perturbation is imposed to the Pt/YSZ interface. This perturbation can lead to the formation of $O_{2(g)}$ which is analyzed online by MS. The aim of the experiment is to obtain information on the stability of YSZ solid electrolyte toward cathodic reduction and on the kinetics of the involved redox couples (O_2/O^{2-}, PtO/Pt). The response time of the system is 0.5s.

Two main perturbation-MS analysis systems have been used :

- Perturbation of the Pt/YSZ interface by cyclic voltammetry (CV) with sweep rates ν ranging from 20mV s^{-1} to 250mV s^{-1} and analysis of the formed $O_{2(g)}$ (if any) by MS. This system has been reported as CV-MS
- Perturbation of the Pt/YSZ interface by double step chronopotentiometry (DSCP) for different applied currents and perturbation times followed by analysis of the formed $O_{2(g)}$ (if any) by MS. This system is reported as DSCP-MS

In both systems the potential (E) has been reported relative to YSZ/Pt,O_2(p_{O2}), where p_{O2} is the working oxygen partial pressure.

VIII.2 Cyclic voltammetry combined with mass spectrometry (CV-MS)

VIII.2.1 The Pt/YSZ interface

The cyclic voltammogram (CV) and the corresponding rate of oxygen evolution reaction measured by MS (CV-MS measurements) in the potential region of YSZ stability is given in Fig. VIII-1. A surface redox couple in the potential region of 100mV to 600mV is obtained. The separation between the anodic and cathodic peak (ΔE = 200mV) indicates that the

process is largely irreversible. This redox couple is certainly related to the oxidation/reduction of Pt at the Pt/YSZ interface (equation VIII-1)

$$PtO_{Pt/YSZ} + 2e^- \rightleftarrows Pt + O^{2-} \qquad \textbf{VIII-1}$$

The insert of Fig. VIII-1 shows furthermore that the onset potential of $O_{2(g)}$ evolution (equation VIII -2) is about 300mV

$$2O^{2-} \rightarrow O_{2(g)} + 4e^- \qquad \textbf{VIII-2}$$

This reaction takes places certainly at the three phase boundary (tpb).

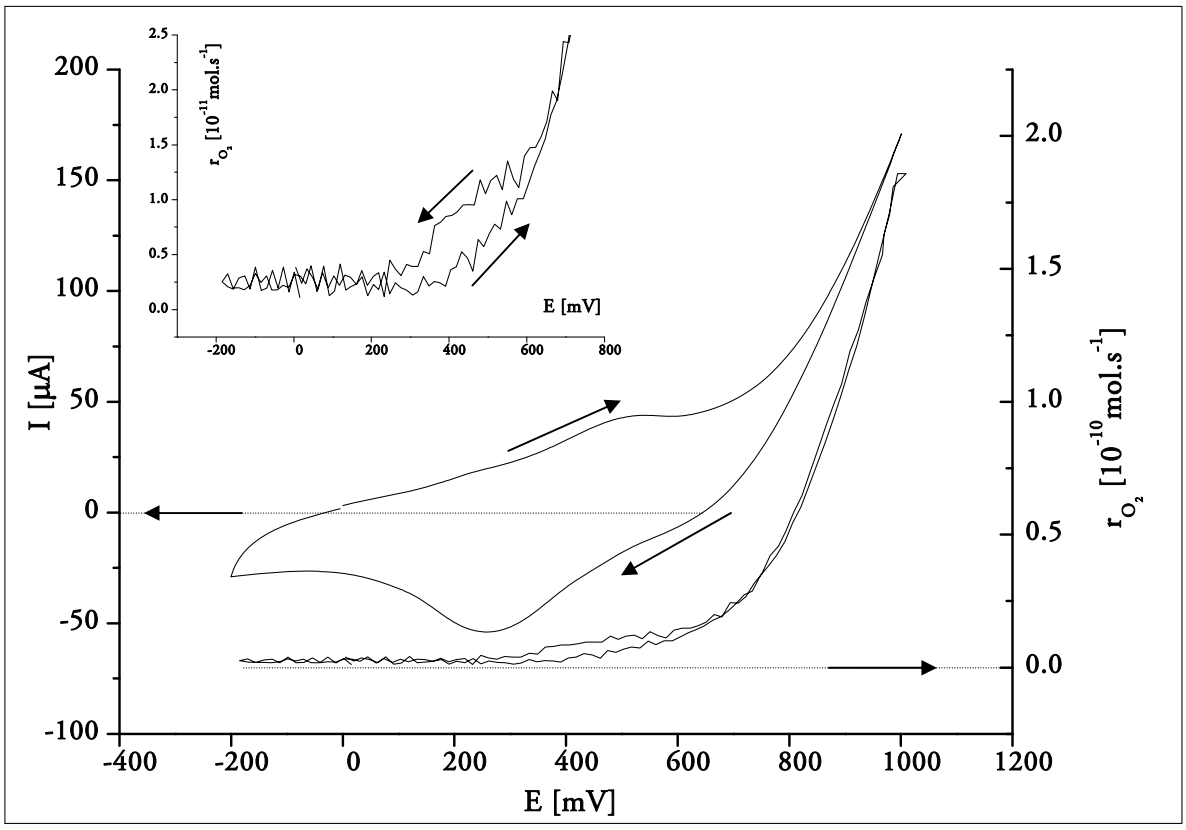

Fig. VIII-1 : Typical CV-MS measurements obtain at Pt/YSZ interface under HV composed of the cyclic voltammogram (left) and corresponding MS results (right). T=400°C, $p_{O2}=10^{-7}$mbar, v=50mV s^{-1}. Insert : Magnification of the MS response in the -200 to 800mV domain.

VIII.2.2 Investigation of the electrochemical stability of YSZ

The influence of cathodic potential limit and partial oxygen pressure (p_{O2}) on the electrochemical stability of YSZ has been investigated.

VIII.2.2.1 Influence of the cathodic potential limit E_c

Fig. VIII-2 shows the effect of the lower cathodic potential limit, E_c, on the CV-MS measurements obtained on the Pt/YSZ interface. For E_c values lower than -250mV a reduction current is observed in the CV during the forward scan. This current increases with decreasing E_c reaching a value of -250 μA for E_c = -1100mV.

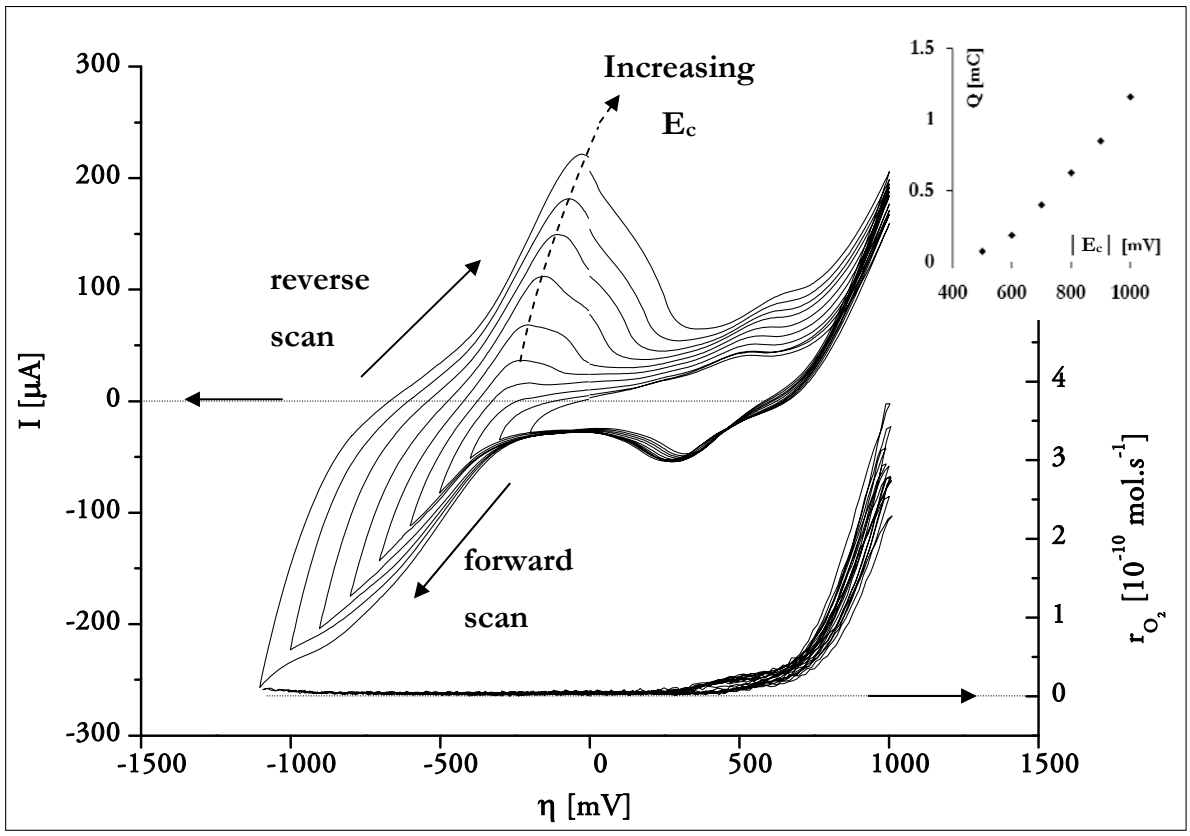

Fig. VIII-2 : CV-MS measurements :Effect of cathodic potential limit E_c (from -200 to -1100mV by steps of 100mV) on cyclic voltammograms of Pt/YSZ interface under HV (left) and corresponding MS results of O_2 evolution (right). Insert : Charges estimated by integration of the anodic peak as a function of cathodic potential limit. T=400°C, $p_{O2}=10^{-7}$mbar, v=50mVs^{-1}

In the reverse scan, an anodic peak is observed which grows and shifts to less negative potentials with decreasing cathodic limit E_c. The fact that the involved anodic charge is almost the same as the cathodic charge indicates that during the cathodic polarization an electrical charge is stored at the Pt/YSZ interface certainly due to YSZ reduction (equation VIII -3)

$$ZrO_2 + 2\delta e^- \rightleftarrows ZrO_{2-\delta} + \delta O^{2-} \qquad \textbf{VIII-3}$$

This stored charge is estimated by integration of the involved cathodic or anodic charge and found to increase almost linearly with the cathodic potential limit E_c (insert of Fig. VIII-2). The involved stored charge (more than 1mC/cm^2) indicates that the stored charge is not limited at the Pt/YSZ interface but penetrates several monolayers inside of the YSZ solid electrolyte. This penetration of charge inside of the YSZ can be explained by the electronic conductivity of the recduced YSZ which creates a new interface $(YSZ)_{reduced}$/YSZ allowing electron transfer through the reduced YSZ.

As is shown in the MS response, no oxygen evolution is involved in this potential domaine (-200mV to -1100mV).

VIII.2.2.2 Influence of the anodic potential limit E_a

Fig. VIII-3 shows the influence of the upper potential limit, E_a, on the CV-MS measurements. This figure shows clearly that the anodic potential limit does not affect the electrochemical behavior of the YSZ solid electrolyte but has a strong effect on the development of the Pt/PtO redox couple. In fact, increasing E_a results in an increase of the involved cathodic charge related to the reduction of PtO and a potential shift to more positive potential of the reduction peak. The stored charge related to this reduction process is estimated by integration of the cathodic peak, and is found to increase linearly with the anodic reverse potential (right insert in Fig. VIII-3). The electrochemical process involved in this potential domain is attributed to the electrochemical formation/reduction of a PtO layer at the Pt/YSZ interface, according to reaction VIII -1.

The involved stored charge (≈ 0.1mC/cm²) indicates that in this case the penetration is very much limited and the stored charge is mainly located at the Pt/YSZ interface under the investigated conditions.

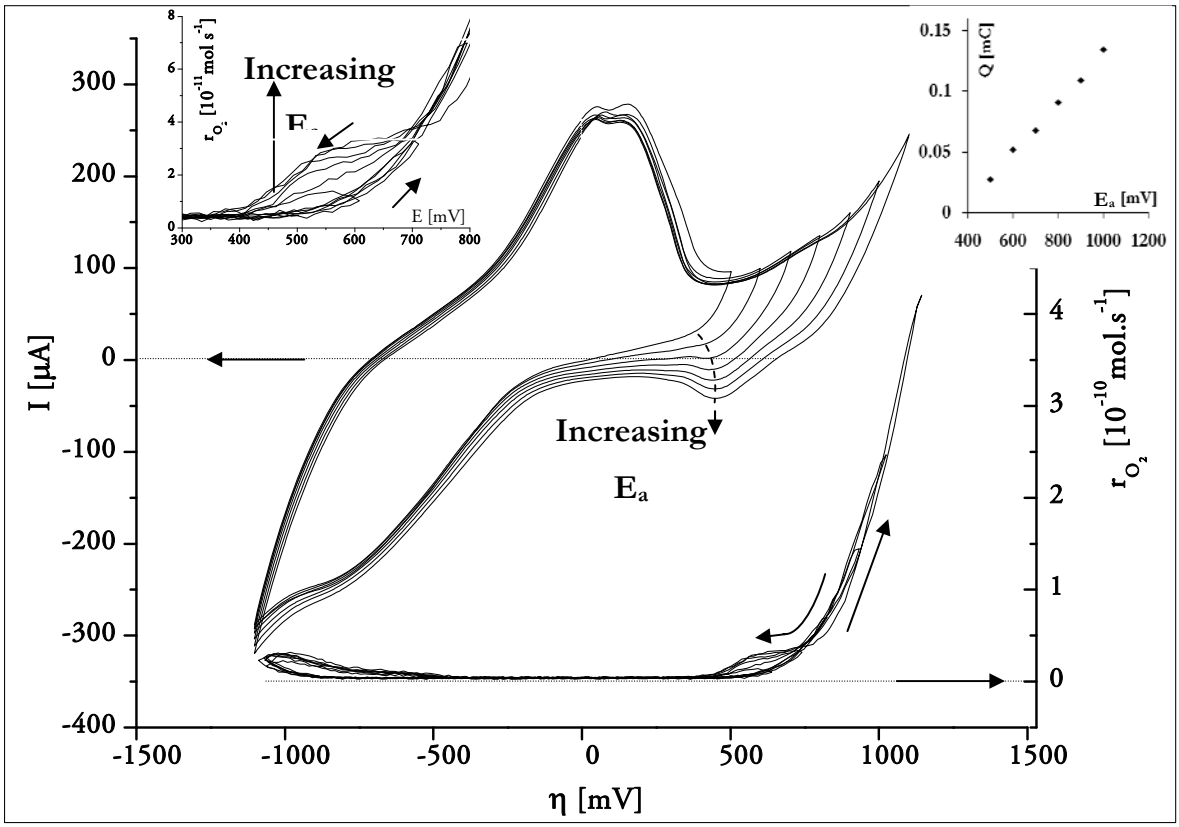

Fig. VIII-3 : CV-MS measurements: Effect of anodic potential limit E_a (from 400mV to 1000mV by steps of 100mV) on the cyclic voltammogram of Pt/YSZ interface under HV (left) and corresponding MS results of O_2 evolution (right). T=400°C, PO_2=10^{-7}mbar, v=50mV s^{-1}. Right insert : Charges estimated by integration of the cathodic peak as a function of anodic potential limit, Left insert: . Magnification of the MS response in the 300 to 800mV domain.

As is shown in the MS response, the rate of oxygen release, r_{O2}, increases as the potential exceeds 300mV. This is attributed to the oxygen evolution reaction (OER) taking place at the triple phase boundary (tpb) according to reaction VIII -2:

When the potential is reversed, this reaction slows down and r_{O2} decrease in a quasi-reversible way until 700mV (confirming a response time < 1s) then remains higher than the forward scan forming a plateau between 750mV and 500mV (r_{O2} = 30 pmolO s^{-1}) before decreasing to zero at 300mV. This process of oxygen release does not seem to be related to

any electrochemical process but rather to the desorption of oxygen species lying at the Pt/gas interface according to reaction VIII -4:

$$Pt\bullet O \rightarrow \frac{1}{2}O_{2(g)} + Pt \qquad \text{VIII-4}$$

VIII.2.2.3 Influence of the oxygen partial pressure p_{O2}

By increasing the oxygen partial pressure in the system, the MS detector was useless. In fact, the high oxygen background ionic current does not allow to measure the electrochemically formed O_2. Hence in this part, only cyclic voltammorgams recorded at different p_{O2} are presented (Fig. VIII-4).

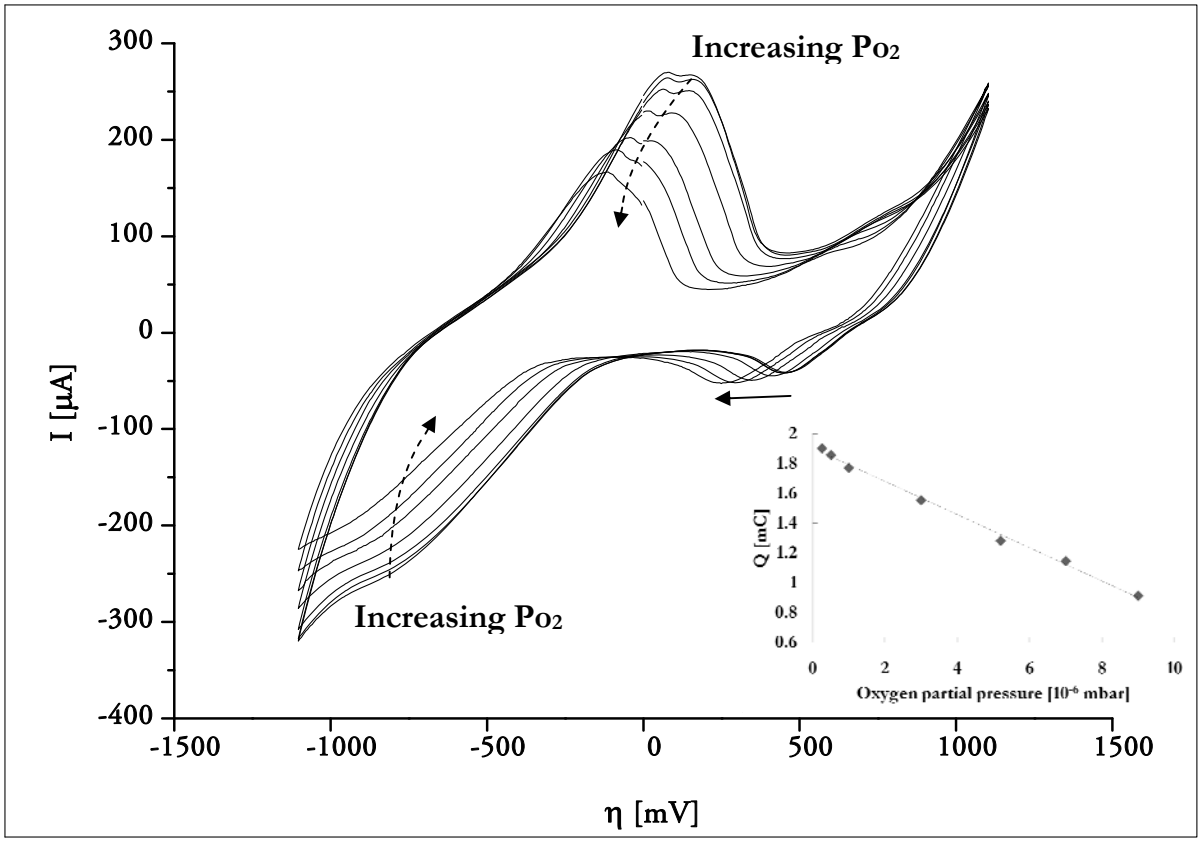

Fig. VIII-4 : CV-MS measurements: Effect of O_2 partial pressure (p_{O2}) on cyclic voltammograms of Pt/YSZ interface under HV , T=400°C, v=50mV.s^{-1}, pO_2= 10^{-7}mbar, 5.10^{-7}mbar, 1.10^{-6}mbar, 3.10^{-6}mbar, 5.10^{-6}mbar, 7.10^{-6}mbar and 9.10^{-6}mbar. Insert gives the charge estimated by integration of the anodic peak.

Fig. VIII-4 shows that increasing p_{O2} affects both the stability of YSZ solid electrolyte and the kinetics of the surface PtO/Pt redox couple. In fact increasing p_{O2} results in a strong decrease of the stored charge during cathodic polarization at E_c = -1100 mV indicating an increase of YSZ stability against electrochemical reduction. Furthermore, the cathodic PtO reduction peak shifts to less positive values with increasing p_{O2}.

VIII.3 Double step chronopotentiometry combined with mass spectrometry (DSCP-MS)

The reactions involved in the Pt/YSZ system (reactions VIII -1, VIII -2, VIII -3 and VIII -4) have been further investigated by DSCP-MS measurements. The double step chronopotentiometry (DSCP) perturbation includes a pretreatment step and two measurement steps. The pretreatment step consists of a constant cathodic current step of -30μA applied for 10s (this insures that the Pt/YSZ interface is in the same initial state before each experiment). The measurement step consists in a constant anodic current (I_a) step during a time t_b (charging) followed by a cathodic current I_c (discharging) step. The influence of the anodic current, I_a, and of the anodic polarization time t_b are investigated.

Fig. VIII-5 shows a typical DSCP-MS (-30μA in the pretreatment, +30μA in the anodic step and -30μA in the cathodic step).

Four main domains can be distinguished in this figure (Fig. VIII-5):

- Domain I (from 0-10s) where the potential reaches a plateau at about -400mV. In this domaine there is no oxygen evolution and the main reaction is the oxidation of reduced YSZ produced during the pretreatment step (reverse of equation VIII -3).
- Domain II where the potential increases rapidily from -400mV to almost the open circuit potential. In this domain both the PtO formation (reverse of equation VIII -1) and oxygen evolution (equation VIII -2) take place. However, the former reaction seems to predominate.

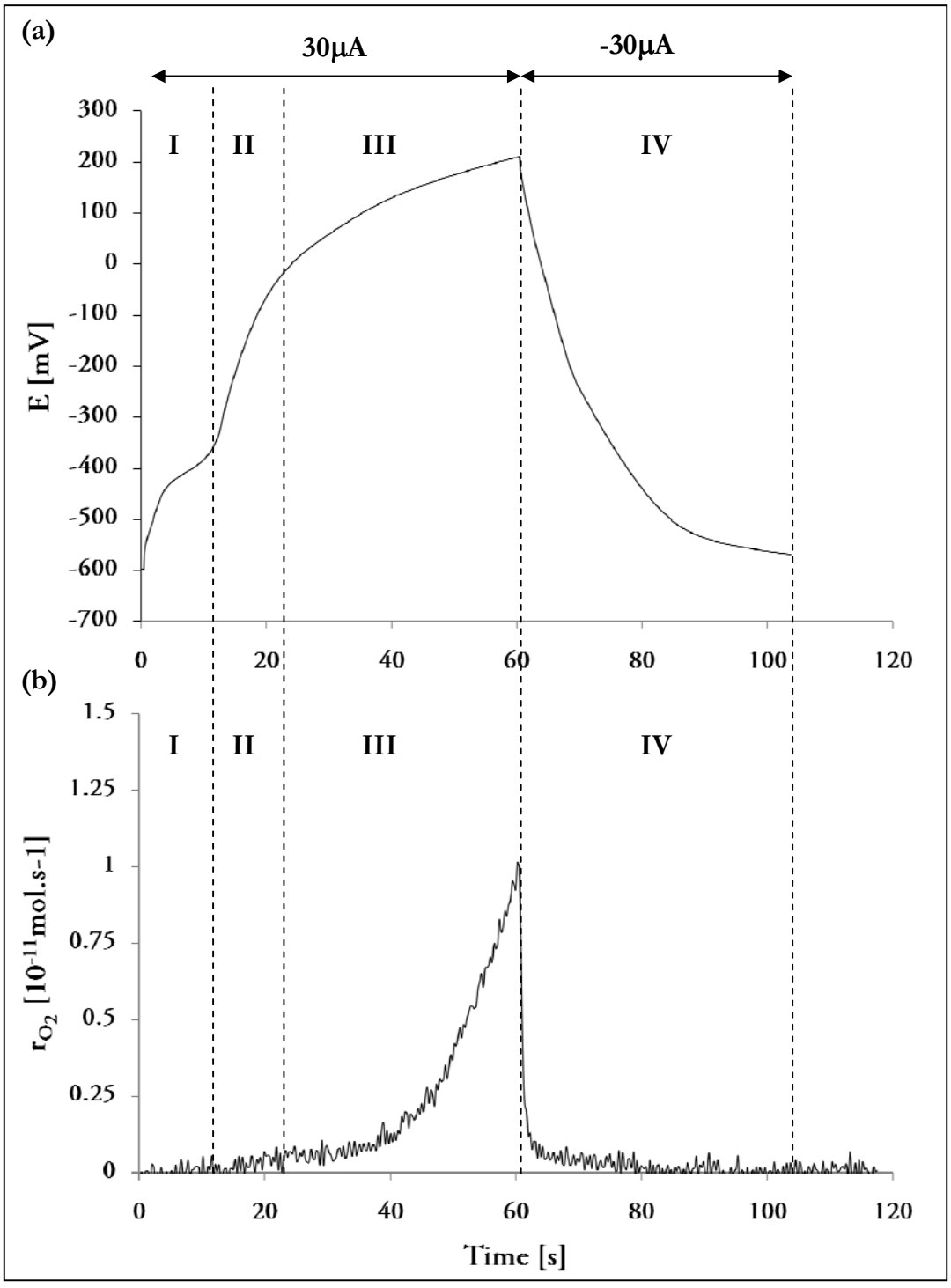

Fig. VIII-5 : Typical DSCP-MS responses obtained at Pt/YSZ interface under HV composed of chornopotentiometric perturbation (a) and corresponding MS measurements of O_2 evolution (b). T=400°C, I_a=30µA, I_c=-30µA, p_{O2}=10^{-7}mbar.
Domain I : YSZ reoxidation, Domain II : PtO formation, Domain III : O^2 evolution, Domain IV : PtO reduction.

● Domain III where the potential increases slowly. In this domain both PtO formation and O_2 evolution take place, however the O_2 evolution (equation X-2) seems to dominate.
● Domain IV where the potential decrease slowly reaching almost the initial value. In this domain the reduction of PtO (equation X-1) dominates.

VIII.3.1 Influence of the applied anodic current, I_a

Fig. VIII-6 displays the influence of the anodic current I_a on the chronopotentiometric curves and on the corresponding oxygen evolution monitored by MS (DSCP-MS measurements). The anodic charging step is performed by applying increasing anodic current from 10μA to 100μA by steps of 10μA during 60s. The current is then reverse to -30μA (discharging step) until the measured potential reaches its initial value (-600mV).

The general features of the responses obtained are similar to those presented in Fig. VIII-5. However, increasing the applied current results in the following modifications:
● Both domains I and II are strongly shortened as expected with increasing I_a.
● Domain IV increases with increasing I_a. This is related with the increasing amount of formed PtO with increasing I_a. The release of O_2 in this domain (Fig. VIII-6 b) under cathodic polarization is very intriguing. This process should involve an oxygen containing species located far from the electroactive Pt/YSZ interface. As suggested in the CV-MS investigation (§ VIII-2), this may involve desorption of oxygen species lying at the Pt/gas interface according to reaction VIII-4. In fact it is speculated that during the anodic polarization step, the oxygen discharged at the tpb diffuses slowly toward the gas exposed interface.

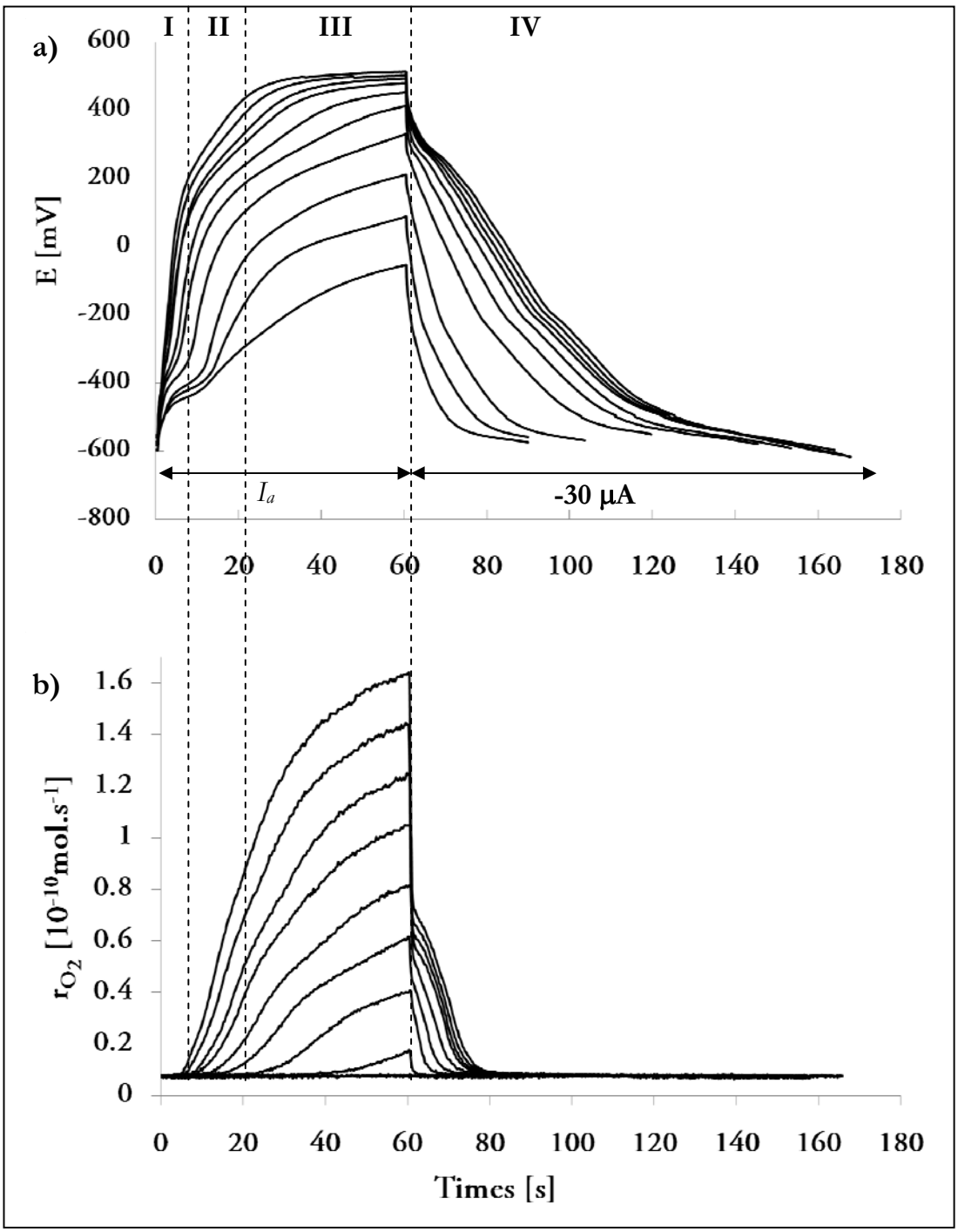

Fig. VIII-6 : DSCP-MS measurements : Current reverse chornopotentiometric transients for anodic polarization with increasing current from 10µA to 100µA by steps of 10µA; cathodic current is kept at -30µA (a) and corresponding MS results of O_2 evolution (b). T=400°C, PO_2=10^{-7}mabr.

VIII.3.2 Influence of the anodic polarization time, t_h

Fig. VIII-7 displays the influence of the anodic holding time t_h on the DSCP-MS measurements. During the charging step, an anodic current of 50μA is applied for increasing holding time (60s to 300s by steps of 60s). The current is then reversed to -50μA until the potential decreases to its initial value -700mV (discharging step).

The general feature of the results obtained here are similar to those reported in Fig. VIII-5 and Fig. VIII-6. However, on the obtained E-t curves (Fig. VIII-7 a) in domain IV, the applied cathodic current induce the reduction of PtO (formed in domain I and II) to metallic platinum. The potential of the electrode returns to the initial potential (E=-700mV at t=0) due to the decrease of PtO surface concentration. The process can be regarded as titration of PtO present at the electrode surface at the end of the anodic polarization by the applied cathodic current. The E-t curves observed in the domain IV are similar to those obtained for a potentiometric titration (E as function of titrant added, $I_c \bullet t$). When the PtO surface concentration drops to zero at the electrode surface, the potential achieves its initial value. In this domain, the time needed for the potential to reach its initial value is reported as the titration time τ. It is related to the surface concentration of PtO. The variation of τ with the anodic polarization time is given in insert of Fig. VIII-7. The titration time, τ, first increases with polarization time t_h, and then saturates at large anodic polarization times (insert Fig. VIII-7 a). Further analysis of the DSCP-MS measurements (Fig. VIII-7) shows that in domain III both O_2 evolution and PtO formation occur simultaneously.

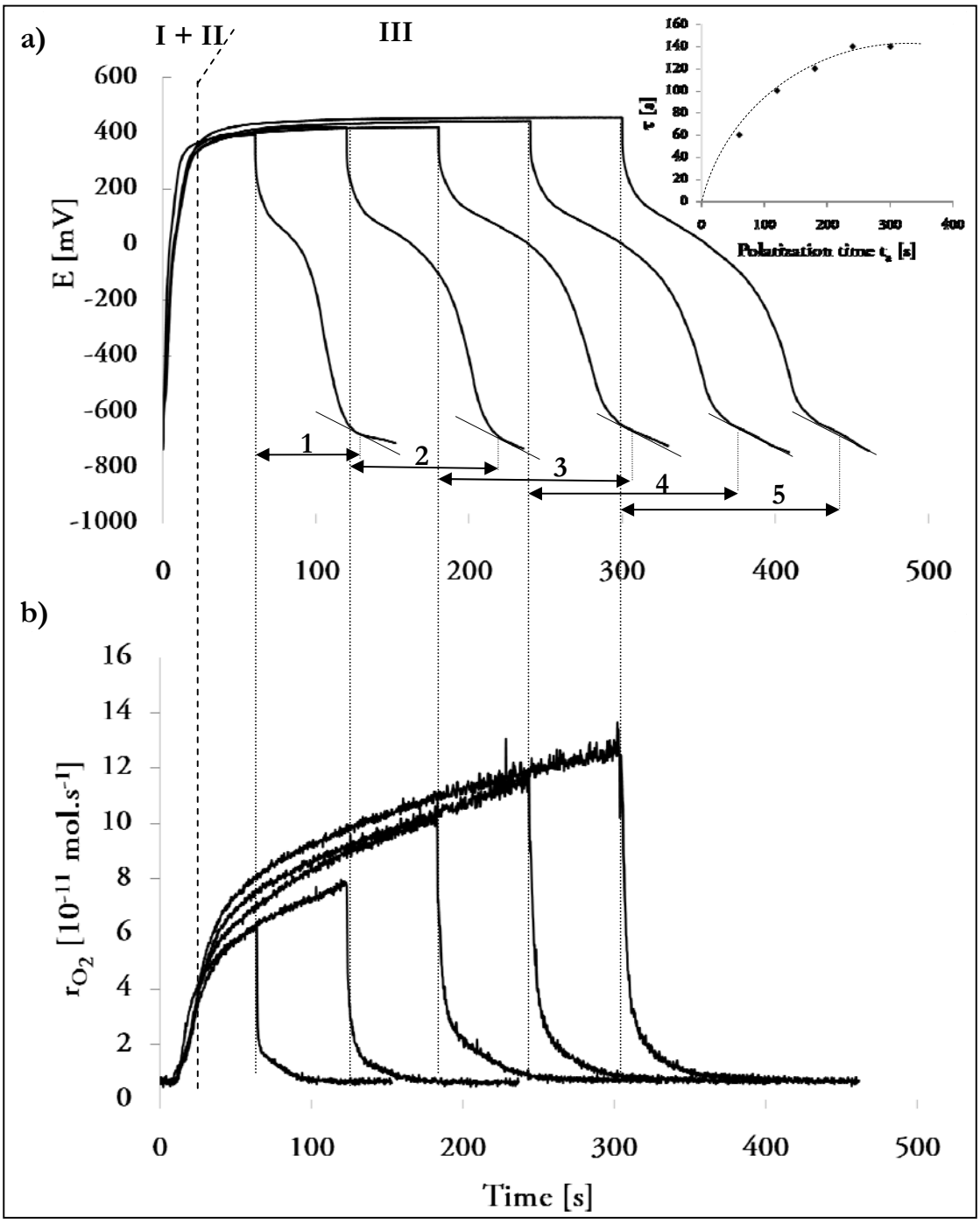

Fig. VIII-7 : DSCP-MS measurements : effect of anodic polarization time on the current reverse chronopotentiometric transients (a) and corresponding MS results of O_2 evolution (b). T=400°C, $p_{O2}=10^{-7}$mbar, I_a=50µA, Ic=-50µA, t_a=60s, 120s, 180 240s and 300s. Insert : Dependence of τ on the polarization time.

One can define the current effieciency of the oxygen evolution reaction η_{O2} (equation VIII -5), PtO formation at the Pt/YSZ interface, η_{PtO}, (equation VIII -6) and Pt•O formation at the Pt/gas interface, η_O, (equation VIII -7).

$$\eta_{O_2} = \frac{Q_{O_2}}{Q_{Total}} \qquad \textbf{VIII-5}$$

$$\eta_{PtO} = \frac{Q_{PtO}}{Q_{Total}} \qquad \textbf{VIII-6}$$

$$\eta_O = \frac{Q_O}{Q_{Total}} \qquad \textbf{VIII-7}$$

where Q_{O2} is the amount of oxygen evolved during the anodic polarization step, determined from the MS results (Fig. VIII-7 b), Q_{PtO} is the amount of PtO reduced electrochemically during the cathodic polarization (Fig. VIII-7 a), Q_O is the amount of oxygen released during the cathodic polarization determined from the MS results (Fig. VIII-7 b) and Q_{Total} is the total applied anodic charge (I_a•t_h).

Fig. VIII-8 and Fig. VIII-9 shows the influence of I_a (t_a =60s) and polarization time t_a (I_a =50μA) on η_{O2}, η_{PtO} and η_O. Increasing I_a and polarization time results in a strong decrease of η_{PtO} with a concomitant increase in η_{O2}. As previously reported at atmospheric pressure (Chapter VI), these results confirm that with increasing anodic holding time, the initially high current efficiency, η_{PtO}, decreases rapidly with a concomitant increase of η_{O2}. In fact, the formation of a PtO layer at the Pt/YSZ double phase boundary appears as a barrier to further oxide growth (auto-inhibiting reaction) without affecting the oxygen evolution reaction. Worthy to notice that η_O increases with the applied anodic current I_a but remains at a constant value independently of the anodic polarization time. This is an indication that saturation of adsorbing sites at the gas exposed Pt is rapidly achieved.

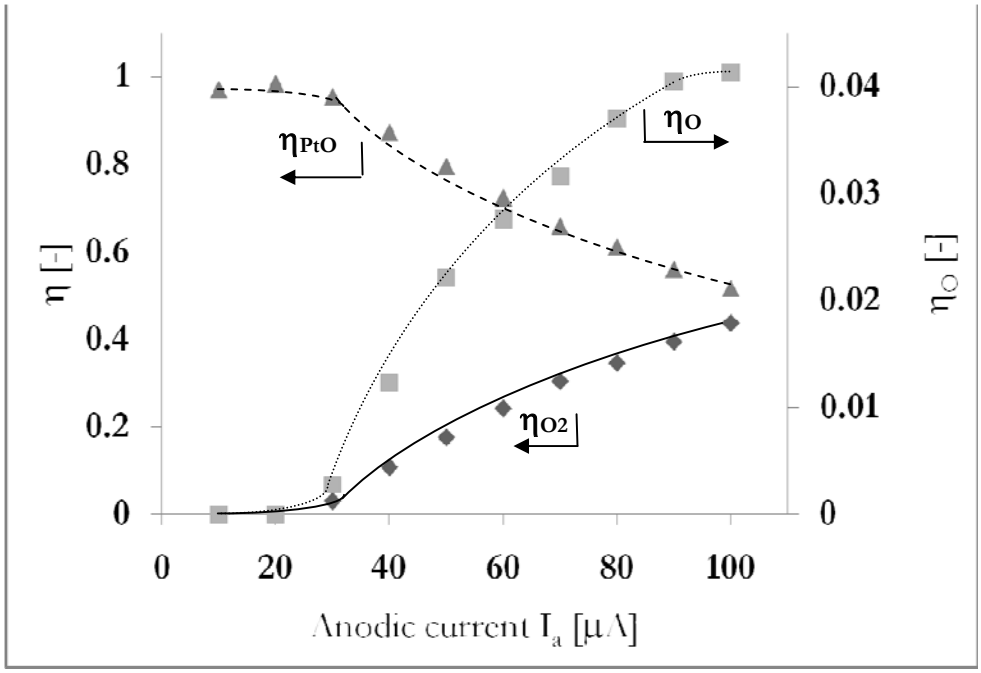

Fig. VIII-8 :Effect of increasing anodic polarization current I_a on the current effienciencies η_{O2} (left), η_{PtO} (left) and η_O (right) determined from steady state DSEMS experiment (Fig. VIII-6)

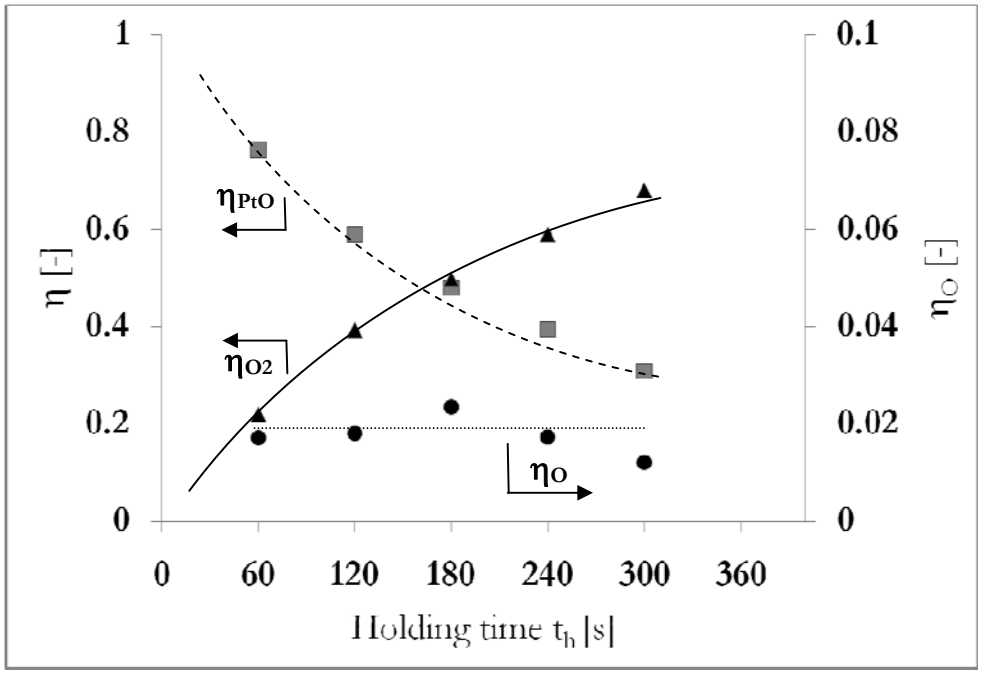

Fig. VIII-9 : Effect of increasing anodic polarization time t_h on the current effienciencies η_{O2} (left), η_{PtO} (left) and η_O (right) determined from steady state DSEMS experiment (Fig. VIII-6)

VIII.4 Discussion

The electrochemical investigation of the Pt/YSZ system, performed in HV under low oxygen partial pressure at 400°C by both CV-MS and DSCP-MS measurements revealed that the O^{2-} ions present in the solid electrolyte are involved in three main different electrochemical processes upon anodic/cathodic polarization:

- Zirconia oxidation/reduction (reaction X-3)
- Platinum oxidation/reduction (reaction X-1)
- Oxygen evolution (reaction X-2)

VIII.4.1 Zirconia reduction/oxidation reaction

The electrochemical process observed in the negative potential domain of the voltamograms is attributed to the progressive reduction/oxidation of YSZ in the vicinity of the Pt/YSZ interface (reaction VIII-3). Because of the absence of oxygen in the gas phase, upon cathodic polarization, zirconia acts as a oxygen source for the formation of O^{2-} ions according to

$$ZrO_2 + 2\delta e^- \rightarrow ZrO_{2-\delta} + \delta O^{2-} \qquad \textbf{VIII-8}$$

This induces a non-stochiometric depletion of oxygen, δ, in the YSZ solid electrolyte lattice which is known in litterature as YSZ blackening [1-5]. This process is comonly reported to be dependent on the oxygen activity in the solid electrolyte, on the temperature and on the oxygen partial pressure [4].

Worth to notice that upon elapsing cathodic polarization time, the reaction front of zirconia reduction advances toward the inside of the solid electrolyte. In fact, in the vicinity of the cathode, YSZ is suggested to behave as a mixed ionic and electronic conductor allowing the electron supply from the platinum cathode to the reactive sites situated at the YSZ subsurface.

VIII.4.2 Platinum oxidation/reduction and oxygen evolution reaction

Under anodic polarization of the Pt/YSZ interface, two reactions take place in parallel: PtO formation (reaction VIII -1) and oxygen evolution (reaction VIII -2). The determination of the current efficiency for each reaction demonstrates that platinum oxidation reaction, taking place at the Pt/YSZ interface, is rapidly limited by an auto-inhibited oxide growth mechanism (Fig. VIII-9) without affecting the oxygen evolution reaction (OER) at the triple phase boundary (tpb). However during the anodic polarization, a fraction of the oxygen discharged at the tpb seems to migrate toward the Pt/gas interface.

One should notice that, according to the thermodynamic investigation proposed by *Berry* [6] and *Vayenas* [7], at the low oxygen partial pressure applied here (p_{O2}=10^{-5} Pa), PtO is thermodynamically unstable. In fact, at 400°C the partial pressure of oxygen should increase up to 1Pa in order to stabilize PtO [6,7]. However, the massive release of gaseous oxygen at the tpb induced by the oxygen evolution reaction (reaction VIII -2) creates a huge local increase of p_{O2} at the platinum gas exposed surface. The species formed at the tpb by O^{2-} discharge are then proposed to populate the Pt/gas interface during the anodic polarization forming PtO at the gas exposed interface ($PtO_{Pt/gas}$). This oxide seems to be stable only under conditions of O_2 evolution.

The effective rate of PtO formation at the binary Pt/YSZ interface and at the Pt/gas interface are estimated according to equation VIII -9 and VIII -10 respectively :

$$R_{PtO}^{eff} = \eta_{PtO} \frac{I}{2F} \qquad \textbf{VIII-9}$$

$$R_{O}^{eff} = \eta_{O} \frac{I}{2F} \qquad \textbf{VIII-10}$$

where I is the applied current during the anodic polarization, η_{PtO} and η_O are the current efficiency of the PtO formation at the Pt/YSZ interface and at the Pt/gas interface respectively.

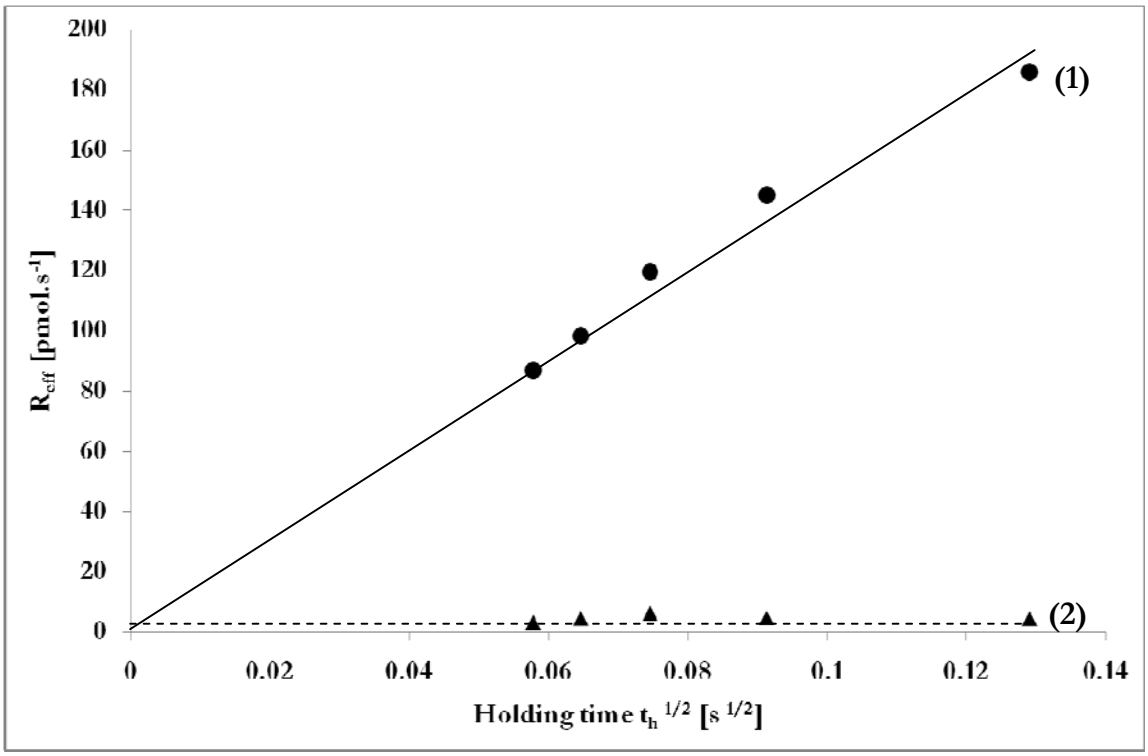

Fig. VIII-10 : Effective rate of PtO formation at the Pt/YSZ double phase boundary (1) and at the Pt/gas surface (2) as a function of the square root of anodic polarization time determined from DSCP-MS experiment (Fig. VIII-6)

As shown in Fig. VIII-10, parabolic time dependence is obtained for R_{PtO}^{eff} suggesting a parabolic PtO formation at the Pt/YSZ. This kinetic law for the electrochemical PtO formation appears similar to that reported at atmospheric pressure (Chapter VI) and is in agreement with the high temperature metal oxidation theory proposed by *Wagner* and its electrochemical interpretation given by *Hoar* & *Price* [8].

VIII.4.3 Proposed model

The mechanism of platinum oxidation previously proposed for a sputtered platinum electrode at atmospheric condition (Chapter VI), involving several oxygen storage locations is confirmed here under HV conditions. Both CV-MS and DSCP-MS measurements revealed a similar oxygen storage mechanism as that previously observed under atmospheric

pressure. However, in HV conditions at low oxygen pressure, one should consider that YSZ becomes electrochemically active endowing the electrolyte with a mixed ionic electronic conducting character in the vicinity of the counter and working electrodes.

Initially one can consider that the system is composed of a homogeneous stochiometric YSZ solid electrolyte supporting pure metallic platinum electrodes. Under polarization, platinum oxidation and oxygen evolution reaction take place at the anode and, because of the lack of gaseous oxygen, zirconia is reduced at the cathode.

Cathode	$ZrO_2 + 2e^- \rightarrow ZrO + O^{2-}$	**VIII-11**
Solid electrolyte	O^{2-} constant solid migration	
Anode	$Pt + O^{2-} \rightarrow PtO + 2e^-$	**VIII-12**
	$O^{2-} \rightarrow \frac{1}{2}O_{2(g)} + 2e^-$	**VIII-13**
	$PtO_{tpb} \rightarrow PtO_{Pt/gas}$	**VIII-14**

At the cathode, the lack of gaseous oxygen induces the reduction of zirconia which acts as oxygen source for O^{2-} ions formation and subsequent migration to the anode. Despite this mixed ionic and electronic conductive character, the YSZ solid electrolyte is expected to mainly behave as an ionic conductor under the experimental conditions. The O^{2-} ion supply to the Pt anode through YSZ is then supposed to be of a constant rate $r=I/2F$ during galvanostatic polarization.

In the first moment of the anodic polarization, the efficiency of PtO formation is close to 1 and that of OER is close to zero, and rapidily a monolayer of PtO is formed at the Pt/YSZ interface. However this PtO formation, which takes place according to a parabolic growth law, is an auto-inhibited reaction and η_{PtO} decreases with elapsing time while η_{O2} increases. In fact, the dominant oxygen evolution reaction is suggested to create a dramatic increase of

oxygen partial pressure in the vicinity of the Pt/gas interface. Under such conditions, the formation of PtO at the gas exposed interface becomes thermodynamically favored and a fraction of atomic oxygen electrochemically formed at the triple phase boundary slowly migrates toward the Pt/gas interface forming PtO exposed to the gas interface.

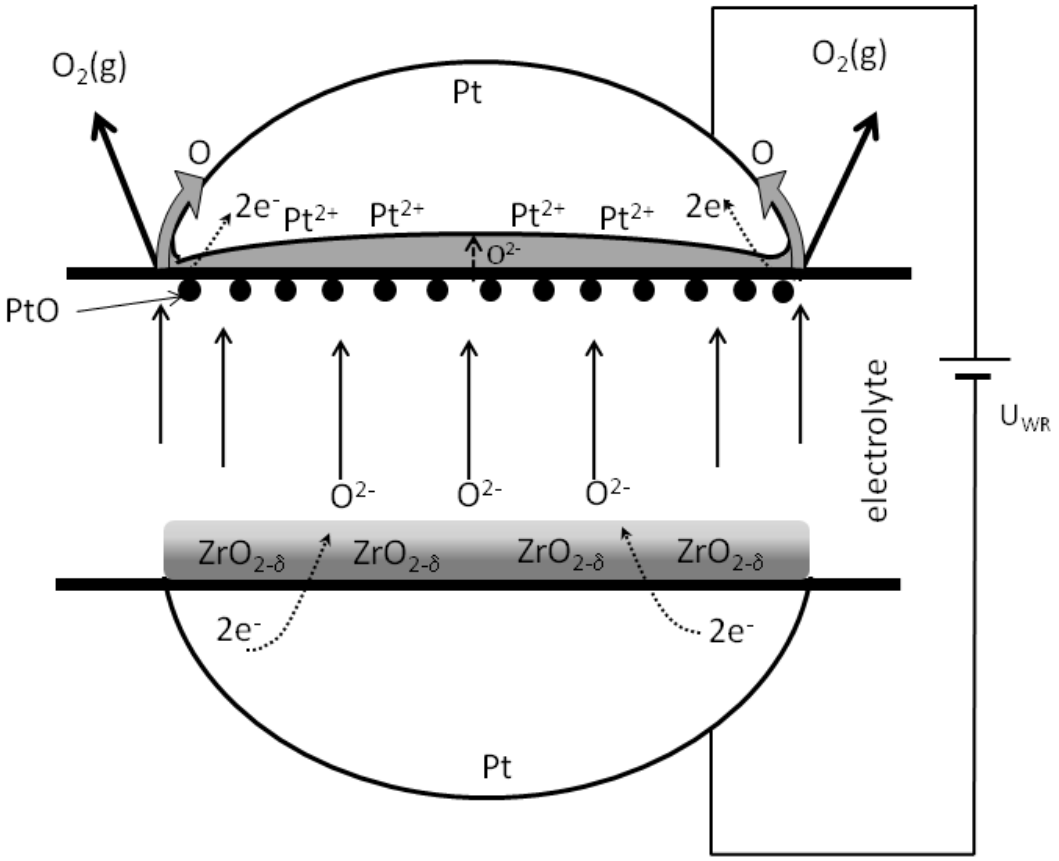

Fig. VIII-11 : Schematic representation of the oxidation and reduction processes during anodic polarization of the Pt/YSZ/Pt system under HV.

VIII.5 Conclusion

In this chapter, the electrochemical investigation of a sputtered platinum electrode deposited on YSZ polycrystalline substrate was performed under high vacuum conditions (p_{O2}=10^{-7} mbar) at 400°C. The coupling of both transient and steady state electrochemical techniques to mass spectrometery (CV-MS and DSCP-MS measurements) allowed to impose a current/potential perturbation while monitoring online the $O_{2(g)}$ formation taking place.

Main findings on the electrochemical behavior of Pt/YSZ system revealed by this original approach are summarized in the following :

● Under cathodic polarization, YSZ is reduced in the vicinity of the Pt/YSZ interface acting as an oxygen source for the formation of O^{2-} ions. This implies YSZ blackening which gives mixed ionic/electronic character to the solid electrolyte. In fact, this allows electron supply from the platinum electrode to the reactive sites involved which are situated at the YSZ subsurface. As consequence the reaction front moves forward to the inside of the YSZ solid electrolyte.

● Under anodic polarization, first a PtO layer is formed at the Pt/YSZ interface according to a parabolic growth law similar to that proposed in the *Wagner* oxidation theory. Based on this model, a mechanism involving O^{2-} diffusion process across the oxide scale is proposed as rate limiting step.

● Under anodic polarization, at a later stage, oxygen evolution reaction (OER) takes place at the triple phase boundary inducing a dramatic increase of oxygen partial pressure in the vicinity of the Pt/gas interface. As a consequence, the thermodynamic stability of PtO rise up allowing the migration of oxygen, discharged at the tpb, toward the gas exposed Pt surface. Worth to mention that this Pt•O species is decomposed when the OER stop and the initial oxygen partial pressure is restored in the vicinity of the Pt/gas interface.

VIII.6 References

1. Luerßen B, Janek J, Günther S, Kiskinovac M, Imbihl R (2002) Physical Chemistry Chemical Physics 4: 2673

2. Xue J, Dieckmann R (1992) Solid State Ionics 53-56: 209

3. Janek J (2000) Solid State Ionics 131: 129

4. Janek J, Korte C (1999) Solid State Ionics 116: 181

5. Katsaounis A, Nikopoulou Z, Verykios XE, Vayenas CG (2004) Journal of Catalysis 222: 192

6. Berry RJ (1978) Surface Science 76: 415
7. Vayenas CG, Michaels JN (1982) Surface Science 120: L405
8. Hoar TP, Price LE (1938) Transactions of the Faraday Society 34: 867

.

CHAPTER IX- ELECTROCHEMICAL OXIDATION OF CO OVER Pt/YSZ CATALYST UNDER HV

In this chapter, the electrocatalytic behavior of Pt/YSZ system was investigated for CO oxidation at 400°C under high vacuum (HV) conditions. The SEMS device of dual chamber reactor configuration was used to impose a single anodic galvanostatic step to the sample in various gas mixture compositions while sampling online the O_2 and CO_2 formation rates (SSCP-MS measurements).

For both oxygen lean (p_{O2} = 10^{-7} mbar and p_{CO} = 6,6.10^{-5} mbar) and oxygen rich (p_{O2} = 3.10^{-4} mbar and p_{CO} = 6,6.10^{-5} mbar) conditions, the CO oxidation reaction is found to be composed of a chemical contribution and an electrochemical contribution without any interaction. As a consequence, the CO electrooxidation process observed under HV is faradaic (Λ<1). CO_2 formation was found to be limited by mass transfer of CO from the gas phase to the tpb in agreement with a simple model of pore diffusion toward the Pt electrode of macroporous structure. However, at current interruption, a remarkable effect is observed as the catalyst remains, for a limited period, in a promoted state before to restore its initial catalytic activity. This remaining enhancement of the catalyst activity is proposed to be related to the P-EPOC phenomenon observed at atmospheric pressure.

IX.1 Introduction

In this chapter, the investigation of CO electrooxidation on Pt/YSZ interface is performed by coupling an electrochemical perturbation (single step chronopotentiometry) to online MS gas analysis (SSCP-MS measurements) under HV in the dual chamber configuration setup (§ VII.2.4.2). The electrochemical perturbation imposed here consisted of a single galvanostatic step at constant anodic current I_a for a given holding time t_h. At current interruption, the Pt/YSZ interface is left under open circuit condition during the whole period of relaxation. Experiments are performed at 400°C in high vacuum conditions and the reactant gases feeds (CO and O_2) are fed separately to the reactor working chamber while the reactor reference chamber is maintained under constant high oxygen pressure $p_{O2}^{ref} = 10^{-2}$ mbar avoiding the YSZ reduction reported in the previous chapter.

IX.2 Electrochemical behavior of Pt/YSZ in O_2 (p_{O2} =10^{-7} mbar) using SSCP-MS measurements

Fig. IX-1 displays the influence of I_a on the galvanostatic step applied at the Pt/YSZ interface in presence of low concentration of O_2 ($p_{O2} = 10^{-7}$mbar). As shown, upon current imposition, oxygen is released to the gas phase according to reaction IX -1 and r_{O2} reaches a steady state value after about 30s.

$$2O^{2-} \rightarrow O_{2(g)} + 4e^- \qquad \textbf{IX-1}$$

Upon current interruption, the rate of oxygen evolution reaction (OER) decreases rapidly back to zero.

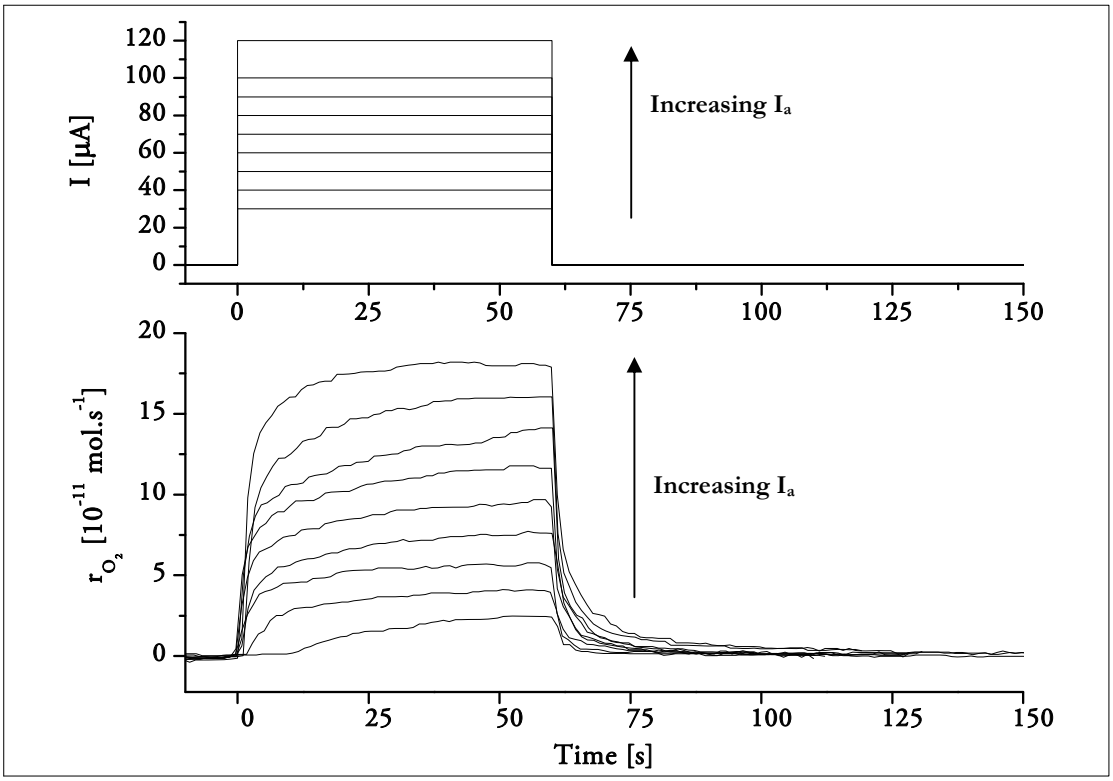

Fig. IX-1: SSCP-MS measurement: Effect of increasing anodic current (from 30 to 100 µA by steps of 10µA and 120µA) of the 90s galvanostatic step on the Pt/YSZ interface under HV, $p_{O2}=10^{-7}$ mbar, T=400°C.

As previously described in Chapter VII, under anodic polarization of the Pt/YSZ interface two reactions take place: the oxygen evolution reaction (reaction IX -1) and the formation of PtO (reaction IX -2).

$$O^{2-} + Pt \rightarrow PtO + 2e^{-} \qquad \text{IX-2}$$

The current efficiency of each of these process (η_{O2} and η_{PtO} respectively) is determined according to :

$$\eta_{O_2} = \frac{Q_{O_2}}{Q_{Total}} \qquad \text{IX-3}$$

$$\eta_{PtO} = 1 - \eta_{O_2} \qquad \text{IX-4}$$

where Q_{O2} is the amount of oxygen (in Coulomb) evolved during the anodic polarization step, determined from the MS measurements (Fig. IX-1) and Q_{Total} is the total charge ($I \bullet t$) passed during the anodic step.

Fig. IX-2 reports the influence of the applied current on the current efficiency of each process. Once again, one see that increasing I_a leads to an increase of η_{O2} with a concomitant decrease of the auto-inhibited PtO formation reaction taking place at the Pt/YSZ interface.

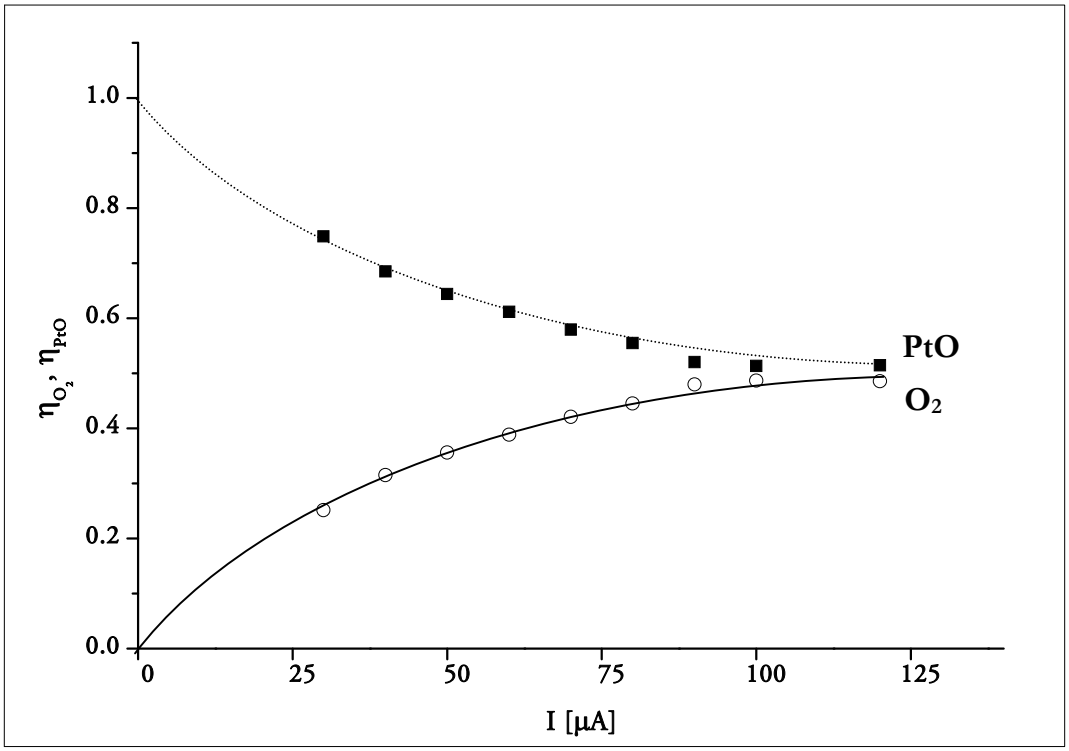

Fig. IX-2: Effect of increasing the anodic polarization current I_a on the the current efficiencies η_{O2} and η_{PtO} from SSCP-MS measurements of Fig. IX-1

IX.3 Oxidation of CO on Pt/YSZ induced by current application using SSCP-MS measurements

A typical SSCP-MS transient observed for CO oxidation over Pt/YSZ catalyst at 400°C under HV (p_{O2} = 10^{-7} mbar, p_{CO}= $6{,}6.10^{-5}$ mbar) during an anodic polarization step is displayed in Fig. IX-3. Initially, the catalytic reaction rate of CO_2 formation under open circuit conditions (reaction IX -5) is 170pmol s^{-1}.

$$\frac{1}{2}O_2 + CO \xrightarrow{Pt} CO_2 \qquad \text{IX-5}$$

At current application (I_a=120μA), gaseous oxygen is released and the rate of CO_2 formation increases simultaneously (Fig. IX-3).

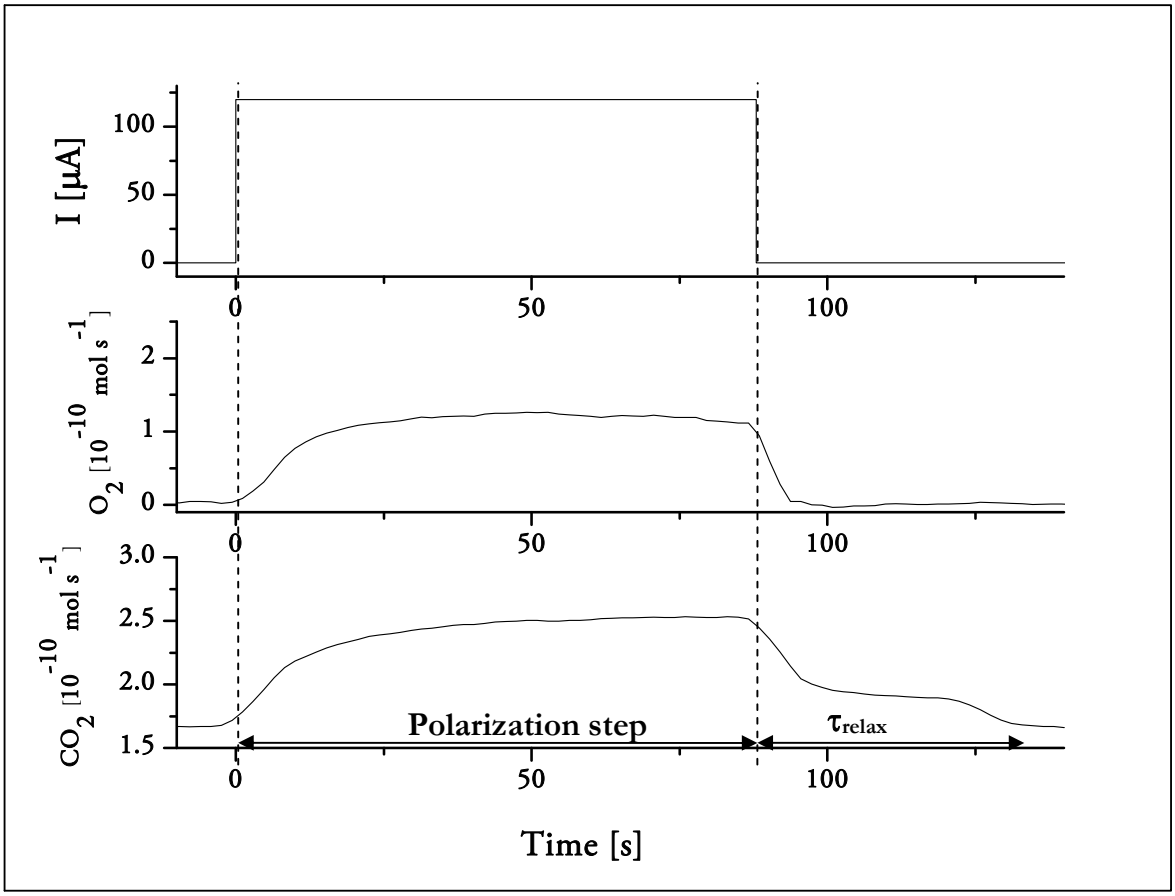

Fig. IX-3: SSCP-MS measurement: Effect of galvanostatic polarization at 120μA during 90s on the catalytic oxidation of CO over Pt/YSZ catalyst under HV, p_{CO}= 6.6.10^{-5} mbar, p_{O2}=10^{-7} mbar, T=400°C.

After 50s of polarization, both rate transients reach steady state (r_{O2} = 100pmol s^{-1} and r_{CO2} =250 pmol s^{-1}). At current interruption, the oxygen release rapidly stops while the CO_2 formation rate first decreases following O_2 decrease then remains at a constant value (190 pmol s^{-1}) for 30s before returning to its initial unpromoted value.

$$O^{2-} + CO \rightarrow CO_2 + 2e^- \qquad \text{IX-6}$$

Worth to notice that concerning the CO_2 fomation, the current application leads to a rate enhancement factor of ρ = 1.5 with a faradaic efficiency of Λ < 1, *i.e.* corresponds to a classical electrochemical process (reaction IX-6). However, the increase in rate observed after current interruption is attributed to the chemical reaction of CO with O_2 from the gas phase (initial decrease) or with PtO (reaction IX-7) formed during the current application step.

$$CO + PtO \rightarrow CO_2 \qquad \text{IX-7}$$

The current efficiency for O_2, CO and PtO formation during anodic polarization is define as:

$$\eta_{O_2} = \frac{Q_{O_2}}{Q_{Total}} \qquad \text{IX-8}$$

$$\eta_{CO_2} = \frac{Q_{CO_2}}{Q_{Total}} \qquad \text{IX-9}$$

$$\eta_{PtO} = 1 - \eta_{O_2} - \eta_{CO_2} \qquad \text{IX-10}$$

where Q_{O2} and Q_{CO2} are the amount of O_2 and CO_2 evolved during the anodic polarization step, determined from the MS results and Q_{Total} is the total charge passed during the anodic step.

IX.3.1 Influence of the gas composition

Fig. IX-4 reports two experiments carried out at two different p_{CO} (3.10^{-5} and $1{,}6.10^{-4}$ mbar) and invariant p_{O2} (10^{-7} mbar) in the working compartment of the reactor. At open circuit, the increase of p_{CO} leads to a decrease in the rate of CO_2 formation. However, upon current imposition, the rate of CO_2 increases more rapidly and reaches higher promoted steady state with increasing CO partial pressure in the system. In parallel, one should notice that the rate of oxygen release diminishes drastically with increasing p_{CO}.

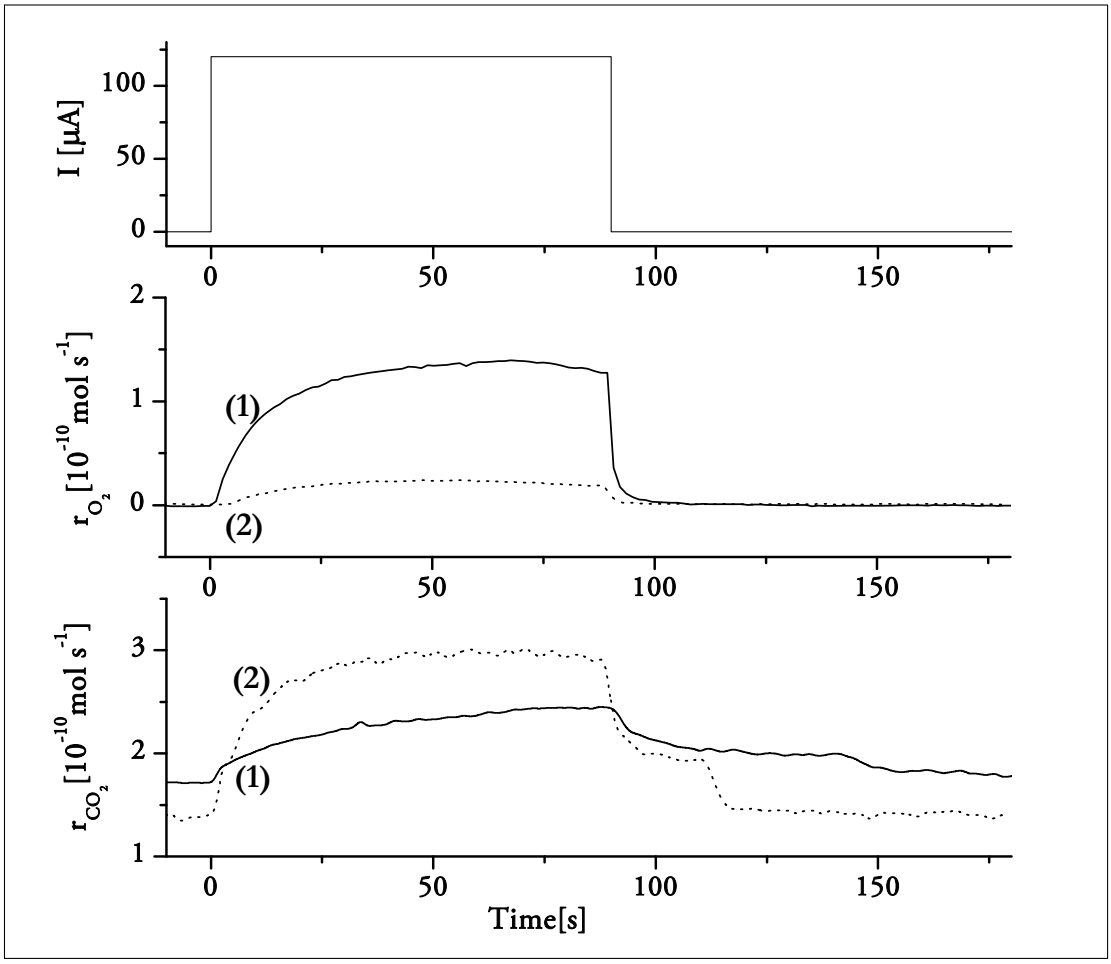

Fig. IX-4: Effect of p_{CO} in the reactor working compartment on the catalytic oxidation of CO over Pt/YSZ catalyst under HV during a galvanostatic polarization at 120µA of 90s, (1) p_{CO}= 3.10^{-5} mbar , (2) p_{CO}= 16.10^{-5} mbar ,p_{O2}=10^{-7} mbar, T=400°C.

Upon current interruption, the rate of oxygen released to the gas phase drops quickly back to zero while the rate of CO_2 formation exhibits a more complex transient. r_{CO2} first decreases to an intermediate value before to return to its initial unpromoted value. Worth to notice that the relaxation time, τ_{relax}, needed for the catalyst to return to the unpromoted state depends on the gas mixture composition *i.e.* becomes shorter with increasing p_{CO}.

The current efficiency has been determined for each process and plotted in Fig. IX-5. One can observe that increasing p_{CO} in the reactor working compartment results in a decrease of

η_{O2} and a η_{CO2} linear increase. However, η_{PtO} seems to be unaffected by the gas mixture composition.

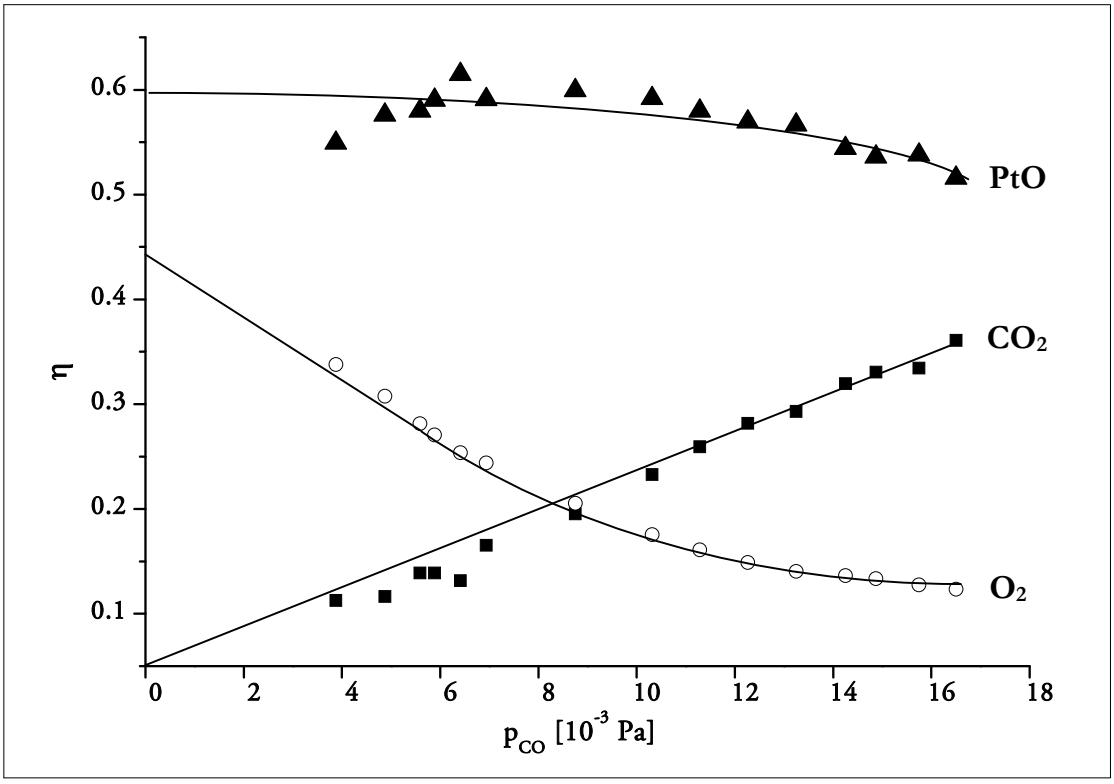

Fig. IX-5: Effect of CO pressure p_{CO} on the current efficiencies η_{O2} , η_{CO2} and η_{PtO} from CP-MS measurements of Fig. IX-4.

IX.3.2 Influence of the anodic current I_a

IX.3.2.1 In absence of $O_{2(g)}$ feed

The gas mixture composition is kept constant (p_{O2} = 10^{-7} mbar and p_{CO} = 6,6 10^{-5}mbar) and the applied anodic current is increased from 30μA up to 120μA by intervals of 10μA then up to 520μA by steps of 100μA (Fig. IX-6). Upon current application, both CO_2 and O_2 are formed. For low anodic current (<120μA), the rate of O_2 formation reaches a steady state after 20s of polarization and for higher applied anodic current (>300μA), r_{O2} passes through a maximum.

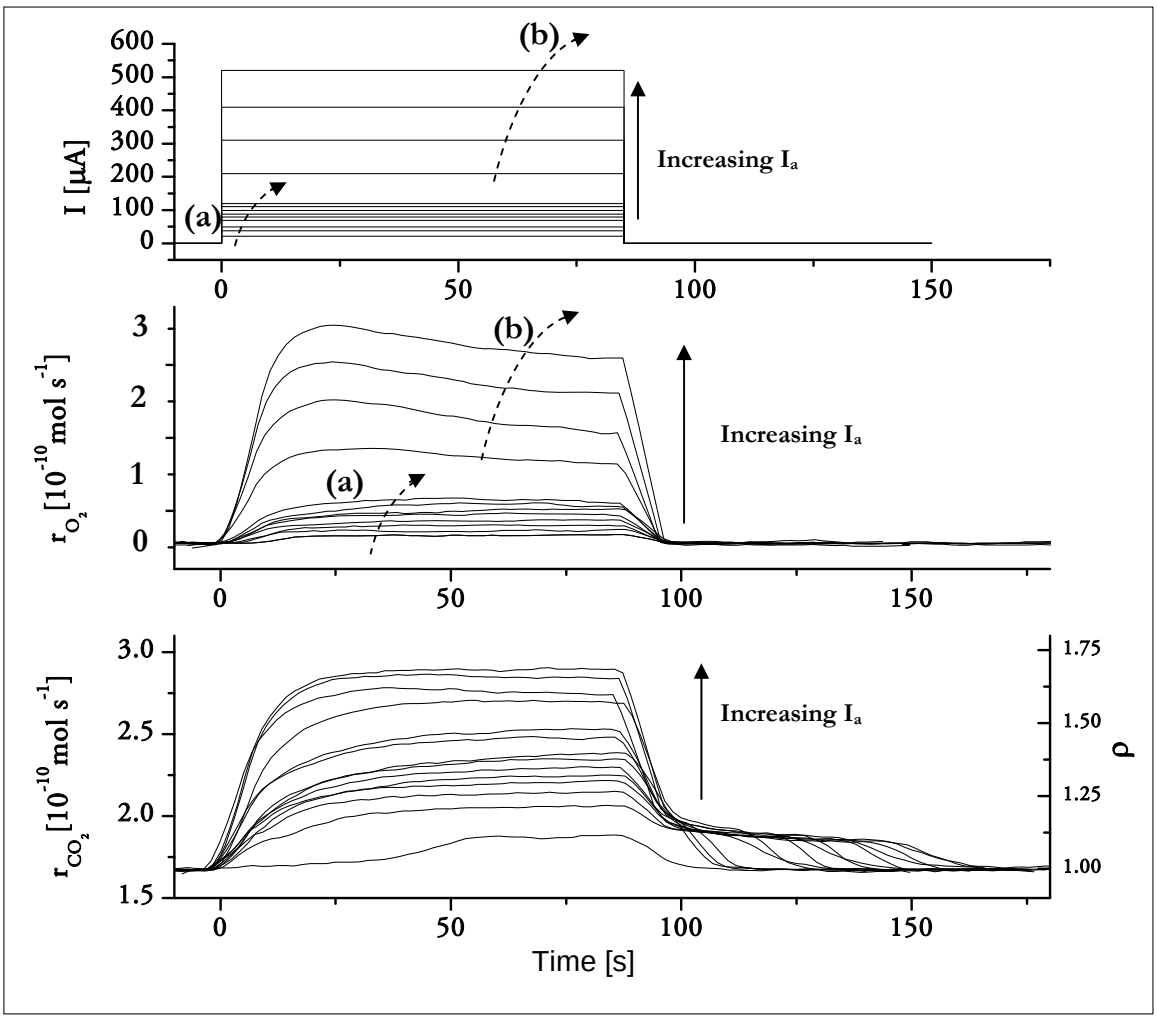

Fig. IX-6: SSCP-MS measurement : Effect of anodic current on the oxidation of CO over Pt/YSZ catalyst under HV. I_a =30 μA to 120 μA by steps of 10 μA (a) then up to 520μA by steps of 100μA (b). p_{CO}= 6.6.10^{-5} mbar, p_{O2}=10^{-7} mbar, T=400°C.

In parallel to this oxygen evolution, the CO_2 formation rate, initially at r_{CO2}^0 = 170 pmol s^{-1}, also increases with increasing anodic current. r_{CO2} increases rapidly in the first time of polarization and then reaches a steady state depending on the applied anodic current.

For all applied anodic current the rate increase observed is faradaic (Λ<1), with rate enhancement ratio, ρ, varying from 1 to 1.7 for increasing anodic current (Fig. IX-6).

At current interruption, the rate of oxygen released to the gas phase quickly drops to zero while the rate of CO_2 formation decreases first to the value of 200pmol s^{-1} where it forms a

plateau before to return to its initial value. The time period of this plateau increases with increasing anodic current. As shown in Fig. IX-7, increasing I_a results in a decrease of η_{CO2} and η_{PtO} while η_{O2} increases.

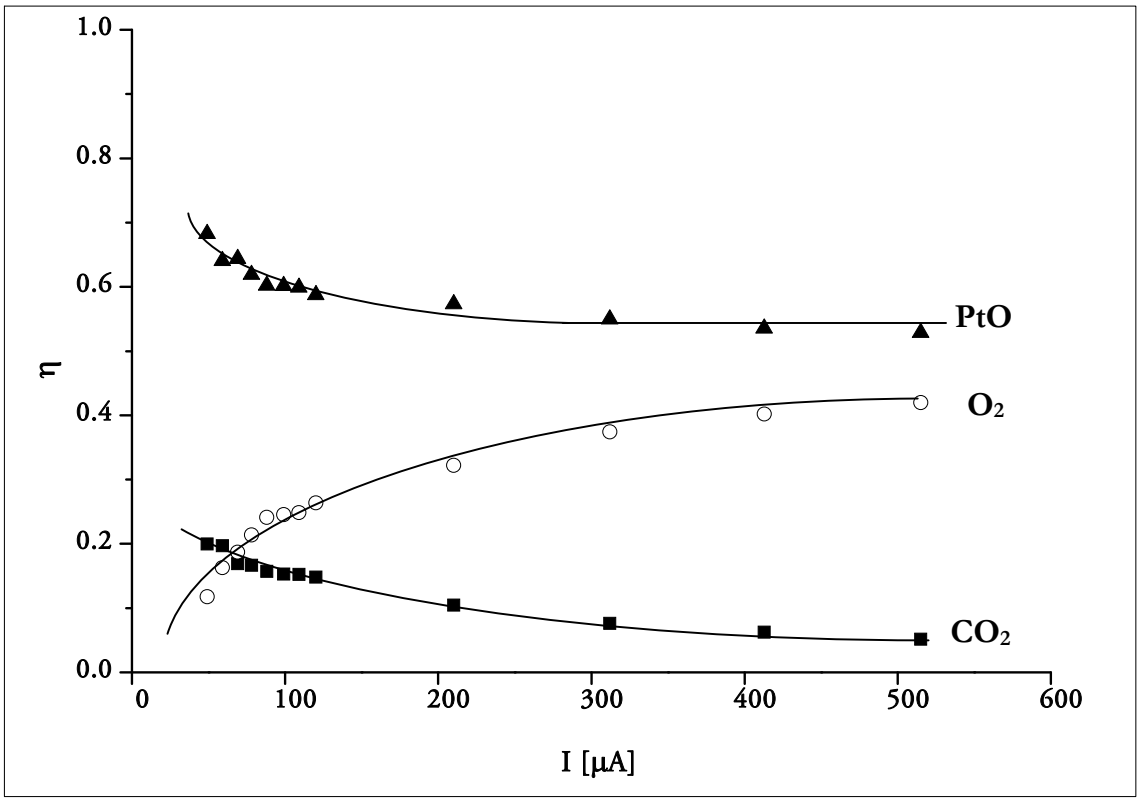

Fig. IX-7: Effect of increasing the anodic polarization current I_a on the the current effienciencies η_{O2} , η_{CO2} and η_{PtO} from CP-MS measurements of Fig. IX-6.

IX.3.2.2 In presence of $O_{2(g)}$ feed

In these experiments an excess of oxygen has been used relative to CO (p_{O2} = 30.10^{-5}mbar and p_{CO} = 6.10^{-5}mbar) and the current applied during the anodic galvanostatic step is increased from 30μA up to 100μA by intervals of 10μA (Fig. IX-8). Only the CO_2 formation rate was monitored is this experiments as the MS was not sensible to the modification of p_{O2} imposed by the applied current.

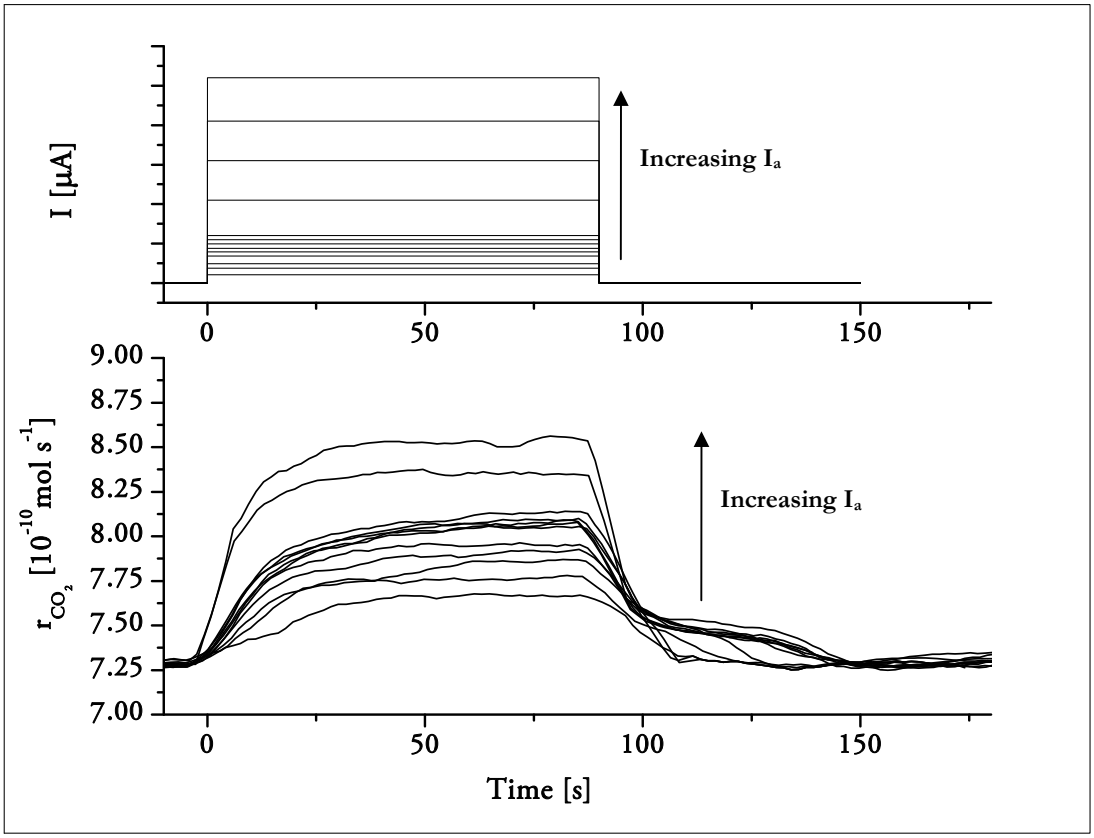

Fig. IX-8: CP-MS measurements : Effect of increasing anodic current of the 90s galvanostatic polarization step on the catalytic oxidation of CO over Pt/YSZ catalyst under HV. I_a =30 µA to 120 µA by steps of 10 µA then up to 520µA by steps of 100µA. p_{CO}= 6.10^{-5} mbar, p_{O2}=30.10^{-5} mbar, T=400°C.

The initial rate of CO_2 formation (under open circuit conditions) is 730pmol s^{-1}. Upon current application the reaction increases within the first 30s and then reaches a steady state. This steady state rate, r_{CO2}^{p} increases with increasing anodic current and exhibits a faradaic behavior (Λ<1). At current interruption, r_{CO2} drops rapidly to an intermediate value (750pmol s^{-1}) where it remains for a certain period of time before to return back to its initial value. For increasing anodic current, the relaxation time needed for the catalyst to return to its initial active state increases.

Worth to notice that adding O_2 feed in the reactor has a dramatic influence on the initial CO_2 formation rate r_{CO2}^{0} but a rather limited impact on Δr ($\Delta r_1 = \Delta r_2$ in Fig. IX-9).

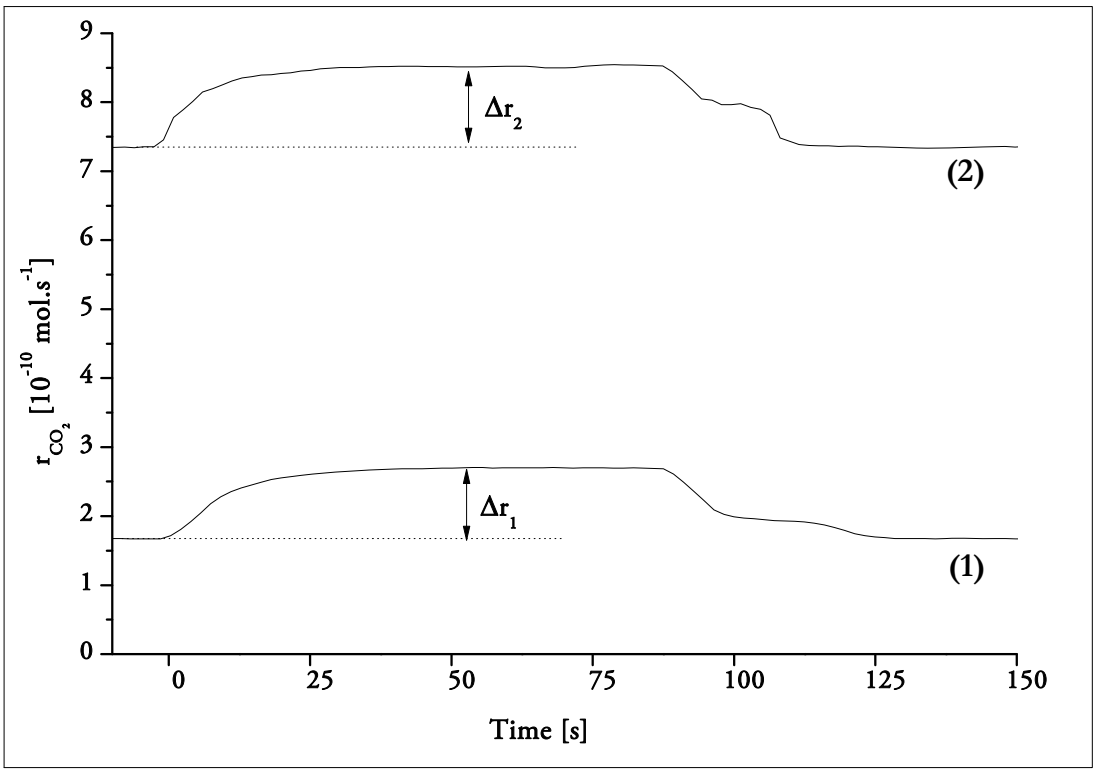

Fig. IX-9: SSCP-MS measurements : Effect of O_2 feed on the catalytic oxidation of CO over Pt/YSZ catalyst under HV. (1) $p_{O2}=10^{-7}$ mbar and $p_{CO}= 6.6.10^{-5}$ mbar, (2). $p_{O2}=30.10^{-5}$ mbar and $p_{CO}= 6.10^{-5}$ mbar, I_a =520 µA, T=400°C.

In fact, the catalytic CO oxidation reaction taking place at the Pt/YSZ system under anodic polarization is suggested to be composed of two contributions: the catalytical CO oxidation taking place at the Pt/gas interface, which is dramatically affected by the presence of excess oxygen in the gas mixture, and the electrocatalytic CO oxidation taking place at the tpb, which is independent of it.

IX.4 Discussion

Fig. IX-2 shows clearly that in absence of CO, under anodic polarization, PtO is formed at the Pt/YSZ interface (reaction XI-2) according to an auto-inhibited process (decrease in rate due to PtO formation) and in parallel O_2 is evolved (reaction XI-1) at the tpb. The formation of O_2 leads to an increase of the oxygen partial pressure (p_{O2}) at the Pt/gas

interface, this increase in p_{O2} induces the migration of oxygen species to the Pt/gas exposed surface (discussed in Chapter VIII).

As CO is fed in the working compartment of the reactor (3.10^{-5} mbar$<p_{CO}<16.10^{-5}$ mbar) in oxygen lean conditions ($p_{O2} = 10^{-7}$ mbar), CO_2 is catalytically formed (reaction XI-5) at the Pt/gas interface. At current imposition, three additional electrochemical reactions take place :

- PtO formation at the Pt/YSZ interface (reaction XI-2)
- O_2 evolution at the tpb (reaction XI-1)
- CO electrooxidation at the tpb (reaction XI-6)

The η_{CO2} of CO_2 formation (reaction XI-6) lies between 10-40%, it increases with p_{CO} and decreases with increasing anodic current I_a. This dependency on both CO concentration and I_a gives strong indications that transport of CO toward the tpb is limiting. In fact, two fluxes can be defined in this process:

□ The flux of CO from the gas phase to the tpb, J_{CO}, depending on CO concentration. According to the molecular flow theory and considering inner diffusion [1], the CO free-molecule flux through the Pt film to the reactive sites, J_{CO}, is given by :

$$J_{CO} = w\sqrt{\frac{8M_{CO}}{\pi RT}}\left(p_{CO}^{*} - p_{CO}^{tpb}\right) \qquad \textbf{IX-11}$$

Where w is a dimensionless probality factor depending on the electrode geometry, R is the gas constant, T is the temperature, M_{CO} the CO molecular mass, p_{CO}^{tpb} and p_{CO}^{*} the CO pressure at the tpb and in the bulk gas phase respectively.

□ The flux of O^{2-} from YSZ to the tpb [2], $J_{O^{2-}}$, depending on J_a, the applied current density. $J_{O^{2-}}$ is supplied electrochemically to the Pt/YSZ interface at constant rate $J_{O^{2-}} = J_a/2F$.

As soon as oxygen evolution takes place at the tpb, it is suggested that $J_{O^{2-}} > J_{CO}$ and that steady state CO concentration drops dramatically at the electrode surface. In this case, the mass transfer of CO to the tpb is the limiting step and assuming that all CO molecules reaching the Pt surface react to form CO_2 according to reaction XI-6 (zero surface

concentration), the probability factor w may be determined from the slope of the linear relation between Δr_{CO2} and p_{CO}. From the results presented in Fig. IX-5, one estimates w = 5,6.10^{-2}. Considering a simple geometry for this pore diffusion process w may be estimated by :

$$w = \frac{2}{3}\frac{r}{L} \qquad \text{IX-12}$$

where r and L are the pore radius and length respectively. The thickness of the Pt electrode being of 1μm, this corresponds to pores of 170nm diameter in agreement with observations made by SEM images (§ VI.3).

One should notice that increasing the oxygen partial pressure p_{O2} in the gas mixture (from p_{O2} = 10^{-7} mbar to p_{O2} = 30.10^{-5} mbar) had a large influence on the initial open circuit reaction rate of CO_2 formation (reaction XI-5) but at current imposition, the electrocatalytic oxidation of CO at the tpb (reaction XI-6) is not affected (Fig. IX-9). This suggests that the total reaction rate of CO_2 formation taking place under anodic galvanostatic polarization is simply the sum of the rate of two independent processes : the catalytic partial CO oxidation taking place at the Pt/gas interface (reaction XI-5) and the electrocatalytic CO oxidation occurring at the tpb (reaction XI-6). This absence of synergy between these two processes shows clearly that under the investigated conditions at current imposition, we are not dealing with a promotional effect of the CO catalysis (no EPOC behavior) but with a classical faradaic enhancement of the CO oxidation [3-7].
However, worthy to note that at current interruption, the reaction rate of CO_2 formation firstly decreases and then remains enhanced for a limited period of time before to return to its initial value (Fig. IX-3). This is suggested to be related to oxygen storage (certainly the above mentioned PtO layer) formed during the anodic polarization.

The ratio Λ_{PtO}, which express the amount of stored oxygen consumed after current interruption, is defined as the ratio of the amount of oxygen consumed by CO oxidation

after current interruption N_{CO2}, to the amount of oxygen stored as PtO during the anodic polarization N_{PtO}.

$$\Lambda_{PtO} = \frac{N_{CO_2}}{N_{PtO}} \qquad \text{IX-13}$$

with

$$N_{PtO} = \eta_{PtO} \frac{It_h}{2F} \qquad \text{IX-14}$$

Where η_{PtO} is the current efficiency for the PtO formation, I the applied current and t_h the holding time of the galvanostatic step.

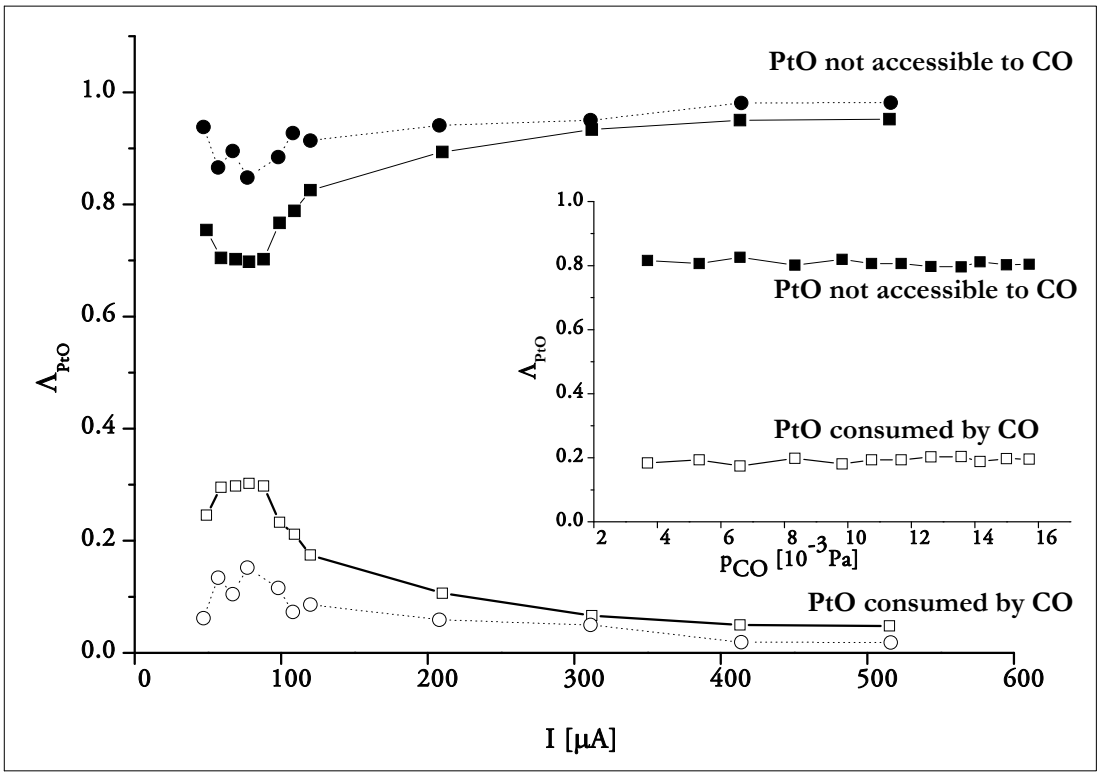

Fig. IX-10: Effect of the anodic polarization current I_a on Λ_{PtO} from SSCP-MS measurements of Fig. IX-6 (solid line) and Fig. IX-8 (dashed line). Insert gives results from Fig. IX-4

As shown in Fig. IX-10, a small fraction (< 30%) of the oxygen stored during the anodic polarization is involved in the CO_2 formation taking place after current interruption. This suggests that the oxygen released at current interruption does not act as promoter as

reported at high pressure (Chapter III). This behavior is certainly related to the fact that this process is diffusion controlled.

IX.5 Conclusion

In this chapter, the electrocatalytic behavior of Pt/YSZ system was investigated for CO oxidation at 400°C under HV conditions. The new probe device in dual chamber reactor configuration (depicted in chapter VII) was used to impose a single anodic galvanostatic step to the sample in various gas mixture compositions while sampling online the O_2 and CO_2 formation rates (SSCP-MS measurements).

- In absence of CO (p_{O2} = 10^{-7} mbar), under anodic polarization, PtO formation and parrallel oxygen evolution reaction occurring at the Pt/YSZ interface and at the tpb respectively were observed in agreement with previous discussion (Chapter VIII).
- In presence of CO (p_{CO}>3.10^{-5} mbar) for both oxygen lean (p_{O2} = 10^{-7} mbar) and oxygen rich (p_{O2} = 30.10^{-5} mbar) conditions, under anodic polarization, it turns out that the CO oxidation reaction is composed of a chemical contribution and an electrochemical contribution without any interaction. As a consequence, the CO electrooxidation process observed under HV is faradaic (Λ<1). CO_2 formation was found to be limited by mass transfer of CO from the gas phase to the tpb in agreement with a simple model of pore diffusion within the macroporous Pt electrode. This can explain the low faradaic efficiency.
- However, at current interruption, a remarkable effect is observed as the catalyst remains, for a limited period, in a promoted state before returning to its initial catalytic activity. This remaining enhancement of the catalyst activity after current interruption is proposed to be due to the formation of a PtO layer at the Pt/YSZ interface which was highlighted in Chapter VIII and related to the P-EPOC phenomenon observed at atmospheric pressure.

IX.6 References

1. Handbook of Vacuum Science and Technology, Hoffman, Singh and Thomas, Academic Press, 1998

2. Vayenas CG, Bebelis S, Pliangos C, Brosda S, Tsiplakides D (2001) Electrochemical Activation of Catalysis: Promotion, Electrochemical Promotion, and Metal-Support Interactions. Kluwer Academic / Plenum Publishers, New York

3. Katsaounis A, Nikopoulou Z, Verykios XE, Vayenas CG (2004) Journal of Catalysis 226: 197

4. Imbihl R, Janek J (2000) Solid State Ionics 136-137: 699

5. Luerßen B, Gunther S, Marbach H, Kiskinova M, Janek J, Imbihl R (2000) Chemical Physics Letters 316: 331

6. Poppe J, Völkening S, Schaak A, Janek J, Imbihl R (2000) Phys. Chem. Chem. Phys. 1: 5241

7. Luerßen B, Mutoro E, Fischer H, Günther S, Imbihl R, Janek J (2006) Angewandte Chemie International Edition 45: 1473

CHAPTER X- GENERAL DISCUSSION AND PROPOSED MODEL

This PhD thesis is part of the research works started several years ago in the "NEMCA group" of Prof. Comninellis at the EPFL. Its subject concerns the permanent electrochemical promotion of Pt catalyst (P-EPOC) supported on YSZ solid electrolyte. Both electrocatalytical and electrochemical approaches are proposed under both atmospheric pressure and high vacuum conditions. Atmospheric investigations are performed in an existing setup widely used for EPOC investigations. The irreversible character of the electrochemical promotion of C_2H_4 combustion over Pt/YSZ catalyst is ascertained to increase in polarization time and the electrochemical investigation of $O_{2(g)}$,Pt/YSZ system reveals a process of PtO formation at the Pt/YSZ interface. HV studies have necessitated the construction of a new setup which allows imposing an electrochemical perturbation (CV or CP) and monitoring at the same time the electrochemical products released in the gas phase. This new electrochemical technique allows to propose an original P-EPOC model involving two different types of promoters where the electrochemical modification of the Pt/YSZ interface is directly related to the observed modification of the Pt/gas catalyst activity.

X.1 General discussion and proposed model

The review of EPOC literature (Chapter II) reminds first the principle of electrochemical promotion which is characterized by the rate enhancement and the faradaic enhancement factors (ρ and Λ). This reversible modification of the catalyst activity, observed during the polarization step, is explained by the rapid migration of sacrificial promoter at the catalyst surface [1]. However, after long term polarization, several systems have exhibited complex open-circuit relaxation transients of reaction rate called Permanent or Persistent EPOC phenomenon (P-EPOC or Pers-EPOC) [2-4]. To quantify this unexpected irreversible character one should introduce new parameters like γ, the permanent enhancement factor (for P-EPOC), or Λ_{OS}, the oxygen storage efficiency (for Pers-EPOC).

The experimental results obtained, under atmospheric pressure during the investigation of C_2H_4 combustion over Pt/YSZ at 375°C (Chapter III), let suppose that the electrochemical promotion (EPOC and P-EPOC) is related to both a rapid and a slow process of promoter formations. In this work, a model is proposed where two different active oxygen states, $O^{\delta 1-}$ and $O^{\delta 2-}$, are created on the gas exposed catalyst (Pt/gas) interface during the imposed anodic polarization.

- $O^{\delta 1-}$ is a highly mobile sacrificial promoter with a moderate reactivity and moderate dipole moment ($P_{O\delta 1}$). Its rapid migration from the triple phase boundary to the Pt/gas interface is considered to be controled by the applied current and to be temperature dependent. At 375°C under a polarization of 0.5mA, $O^{\delta 1-}$ is estimated to have an average lifetime at the catalyst surface of about 30 seconds upon current interruption. This promoter is responsible for the EPOC phenomenon.
- $O^{\delta 2-}$, is a very stable promoter presenting a large dipole moment ($P_{O\delta 2} > P_{O\delta 1}$) with an infinite lifetime at the catalyst surface (non-reactive promoter). The presence of this type of promoter is expected to be limited by a slow diffusion process, *i.e.*

temperature dependent but independent of the applied current. This promoter is responsible for the P-EPOC phenomenon.

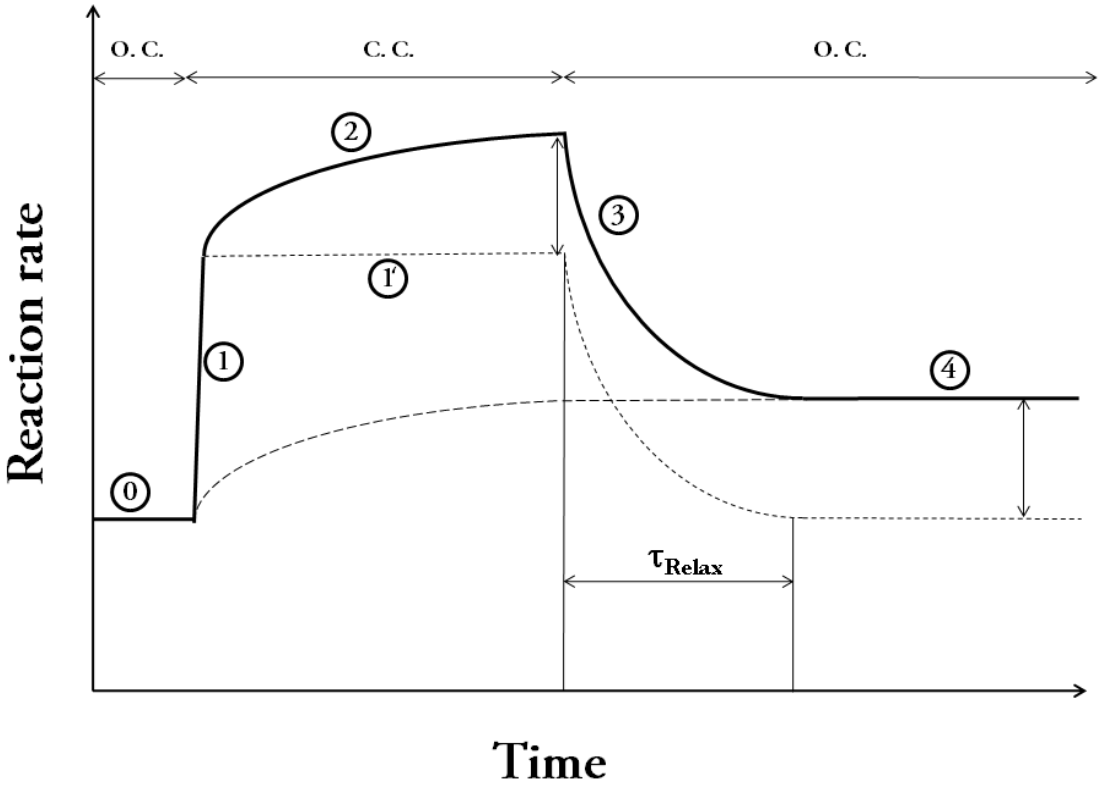

Fig. X-1 : Schematic representation of a typical electrochemical promotion (EPOC and P-EPOC) transient. (0) Open circuit reaction rate r_0. (1) dramatic reaction rate increase upon current application (1') actual steady state of the $O^{\delta 1}$ promoters (EPOC) (2) apparent steady state observed during long anodic polarization (3) holding time dependent slow relaxation of duration τ_{Relax} upon current interruption and (4) final new permanently enhanced reaction rate (P-EPOC)

Fig. X-1 shows a schematic representation of typical electrochemical promotion (EPOC and P-EPOC) transient according to this model. Before polarization (0 in Fig. X-1), ethylene combustion occurs over Pt/YSZ catalyst at the open circuit reaction rate r_0. Upon current application, electrogenerated promoter migrates from the tpb to the Pt gas exposed catalyst surface, creating both $O^{\delta 1-}$ and $O^{\delta 2-}$ promoters. However, in the initial time of polarization (1 in Fig. X-1) only the mobile $O^{\delta 1-}$ promoters may populate rapidly the catalyst active

surface while the slow diffusion controlled $O^{\delta 2-}$ promoters populate the catalyst surface much later. As a consequence, considering equations III-20 and III-21, the rapid increase of $\theta_{O\delta 1}$ leads to a rapid increase of the catalyst work function $\Delta\Phi_1$ with a concomitant dramatic incresase in the reaction rate (1 in Fig. X-1) .

$$\Delta\Phi_1 = \frac{eN_M}{\varepsilon_0}\left(P_{O^{\delta 1}}\theta_{O^{\delta 1}}\right) \qquad \textbf{X-1}$$

where $P_{O\delta 1}$ is the dipole moment and $\theta_{O\delta 1}$ the coverage of the $O^{\delta 1-}$ promoters.

$O^{\delta 1-}$ migration being current controlled, one may assume a supply rate of $O^{\delta 1-}$ promoter equal to $I/2F$. Considering $N_{Pt/gas}$ active sites at the catalyst surface, this process should be saturated after $2FN_{Pt/gas}/I$ seconds, *i.e.* about 34s (I=0.5mA and $N_{Pt/gas}$ =109nmol). So this enhancement process is rapidly limited and the steady state is rapidly reached after few minutes of polarization (1' in Fig. X-1). Nontheless, the stable $O^{\delta 2-}$ promoters are then expected to gradually diffuse toward the Pt/gas interface and so rise the catalyst work function according to equation III-21 with concomitant increase in the reaction rate (2 in Fig. X-1) :

$$\Delta\Phi_2 = \frac{eN_M}{\varepsilon_0}\left(P_{O^{\delta 2}}\theta_{O^{\delta 2}}\right) \qquad \textbf{X-2}$$

where $P_{O\delta 2}$ is the dipole moment and $\theta_{O\delta 2}$ the coverage of the $O^{\delta 2-}$ promoters.

Worth to notice that, because of the usual very large time constants of $O^{\delta 2-}$ promoters, during a classical EPOC experiment (short polarization time), the change in $\theta_{O\delta 2}$ is expected to be rather small, leading to a very slow reaction rate increase in this regime which may then be seen as an apparent steady state with regard to the experiment duration. However, even in case of limited presence of $O^{\delta 2-}$ at the catalyst surface, it is expected that the dipole moment, $P_{O\delta 1}$, of $O^{\delta 1-}$ promoter already present at the Pt/gas interface should be affected by the increasing value of $\theta_{O\delta 2}$. During this apparent steady state period, the slow diffusion of $O^{\delta 2-}$ promoter is then expected to increase the average lifetime of $O^{\delta 1-}$ promoter present at the catalyst surface.

At current interruption (3 in Fig. X-1), the flux of electrogenerated oxygen promoter stops and so ends the creation of fresh $O^{\delta 1-}$ and $O^{\delta 2-}$ promoters. $\theta_{O\delta 1}$ will then decrease back to almost zero after τ_D related to the stability of these promoters, while the highly stable $O^{\delta 2-}$ promoters are expected to remain at the catalyst surface. Finally, after long relaxation time (4 in Fig. X-1), $O^{\delta 2-}$ promoters will then keep the catalyst in a new promoted state even after current interruption, *i.e.* $O^{\delta 2-}$ is responsible for P-EPOC. Worth to recall that increasing polarization time rises up the $O^{\delta 1-}$ dipole moment and so increases the stability of $O^{\delta 1-}$ promoter at the Pt/gas surface (increase of τ_D). This fact should then lead to decreasing values of $O^{\delta 1-}$ consumption rate after current interruption in agreement with the experimental relation found between the $O^{\delta 1-}$ average lifetime (τ_D) at the catalyst surface and the square root of the polarization time (Fig. III-15).
In this model, $O^{\delta 1-}$ promoter species, whoes population at the Pt/gas interface rises quickly to steady state, must be related to the sacrificial promoter presented in the state-of-the-art of EPOC (*e.g.* highly mobile, reactive presenting a moderate lifetime at the catalyst surface and formation at the tpb). On the opposite, the second type of promoter $O^{\delta 2-}$, *i.e.* highly stable at the catalyst surface, may be related to the electrochemical formation of platinum oxide which subject to controversy.

The electrochemical investigations of the $O_{2(g)}$,Pt/YSZ system demonstrate that upon an anodic polarization two parallel reactions take place, *i.e.* platinum oxidation (equation VI-2) at the binary Pt/YSZ interface and oxygen evolution (OER) (equation VI-1) at the triple phase boundary (tpb). The current efficiencies of these two reactions η_{PtO} and η_{O2} were determined (equation VI-3 and VI-4) suggesting that PtO formation is an auto-inhibited reaction at the Pt/YSZ interface (η_{PtO} initially close to one, decreases with elapsing time). In fact, the limiting step of the PtO formation is related to the transport of O^{2-} across the oxide scale (*Wagner* model) [5,6] or incorporation into the oxide scale (place exchange mechanism) [7].

In addition, further investigation, performed under high vacuum (HV) conditions, described in Chapters VII and VIII, allowed to develop new electrochemical techniques (CV-MS and DSCP-MS measurements) used for the electrochemical and electrocatalytic studies under HV. With this technique, the oxygen evolution reaction taking place at the tpb, in parallel to the formation of PtO at the Pt/YSZ interface, is observed by MS. The dramatic oxygen release observed during the polarization is proposed to increase the partial pressure of oxygen nearby the Pt/gas interface which stabilizes thermodynamically the oxidized state of platinum (PtO) [8,9]. As a consequence, oxygen discharged at the tpb, which is strongly bonded to platinum, can diffuse toward the gas exposed interface during anodic polarization. This process appears to be limited (η_O < 0.3), however, η_O is found to increase with increasing current and is independent of the polarization time (Fig VIII-8 and Fig VIII-9).

All these results allow to propose a general model for the electrogeneration of $O^{\delta}{}_2$ promoters during an anodic polarization involving three processes:

- The rapid formation of a thin PtO submonolayer at the Pt/YSZ interface.
- A deeper oxidation of platinum toward the Pt bulk according to the *Wagner* model at low holding potential and according to a place exchange mechanism at higher holding potential.
- The slow diffusion, toward the Pt/gas interface, of strongly bonded oxygen, (equation VIII-14), *i.e.* population of Pt/gas interface by $O^{\delta}{}_2^-$ promoters.

Worth to notice that the third process, which is directly related to P-EPOC, is highly influenced by the experimental conditions because thermodynamic stability of PtO at the gas exposed surface is of major importance (Chapter VIII). This will explain that P-EPOC is observed at low temperature where PtO is thermodynamically favoured and that Pers-EPOC is observed at higher temperature.

This model of electrochemical PtO formation can be related to the electrocatalytic behavior of Pt/YSZ for CO oxidation under HV (Chapter IX). For both oxygen lean (§ IX-3.2.1) and oxygen rich (§ IX-3.2.1) conditions, the CO oxidation reaction is found to be composed of a

chemical contribution (reaction IX-5) and a faradaic electrochemical contribution (reaction IX-6) without any synergic effect. In addition, CO_2 formation is found to be limited by CO mass transfer across the macroporous structure of the Pt electrode. At current interruption the catalyst remains, for a limited period, in an enhanced state before returning to its initial state. Again, this remaining enhancement of the catalyst activity is proposed to be related to the previously mentioned oxygen storage (PtO) which is consumed afterwards by the catalytic reaction.

X.2 References

1. Vayenas CG, Bebelis S, Pliangos C, Brosda S, Tsiplakides D (2001) Electrochemical Activation of Catalysis: Promotion, Electrochemical Promotion, and Metal-Support Interactions. Kluwer Academic / Plenum Publishers, New York
2. Nicole J (1999) Etude de la promotion électrochimique de l'oxydation catalytique de l'éthylène sur des oxydes métalliques, EPFL
3. Wodiunig S (2000) Electrochemical Promotion of RuO_2 Catalysts for the Gas Phase Combustion of Ethylene, Ecole Polytechnique Fédérale
4. Jaccoud A (2006) Electrochemical promotion of Pt catalysts for gas phase reaction, EPFL
5. Hoar TP, Price LE (1938) Transactions of the Faraday Society 34: 867
6. Cabrera N, Mott NF (1949) Reports on Progress in Physics 12: 163
7. Eley DD, Wilkinson PR (1960) Proceedings of the Royal Society of London. Series A. Mathematical and Physical Sciences 254: 327
8. Berry RJ (1978) Surface Science 76: 415
9. Vayenas CG, Michaels JN (1982) Surface Science 120: L405

List of Symbols

1 Acronyms

AFM	Atomic Force Microscopy
CE	Counter Electrode
CV	Cyclic Voltammetry
DEMS	Differential Electrochemical Mass Spectrometry
DSCP	Double Step Chronopotentiometry
ERS	Electrochemical Reaction Site
EPOC	Electrochemical Promotion Of Catalysis
GC	Gas Chromatography
HV	High Vacuum
Me	Metal
MIEC	Mixed Ionic Electronic Conductor
ML	Monolayer
MS	Mass Spectrometry
NEMCA	Non faradaic Electrochemical Modification of Catalyst Activity
OCV	Open-circuit potential
OER	Oxygen Evolution Reaction
PEEM	PhotoElectron Emission Microscopy
P-EPOC	Permanent Electrochemical Promotion Of Catalysis
Pers-EPOC	Persistent Electrochemical Promotion Of Catalysis
QMS	Quadrupole Mass Spectrometer
RDS	Rate Determining Step
RE	Reference Electrode
SEM	Scanning Electron Microscopy
SEMS	Solid Electrochemical Mass Spectrometry
SPEM	Scanning Photoelectron Microscopy

SOFC	Solid Oxide Fuel Cell
STM	Scanning Tunneling Microscopy
SSCP	Single Step Chronopotentiometry
TOF	Turn Over Frequency
tpb	Triple phase boundary
TPD	Temperature Programmed Desorption
WE	Working Electrode
XPS	X-ray Photoelectron Spectroscopy
XRD	X-Ray Diffraction
YSZ	Yttria Stabilzed Zirconia

2 Roman Symbols

Symbol	Meaning	Units
A	Electrode surface area	[cm^2]
C	Collection efficiency	[-]
C_i	Concentration of i species	[mol L^{-1}]
C_{ox}^*	Bulk concentration of ox species	[mol L^{-1}]
D	Detection efficiency	[-]
D_i	Diffusion coefficient of i species	[cm^2 s^{-1}]
D_{ox}	Diffusion coefficient of ox species	[cm^2 s^{-1}]
E	Potential	[V]
E_a	Anodic upper potential limit	[V]
E_c	Cathodic lower potential limit	[V]
E_H	Anodic holding potential	[V]
E_m	Hopping energy	[kJ]
E_{OC}	Open-circuit potential	[V]
F	Faraday constant	[C]
F_i	Flux of i species	[mol V^{-1} s^{-1}]
G	Free Enthalpy	[kJ mol^{-1}]
ΔG	Free Enthalpy change	[kJ mol^{-1}]
h	Planck constant	[J s]
H	Enthalpy	[kJ mol^{-1}]
ΔH	Enthalpy change	[kJ mol^{-1}]
I	Current	[A]
I_a	Anodic holding current	[A]
I_c	Cathodic holding current	[A]
I_0	Exchange current	[A]
I_{eff}	Effective current for oxide formation	[A]
I_f	Faradaic current	[A]
I_p	Peak current	[A]

I_X	Ionic current of *X* species	[A]
J_X^{Sample}	Gas flow of X released from sample surface	[mol s^{-1}]
$J_X^{Sniffer}$	Gas flow of X entering in the sniffer	[mol s^{-1}]
$J_X^{Topreactor}$	Gas flow of X exiting from the reactor detection hole	[mol s^{-1}]
k	Reaction rate constant	[mol s^{-1}]
K	Clausing factor	[-]
K^0	Equilibrium rate constant	[-]
K_{CO}^0	MS calibration coefficient for CO	[A.Pa^{-1}]
K_{CO2}^0	MS calibration coefficient for CO_2	[A.Pa^{-1}]
K_{O2}^0	MS calibration coefficient for O_2	[A.Pa^{-1}]
k_{ad}	Adsorption rate constant	[mol s^{-1}]
k_L	Linear rate constant	[mol s^{-1}]
k_{Log}	Logarithymic rate constant	[mol s^{-1}]
k_p	Parabolic rate constant	[mol $s^{-1/2}$]
k_p^0	Parabolic rate constant at zero overpotential	[mol s^{-1}]
k_b	Boltzmann constant	[J/K]
L	Distance	[m]
L_t	Critical tunneling distance	[m]
M_x	Molecular mass of *X* species	[kg mol^{-1}]
m_e	Electron mass	[kg]
N	Total MS efficiency	[-]
N_0	Amount of adsorbed oxygen	[mol]
N_F	Maximum amount of promoters supplied	[mol]
N_M	Surface atom density	[mol]
$N_{Pt/gas}$	Amount of reactive sites at the catalyst surface	[mol]
N_R	Amount of oxygen atoms consumed after current interruption	[mol]
p_{C2H4}	Ethylene partial pressure	[Pa], [mbar]
p_{CO}	Carbon monoxide partial pressure	[Pa], [mbar]
p_{O2}	Oxygen partial pressure	[Pa], [mbar]

$p_{O2}^{reference}$	Oxygen partial pressure in the reference compartment of the reactor	[Pa], [mbar]
$p_{O2}^{working}$	Oxygen partial pressure in the working compartment of the reactor	[Pa], [mbar]
p^{HV}	Pressure in the HV main chamber	[Pa], [mbar]
$p^{Sniffer}$	Pressure in the Sniffer	[Pa], [mbar]
P_j	Dipole moment of j species	[D]
PS	Pumping speed	[L s^{-1}]
Q_{NiO}	Amount of NiO anodically formed	[C]
Q_O	Amount of O released after current interruption	[C]
Q_{PtO}	Amount of PtO anodically formed	[C]
Q_{Total}	Equivalent amount of charge passed during anodic polarization	[C]
R	Ideal gas constant	[J mol^{-1} K^{-1}]
R_p	Polarization resistance	[Ω]
r	Reaction rate	[mol s^{-1}]
r^0	Initial reaction rate (Before polarization)	[mol s^{-1}]
r'	Final reaction rate (After polarization)	[mol s^{-1}]
r_{el}	Faradaic rate	[mol s^{-1}]
r_{CO2}	CO_2 formation rate	[mol s^{-1}]
r_{O2}	O_2 formation rate	[mol s^{-1}]
R_{eff}	Effective oxide formation rate	[mol s^{-1}]
S_i	Section of sniffer entrance	[m]
S	Entropy	[kJ K^{-1} mol^{-1}]
ΔS	Entropy change	[kJ K^{-1} mol^{-1}]
T	Temperature	[C]
t_D	Desorption time	[s]
t_e	Electron transference number	[-]
t_h	Hole transference number	[-]
t_H	Holding time	[s]

t_{ion}	Ionic transference number	[-]
TOF_0	Open-circuit turn over frequency	[s^{-1}]
TOF_p	Closed-circuit turn over frequency	[s^{-1}]
u_i	Mobility of I species	[$cm^2\ V^{-1}\ s^{-1}$]
ΔU_e	Energy difference between the Fermi level and the metal conduction band	[eV]
ΔU_{WR}	Potential difference between working and reference electrode	[V]
V_{ox}	Number of moles of metal to form 1 mole of oxide	[-]
V_0	Volume of the sniffer	[cm^3]
$V_{reference}$	Volume of the reference compartment of the reactor	[cm^3]
$V_{working}$	Volume of the working compartment of the reactor	[cm^3]
W	Probability	[-]
z	Charge of ionic species	[-]

3 Greek Symbols

Symbol	Meaning	Units
α_a	Anodic charge transfer coefficient	[-]
α_c	Cathodic charge transfer coefficient	[-]
γ	Permanent rate enhancement factor	[-]
ε^0	Permittivity of free space	[C^2 N^{-1} m^{-2}]
η	Overpotential	[V]
η_{act}	Activation overpotential	[V]
η_{NiO}	Current efficiency for NiO formation	[-]
η_{PtO}	Current efficiency for PtO formation at the Pt/YSZ interface	[-]
η_O	Current efficiency for PtO formation at the Pt/gas interface	[-]
η_{O2}	Current efficiency for O_2 formation	[-]
θ_O	Promoter coverage	[-]
$\theta_{O\delta 1}$	O^{δ_1} promoter coverage	[-]
$\theta_{O\delta 2}$	O^{δ_2} promoter coverage	[-]
Λ	Faradaic enhancement factor	[-]
Λ_{OS}	Oxygen storage efficiency	[-]
μ_i	Chemical potential	[J mol^{-1}]
μ_i^*	Electrochemical potential	[J mol^{-1}]
ρ	Rate enhancement factor	[-]
σ	Conductivity	[S m^{-1}]
τ	Time constant detection	[s]
τ_D	Promoter lifetime	[s]
τ_{Relax}	Open circuit relaxation time	[s]
Φ	Galvani potential	[V]

$\Delta\Phi_w$	Work function change	[eV]
ν	Vibrationnal frequency	[s]
	Scan rate	[V s^{-1}]
Ω	Volume of oxide per metal ion	[m^3]

Cyril FALGAIRETTE

Ch. des Rosiers, 3
1004 Lausanne Suisse
Tel : +41(0)76/571.78.99
Email : cyril.falgairette@a3.epfl.ch

28 (Born June 25, 1981)
French citizenship, Single

Education

2006-present	PhD Thesis: *Electrochemical Promotion Of Catalysis*, Group of Electrochemical Engineering GGEC, Prof.Comninellis, EPFL, Lausanne, Switzerland
2005-2006	Minor in Management of Technology and Entrepreneurship EPFL, Lausanne, Switzerland
2000-2005	Master of Science in Chemical and Biological Engineering EPFL, Lausanne, Switzerland
1999-2000	Post-Secondary preparatory school in Physics-Chemistry, Lycée Thiers, Marseille, France
1999	Baccalaureat Général Scientifique, Lycée Lacordaire, Marseille, France

Professional experience and internships

2006-present	Part time research assistant for the teaching of undergraduates EPFL students
2008-1 month	Internship by Prof. Janek (Pulsed Laser Deposition), JLU, Giessen, Germany
2005-4 month	Internship GGEC (Boron Doped Diamond Electrode), EPFL, Lausanne, Switzerland
2004-3 month	Internship GGEC (Nanoparticles), EPFL, Lausanne, Switzerland
2002-2004	Teaching assistant General Chemistry, Prof. Friedli, EPFL, Lausanne, Switzerland

Languages

French : Mother tongue | English : Fluent | German: Good Knowledge

Publications

8) C.Falgairette, C.Xia, Y.D.Li, W. Harbich, G. Foti, C.Comninellis, *Investigation of Pt/YSZ interface at low partial pressure by solid electrochemical mass spectrometry under high vacuum conditions*, Journal of Applied Electrochemistry (submitted manuscript)

7) C.Falgairette, C.Xia, Y.D.Li, W. Harbich, *Solid Electrochemical Mass Spectrometry (SEMS) applied to Pt/YSZ under high vacuum conditions*, Journal of Applied Electrochemistry (submitted manuscript)

6) S.Souentie, C.Falgairette, Ch.Comninellis, *Electrochemical investigation of the $O_{2(g)}$,Ni/YSZ system using cyclic voltammetry*, Journal of Electrochemical Society (accepted manuscript)

5) S.Souentie, C.FalgairetteCh.Comninellis, *Investigation of the "permanent" electrochemical promotion of catalysis (P-EPOC) by electrochemical mass spectrometry (EMS) measurements*, Electrochemistry Communications (2009)12:2, pp. 323-326

4) G.Fóti, A.Jaccoud, C.Falgairette, Ch.Comninellis, *Charge storage at the Pt/YSZ interface*, Journal of Electroceramics (2009) 23 (2-4), pp. 175-179

3) C.Falgairette, G.Fóti, *Oxygen storage in O_2/Pt/YSZ cell*, Catalysis Today (2009) 146 (3-4), pp. 274-278

2) C.Falgairette, A.Jaccoud, G.Fóti, Ch.Comninellis, *The phenomenon of "permanent" electrochemical promotion of catalysis (P-EPOC)*, Journal of Applied Electrochemistry (2008) 38 (8), pp. 1075-1082

1) A.Jaccoud, C.Falgairette, G. Fóti, Ch.Comninellis, *Charge storage in the $O_{2(g)}$,Pt/YSZ system*, Electrochimica Acta (2007) 52 (28), pp. 7927-7935

Presentations

○ C.Falgairette, G.Fóti, Ch.Comninellis, *Persistent-EPOC related to charge storage at the Pt/YSZ interface,* EFEPOC-EPOCAP conference, September 29-October 3, 2008, Oleron, France

○ C.Falgairette, G.Fóti, Ch.Comninellis, *Charge storage at the Pt/YSZ interface*, EFEPOC-OREPOC conference, 1-5 October, 2007 ,Thessaloniki, Greece

Posters

○ C.Falgairette, G.Fóti, Ch.Comninellis, *Linear sweep voltammetric study of Pt electrodes in solid electrolyte cell*, 4th European Summer School on Electrochemical Engineering (ESSEE4),17-22 September, 2006 , Palić, Serbia and Montenegro